

**Aqueous-phase electrical discharges:
generation, investigation and application for
organics removal from water**

Dissertation

zur Erlangung des akademischen Grades eines
Doktors der Naturwissenschaften

– Dr. rer. nat. –

vorgelegt von

Svetlana Gasanova

geboren in 1988

Institut für Instrumentelle Analytische Chemie
der
Universität Duisburg-Essen

2013

Die vorliegende Arbeit wurde im Zeitraum von Oktober 2010 bis September 2013 im Arbeitskreis von Prof. Dr. Torsten C. Schmidt am Institut für Instrumentelle Analytische Chemie der Universität Duisburg-Essen durchgeführt.

Tag der Disputation: 25.11.2013

Gutachter:	PD Dr. Ursula Telgheder
	Prof. Dr. Volker Buck
Vorsitzender:	Prof. Dr. Eckart Hasselbrink

Abstract

The inability of the existing methods of water treatment to completely degrade recalcitrant organic contaminants and the use of chemical substances in water treatment process forces the scientific world to develop alternative decisions for water treatment. In the present study, a novel method of water treatment based on application of electrical discharges was investigated. Owing to the simultaneous initiation of physical effects (shock waves, thermal effects, UV/Vis light emissions) and chemical reactions (formation of reactive radicals), the method of electrical discharges is supposed to be environmentally friendly as no additional chemicals are required. It represents the main advantage over such competing methods of water treatment as Advanced Oxidation Processes.

This study was aimed to investigate the applicability of electrical discharges generated directly in water for organics removal. The approach undertaken in the present study included the description of the discharge generation, its investigation as well as the demonstration of organics removal.

The electrical discharge generation was performed directly in water using nanosecond high-voltage pulses of direct current (maximal pulse rise time of 800 ns) applied across the large area electrodes (effective area of each electrode is 2 cm²). Special attention was paid on the effect of the electrode coating. The usual problem of streamer reproducibility in time was also highlighted and successfully solved.

The investigation of the obtained electrical discharges was carried out using emission spectrometry which enabled to estimate their physical and chemical activities. Underwater electrical discharges were shown to be a source of intense light radiation in the entire optical region (200-800 nm). Besides, underwater electrical discharge phenomenon was demonstrated to lead to the formation of various reactive species including a very strong oxidant – hydroxyl radical. The created plasma was also characterized in terms of the basic plasma parameters – plasma temperature and electron density.

Among all the experimental parameters, special attention was paid on the impact of average electric field strength and solution conductivity on electrical discharges. It was found that solution conductivity tested in the range of 0.3 μ S/cm – 10 mS/cm made different effects on the discharge inception, physical and chemical activities of the electrical discharges. Thus, higher solution conductivity facilitated

electrical discharge generation and led to the more intense light radiation; however, decreased the formation of reactive species. It was also found that high values of average electric field strength facilitated electrical discharge generation as well as enhanced its physical and chemical activities.

The applicability of the electrical discharges for water treatment was proved on the example of degradation of recalcitrant compounds: five pharmaceuticals (diclofenac, iopamidol, metoprolol, bisphenol A and carbamazepine) and trifluoroacetic acid. The method of electrical discharges was shown to be effective for removal of the selected compounds (removal rates up to 92%), however, the energy consumption was high. The latter aspect represents a challenge for this water treatment technique and should be improved in the future work.

The experimental work carried out in the present study enables to conclude that electrical discharges in water have a great potential as a novel, chemical-free method of water treatment which could represent an alternative to the conventional methods. The main outputs of the study could be used for the future investigation of underwater electrical discharge phenomenon as well as for the future development of this method of water treatment.

Abstract

Nachteile der bestehenden Verfahren zur Wasseraufbereitung sind unvollständiger Abbau von organischen Verunreinigungen und die Verwendung von chemischen Substanzen. Daher ist es erforderlich alternative Verfahren zur Wasseraufbereitung zu entwickeln. In der vorliegenden Studie wurde ein neues Verfahren zur Wasseraufbereitung basierend auf elektrische Entladungen entwickelt und untersucht. Durch die gleichzeitige Nutzung von physikalischen Effekten (Stoßwellen, thermische Effekte, UV/VIS Strahlung) und chemischen Reaktionen (Bildung der reaktiven Radikale) soll das Verfahren den Abbau von ozonrefraktären Stoffen ermöglichen.

Im Rahmen der vorliegenden Dissertation wurde die Anwendbarkeit der im Wasser generierten elektrischen Entladungen für den Abbau von organischen Stoffen untersucht. Dazu gehörten Studien zur Plasmagenerierung, Plasmacharakterisierung und dem Abbau von ausgewählten organischen Substanzen.

Die Entladungsbildung im Wasser wurde unter Verwendung von Hochspannungsimpulsen im nanosekunden Bereich (maximale Flankensteilheit 800 ns) an großflächigen Elektroden (wirksame Fläche jeder Elektrode 2 cm²) durchgeführt. Das besondere Augenmerk wurde auf den Einfluss der Elektrodenbeschichtung auf die Plasmagenerierung gelegt. Reproduzierbare Streamer konnten unter Verwendung einer α -Al₂O₃-Beschichtung erreicht werden.

Die Untersuchung der elektrischen Entladungen erfolgte durch Emissionsspektrometrie. Intensive Strahlung im optischen Bereich (200-800 nm) konnte beobachtet werden. Außerdem konnte nachgewiesen werden, dass die elektrischen Entladungen im Wasser zur Bildung von verschiedenen reaktiven Spezies einschließlich eines sehr starken Oxidationsmittels – Hydroxyl-Radikal – führen. Das generierte Plasma wurde auch im Hinblick auf die grundlegenden Plasmaparameter – die Plasmatemperatur und die Elektronendichte – charakterisiert.

Es wurde ein besonderes Augenmerk auf die Auswirkungen der durchschnittlichen elektrischen Feldstärke und Leitfähigkeit der Lösung auf elektrische Entladungen gelegt. Es wurde festgestellt, dass die Entladungsbildung, physikalischen und chemischen Effekte von der Leitfähigkeit im Bereich von 0.3 μ S/cm – 10 mS/cm abhängen. Somit erleichtert die hohe Leitfähigkeit der Lösung die Entladungsbildung und führt zur intensiveren Lichtstrahlung, die Bildung von

reaktiven Spezies wird jedoch verringert. Es wurde auch festgestellt, dass die hohe durchschnittlichen elektrischen Feldstärken die Entladungsbildung fördert sowie die physikalischen und chemischen Effekte verstärkt.

Die Anwendbarkeit der elektrischen Entladungen zur Wasseraufbereitung wurde am Beispiel des Abbaus ausgewählter ozonrefraktärer Verbindungen gezeigt. Als Modellverbindungen wurden die pharmazeutischen Substanzen Diclofenac, Iopamidol, Metoprolol, Bisphenol A und Carbamazepin und Trifluoressigsäure verwendet. Es konnte ein Abbau bis zu 92% erreicht werden, obwohl der Energieverbrauch im Bereich von mg/kWh lag.

Die vorliegende Studie lässt den Schluss zu, dass elektrische Entladungen im Wasser ein großes Potenzial für die chemikalienfreie Behandlung von kleinen Abwassermengen besitzen.

Table of content

Abstract.....	i
Table of content.....	v
List of tables.....	x
List of figures.....	xi
Abbreviations and marks.....	xv

CHAPTER 1: INTRODUCTION

1.1. The water treatment issue.....	1
1.2. Removal of pollutants by electrical discharges.....	3
1.3. Research goals.....	4
1.4. Thesis organization.....	5
1.5. List of literature.....	7

CHAPTER 2: ELECTRICAL DISCHARGE GENERATION IN AQUEOUS SOLUTION

Chapter scope.....	11
2.1. Literature survey	
2.1.1. Electrical discharge mechanism.....	12
2.1.1.1. Breakdown in gases	12
2.1.1.2. Breakdown in liquids	13
2.1.1.3. Breakdown of solid dielectrics.....	14
2.1.2. Electrode configurations.....	15
2.1.3. Factors influencing electrical discharge formation in liquid.....	16
2.1.3.1. Electrode coating	16
2.1.3.2. Temporal characteristics of electric pulses.....	23
2.1.3.3. Method of electrical excitation	24
2.1.3.4. Polarity of electric pulses.....	25
2.1.3.5. Solution conductivity.....	26
2.1.3.6. Electric field strength.....	28
2.1.4. Effects induced by underwater electrical discharges.....	29

2.1.4.1. Physical effects.....	29
2.1.4.2. Chemical reactions.....	30
2.2. Experimental	
2.2.1. Overall view of experimental setup.....	32
2.2.1.1. High-voltage equipment.....	32
2.2.1.2. Circulation system.....	34
2.2.2. Electrode coatings.....	35
2.2.3. X-ray diffraction spectra and Scanning Electron Microscope imaging...	35
2.2.4. Chemical methods.....	36
2.2.4.1. Determination of hydrogen peroxide.....	36
2.2.4.2. Determination of hydroxyl radical.....	37
2.3. Results and discussions	
2.3.1. Equivalent electric circuit of the discharge gap.....	38
2.3.2. Factors influencing electrical discharge inception	39
2.3.2.1. Electrode coating	39
2.3.2.2. Electric field strength.....	51
2.3.2.3. Solution conductivity.....	52
2.3.2.4. Pulse repetition rate.....	55
2.3.3. Electrical discharge formation.....	56
2.3.4. Energy per electric pulse.....	57
2.3.5. Chemical activity of underwater electrical discharge.....	59
2.3.5.1. Effect of the solution conductivity.....	60
2.3.5.2. Effect of the pulse repetition rate.....	62
2.4. Summary	64
2.5. List of literature	65
 CHAPTER 3: PLASMA DIAGNOSTICS	
Chapter scope.....	71

3.1. Literature survey

3.1.1. Electrical discharge propagation	72
3.1.1.1 Streamer branching.....	72
3.1.1.2. Streamer length.....	73
3.1.1.3. Propagation velocity.....	73
3.1.2. Radiative processes induced by underwater plasma discharges.....	74
3.1.2.1. Discharge continuum.....	74
3.1.2.2. Line spectrum of primary species.....	77
3.1.3. Plasma parameters	80

3.2. Experimental

3.2.1. Instrumentation.....	83
3.2.1.1. Reactor modification for spectroscopic measurements.....	83
3.2.1.2. Optical equipment.....	84
3.2.2. Determination of plasma parameters.....	86
3.2.2.1. Gas temperature measurements.....	86
3.2.2.2. Electron density measurements.....	87
3.2.3. Solution saturation with Ar and N ₂	88

3.3. Results and discussions

3.3.1. Imaging diagnostic of electrical discharge.....	89
3.3.1.1. Discharge imaging.....	89
3.3.1.2. ICCD imaging.....	92
3.3.2. Discharge continuum.....	94
3.3.2.1. General view.....	94
3.3.2.2. Effect of the solution conductivity.....	95
3.3.2.3. Effect of the electric field strength.....	96
3.3.2.4. Temporal evolution of discharge continuum.....	97
3.3.3. Post-discharge emission spectrum.....	100
3.3.3.1. Reactive species and the respective emission lines.....	100
3.3.3.2. Effect of the solution conductivity.....	103
3.3.3.3. Effect of the applied electric field.....	105
3.3.3.4. Temporal evolution of reactive species.....	106

3.3.3.5. Effect of the solution saturation with gases.....	109
3.3.4. Plasma temperature analysis.....	112
3.3.5. Electron density.....	115
3.3.5.1. Effect of solution conductivity.....	116
3.3.5.2. Effect of the electric field strength.....	118
3.3.5.3. Temporal evolution of electron density.....	119
3.3.5.4. Effect of solution saturation of gases.....	121
3.3.5.5. Numerical values of electron density	123
3.4. Summary.....	124
3.5. List of literature.....	125
 CHAPTER 4: DEGRADATION OF ORGANIC COMPOUNDS	
Chapter scope.....	129
4.1. Literature survey	
4.1.1. Current studies on removal of organics by electrical discharges.....	130
4.1.2. Pharmaceutical compounds.....	131
4.1.2.1. Diclofenac (DFC)	132
4.1.2.2. Iopamidol (IOP)	133
4.1.2.3. Metoprolol (MP)	134
4.1.2.4. Bisphenol A (BPA)	135
4.1.2.5. Carbamazepine (GBZ)	137
4.1.3. Trifluoroacetic acid (TFA)	138
4.2. Experimental	
4.2.1. Reactor configuration.....	140
4.2.2. Chemicals.....	141
4.2.3. HPLC measurements.....	141
4.2.4. Degradation of TFA.....	142
4.2.5. Calculation of energy efficiency.....	143

4.3. Results and discussions	
4.3.1. Removal of pharmaceuticals.....	144
4.3.1.1. Effect of the initial concentration.....	145
4.3.1.2. Effect of the reactor configuration.....	146
4.3.1.3. Effect of the solution conductivity.....	147
4.3.2. Degradation kinetics.....	150
4.3.3. Transformation products of DFC.....	156
4.3.4. Energy efficiency.....	160
4.3.4.1. Effect of the treatment time.....	160
4.3.4.2. Effect of the initial concentration.....	161
4.3.4.3. Effect of the reactor configuration.....	161
4.3.5. Degradation of TFA.....	163
4.4. Summary	165
4.5. List of literature	166
CONCLUSIONS.....	180
OUTLOOK.....	182
ACKNOWLEDGEMENTS.....	183
Curriculum Vitae.....	184
List of publications.....	185
Erklärung der eigenständigen Anfertigung der Arbeit.....	186

List of tables

Table 1	Dielectric properties of some dielectric materials used for the DBD generation	p.20
Table 2	Properties of α -Al ₂ O ₃	p.21
Table 3	Properties of electrode coatings	p.39
Table 4	Possible routes of interactions of water molecules being in vapor with electrons	p.77
Table 5	Duration of the light emission of reactive species in excited state formed by underwater electrical discharge	p.109
Table 6	Values of $\Delta\lambda_{1/2}$ (nm) of the H α line with and without solution saturation with Ar and N ₂	p.122
Table 7	Observed pseudo-first order rate constants of degradation of pharmaceuticals in flow and batch reactors for C ₀ = 1, 10 and 100 mg/L	p.153
Table 8	Energy efficiency of DFC, IOP, MP, BPA and CBZ degradation at the fixed removal rate of 10, 21, 9, 5 and 4%, respectively, in the batch and flow reactors	p.162

List of figures

Figure 1	Breakdown stages	p.12
Figure 2	Basic electrode configurations	p.15
Figure 3	Location of the dielectric layer in discharge gap	p.19
Figure 4	Different modifications of dielectric layer for electrical discharge generation	p.23
Figure 5	Example current and voltage waveforms of 1 kHz AC and 300 Hz short-pulse DC excitation of DBD	p.25
Figure 6	Reactive species formed by underwater electrical discharge	p.31
Figure 7	Overall view of experimental setup (Chapter 2)	p.32
Figure 8	Plasma reactor	p.33
Figure 9	Equivalent electric circuit of the discharge gap	p.38
Figure 10	Scanning electron microscope images of GAC50	p.40
Figure 11	Formation of H_2O_2 with GAC50	p.41
Figure 12	Current and voltage waveforms for GAC50	p.42
Figure 13	Scanning electron microscope images of GAC250	p.43
Figure 14	Current and voltage waveforms for GAC250	p.44
Figure 15	Formation of H_2O_2 and HTA with GAC250	p.45
Figure 16	Scanning electron microscope images of WAC500	p.47
Figure 17	Current and voltage waveforms of electrical discharge generated with WAC500	p.48
Figure 18	Formation of H_2O_2 and HTA with WAC500	p.49
Figure 19	X-ray diffraction spectra of the ceramic coatings	p.50
Figure 20	Influence of the inter-electrode distance on the threshold voltage of the electrical discharge inception	p.51
Figure 21	The effect of solution conductivity on the threshold voltage of the electrical discharge inception	p.53

Figure 22	Voltage waveforms of electrical discharge generated at different values of solution conductivity	p.55
Figure 23	Current waveforms of electrical discharge generated at different values of solution conductivity	p.55
Figure 24	Calculation of the energy per electric pulse on the example of solution conductivity of 2 mS/cm	p.58
Figure 25	Effect of the solution conductivity on the energy per electric pulse	p.58
Figure 26	HTA formation in solutions of different conductivity and Effect of the solution conductivity on the HTA formation	p.61
Figure 27	H ₂ O ₂ formation in solutions of different conductivity and Effect of the solution conductivity on the H ₂ O ₂ formation	p.61
Figure 28	Effect of the pulse repetition rate on HTA and H ₂ O ₂ formation	p.63
Figure 29	Dependence of spectral radiance on the wavelength at different temperatures	p.76
Figure 30	Radiolysis of water	p.79
Figure 31	Density – gas temperature plane	p.82
Figure 32	Placement of the optical equipment relating to the plasma reactor	p.83
Figure 33	Block scheme of experimental setup (Chapter 3)	p.84
Figure 34	Calibration of the emission spectrometer with a HeNe laser	p.85
Figure 35	Image of the electrical discharge for $\sigma = 0.1$ mS/cm	p.90
Figure 36	Image of the electrical discharge for $\sigma = 1$ mS/cm	p.90
Figure 37	Effect of the solution conductivity on the discharge shape	p.91
Figure 38	Image of a spark discharge	p.92
Figure 39	Time-resolved ICCD camera images of an underwater electrical discharge	p.93
Figure 40	Time-resolved profiles of the discharge light collected in the range of 120 – 1090 nm	p.93
Figure 41	Continuous spectrum of underwater electrical discharge	p.95
Figure 42	Effect of the solution conductivity on the discharge intensity	p.95

Figure 43	Effect of the averaged electric field strength on the discharge intensity	p.97
Figure 44	Time-resolved discharge continuum	p.98
Figure 45	Temporal evolution of the discharge light	p.99
Figure 46	Effect of the solution conductivity on the discharge light duration	p.100
Figure 47	Post-discharge emission spectrum of reactive species	p.101
Figure 48	Effect of the solution conductivity on the radical formation by electrical discharges	p.104
Figure 49	Effect of the average electric field strength on the radical formation by electrical discharges	p.106
Figure 50	Temporal evolution of the OH emission line (309 nm)	p.108
Figure 51	Effect of the solution conductivity on the radical emission line intensity	p.108
Figure 52	Effect of the solution saturation with N ₂ on the post-discharge emission spectrum	p.110
Figure 53	Emission spectrum of reactive species formed by underwater electrical discharge when saturating with Ar	p.111
Figure 54	Comparison of OH, H _α and O emission lines in the case of no gas bubbling, saturation with N ₂ and Ar	p.112
Figure 55	Effect of experimental parameters (solution conductivity and electric field strength) on the position of the continuum maximum	p.113
Figure 56	Effect of the saturation of solution with N ₂ and Ar on the discharge continuum maximum	p.115
Figure 57	Example of the H _α line treatment	p.116
Figure 58	Effect of the solution conductivity on the H _α line broadening	p.117
Figure 59	Effect of the solution conductivity on the $\Delta\lambda_{1/2}$ of the H _α line	p.118
Figure 60	Effect of the average electric field strength on the H _α line broadening	p.119
Figure 61	Effect of the average electric field strength on the $\Delta\lambda_{1/2}$ of the H _α line	p.119
Figure 62	Time-resolved H _α line profiles	p.120

Figure 63	Temporal dependence of the $\Delta\lambda_{1/2}$ of H_{α} line	p.120
Figure 64	Effect of the solution saturation with Ar and N_2 on the broadening of the H_{α} line	p.122
Figure 65	Structural formula of diclofenac	p.132
Figure 66	Structural formula of iopamidol	p.133
Figure 67	Structural formula of metoprolol	p.134
Figure 68	Structural formula of bisphenol A	p.135
Figure 69	Structural formula of carbamazepine	p.137
Figure 70	Structural formula of trifluoroacetic acid	p.138
Figure 71	Reactor configurations used in the present study: a batch reactor and a flow reactor (Chapter 4)	p.141
Figure 72	Effect of the initial concentration of pharmaceuticals on the removal rates in the batch reactor and in the flow reactor	p.144
Figure 73	Effect of the solution conductivity on the removal rates of diclofenac, iopamidol, metoprolol, bisphenol A and carbamazepine	p.148
Figure 74	Degradation curves of diclofenac, iopamidol, metoprolol, bisphenol A and carbamazepine in the batch and the flow reactors at initial concentrations of 1, 10 and 100 mg/L	p.151-152
Figure 75	First order degradation plots on the example of iopamidol in the flow reactor	p.153
Figure 76	HPLC chromatograms of diclofenac before and after plasma treatment recorded at 254 nm	p.157
Figure 77	Absorption spectra of diclofenac and its transformation products	p.158
Figure 78	The main degradation products of diclofenac reported in literature	p.159
Figure 79	Effect of the treatment time on the energy yield on the example of diclofenac degradation	p.161
Figure 80	Ion chromatograms of TFA before and after plasma treatment	p.164

Abbreviations	Marks
AOP – advanced oxidation process	T_i – ion temperature
WTP – water treatment plant	T_e – electron temperature
VOC – volatile organic compound	T – plasma gas temperature
NSAID – non-steroidal anti-inflammatory drug	T_{bb} – blackbody temperature
DFC – diclofenac	α – emission coefficient; fractional width from line center
IOP – iopamidol	N_e – electron density
BPA – bisphenol A	$\Delta\lambda_{1/2}$ – full width at half maximum of emission line
MP – metoprolol	E_{pulse}, E_p – energy per electric pulse
CBZ – carbamazepine	ϵ_r – relative permittivity
ICM – X-ray contrast media	ϵ_0 – vacuum permittivity
HFC – hydrofluorocarbons	A – area of dielectric layer; absorbance
HCFC - hydrochlorofluorocarbons	d – thickness of dielectric layer; distance between electrodes
NTP – nonthermal plasma	C_d – capacity of ceramic layer
DBD – dielectric barrier discharge	C_s – capacity of aqueous solution
DC – direct current	R_d – resistivity of ceramic layer
AC – alternating current	R_s – resistivity of aqueous solution
HV – high voltage	r – radius of pinhole; radius of curvature of electrode tip
AEFS – average electric field strength	ϵ – molar extinction coefficient
GAC50 – grey alumina coating 50 μm thick	l – length of light path
GAC250 – white alumina coating 250 μm thick	C – concentration
WAC500 – white alumina coating 500 μm thick	U, V_0 – voltage across electrodes
XRD – X-ray diffraction	I – electric current; light intensity
HTA - 2-hydroxyterephthalic acid	F – pulse repetition rate
TFA – trifluoroacetic acid	σ – solution conductivity
NaTA - disodium salt of terephthalic acid	\emptyset – diameter
MCP – multichannel plate	E_{red}^0 – <i>standard reduction potential</i>
ICCD – intensified charge coupled device	E_{ox}^0 – <i>standard oxidation potential</i>
FR – flow reactor	P – discharge power
BR – batch reactor	C_0 – initial concentration
HPLC - high performance liquid chromatography	V – solution volume
MS – mass spectrometry	X – conversion of initial compound
DAD – diode array detector	W – removal efficiency
PFC - polyfluorinated compound	

CHAPTER 1: INTRODUCTION

1.1. The water treatment issue

In the world of rapidly growing economy and climate change, the consumption of organic compounds is continuously increasing. The production of chemicals of different toxicity and recalcitrance reaches high levels. Everyday new organic substances that could become recalcitrant contaminants are being synthesized and charged into the environment. These facts represent the main challenges in the development of new and effective water treatment methods.

In recent years, many studies have reported on incomplete elimination of a number of organic substances by the conventional water treatment (Creese *et al*, 2004, Ternes *et al*, 1998). As a result, organic residuals were found in water treatment plant effluents, groundwater, surface water as well as drinking water samples. It might lead to the accumulation of the organics in human body causing chronic diseases. The high stability of some organic compounds, such as pharmaceuticals, for instance, does not allow of their biodegradation, therefore advanced water treatment is required. Nowadays, a variety of methods based on chemical destruction of organic pollutants are being developed. Among them there are chlorination, such relatively new techniques of water purification as ozonation (also in combination with UV), Advanced Oxidation Processes (AOPs) and photocatalysis.

Chlorination has been implemented for years as a method of water disinfection. It was also used for the elimination of organics on molecular level. Usually two main disadvantages of chlorination as a water treatment method are reported: (i) – the formation of carcinogenic chlorinated hydrocarbons resulted from the reaction of chlorine with organic pollutants (Dunnick *et al*, 1993); (ii) – the low

oxidation potential of chlorine ($E_{\text{ox}}^0(\text{Cl}_2) = 1.36 \text{ V}$) which results in incomplete elimination of organic pollutants.

With time, chlorination was replaced by ozonation which is commonly used as a final step in modern water treatment plants (WTP). The combination of ozonation with UV irradiation is being intensively implemented in many WTPs to purify water till the drinking level. The principle of water purification by ozone consists in the oxidation of organics by highly reactive and short-lived oxygen atoms ($E_{\text{ox}}^0(\text{O}^\bullet) = 2.42 \text{ V}$) formed from the destruction of unstable ozone molecules. Although ozone was accepted as being safe (Lake *et al.*, 2001), water treatment application requires significant dosages of ozone (7-15%).

Currently, many research groups are developing a variety of Advanced Oxidation Processes that are aiming on the generation of highly reactive hydroxyl radicals ($E_{\text{ox}}^0(\text{OH}^\bullet) = 2.82 \text{ V}$) for successful degradation of organics. Although some AOPs are quite promising, still some organic compounds remain undestroyed. Moreover, water treatment by all AOPs (Fenton, H_2O_2 , O_3 etc.) requires undesirable addition of chemical substances. The subsequent removal of the supplementary chemicals and their recycling is also a big issue. Among other disadvantages, there are storage of oxygen for ozone-based processes and high costs of UV lamps for UV-based processes.

Photocatalysis is also extensively investigated as a novel water treatment technique. The destruction of organics by photocatalysis is based on semiconductor photochemistry. The main obstacle of photocatalysis is the separation of catalyst in suspension. Since photocatalysis is considered to be an AOP, the disadvantages of AOPs listed above could be attributed to photocatalysis as well. Additionally, because the photocatalytic oxidation of organics is preceded by the adsorption of the pollutant on the surface of the catalyst, there is a risk that the pollutant remains adsorbed, but not degraded.

In order to avoid the limitations and disadvantages of the existing water treatment techniques the alternative ones are to be developed. The first and the main requirement to the novel technique is the chemical-free treatment. Secondly, the water treatment should result in the complete mineralization in order to avoid the possible formation of toxic and recalcitrant by-products. The third aspect concerns the treatment costs which should not be incredibly high. Finally, the successful water

treatment technique should be applicable for both – water disinfection and degradation of organics on molecular level.

1.2. Removal of pollutants by electrical discharges

Recently, electrical discharges have attracted a great interest as a novel tool for pollution control. From this point of view, wide range of application of electrical discharges includes the degradation of air pollutants such as Volatile Organic Compounds (VOCs) (Penetrante *et al*, 1993, McAdams *et al*, 2001, Grabowski *et al*, 2006), water disinfection (Sato *et al*, 1996, Li *et al*, 2006, Mizuno *et al*, 1988) and removal of organic compounds dissolved in water (Magureanu *et al*, 2007, Gerrity *et al*, 2010, Hoebein *et al*, 1999).

The discharge systems for the operation in air were characterized by the moderate costs and relative simplicity in terms of electrical discharge generation (Urashima *et al*, 2000, Eliasson *et al*, 1991, Van Durme *et al*, 2007, Chen *et al*, 2009, Futamura *et al*, 2002). However, when the technology expended its application on the water pollution control, the first obstacles appeared. The main problem was the transfer of the electrical discharge and the induced effects from gas phase to liquid. Since the direct generation of electrical discharge in liquid is much more complicated than in gas phase, the new reactors were designed in the way that the electrical discharges still took place in gas phase, but in proximity of the contaminated water layer (Belosheev *et al*, 1998, Magureanu *et al*, 2010, Lukes *et al*, 2011, Hoebein *et al*, 1999, Sano *et al*, 2002). However, the question, how efficient is such a treatment, caused a great concern as the most reactive part of the system - boundary between water and gas – occupied a small volume. This limitation could be eliminated by the more efficient generation of electrical discharge directly in water. The great advance in the understanding of underwater electrical discharge phenomenon achieved in the last two decades (Babaeva *et al*, 2008, Bruggeman *et al*, 2009, Clements *et al*, 1987, Starikovskiy *et al*, 2011, Marinov *et al*, 2011) allowed to start the investigation of organics removal by electrical discharges generated directly in water. However, most of systems still resort to the aid of gas phase in the generation of electrical discharge, for instance, the discharges in water with gas bubbles (Kurahashi *et al*, 1997, Ihara *et al*, 1999, Miichi *et al*, 2002, Gershman *et al*, 2007, Shih *et al*, 2010). The least studies

report on the investigation of organics removal by electrical discharges generated fully in water.

Electrical discharges in water produce conductive channels - streamers – which are filled with plasma. Plasma is the most abundant state of matter as 99.9% of the universe is comprised of plasma. The definition of “plasma” was firstly introduced by Irving Langmuir in the year 1928 (Langmuir *et al*, 1928). The modern definition of plasma says that it is an ionized gas consisting of positive ions and free electrons in proportions resulting in more or less no overall electric charge, typically at low pressures (as in the upper atmosphere and in fluorescent lamps) or at very high temperatures (as in stars and nuclear fusion reactors).

Non-thermal plasmas (NTP) utilized in chemical processing is not in thermal equilibrium as the electron temperature (T_e) much exceeds the ion temperature (T_i): $T_e \gg T_i$. On the contrary, in thermal plasmas all components are in local thermodynamic equilibrium and occur at almost equally high temperature ($T_e \simeq T_i$). In contrast to thermal plasma, in NTP, it is more energy efficient to not feed energy equally into all degrees of freedom within a gas or plasma, but only into those degrees of freedom that can efficiently create the desired final reaction products for the particular application (Parvulescu *et al*, 2012). Thus, high energy electrons of NTP are capable of dissociating and/or ionizing water molecules to form reactive primary and secondary species which would then attack the organic pollutants.

Owing to the ability to form reactive species *in situ*, i.e. without the addition of chemicals, and the variety of physical effects induced simultaneously with the chemical reactions, electrical discharges generated in water are considered to be a novel, effective and environmentally friendly tool for water treatment. This technology is being rapidly developed on the laboratory scale, used for a small-scale water treatment (e.g. “AquaSpark” Ltd.) and patented by research groups and companies (e.g. US patents: 5464513, 5630915, 4169029, R.F. Patents: 2136600, 2178774).

1.3. Research goals

The experimental work carried out in the present study had three main goals: (i) generate an electrical discharge in water; (ii) characterize the obtained electrical discharge and (iii) check the capability of the obtained and characterized electrical

discharge for organics removal from water. In this subchapter, the thesis goals are discussed, while the more specific objectives followed from each goal are presented in the Chapter scope of the relevant chapter.

The first goal arose from the fact that the generation of electrical discharges in liquids is not simple compared to gas discharges. Many experimental parameters have to be considered and the optimal values have to be found for the successful generation of electrical discharges that would not cease with time.

The second goal comes from the necessity to provide the understanding of physical and chemical effects induced by the obtained discharges. This is an integral part of the research which enables to get an insight into the electrical discharge nature. The understanding of the process nature, in turn, enables to optimize the parameters for the most beneficial operation.

The third goal finalizes the present research and defines whether or not the electrical discharges have a future as a tool for water treatment. It should be noted that the organic substances selected for the present study are characterized by a very high recalcitrance which successful degradation is a great challenge for a developing water treatment technique.

The fourth and the most general aim was to undertake a systematic approach, which enabled to work out all three aspects of underwater electrical discharge – generation, investigation and application – within one study.

1.4. Thesis organization

The dissertation is divided into three main parts, each of them corresponds to the one of the three goals listed above. Following the present Chapter 1, Chapter 2 describes the generation of electrical discharge in water, Chapter 3 is devoted to the plasma diagnostics and, in Chapter 4, the degradation of pharmaceutical compounds by electrical discharges is discussed. Each chapter starts with the short Chapter scope discussing the objectives and the main approaches to achieve the goal. It is followed by the Literature survey, which describes the theoretical background, achievements to date and the current research trends of the topic. The Experimental part of each chapter summarizes the descriptions of experimental apparatuses, techniques, methods and experimental procedures used during the experimental investigation. The

Results and Discussions part is the most essential part of each chapter which contains the description of obtained results, their analysis, verification or disapproval of hypotheses. The Summary highlights the most important achievements.

1.5. List of literature

- Babaeva** N.Y., Kushner M.J. 2008. Streamer Branching: The Role of Inhomogeneities and Bubbles. *IEEE Trans Plasma Sci.* 36(4), 892-893
- Belosheev** V.P. 1998. Leader discharge over a water surface in a Lichtenberg figure geometry. *Tech Phys.* 43, 1329-1332
- Bruggeman** P., Leys C. 2009. Non-thermal plasmas in and in contact with liquids. Topical Review. *J Phys D: Appl Phys.* 42, 1-28
- Chen** H.L., Lee H.M., Chen S.H., Chang M.B., Yu S.J., Li S.N. 2009. Removal of volatile organic compounds by single-stage and two-stage plasma catalysis systems: a review of the performance enhancement mechanisms, current status, and suitable applications. *Environ Sci Technol.* 43(7), 2216-2227
- Clements** J.S., Sato M., Davis R.H. 1987. Preliminary investigation of prebreakdown phenomena and chemical reactions using a pulsed high-voltage discharge in water. *IEEE Trans Ind Appl.* IA-23, 224-235
- Creese** A., Gasman N., Mariko M. 2004. The World Medicines Situation. World Health organization
- Dunnick** J.K., Melnick R.L. 1993. Assessment of the carcinogenic potential of chlorinated water: experimental studies of chlorine, chloramine, and trihalomethanes. *J Natl Cancer Inst.* 85(10), 817-22
- Eliasson** B., Kogelschatz U. 1991. Nonequilibrium volume plasma chemistry processing. *IEEE Trans Plasma Sci.* 19(6), 1063-1077
- Futamura** S., Zhang A., Einaga H., Kabashima H. 2002. Involvement of catalyst materials in nonthermal plasma chemical processing of hazardous air pollutants. *Catal Today.* 72(3-4), 259-265
- Gershman** S., Mozgina O., Belkind A., Becker K., Kunhardt E. 2007. Pulsed electrical discharge in bubbled water. *Contrib Plasma Phys.* 47(1-2), 19-25
- Gerrity** D., Stanford B.D., Trenholm R.A., Snyder S.A. 2010. An evaluation of a pilot-scale nonthermal plasma advanced oxidation process for trace organic compound degradation. *Water Res.* 44, 493-504
- Grabowski** L.R. 2006. Doctoral Dissertation: Pulsed corona in air for water treatment. Technical University Eindhoven, Eindhoven, 127 pages

Hoeben W., Velduizen E.M. van, Rutgers W.R., Kroesen G.M.W. 1999. Gas phase corona discharges for oxidation of phenol in aqueous solution. *J Phys D: Appl Phys.* 32(24), L133-L137

Ihara S., Miichi T., Satoh S., Yamabe C., Sakai E. 1999. Ozone generation by a discharge in bubbled water. *Jpn J Appl Phys.* 38, 4601-4604

Kurahashi M., Katsura S., Mizuno A. 1997. Radical formation due to discharge inside a bubble in liquid. *J Electrostatics.* 42, 93-105

Lake L.R. 2001. Secondary direct food additives permitted in food for human consumption. Food and drug administration agency. Rules and regulations. 66(123), 33829-33830

Langmuir I. 1928. Oscillations in ionized gases. *Proc Natl Acad Sci USA.* 14, 627-637

Li Z., Sakai S., Yamada C., Wang D., Chung S., Lin X., Namihira T., Katsuki S., Akiyama H. 2006. The effects of pulsed streamerlike discharge on cyanobacteria cells. *IEEE Trans Plasma Sci.* 34, 1719-1725

Lukes P., Clupek M., Babicky V. 2011. Discharge filamentary patterns produced by pulsed corona discharge at the interface between a water surface and air. *IEEE Trans Plasma Sci.* 39(11), 2644-2645

Magureanu M., Mandache N.B., Parvulescu V.I. 2007. Degradation of organic dyes in water by electrical discharges. *Plasma Chem Plasma Proces.* 27(5), 589-598

Magureanu M., Piroi D., Mandache N.B., David V., Medvedovici A., Parvulescu V.I. 2010 Degradation of pharmaceutical compound pentoxifylline in water by non-thermal plasma treatment. *Water Res.* 44, 3445-3453

Marinov I.L., Guaitella O., Rousseau A., Starikovskaia S.M. 2011. Successive nanosecond discharges in water. *IEEE Trans Plasma Sci.* 39(11), 2672-2673

McAdams R. 2001. Prospects for non-thermal atmospheric plasmas for pollution abatement. *J Phys D: Appl Phys.* 34(18), 2810

Miichi T., Hayashi N., Ihara S., Satoh S., Yamabe C. 2002. Generation of radicals using discharge inside bubbles in water for water treatment. *Ozone Sci Eng.* 24, 471-477

Mizuno A., Hori Y. 1988. Destruction of living cells by pulsed high-voltage application. *IEEE Trans Ind Appl.* 24, 387-394

Parvulescu V.I., Magureanu M., Lukes P. 2012. Plasma chemistry and catalysis in gases and liquids. Wiley-VCH Verlag & Co. KGaA, Weinheim, Germany. Print ISBN: 978-3-527-33006-5, 401 page

Penetrante B.M. and Schultheis S.E. 1993. Non-thermal plasma techniques for pollution control: Parts A and B. NATO ASI Series G, Springer-Verlag Berlin and Heidelberg GmbH & Co. K, Berlin, Germany. ISBN-10: 364278478X 440 pages

Sano N., Kawashima T., Fujikawa J., Fujimoto T., Kitai T., Toyoda A. 2002. Decomposition of organic compounds in water by direct contact of gas corona discharge: influence of discharge conditions. Ind Eng Chem Res. 41(24), 5906-5911

Sato M., Ohgiyama T., Clements J.S. 1996. Formation of chemical species and their effects on microorganisms using a pulsed high-voltage discharge in water. IEEE Trans Ind Appl. 32(1), 106-112

Shih K.Y., Locke B.R. 2010. Chemical and physical characteristics of pulsed electrical discharge within gas bubbles in aqueous solutions. Plasma Chem Plasma Process. 30(1), 1-20

Starikovskiy A., Yang Y., Cho Y.I., Fridman A. 2011. Non-equilibrium plasma in liquid water: dynamics of generation and quenching. Plasma Sources Sci Technol. 20, 1-7

Ternes T.A. 1998. Occurrence of drugs in German sewage treatment plants and rivers. Water Res. 32(11), 3245-3260

Urashima K., Chang J.-S. 2000. Removal of volatile organic compounds from air streams and industrial flue gases by non-thermal plasma technology. IEEE Trans Dielectr Electr Insul. 7(5), 602-614

Van Durme J., Dewulf J., Leys C., Van Langenhove H. 2007. Combining non-thermal plasma with heterogeneous catalysis in waste gas treatment: a review. Appl Catal B: Environ. 78(3-4), 324-333

CHAPTER 2: ELECTRICAL DISCHARGE GENERATION IN AQUEOUS SOLUTION

Chapter scope

The generation of electrical discharges is not simple due to the high power needed and dissipated during this process. Many efforts to generate electrical discharges directly in liquids have been undertaken. The difficulty of the electrical discharge generation directly in liquid consists in the fact that the mechanism of the liquid discharge is not known. Liquids are denser media than gases, therefore higher energies for the discharge inception are needed.

This chapter describes the first step on the way of application of underwater electrical discharge for organics removal - electrical discharge initiation. The effect of the different parameters on the electrical discharge inception in aqueous solution is studied. The monitoring of the electrical discharge generation was carried out visually. The tools employed for explanation of the observed phenomena include: (i) analysis of voltage and current waveforms, (ii) analysis of equivalent electric circuit and (iii) chemical methods. The latter tool implies the analysis of reactive species formation resulted from the electrical discharge.

The main aim at this step is the generation of a reproducible electrical discharge in aqueous solution. The objectives include: (i) design of a plasma reactor; (ii) find out what parameters and in what extent influence the electrical discharge inception; (iii) search for the optimal conditions of the electrical discharge inception; (iv) evaluation of the chemical activity of the underwater electrical discharge.

2.1. Literature survey

2.1.1. Electrical discharge mechanism

2.1.1.1. Breakdown in gases

Electrical breakdown of gases implies the formation of a discharge channel between two electrodes separated by a gas gap, when the applied voltage exceeds a certain value. It is accompanied by a number of effects including light flash and sound. The main breakdown mechanism is the impact ionization followed by an electron attachment. Other possible mechanisms include photoionization and electron detachment from negative ions. Electrons accelerate in the electric field impacting gas molecules and giving the birth to the new electrons. The development of an electron avalanche is shown in figure 1(a). As the strength of the electric field increases, the impact ionization also increases, which leads to the formation of the independent electron avalanches until the discharge gap gets filled with plasma. The plasma consists of positive ions left after the previous avalanches and electrons formed by the following avalanches. The expansion of the plasma channel is caused by the constant formation of new avalanches. The formation of a streamer is shown in figure 1(c). If the plasma channel reaches the cathode, the full breakdown over the discharge gap occurs (figure 1(e)). Otherwise, the partial discharges take place (figure 1(c) and (d)).

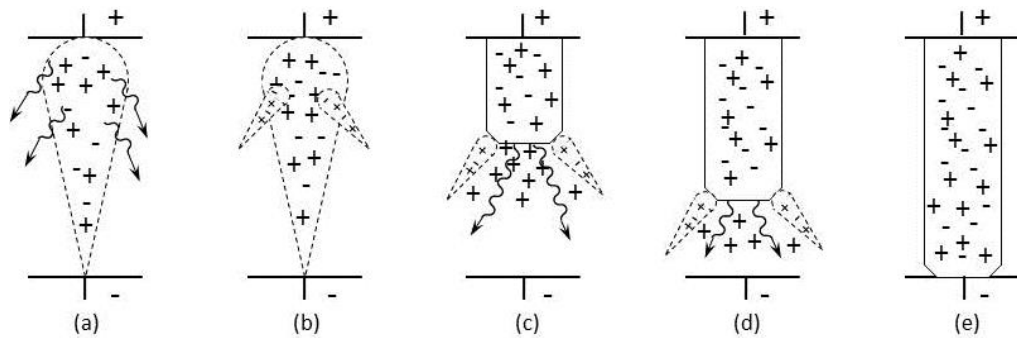


Figure 1. Breakdown stages: (a) – the grows of an electron avalanche; (b) – formation of secondary avalanches; (c), (d) – the grows of a positive streamer; (e) – full electric breakdown (Yurikov *et al*, 1982)

The photons created in the head of an electron avalanche lead to the formation of the secondary avalanches that grow in front of the streamer and from its sides. The avalanche development leads to the enhancement of the electric field in the discharge gap towards the cathode. The propagation velocity of a positive streamer is $10^8 - 10^9$ cm/s (Yurikov *et al*, 1982).

2.1.1.2. Breakdown in liquids

Unlike in gases, liquid dielectrics are characterized by a higher particle density and a higher value of electrical breakdown strength. The first feature implies that the electrons cannot accelerate in liquids due to a very short mean free path. The second feature means that the molecules in liquids have higher ionization potential than in gases. Despite there is no single breakdown mechanism, electric breakdown in liquids has much in common with the one in gas phase. Historically, there are two theories of the breakdown in liquids. Depending on experimental conditions, the breakdown mechanism is described in terms of a bubble theory or the electron avalanches are assumed to be formed directly in liquid.

The bubble theory

A bubble-initiated breakdown implies that the discharge track includes both gas and liquid phase: electric discharge initiation takes place in the gas phase with the following propagation into the liquid. The breakdown inception is always related to the existence or the formation of localized, low-density regions (micro-bubbles). This theory was originally created and developed by Bunkin and Bunkin (Bunkin *et al*, 1992). The authors entitled these regions as “bubbstons” and explained their existence in liquids by the presence of impurities spread across the entire solution volume. Second possible reason of the pre-existence of the bubbles is their formation due to the Joule heating of the conductive liquid due to the intense electric current flow. It should be noted that the first case is more probable for industrial liquids containing impurities i.e. dissolved gases, ion clusters, solid particles etc, whereas in the pure liquid dielectrics the gas micro-bubbles are likely formed onsite. Thus, the breakdown in the liquid is coupled to the existence or formation of low density regions and microbubbles (Kolb *et al*, 2008, Joshi *et al*, 2009, Lewis *et al*, 2003). After the micro-bubble nucleation through one of the described mechanisms, the

electrical breakdown initiation in the gas phase occurs. Its inception can be described by the breakdown mechanism in gases. Electrons are injected into the bubble localized near the electrode surface and accelerated by the electric field. When the streamer reaches the bubble wall (liquid/bubble interface), electric current increases and the charges get deposited on the bubble wall. The following propagation mechanism is explained by the constant formation of a gaseous cavity around the discharge channels, where electron avalanches take place. It should be noted that the heat release and bubble formation is only possible for the long voltage pulses ($> 1 \mu\text{s}$).

Direct ionization of liquid

This breakdown theory assumes that electrical discharges in liquid can be formed in the absence of the gas bubble formation and without thermal effects (Starikovskiy *et al*, 2011, Marinov *et al*, 2011), but through the direct ionization of the molecules and atoms in liquid. However, two strong arguments against this theory are usually put forward. The first one consists in the fact that the electron avalanche development in liquid is nearly negligible due to the large scattering cross sections of the electrons. It makes impossible for electrons to gain the high kinetic energy in such a dense media like liquid water. Second fact consists in inability of free electrons to exist in liquid because of the rapid solvation (1 ps, Laenen *et al*, 2000). However, despite all the contras, Starikovsky *et al*, 2011 have recently reported on the successful ionization of liquids (water) by the direct electron impact ionization. It became possible, when the electric field near the electrode was of one order of magnitude higher than the critical value of the breakdown. For realization of this mechanism the authors used very short voltage pulses and a rod high-voltage electrode ($U = 220 \text{ kV}$, pulse duration = 400 ps, electrode diameter at the tip = 100 μm).

2.1.1.3. Breakdown of solid dielectrics

Thermal processes play the most important role in breakdown of solid dielectrics unlike in gases, where the breakdown is mainly an electrical phenomenon. Displacement and active current flow through the dielectric exposed to the high electric field. The displacement current is caused by the polarization of the molecules in the dielectric. The active current is caused by the dielectric losses and increases as

the temperature of the dielectric increases until the breakdown takes place. The main feature of thermal breakdown of solid dielectrics is that it is a very slow process, since it develops with the heating of the dielectric in the electric field. Thermal breakdown is normally localized in the area of the poor heat dissipation. The threshold voltage for thermal breakdown depends on a number of factors: the repetition rate of the applied electric field, cooling conditions, thermal parameters of the dielectric material etc.

2.1.2. Electrode configurations

There are different electrode configurations used to generate electrical discharge in liquids (figure 2): point-to-point, point-to-plate, plate-to-plate, wire-cylinder geometries.

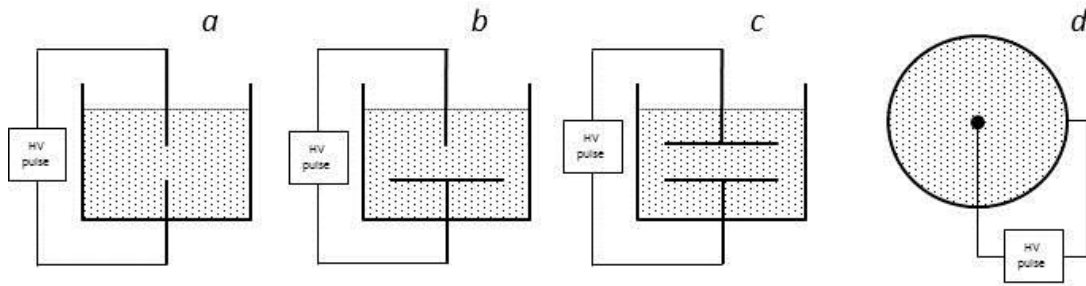


Figure 2. Basic electrode configurations: (a) – point-to-point, (b) – point-to-plate, (c) – plate-to-plate, (d) – wire-cylinder

The electrode configuration with a strongly asymmetric geometry – point-to-plate - is the most commonly used to generate electrical discharge through the direct ionization of liquids. The electrical discharge generated in such a way is a classic corona discharge. Point-to-plate geometry implies that the inter-electrode distance is much greater than the diameter of the point electrode. In such configurations, a point electrode represents a tip and is usually used as a high voltage electrode to concentrate the electric field for the liquid phase discharge. The electrical discharge initiation with point-to-plate geometry is determined by the amplitude of the applied voltage pulse and the curvature radius of the tip. Point-to-point and point-to-plate electrode

geometries are difficult to implement to the commercial applications because of the limited lifetime of the tip electrodes resulting from the destruction of the electrode tip. Besides, the electrical discharge generated in this way occupies a very small volume. The use of a wire-cylinder electrode configuration is another way to create the spatial non-uniformity of the electric field. In this case, the critical parameters of the electrical discharge generation are the radii of the wire and the cylinder (Lukes *et al*, 2009).

Symmetric electrode configuration, where both electrodes have the same shapes and are characterized by a large electrode area (plate-to-plate, figure 2(c), Hartmann *et al*, 2007) are used for the electrical discharges initiated through the DBD discharge (the nature of DBD is discussed in details in the next subchapter). In this case, one or two electrodes are covered with a dielectric layer. In general way, classical coronas have higher electron energy than the barrier discharges (Morrow *et al*, 1997, Braun *et al*, 1991, Babaeva *et al*, 2008, Dhali *et al*, 1987). Average electron energies in the streamer heads are 5-15 eV for coronas (Namihira *et al*, 2007) and 2-6 eV for DBDs. Electric field strength near the electrode tip in case of coronas is much higher than that on the electrode surface in case of DBDs, where the field is much more homogeneous. Random distribution of lots of simultaneous discharges distinguishes the DBD from corona discharges. The latter fact suggests that DBD would be commonly used for treatment of large surfaces and volumes, whereas coronas would be used for such cases where a small plasma volume is needed. Thus, plate-to-plate electrode geometry is widely used for such applications as surface treatment, water purification, ozone generation etc.

2.1.3. Factors influencing electrical discharge formation in liquid

2.1.3.1. Electrode coating

The role of dielectric material

The presence of a dielectric significantly affects the electrical discharge generation as it modifies the electric field configuration and acts as an electron supplier. In the DBD generation, electrode coating serves for two main purposes: (i)

to avoid the transition to spark discharge by preventing charge carrier flow through the surface; (ii) to enhance the electric field by storing surface charges and electron accumulation.

The partial discharge (e.g. corona) means that the discharge channels, formed on the surface of one electrode, do not reach the surface of the opposite electrode. However, under certain conditions, corona has a tendency to turn into the spark discharge. Spark discharges occur when streamer head reaches an opposite electrode building the conductive bridge. Electric current starts flowing between the electrodes and the discharge is no longer partial. Spark discharges are characterized by a very high energy (E_{pulse} up to a few kJ) and temperature (T up to a few thousand degrees) and lead to electrode erosion or complete destruction. Therefore, sparks should be avoided when generating electrical discharges for the water treatment purposes. Besides, the current build-up between the electrodes, when sparking, leads to substantial heating of the surrounding media. One of the ways to avoid the spark discharges is to reduce the amount of current by using a dielectric coating for an electrode – dielectric barrier. In other words, a dielectric layer is to protect an electrode from the rapid destruction and provide a long lifetime of an electrode surface.

Second purpose of a dielectric coating is that it allows of achieving the electric field enhancement needed for the electrical discharge inception. The charge cannot be accumulated on the conductive surface of the metal electrode as the constant electron leakage occurs when exposed to the electric field. Thus, an insulation of the metal electrode is required. Moreover, the use of a dielectric allows of increasing the capacitance in the discharge gap, which leads to the higher breakdown voltage required and more input energy stored in the system prior to the discharge. When the threshold electric field of the electrical discharge is achieved, the dielectric layer starts discharging yielding the electrical discharge. Two main parameters of a dielectric that determine its properties are: (i) dielectric strength and (ii) relative permittivity.

The dielectric strength characterizes the ability of a dielectric to withstand the high electric field without breaking down. For the DBD generation in liquid, the breakdown in solid phase (dielectric layer) must be prevented. For this purpose, the dielectric material must have a high value of the dielectric strength. Generally speaking, dielectric strength determines stability of a dielectric material, which determines its lifetime.

The relative permittivity (ϵ_r), also known in literature as dielectric constant, is responsible for the ability of a dielectric to polarize under the applied electric field. The higher the ϵ_r value, the more efficient is the polarization, the more energy will be stored by the dielectric layer. Due to the ability to be polarized, the dielectric layer can be considered as a capacitor when exposed to electric field. The relative permittivity determines the properties of this capacitor, therefore, it is the main characteristic of a dielectric material along with the dielectric strength. Among other important parameters of a dielectric material, there are dielectric resistivity, dielectric loss tangent etc. Since the influence of these parameters is not crucial in present study, their detailed consideration is omitted. The capacitance of the dielectric (C_d) layer is expressed by the equation:

$$C_d = \frac{\epsilon_r \epsilon_0 A}{d} \quad (1)$$

where ϵ_r is the relative permittivity of a dielectric, ϵ_0 is the vacuum permittivity, d is the thickness of the dielectric layer and A is its surface area.

The charge accumulated in the dielectric layer is proportional to the ratio ϵ_r/d . The linear dependence of the discharge current from this ratio was found by Gibalov *et al*, 1998, who tested the wide range of ϵ_r/d values. Varying the relative permittivity and thickness of a dielectric layer, one can adjust C_d suitable for the DBD formation. On the one hand, C_d must be high enough to store the amount of energy required for the discharge inception. On the other hand, a barrier with too high values of C_d requires unachievably high values of applied voltage, so a compromise must be made in search for the appropriate layer thickness and the dielectric material.

Depending on the desired C_d , one or two electrodes could be covered with dielectric (figure 3). In case of both electrodes covered, the total capacitance is theoretically doubled compared to the case in which one electrode is covered and another one is a bare metal, provided that the thickness is constant in both cases. However, the studies show (Meiners *et al*, 2010, Heuser *et al*, 1985) that in the situation when only one electrode is covered the transferred charge is much higher than that in case of both electrodes covered. The authors also concluded that the use of only one barrier increases the plasma efficiency.

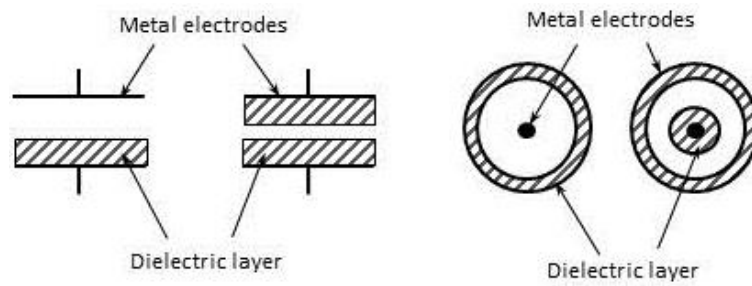


Figure 3. Location of the dielectric layer in discharge gap

Coating material

Dielectric material is one of the crucial parameters for the DBD generation. A successful dielectric material must possess the following properties:

- high value of the relative permittivity
- high value of the dielectric strength
- low value of the heat loss
- low value of the dielectric loss
- high value of the electrical resistivity
- good mechanical stability
- chemical inertness

Typical electrode coatings used for the DBD generation include glass, quartz, ceramics and polymers - materials of low heat loss, high dielectric strength and high dielectric constant. The influence of different dielectric materials on the DBD generation is a subject of investigation of many research groups (Hartmann *et al*, 2009, Lukes *et al*, 2009, Kogelschatz *et al*, 2010, Laroussi *et al*, 2002, Miclea *et al*, 2001, Piroi *et al*, 2010, Kostov *et al*, 2009, Akishev *et al*, 2003, Williamson *et al*, 2006).

The reactivity of DBD can be improved by increasing the permittivity of the dielectric layer. Therefore, the materials with relatively low values of permittivity such as quartz and glass are mainly used for low-energy applications of DBD (e.g. discharges in gas phase) such as ozone generation. The use of materials with extremely high permittivity (Sr-containing materials) leads to the very high values of electron density (up to 10^{19} cm^{-3}) and the generation of thermal plasmas (T values of

up to 10^4 K) (Meiners *et al*, 2010, Li *et al*, 2004, Li *et al*, 2007). Most of authors, dealing with the DBD generation directly in liquid, use different variations of ceramic coatings due to their optimal value of permittivity, compared to glass and quartz, and at the same time a high stability with regard to chemical reactions.

Table 1. Dielectric properties of some dielectric materials used for DBD generation

Coating material	ϵ_r	Reference	Dielectric strength (MV/m)
Quartz	4.22	Naz <i>et al</i> , 2012	-
Glass	8.63	-	9.8 – 13.8
Ceramics: almandine, corundum	10-12	Lukes <i>et al</i> , 2009, Sein <i>et al</i> , 2008	13.4
Sr-containing ceramics	120-300	Li <i>et al</i> , 2007, Li <i>et al</i> , 2004, Meiners <i>et al</i> , 2010	-

Alumina (Al_2O_3) is the most widely used material in the family of ceramics. It is made of the available raw materials and is relatively cheap giving the good opportunities for its industrial application. The key properties of alumina include (Accuratus):

- hard, wear-resistant
- excellent dielectric properties from low-frequency DC to GHz frequencies
- resistance to strong acid and alkali attack at elevated temperatures
- good thermal conductivity
- excellent size and shape capability
- high strength and stiffness
- availability in purity ranges from 94% to 99.5% (for the most demanding high temperature applications)

Alumina is usually found in the crystalline form - α -Al₂O₃, which properties are summarized in Table 2 (Cheng *et al*, 2006, Accuratus):

Table 2. Properties of α -Al₂O₃

Parameter	Unit	Value
ϵ_r (1 kHz)		9.8
Dielectric loss tangent (1 kHz)	$\times 10^{-4}$	2.5
Volume resistivity	Ω/cm	10^{14}
Insulation intensity	kV/mm	33 - 38
Density	g/cm^3	3.9
Coefficient of thermal expansion	$10^{-6}/\text{C}^\circ$	8.4
Resistance against bending	Mpa	300
Resistance against heat impact		Excellence
Resistance against mechanical impact		Excellence

Surface morphology

In many applications of DBD large electrode areas are required. However, it is more difficult to generate electrical discharge using large electrode areas (e.g. plate-to-plate and cylinder-cylinder electrode geometries) than using the small ones (e.g. point-to-plate electrode geometries) due to the homogeneous distribution of electric field. Therefore, for successful generation of electrical discharges spatial non-uniformities are required. In general way, the probability of the breakdown increases for the surfaces with imperfections, which are able to locally enhance the electric field. For the electrical discharge formation through DBD with large electrode areas, these imperfections are created artificially. A highly non-uniform electric field can be generated modifying the shape of metal electrodes or changing dielectric layer

microstructure. Some most common ways of the electrode surface modification are presented in figure 4.

It was shown that metal wire meshes could be used as electrodes (Wang *et al*, 2006, Qian *et al*, 2012, Tepper *et al*, 2002, Hensel *et al*, 2008). Meshed sheets can be wrapped around a cylinder (for wire-cylinder electrode configurations) or placed in a plate-parallel position (for plate-to-plate electrode geometries, figure 4(a)). The meshes are covered with a dielectric layer and electrical discharge develops at the mesh wires or on its nodal points. (Trunec *et al*, 1998) investigated the role of meshes in the DBD generation. Calculations have shown that meshes do not make any influence on the local enhancement of the electric field. However, the authors explained the role of the meshed electrodes in the discharge generation by the fact that the meshes have smaller resistance than flat electrodes.

Recent studies have reported on the role of surface morphology of the dielectric layer in DBD generation (Hensel *et al*, 2004, Lukes *et al*, 2009). The presence of small cavities (porosity) in the dielectric layer is supposed to facilitate the DBD initiation. For this, the electrode could be covered with a dielectric layer with porosity (figure 4(b)). The active role of porous material for DBD generation consists in the formation of micro-discharges inside the pores. Pores are assumed to serve as the points, where electromagnetic field is enhanced. If the pores of a big diameter are used ($>100\text{ }\mu\text{m}$), the DBD could be considered as a diaphragm or capillary discharge. Typical pore diameters for the DBD generation vary from 1 to $80\text{ }\mu\text{m}$. Thermal plasma-spray technology is used for porous ceramic deposition on the metal surfaces. The mechanism of pores functioning consists in the fact that the pores serve as conductive channels and thus provide the direct contact between metal electrode and the liquid.

Hong *et al*, 2010, Mahoney *et al*, 2010, Baerdemaeker *et al*, 2007, Jang *et al*, 2011, Sato *et al*, 1999 reported on the generation of electrical discharge through a hole in the dielectric layer placed in between the electrodes (figure 4(c)). Depending on the ratio of the dielectric thickness (d) to the radius of the hole (r), this type of discharge is attributed to the capillary ($d/(2r) \gg 1$) or diaphragm ($d/(2r) \simeq 0.1 - 1$) discharge which functioning differs from the operation of the classical DBD. In this case, the discharge generation takes place in the hole filled with the conductive liquid. The discharge is assumed to begin with the breakdown of a water bubble formed in the hole nucleated by the ohmic heating when the HV is applied across the electrodes.

Thus, the main advantage of both capillary and diaphragm discharge is that they are electrodeless discharges, which enables to avoid the electrode corrosion.

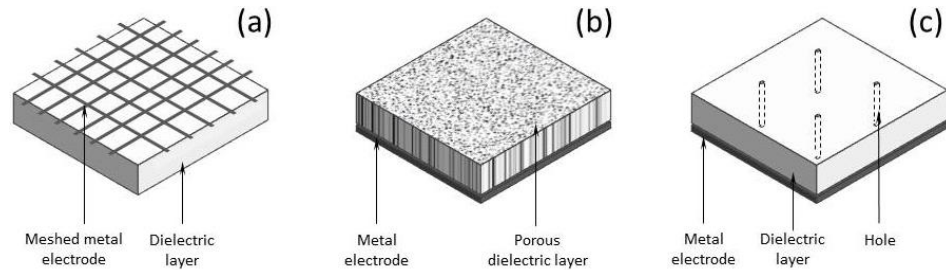


Figure 4. Different modifications of dielectric layer for electrical discharge generation: a – meshed metal electrode covered with dielectric layer; b – dielectric layer with open porosity; c –holes in the dielectric layer

2.1.3.2. Temporal characteristics of electric pulses

The electrical discharge ignition requires sudden application of a strong electric field. The efficiency of the energy transfer increases with the decrease of HV pulse width. Temporal characteristics of a HV pulse such as pulse rise time, pulse width and pulse decay time determine in significant way the costs of the power supply. The power supplies producing pulsed DC voltage create HV pulses with shorter rise and fall times than HV pulses of high-frequency AC power supplies.

The pulse width of the applied voltage determines many important discharge properties such as initiation time, propagation velocity, plasma temperature etc. Basically, two types of discharges are distinguished: short-pulse discharges with pulse rise-time from picoseconds to ten nanoseconds. To use the longer pulse rise times ($>10 \mu\text{s}$) is not reasonable due to the heat dissipation instead of the electric field enhancement.

Pulse rise time and pulse duration define the mechanism of the liquid discharge. Briefly, short HV pulses allow the direct ionization of liquid, where the electron impact mechanism is realized. The short rise time does not allow of the heat dissipation near the electrode and, thus, the surrounding liquid remains unheated. Starikovskiy *et al*, 2011 reported on the electrical breakdown directly in liquid using

HV pulses with picosecond rise time. The propagation velocity in their experiments reached the value of 5000 km/s. No bubble or void formation was observed.

Long HV pulses, on the contrary, do not allow of the electron acceleration in the extent as it is for the short HV pulses. In this case the time of the HV application is enough to heat the surrounding liquid media and nucleate a water bubble. The electric discharge therefore starts in this bubble with the following propagation into the liquid phase.

Thus, on the basis of the experimental results one may conclude that, firstly, the pulse width of the applied voltage directly determines the discharge mechanism and, therefore, all subsequent discharge phenomena. Secondly, the shorter electric pulse, the faster is the current dissipation in the discharge gap, the higher is the plasma density and, therefore, the more efficient use of the input power is expected.

2.1.3.3. Method of electrical excitation

Accumulated surface charges on the surface of a dielectric layer can be neutralized either by alternating current (AC) or by pulsed direct current (DC). Regarding to the electric current nature, there are two operation modes to drive electrical discharge: high-frequency AC and short-pulse DC.

The first type is characterized by a series of micro-discharges generated during one positive or negative half-period (figure 5(a)). The spikes on the current waveform correspond to the micro-discharges. In case of the short-pulse DC excitation (figure 5(b)), only one event of discharge takes place per one electric pulse. In case of the DC excitation, a higher discharge current and a higher initial electric field are achieved, which results in the higher plasma-chemical production. Analysis of experimental studies on the influence of the electric current nature allows to conclude that the short-pulse DC excitation produces higher power levels than high-frequency AC excitation. Williamson *et al*, 2006 explained the difference in AC and DC excitation by a different value of the threshold electric field of the breakdown. For the AC excitation, the voltage value needed for the electrical discharge inception is essentially the static breakdown voltage. For the DC excitation, where the pulse width is much shorter and the application of voltage occurs much faster, the breakdown voltage exceeds the static breakdown voltage. Thus, the electric field strength at the breakdown is higher for the DC excitation. Therefore electrical discharge inception and all subsequent

processes are characterized by a higher power using the short-pulse DC current rather than AC.

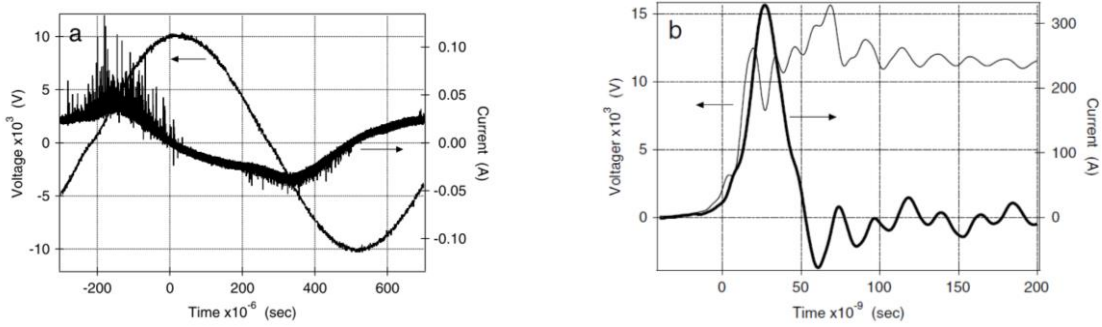


Figure 5. Example current and voltage waveforms of (a) 1 kHz AC and (b) 300 Hz short-pulse DC excitation of DBD (Williamson *et al*, 2006)

2.1.3.4. Polarity of electric pulses

The electrical discharge initiation can be triggered either at the cathode or at the anode surface. The effect of the polarity on the liquid phase discharges follows from the fact that ions and electrons are characterized by different values of mobility. Studies report on the following regularities: (i) threshold voltage of an electrical discharge is lower for the anode-initiated discharges; (ii) the polarity of a high-voltage electrode influences the discharge morphology and propagation velocity.

Computer simulations (Qian *et al*, 2006) and laboratory experiments (Joshi *et al*, 2003, Joshi *et al*, 2004) showed that the electric field required for the electrical discharge generation was lower for the discharges initiated on the anode surface. Therefore the threshold voltage is lower when a high-voltage electrode is biased positively rather than negatively (Korobeinikov *et al*, 2002, Jones *et al*, 1995). Thus, when a symmetrical electrode configuration is used, the breakdown is initiated easily at the anode.

The effect of the polarity on the electrical discharge initiation was extensively investigated by Qian *et al*, 2006. The authors proposed a microscopic model of the discharge initiation which takes into account a large difference in velocities of ions and electrons. In case of positive polarity, the electrons move very fast inside the bubble towards the anode surface. Positive ions move in the opposite direction, but

due to the incomparably lower velocity, the cations do not reach the bubble wall by the time the electrons reach the anode surface. Electric field inside the bubble is collapsed, whereas the electric field in the bulk is enhanced. In case of negative polarity, electrons are injected from the cathode and move very fast towards the bubble wall. The heavy and slow positive ions do not reach the cathode surface by the time the electrons are deposited on the bubble wall or penetrate into the solution bulk. Meanwhile, the electric field inside the bubble is enhanced compared to the electric field in the bulk. Thus, the charge density in the bubble neighborhood is smaller for the cathode-initiated discharge than that for the anode discharges.

Thus, depending on the polarity, the charges are supplied or needed to be supplied for the electrical discharge inception. Electrons either fall into the bubble from the surrounding solution i.e. are extracted from the bubble/liquid interface; or impact the bubble/liquid interface from inside the bubble. The different strength of the electric field for positive and negative polarities causes the dependence of threshold voltage, streamer morphology and propagation velocity from the sign of the applied current.

It should be noted that all considerations described above are attributed to the a priori formation of a bubble prior to the discharge inception, i.e. the bubble theory is assumed to be a dominant mechanism. In case of the direct electron impact ionization of liquid, one should not expect the influence of the polarity on the electrical discharge initiation as the stochastic phenomena (electron avalanches) take place.

2.1.3.5. Solution conductivity

The effect of the solution conductivity was shown by many authors to have a large influence on the electrical discharge initiation. In liquids, the discharge current is transferred by the solvated ions, but not by the free electrons as it is in metals, for instance. The solvated ions compensate the space charge electric field on the growing streamer head, thus strongly influencing electrical discharge propagation. Distilled water has an electric conductivity of $0.06 \mu\text{S/cm}$ (25°C) and a relative dielectric constant of 78.4 (25°C). The high resistivity of the distilled water allows of using it as an insulator. The advantage of such application is that its insulating and dielectric

properties are easily variable. The addition of ionic compounds such as salts, acids or alkalis into water changes its conducting properties.

The aqueous solution may act either as a capacitor or as a resistor depending on the solution conductivity. When the pure water is used, the resistivity of the water layer is high, and the gap between electrodes acts as a capacitor. The input power is discharged through the surrounding media of a high resistivity. The displacement current in this case is larger than the conduction current and the capacitor is not fully discharged. It results either in the low discharge power or in no discharge initiation. In order to facilitate the electrical discharge, the conductivity of water is increased. It results in the conduction current larger than the displacement current and electrical discharge occurs. Thus, solution conductivity directly determines the initiation of electrical discharge.

Another issue, related to the influence of solution conductivity, concerns the threshold voltage of the electrical discharge. Results found in literature show controversial results. *Sunka et al*, 2001 demonstrated that solution conductivity has no impact on the threshold voltage. *Shih et al*, 2010 required the higher voltage values for higher solution conductivity to initiate electrical discharge. *Zhu et al*, 2009, on the contrary, found that the electrical discharge initiation voltage decreases with increase of solution conductivity. The increase of solution conductivity leads to the higher current flow and more intense ohmic heating facilitating vaporization processes. Since electrical discharge initiation is preceded by the water vaporization as discussed above, the increase in solution conductivity will more likely facilitate electrical discharge formation and, therefore, decrease the threshold voltage.

Investigating the influence of solution conductivity, all authors agree that the increase in solution conductivity leads to the higher power and plasma densities, higher plasma temperature and more intense UV radiation during the electrical discharge. However, at the same time, the short streamer length was observed in case of high solution conductivities and explained by a large discharge current flow due to the faster compensation of the space charge electric fields on the head of streamers. The shorter streamer length, i.e. the less plasma-water contact, results in the lower probability of the plasma-chemical reactions.

2.1.3.6. Electric field strength

Liquid phase discharges require large electric fields to create the pre-existing current for heating and to sustain discharge propagation (Shih *et al*, 2010). Electric field required for the electrical discharge inception in liquids are much higher ($\sim 10^9$ V/m) than the one in gas phase ($\sim 10^6$ V/m). Liquid breakdown would take place when the space field at a certain place in the discharge gap becomes equal to the external electric field at the same location. Therefore, the main parameter determining almost all electrical discharge properties is the electric field strength. The significance of this parameter is reported in every study that deals with electrical discharge generation. The averaged electric field strength (AEFS) is defined by the distance between electrodes and the applied voltage. The correlation between these values for symmetric plate-to-plate electrode configuration gives:

$$E = U/d \quad , \quad (2)$$

where E is the averaged electric field strength (V/m), d is the distance between electrodes (m), U is the magnitude of the applied voltage (V). From this equation it could be concluded that the applied voltage is not the most important parameter, but the averaged applied electric field. However, in most of studies the influence of the electric field is replaced by the influence of the applied voltage. The reason to that is because the construction of the discharge chambers does not always allow the change of the distance between electrodes and, therefore, d value is assumed to be constant. In such cases, the only possible way to enhance the AEFS is to increase the applied voltage. For those cases when the inter-electrode distance is easily variable, there is no need to use high values of voltage as the same value of AEFS could be reached by the shortening the inter-electrode distance at the constant voltage.

The shorter inter-electrode distance and the higher applied voltage will result in the higher AEFS and the denser plasma formation. However, even when the applied voltage is low, the spark discharge may occur if the inter-electrode distance is too short. On the other hand, the large discharge gaps are characterized by the high divergent fields at the electrodes and low averaged electric fields in the bulk. Homogeneous electric field is difficult to obtain for long inter-electrode distances (d

is in the range of cm), therefore, the generation of electrical discharge with large discharge gaps is complicated.

The calculation of the electric field strength becomes more complicated for asymmetric electrode configurations, as the electric field at the pin electrode instead of the AEFS across the gap should be considered. The AEFS is not relevant for sharp pins and long gaps because the electric field for the plasma initiation is concentrated around the pin and defined by:

$$E \sim U/r \quad (3)$$

where E is the electric field near the electrode tip (V/m), U is the applied voltage and r is the radius of curvature of the tip (m). From this equation, a lower applied voltage is needed to generate corona discharge using sharper needles as in this case a higher electric field will be achieved.

2.1.4. Effects induced by underwater electrical discharges

The generation of underwater electrical discharges causes the formation of a number of physical and chemical effects. Among them, thermal effects and UV/Visible light emissions play a significant role. Besides, electrical discharges cause the formation of pressure shock waves. The input power is also spent on the formation of the water steam, dissociation and ionization. The simultaneous induction of both physical effects and chemical reactions by electrical discharges is the main advantage in terms of the application for water treatment.

2.1.4.1. Physical effects

Electrical discharges are a source of intense UV radiation, which is of a great interest as the UV leads to photochemical reactions (Lukes *et al*, 2008). The effect of the UV results either in the direct photolysis of the organic compounds or in the formation of highly reactive species which then attack organics. The efficiency of the UV radiation increases with the plasma power increase, thus, in general, more

energetic arc and spark discharges are considered to be more efficient sources of UV than corona and streamer discharges.

The non-thermal plasma (NTP) produced by corona and streamer discharges implies the formation of plasma without heating of the bulk volume. Although, the temperature inside the discharge channels could be very high the localized nature and small volume of the discharge channels enable to support the thermal energy in the small volume and at the same time sustain moderate (room) temperature of the bulk solution. Thus, unlike in thermal plasmas, the use of NTP avoids the large thermal losses and prevents the damage of the nearby surfaces such as reactor walls, electrodes, reactor parts. Pyrolysis of organic compounds by NTP is possible, but since the thermal regions are characterized by a very small volume, the efficiency of the thermal decomposition is low. The greatest contribution of thermal effects consists in thermal dissociation of water molecules with the formation of primary reactive species.

The high-amplitude ultrasound waves could be generated by an electrical discharge. The rapid energy expansion in the radial direction follows the electrical discharge generation, which produces the shock waves in the surrounding liquid phase (Stelmashuk *et al*, 2012). However, an electrical discharge is not an efficient source of the shock waves. (Naugol'nykh *et al*, 1974) reported that only 8% of the total input power spends on the shock waves formation by underwater electrical discharges.

2.1.4.2. Chemical reactions

The high chemical efficiency is the main advantage of underwater electrical discharges. Electrons in the plasma discharge zone could reach the energy of up to 10 eV. The energetic electrons along with the energetic photons trigger many chemical processes. The mechanism of discharge generation in liquid phase, as discussed before, includes the formation of the gas phase, where the electrical discharge inception occurs. The chemical activity of underwater electrical discharges, thus, is related to the chemical reactions in the water steam filling the bubble (reactive species being in the plasma state) and subsequent reactions in the bulk solution.

The majority of experimental data report that the electrical breakdown in a water bubble yields the formation of such species as hydroxyl, hydrogen and oxygen radicals. The water dissociation by the non-elastic electron impact of the water

molecules is considered as the main mechanism of the radical formation. The primary species are highly reactive, but short-lived, therefore their monitoring utilizes high-speed and high-sensitive techniques such as emission spectrometry.

The water bubbles rapidly collapse and the high-temperature zone (discharge channels) decays in time. It is followed by the formation of a variety of species in a cooler zone surrounding the discharge channels. These species include hydrogen peroxide, ozone, molecular oxygen, hydrogen etc, which are characterized by a higher stability than the reactive radicals and can diffuse into the bulk solution. It makes possible to detect and quantify the secondary species by the chemical methods. The formation of hydrogen peroxide (H_2O_2) is of a special significance. The fact that it could act as a reductant ($E_{\text{red}}^0 = -0.7 \text{ V}$) and a relatively powerful oxidant ($E_{\text{ox}}^0 = 1.77 \text{ V}$), H_2O_2 plays an important role in the destruction of organic molecules.

Electrons impacting the bubble/liquid interface become solvated. The probability of the electron solvation, however, is low due to the low possibility of the occurrence of electron in the liquid phase (Buxton *et al*, 2006). There are very few studies reporting on the successful detection of the \bar{e}_{aq} . The significance of the \bar{e}_{aq} consists in its ability to form superoxide radical ($\text{O}_2^{\cdot-}$), which could act as an oxidizing or reducing agent dependent on the conditions. Other studies report on the formation of $\text{O}_2^{\cdot-}$ through the reaction of molecular oxygen and hydrogen radicals (Sahni *et al*, 2006).

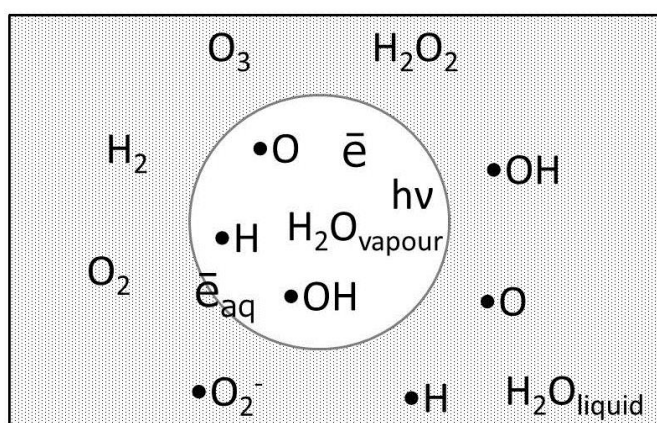


Figure 6. Reactive species formed by underwater electrical discharge

2.2. Experimental

2.2.1. Overall view of experimental setup

The overall view of experimental setup used for the experiments described in the present chapter is presented in figure 7. Generally, the equipment could be divided into two parts: the high-voltage equipment (figure 7(a)) and the circulation system (figure 7(b)).

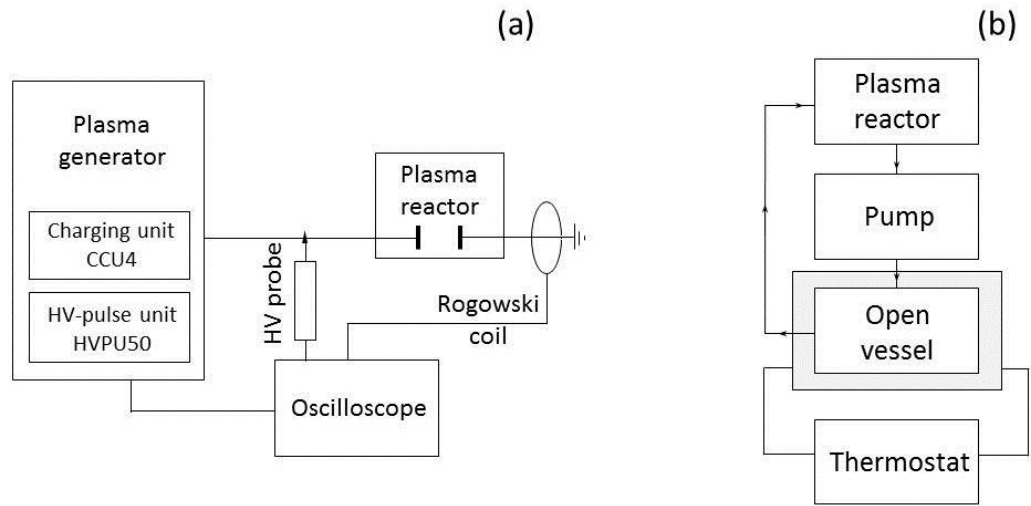


Figure 7. Overall view of experimental setup: (a) the high-voltage equipment; (b) – circulation system

2.2.1.1. High-voltage equipment

Plasma generator

The plasma generator used in the present study was developed by PPT Puls-Plasmatechnik GmbH (Dortmund, Germany). It consists of two main components: a HV-Capacitor (Charging Unit CCU4) and a HV-Pulse-Unit HVPU50. The HV-pulse unit contains a capacitor with a loading capacity of 500 nF. The charging unit is used to produce an initial voltage pulse with a relatively long pulse rise-time and low voltage amplitude (up to 3.2 kV); the electric pulse then is shortened (pulse rise time up to 800 ns) and transformed by the HV pulse unit yielding a maximal voltage of 50

kV. High-voltage pulses of the direct current (DC) have sinusoidal form with maximal pulse repetition rate of 200 Hz.

Plasma reactor

The generation of electrical discharge in the present study was carried out in a plasma reactor. Its cross section is shown in figure 8. The plasma reactor consists of a quartz cylinder and two Teflon[®] electrode holders. Two round titanium electrodes with a radius of 1 cm and a thickness of 0.5 cm are placed parallel. One of the electrodes is covered with an electrode coating and connected to the HV-power supply, another electrode is grounded. From the back side either electrode is connected to a screw to provide electrical contacts with the power supply or with the ground. The stainless steel screws enable the electrode distance variations from 1.04 to 3.24 cm. The total volume of the plasma reactor could be varied from 20 to 45 mL.

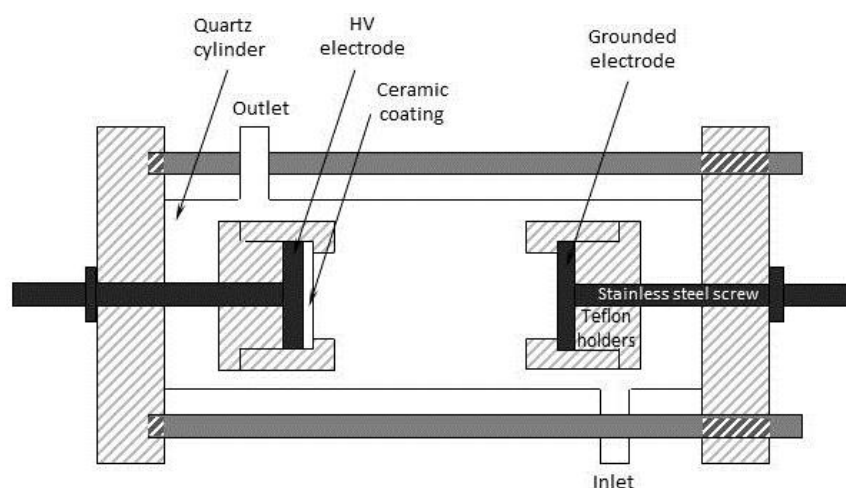


Figure 8. Plasma reactor

In order to minimize the inductance of the system, the HV cable connecting the plasma generator and the plasma reactor should be as short as possible. However, its length is determined by the relative location of the plasma reactor and the plasma generator. In the present study, the length of this cable was 1 m.

Oscilloscope measurements

The characteristics of the voltage and current across the electrodes were measured by a two channel oscilloscope (Tektronix TDS 2012C, USA) which was triggered by the HV pulse unit. A high voltage probe PVM-1 (1000:1 attenuation, North Star High Voltage, USA) was used for voltage measurements and a Rogowski current transducer (2.00 mV/A, PEM Ltd., UK) was used for current measurements. The characteristics of electric pulses were determined as follows:

- The electric pulse amplitude is the difference between the initial and the maximal values of the electric pulse
- The pulse rise time was determined as the time during which the signal increases from 5 to 95 % of the amplitude
- The pulse fall time was determined as the time during which the signal decrease from 95 to 5 % of the amplitude
- The pulse duration was determined as the full width at half maximum of the electric pulse
- The pulse energy was calculated by integrating the transient power curve by time

2.2.1.2. Circulation system

In the present study, the plasma reactor was incorporated into a circulation system (figure 7(b)), which served for two main purposes. Firstly, since the electrical discharge generation is accompanied by intense thermal emissions, the cooling of the aqueous solution is required in order to keep the constant solution temperature. When the pulse repetition rate is high enough (≥ 10 Hz), the solution is heated by $\sim 1^\circ\text{C}/\text{min}$. Thus, at the long operation the thermal effects may influence significantly the physical and chemical properties of the solution. Besides, the increased temperature might cause the destruction of the reactor parts as well as the electrode coatings. Secondly, since the mixing of the solution is required. The active volume of plasma reactor which is exposed to electrical discharge is varied from 2.1 ml to 5.1 mL (depending on d), while the total volume is 45 mL. For the degradation of organic compounds, the larger solution volumes are required.

Solution from the plasma reactor is transported by a magnetic drive pump (Iwaki Magnet Pump, model MD-30FX) to a double-walled open flask. The flask is connected to a thermostat (Huber Kaeltemaschinenbau GmbH, Offenburg, Germany) which supports the solution temperature of 20 °C. The solution from the flask is transported back into the plasma reactor. The maximal volume of the water cycle is 270 mL.

Electrical discharges were generated in aqueous solutions with different values of solution conductivity. It was adjusted by sodium sulfate and measured by a conductometer 712 Metrohm (Model 1.712.0010, Herisau, Switzerland).

2.2.2. Electrode coatings

Three ceramic coatings with different composition and thickness were examined in this study with respect to electrical discharge formation. First electrode coating – Grey Alumina Coating of 50 μm thick (GAC50) - was produced by Medicoat AG (Maegenwil, Switzerland) using DC arc plasma-spray technique. The coating represented a mixture of α - and γ - Al_2O_3 . Second electrode coating – Grey Alumina Coating of 250 μm thick (GAC250) - was produced from the mixture of α - and γ - Al_2O_3 by TU Ilmenau, Germany using inductively coupled plasma-spray technique. Third electrode coating – White Alumina Coating of 500 μm thick (WAC500) - was made of Rubalit 708 HP material (CeramTec GmbH, Germany). The sintered layer consists of almost pure (96 %) α - Al_2O_3 with no porosity.

2.2.3. X-ray diffraction spectra and Scanning electron microscope imaging

Phase identification of all three coatings was carried out using X-ray diffraction (XRD) method with CuK_α radiation. The XRD spectra were measured by an X-ray diffractometer (D8 Advance, Bruker AXS GmbH, Germany) from 5° to 90° 2-theta angular range. The morphology of coating surfaces was characterized using an environmental scanning electron microscope (ESEM, Quanta 400 FEG, FEI Company, USA).

2.2.4. Chemical methods

2.2.4.1. Determination of hydrogen peroxide

The generation of underwater electrical discharge is accompanied by the formation of hydrogen peroxide (H_2O_2). In the present study, the change of H_2O_2 concentration was used as an indicator of electrical discharge generation. Due to its relatively high stability, H_2O_2 can be found in the solution long after its formation (the lifetime is up to a few days). In the present study, H_2O_2 was quantified colorimetrically using Allen's method (Allen *et al.*, 1952). The fundamental reaction in this method is redox reaction between H_2O_2 and I^- :



The oxidation of the iodide ion by H_2O_2 to form molecular iodine (equation 4) is followed by the formation of triiodide ion in the excess of iodide ions (equation 5). The formed triiodide ion (yellow color) is measured colorimetrically. Its amount is equal to the amount of the formed H_2O_2 . The concentration of I_3^- was calculated according to the Lambert-Beer's Law:

$$A = \varepsilon \cdot l \cdot C, \quad (6)$$

where A is the absorbance (a.u.), ε is the molar extinction coefficient ($\text{L}/(\text{mol} \cdot \text{cm})$), l is the length of the light path (cm), C is the concentration (mol/L).

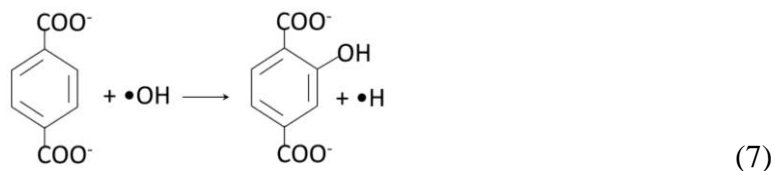
Iodide anion was formed onsite through the reaction between reagents A and B. The reagent A: 1 g of NaOH, 33 g of KI, 0.1 g of $(\text{NH}_4)_6\text{Mo}_7\text{O}_{24} \cdot 4\text{H}_2\text{O}$ in 500 ml of distilled water. The reagent B: 10 g of KHP in 500 ml of distilled water. 1 ml of the reagent A, 1 ml of the reagent B and 1 ml of the sample solution containing H_2O_2 were mixed and transported into the quartz cuvette. The absorbance was measured at 350 nm with a Lambda 25 UV-VIS spectrophotometer (Perkin Elmer, LAS GmbH). The sampling was carried out after 5, 10, 15, 20, 30, 40, 50, 60 and 90 min of the operation.

2.2.4.2. Determination of hydroxyl radical

Hydroxyl radical (OH^\bullet) is another reactive specie, along with hydrogen peroxide, which is formed in the aqueous solution exposed to electrical discharges. The lifetime of OH^\bullet (up to a few ms) is much shorter than that of H_2O_2 , therefore, for its quantification a direct method described by Mason *et al*, 1994 was employed.

Quantification of hydroxyl radicals was carried out using disodium salt of terephthalic acid (NaTA) (Saran *et al*, 1999). NaTA (non-fluorescent) is known as an OH^\bullet scavenger; it reacts with OH^\bullet to form 2-hydroxyterephthalic acid (HTA, fluorescent) according to equation 7. The concentration of HTA was determined by its fluorescence, which yield is proportional to the OH^\bullet concentration in the solution in the excess of NaTA.

The HTA fluorescence yield was measured with an RF 5301 PC spectrofluorophotometer (Shimadzu, Germany). The excitation wavelength was set at 315 nm and the fluorescence spectra of the solution were collected in the range of 320 nm - 500 nm. The peak intensity was quantified for each solution at the emission wavelength of 425 nm.



Mason *et al*, 1994 reported on the reduced yield (up to 35%) of this reaction in solutions with considerable content of O_2 . Since all solutions investigated in the present work were exposed to the air, one cannot precisely calculate the amount of OH^\bullet by this method. However, the quantification of HTA enables to estimate the increase or decrease of OH^\bullet concentration, thus, along with H_2O_2 , serving as a parameter to estimate the chemical efficiency of electrical discharge.

2.3. Results and discussions

2.3.1. Equivalent electric circuit of the discharge gap

Equivalent electric circuit of the plasma discharge gap used in this study is presented in figure 9.

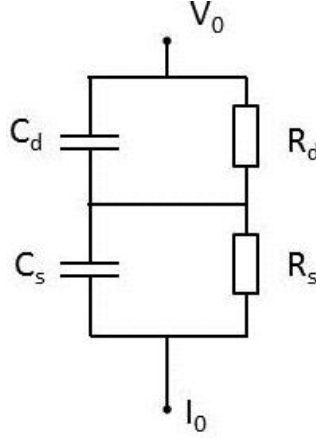


Figure 9. Equivalent electric circuit of the discharge gap

In figure 9, I_0 is the total current and V_0 is the voltage across the electrodes; C_d and R_d are, respectively, the capacity and resistivity of the ceramic layer covering the high-voltage electrode; C_s and R_s are, respectively, the capacity and resistivity of the aqueous solution in which the electrodes are submerged. The successful generation of electrical discharge implies the breakdown on the discharge gap simultaneously with no breakdown of the electrode coating. For this, the properties of the aqueous solution and electrode coating should be investigated in order to find the optimal values of C_d , R_d , C_s and R_s . Electrode coatings with different composition and thickness were tested in order to adjust C_d and R_d values, while the solution properties (C_s and R_s) were kept constant. On the contrary, C_d and R_d were kept constant when adjusting the C_s and R_s values.

2.3.2. Factors influencing electrical discharge inception

2.3.2.1. Electrode coatings

In the present work ceramics was chosen as a coating material for the generation of electrical discharge in aqueous solution with large-area electrodes. The present chapter describes the influence of coating parameters – composition, thickness and surface structure – on the electrical discharge inception. In this chapter the capacity and resistivity of the dielectric layer were varied, whereas the capacity and resistivity of the aqueous solution were kept constant.

The electrical discharge generation was mainly monitored visually. The visual control was also accompanied by the current and voltage waveform analysis and the formation of reactive species (hydroxyl radical (OH^\bullet) and hydrogen peroxide (H_2O_2)). The properties of the tested electrode coatings are summarized in table 3. GAC50 is an electrode coating made of a mixture of α - and γ - Al_2O_3 with the thickness of 50 μm and provided with porosity. GAC250 is an electrode coating with the same characteristics as GAC50, but with a bigger thickness (250 μm). WAC500 is an electrode coating made of a pure α - Al_2O_3 (96%) of 500 μm thick without porosity.

Table 3. Properties of electrode coatings

Coating	Producer	Composition	Thickness (μm)	Porosity
GAC50	Medicoat AG	Mixture of α - and γ - Al_2O_3	50	Yes
GAC250	TU Ilmenau	Mixture of α - and γ - Al_2O_3	250	Yes
WAC500	Ceram Tec GmbH	Pure α - Al_2O_3	500	No

Electrode coating GAC50

No electrical discharge generation under any conditions was observed using grey alumina with the thickness of 50 μm as a coating material (GAC50). Increase of the spatially averaged electric field strength (AEFS) up to 18 kV/cm ($d = 1.5$ cm, $U =$

27 kV) resulted in the arc discharge. Therefore, this value of the AEFS was found to be a limit for the given coating, above which the full breakdown of the electrode gap occurs. The change of solution conductivity that was ranged from 100 $\mu\text{S}/\text{cm}$ to 2 mS/cm did not make any positive influence on the electrical discharge generation.

The arc discharges have led to the coating destruction as lots of craters and fractures appeared on the surface of GAC50 exposed to high-voltage pulses. Scanning electron microscope images of the coating surface with length scales of 10 and 500 μm are presented in figure 10. The surface deterioration evidences the lack of mechanical stability of GAC50. The craters were assumed to be caused by the breakdown in the ceramic layer, which has led to the surface destruction.

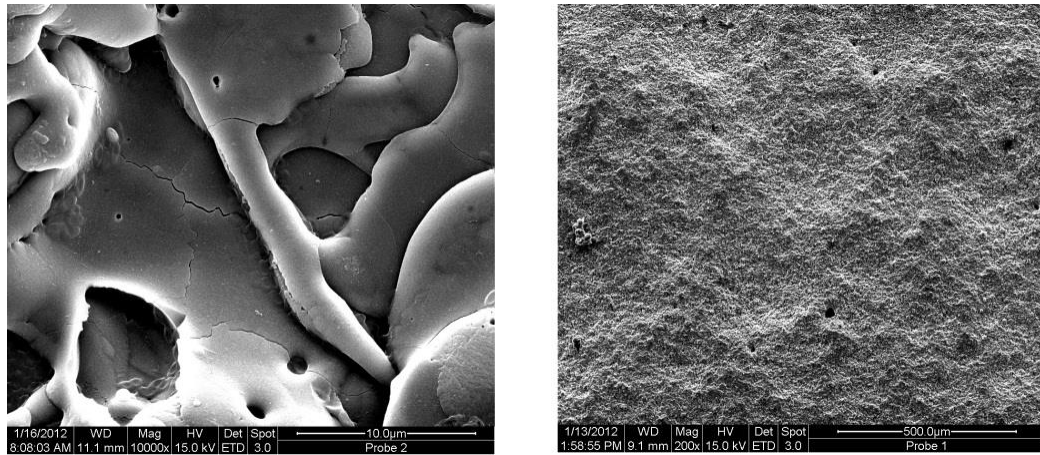


Figure 10. Scanning electron microscope images of GAC50 (conditions are listed in the Experimental part)

Significant amount of H_2O_2 was formed in the aqueous solution using GAC50 and measured using chemical methods. Both processes – electrical discharge and electrolysis – might lead to the H_2O_2 formation. Since the electrical discharge generation was not observed, it was assumed that the main source of H_2O_2 were electrochemical reactions. H_2O_2 formation results from the dimerization of hydroxyl radical (equation 9) formed by the anodic oxidation (equation 8):



The change of H_2O_2 concentration with time is shown in figure 11. H_2O_2 was produced by GAC50 in amount of $80\text{ }\mu\text{M}$ after 90 min of applying high voltage pulses ($U = 26\text{ kV}$, $d = 1.5\text{ cm}$, $\sigma = 1\text{ mS/cm}$). The most rapid increase of the concentration occurs during the first 50 minutes. Small change of the H_2O_2 concentration during the last forty minutes of operation suggests that the stationary concentration is achieved and the rate of H_2O_2 formation is equal to the rate of its decomposition.

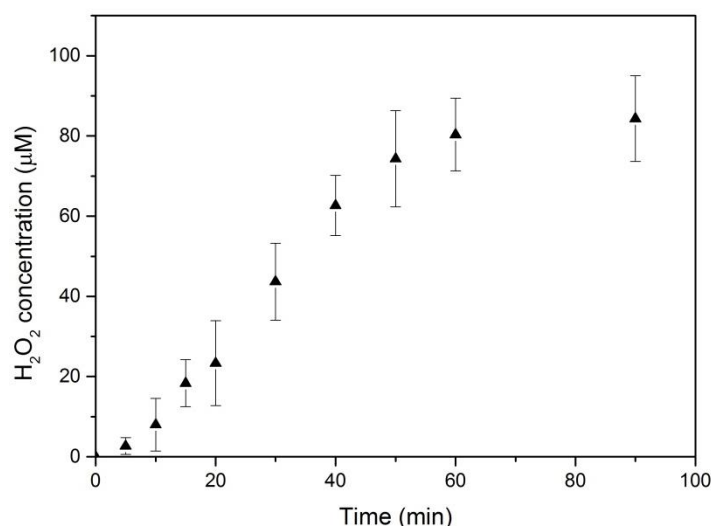


Figure 11. Formation of H_2O_2 with GAC50

The waveforms of the current and voltage across the discharge gap are presented in figure 12 for solution conductivity of 2 mS/cm . Peak of the current waveform is shifted with respect to the peak of voltage waveform indicating the presence of a capacitance in the electric circuit. The peak on the current waveform is essentially the displacement current and, as it is clearly seen from the figure, it is not followed by the discharge current. Despite the ceramic layer of GAC50 acts as a capacitance, its resistance is not high enough to insulate the metal surface and avoid the leakage of electrons, which is evidenced by electrolysis. Thus, the reason of electrolysis in case of GAC50 is poor insulating properties of the ceramic layer. The low resistance of GAC50 can be explained by a number of factors including porous surface structure, low density, amorphous structure of $\gamma\text{-Al}_2\text{O}_3$, insufficient thickness of the layer.

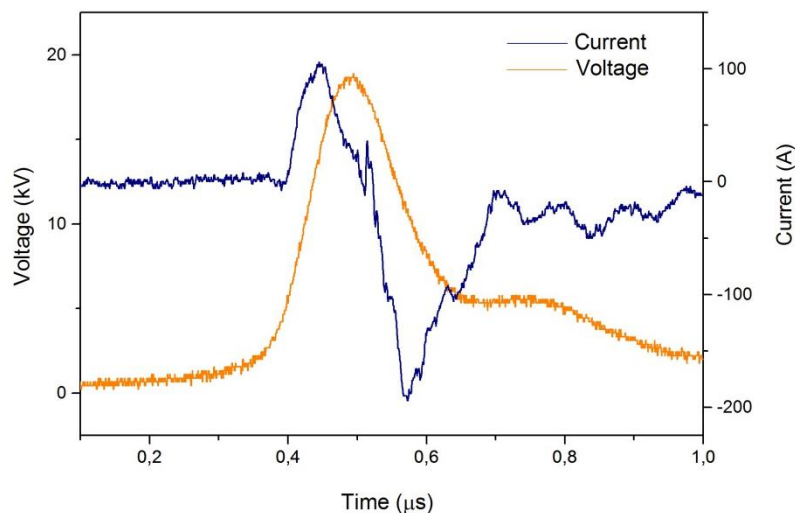


Figure 12. Current (blue) and voltage (yellow) waveforms for GAC50

Because of the poor mechanical stability, GAC50 is unable of protecting the metal electrode from destruction and corrosion. Poor insulating properties of GAC50 make it unable of acting as a barrier for electrons. Thus, the input energy in case of GAC50 is spent on the electrochemical processes (i.e. electrolysis) instead of the electrical discharge generation.

Electrode coating GAC250

In order to check the effect of the coating thickness on its ability of electrical discharge generation, a thicker electrode coating with the same composition as GAC50 was used. The new coating – GAC250 – was five times thicker (250 μm) than the previous one.

With this coating, electrical discharge was observed for the wide range of electric field values. The threshold value of AEFS for the electrical discharge inception was found to be 7.3 kV/cm ($U = 22$ kV, $d = 3$ cm), whereas the upper limit was found to be 20 kV/cm ($U = 30$ kV, $d = 1.5$ cm). Further decrease of the electrode distance and/or increase of the voltage pulse amplitude has led to the formation of arc discharges. Change of the solution conductivity that was ranged from 100 $\mu\text{S}/\text{cm}$ to 2 mS/cm did not make any influence on the threshold value of AEFS for electrical discharge generation. Solution conductivity only influenced the brightness and the shape of the electrical discharges.

The arc discharges did not lead to the formation of craters on the surface of GAC250, however, GAC250 was fractured after exposure to the high-voltage pulses

(figure 13). It suggests that the breakdown of the coating did not take place, however, the mechanical stability of the coating was not significantly improved by the increase of its thickness.

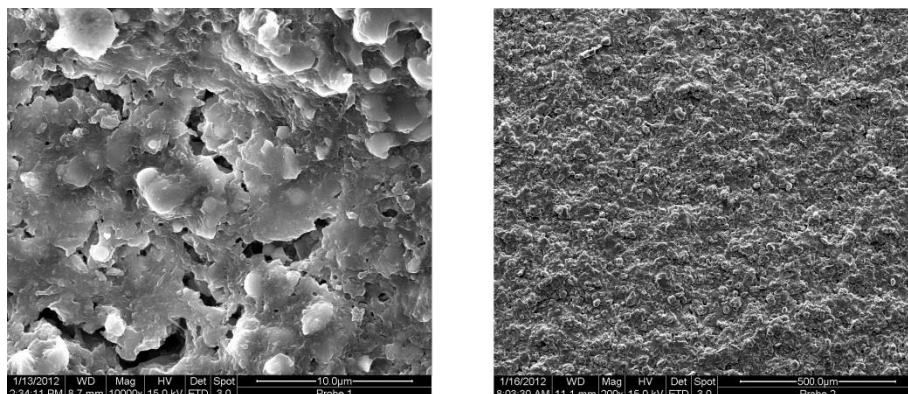


Figure 13. Scanning electron microscope images of GAC250 (conditions are listed in the Experimental part)

The waveforms of the current and voltage across the discharge gap are shown in figure 14 for solution conductivity of 2 mS/cm. Differences in current and voltage waveforms for GAC250 were observed in comparison with the ones for GAC50. The first maximum of the current waveform was observed at 460 ns as it was in case of GAC50 indicating the charging of the capacitor. The following current decrease simultaneously with the voltage increase corresponds to the fully charged capacitor. As the voltage drops down, the discharge current starts flowing. The second current maximum (520 ns) is related to the electrical discharge (i.e. discharge current). The small amplitude of the discharge current, however, suggests that the discharge is very weak. The increase of the discharge brightness and at the same time the increase of the second maximum was observed when the applied voltage was increased. Thus, unlike in GAC50, GAC250 was able of the electrical discharge generation which was visually observed and confirmed by the current and voltage waveforms.

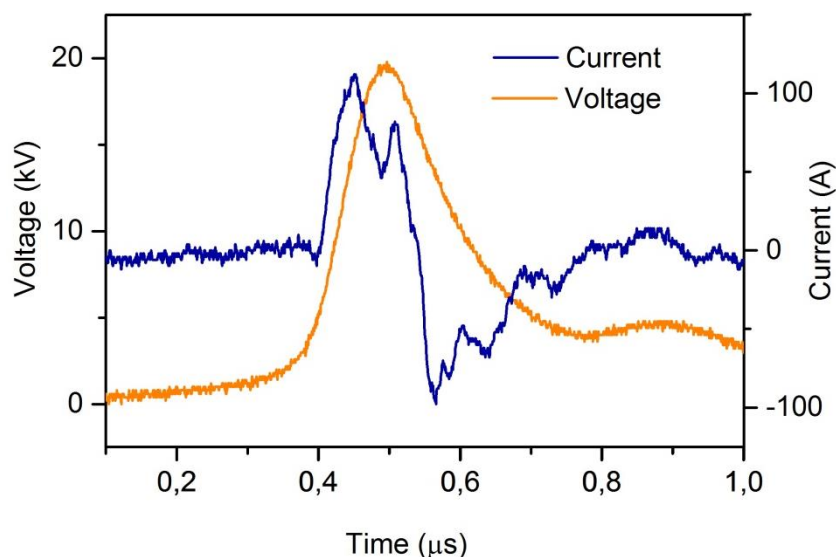


Figure 14. Current (blue) and voltage (yellow) waveforms for GAC250

The presence of two processes – electrical discharge and electrolysis – obstructs the description of the phenomena. In order to find out, whether or not electrolysis occurs simultaneously with the electrical discharge generation using GAC250, H_2O_2 formation was measured with and without electrical discharge. For the experiments in the absence of electrical discharge, the voltage was set at the value slightly below the threshold for the electrical discharge inception ($U = 20 \text{ kV}$, $d = 3 \text{ cm}$). With no electrical discharge, the concentration of H_2O_2 was below the detection limit of the used technique ($C_{\text{H}_2\text{O}_2} < 0.01 \text{ } \mu\text{M}$ after 90 min of operation). This experiment indicates the negligible part of electrolysis in the electrical discharge generation using GAC250. The concentration of H_2O_2 on the edge of the detection limit was measured in the presence of electrical discharge ($C_{\text{H}_2\text{O}_2} = 1 \text{ } \mu\text{M}$ after 90 min of operation, figure 15(a)). It indicates the low chemical activity of the electrical discharge using GAC250. The formation of H_2O_2 during the electrical discharge proceeds through the recombination of hydroxyl radical (OH^\bullet) according to equation 9. However, unlike in the electrochemical formation of OH^\bullet by oxidation of hydroxyl anions on the anode surface, the formation of OH^\bullet by underwater electrical discharge is due to the plasma-chemical reactions. The mechanism of the plasma-chemical splitting of water molecules will be discussed in the next chapter.

Thus, the electrical discharge generation could also be monitored by measuring the formation of OH^\bullet . The change of OH^\bullet concentration with and without of electrical discharge is shown in figure 15(b). The black squares correspond to the

OH^\bullet formation in the absence of discharge. The grey circles correspond to the OH^\bullet formation when electrical discharge takes place. The fact that electrolysis does not take place in using GAC250 is evidenced by the negligibly low concentration of OH^\bullet in the case of absence of electrical discharge ($C_{\text{HTA}} < 2 \text{ nM}$ after 90 min of operation). In the presence of electrical discharge the amount of OH^\bullet increased significantly ($C_{\text{HTA}} = 22 \text{ nM}$ after 60 min of applying high voltage). This result indicates that the main source of OH^\bullet is the plasma-chemical reactions rather than electrolysis. The observed decrease of OH^\bullet concentration after 60 min of operation (figure 15(b)) is explained by the fact that the generation of electrical discharge generated using GAC250 starts ceasing after this time.

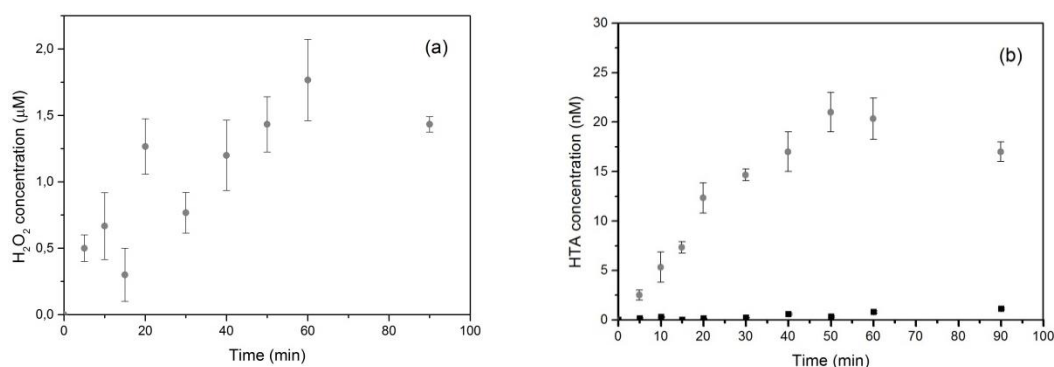


Figure 15. Formation of (a) - H_2O_2 and (b) - HTA with GAC250 (the amount of HTA is taken as a measure of OH^\bullet formation, see the Experimental part)

Besides the ability of electrical discharge generation, GAC250 demonstrated another effect that consisted in the disappearance of the discharge channels. It was noted that the number of the discharge channels decreased with time until they completely faded. The time during which the discharges were observable varied from 20 min to 1 hour depending on the AEFS and solution conductivity. At low values of the AEFS and low solution conductivity the discharges were more long-lived than at the high values of AEFS and solution conductivity. Revival of the faded electrical discharges became possible only after the solution was removed from the system and the electrodes were dried up.

This effect was discussed in the literature (Lukes *et al*, 2009) and explained by the formation of the surface charge on the ceramic layer. The accumulated charges reduce the electromagnetic field on the ceramic electrode acting as a screen. The authors proposed either to vary periodically the polarity of the applied voltage (e.g. by

using an AC source) or to use relevant ions in order to extend the time of the discharge. The polarity could be changed using alternating current which, however, contradicts the conditions chosen for the present study. Following to the second suggestion of the authors, solution composition was changed, but it made no visible effect on the extension of the discharge life time.

In the present study, the explanation of the observed phenomenon concerns the surface structure of the coating. GAC250 was provided with porosity, which is supposed to be necessary for the electrical discharge generation (Lukes *et al*, 2009, Hartmann *et al*, 2009). The pores are supposed to be the points where the electric field is enhanced which facilitates electrical discharge formation. However, at the same time porosity can play a negative role. In aqueous solution exposed to electric field, pores can be clogged by ions of the solution. It prevents the following electrical discharge formation.

In general, GAC250 acted as a better barrier than GAC50. It had worse dielectric, but better insulating properties, which resulted in the electrical discharge generation and prevention of electrolysis. Insufficient mechanical stability, however, suggests that further improvement of the coating properties is required. The issue of streamer disappearance can be solved by using the coating without porosity.

Electrode coating WAC500

One of the ways to improve properties of the electrode coating is to change its composition. Amorphous structure of grey alumina is supposed to have worse stability than more structured white alumina. Admixtures of γ -Al₂O₃ in the grey alumina significantly deteriorate the mechanical stability and dielectric properties of aluminium oxide.

The γ -Al₂O₃ unit cell has a tetragonal cell structure. In the pure γ -Al₂O₃ phase, the termination points are oxygen atoms. Thus, the surface is planar and is expected to be unstable. The α -Al₂O₃ unit cell has a hexagonal cell structure, with a rhombohedral primitive cell. In the pure α -Al₂O₃ phase, the termination points are aluminium atoms and the surface is non-planar and therefore more stable. Thus, the most stable phase of Al₂O₃ is pure α -Al₂O₃, whereas the mixture of different Al₂O₃ phases is less stable and less dense (Ahn *et al*, 1997).

The third electrode coating used in this work – WAC500 - was made of almost pure α -Al₂O₃ (96%) with the thickness of 500 μ m. No porosity was attached to the

WAC500 in order to eliminate the effect of streamer disappearance. Five pinholes were drilled through the coating to serve as spots of electromagnetic field enhancement. The pinholes had a diameter of 0.1 mm, which was assumed to be sufficient to distort electric field, but at the same time not to be deadly clogged by ions of the solution. Thus, the electric discharges generated with WAC500 and GAC250 differed by the nature from each other. The discharges with GAC250 were attributed to DBDs, whereas the discharges with WAC500 were attributed to the diaphragm discharges. The diaphragm discharges in the present study differed by the ones described in the literature as the diaphragm was positioned not in the middle of the electrode gap, but was directly adjoined to the electrode.

Five discharge channels, each positioned exactly at the pinhole, were formed using WAC500. The threshold value of the AEFS for electric discharge inception was found to be 7 kV/cm ($U = 21$ kV, $d = 3$ cm). The upper limit of the AEFS was found to be 28.7 kV/cm ($U = 43$ kV, $d = 1.5$ cm). The effect of solution conductivity on the electrical discharge generation with WAP500 was similar to the one with GAP250.

No deterioration of the coating was detected after the WAC500 was exposed either to high-voltage pulses and/or spark discharges (figure 16). No cracks or craters on the surface of WAC500 showed the high mechanical stability of the coating. It could be explained by both – the thicker ceramic layer and the coating composition.

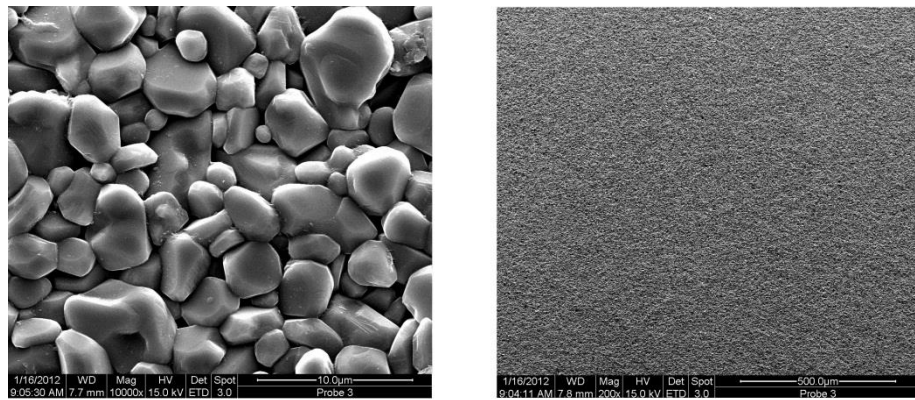


Figure 16. Scanning electron microscope images of WAC500 (conditions are listed in the Experimental part)

The waveforms of current and voltage across the discharge gap with WAC500 are presented in figure 17 for $U = 25$ kV, $d = 3$ cm, $\sigma = 2$ mS/cm. The discharge current with WAC500 (~ 220 A) is much higher than the discharge current with

GAC250. The peak of current and voltage pulses are not shifted as it was in the case of GAC250 suggesting that the capacitive properties of the coating were changed. The increase of the layer thickness has led to the decrease of its capacitance according to the equation 1. Assuming that $\epsilon_r \epsilon_0$ value does not vary significantly for the tested coatings, the capacitance of WAC500 then is ~10 times less than the capacitance of GAC50 and 2 times less than the capacitance of GAC250. Thus, WAC500 had the poorest capacitive properties among the tested coatings, therefore failed to act as dielectric barrier, which reflected in the current and voltage waveforms.

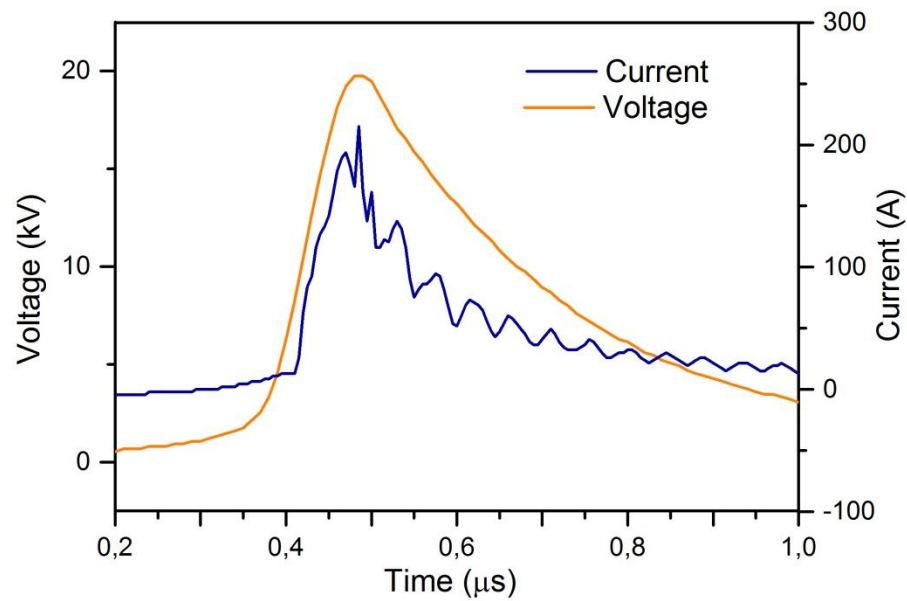


Figure 17. Current (blue) and voltage (yellow) waveforms of electrical discharge generated with WAC500

Despite the bad capacitance, WAC500 was expected to demonstrate better insulating properties. In order to examine the ability of WAC500 to act as an insulator and act as a barrier for electrons, the formation of H_2O_2 was measured using WAC500. As well as in the case of GAC250, two processes – electrolysis and plasma-chemical reactions may lead to the H_2O_2 formation. Therefore, H_2O_2 formation was measured with and without electrical discharges. The measurements of H_2O_2 by electrolysis was carried out using $U = 20$ kV, $d = 3$ cm and $\sigma = 1$ mS/cm in the absence of electrical discharge. As the concentration of H_2O_2 was below the detection limit after 90 min of operation, it was concluded that electrolysis took a negligible part. The formation of H_2O_2 by recombination of OH^\bullet resulted from the plasma-chemical reactions, was measured with $U = 30$ kV, $l = 3$ cm, $\sigma = 1$ mS/cm in

the presence of electrical discharge. The increase of H_2O_2 concentration with time is shown in figure 18(a) and it achieves the value of $23\ \mu\text{M}$ after 90 min of operation. To confirm this result, the formation of OH^\bullet was measured with and without electrical discharge (figure 18(b)). The concentration of HTA on the edge of detection limit was measured without electrical discharge (black squares). The considerable increase of HTA concentration with time in the presence of electrical discharge (grey circles) indicates the plasma-chemical nature of OH^\bullet formation. Thus, these results allow the conclusion that WAC500 had very good insulating properties, which have led to the prevention of electrolysis. The fact that much higher amounts of OH^\bullet and H_2O_2 were formed by the electrical discharges with WAC500 than with GAC250 allows to conclude that the discharge with WAC500 were characterised by a higher chemical activity.

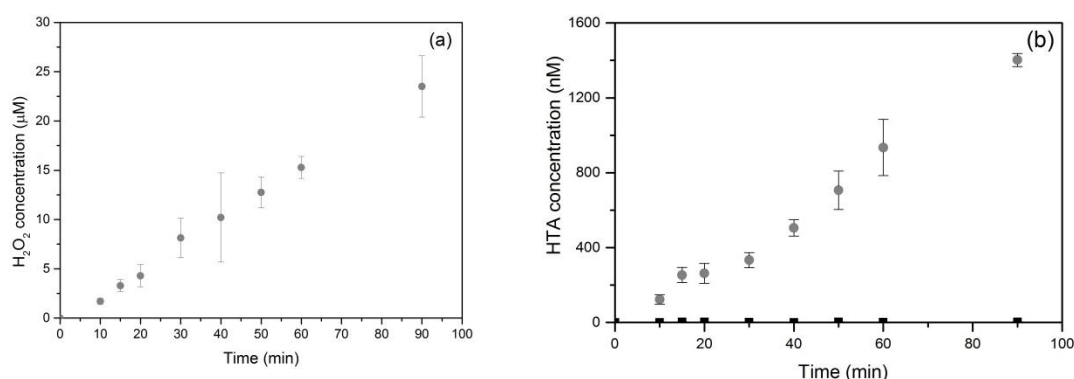


Figure 18. Formation of H_2O_2 and HTA with WAC500

Unlike in GAC250, electrical discharges generated with WAC500 did not disappear over the entire time of the coating usage, nor did the discharges pale or become thinner with time. The coating lifetime was estimated to vary from 20 to 30 hours of continuous operation depending on the experimental conditions. All further experiments described in the present study were carried out using WAC500.

A remark about plasma-spray technique

As it was discussed above, mechanical stability, dielectric and insulating properties of electrode coating are determined by the layer thickness and the coating composition. Therefore, it is crucial to use materials with certain composition which do not change their properties under any conditions.

After the failure of GAC50 to generate electrical discharge, the decision was

made to change the coating composition from grey to white alumina. The new coating was produced using a plasma-spray technique and was supposed to consist of pure α - Al_2O_3 which was evidenced by the white colour. However, the XRD spectra of the new coating revealed that it contained significant amount of γ - Al_2O_3 (figure 19). Thus, after the determination of the coating composition by XRD analysis, the material of the new coating was defined as grey alumina. The question arises, what were the reasons of the uncontrolled phase transformation?

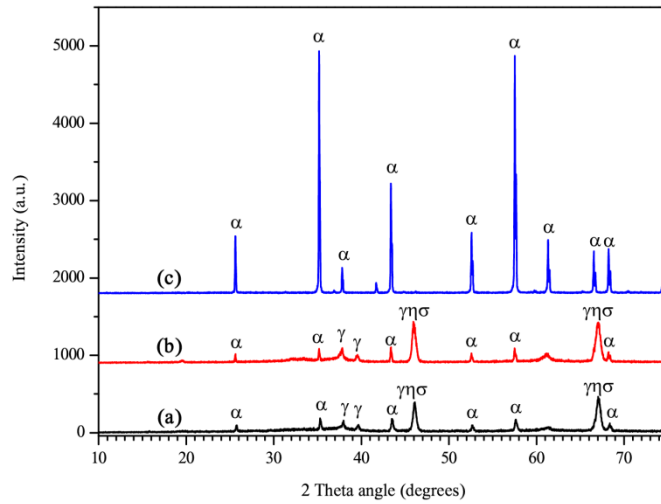
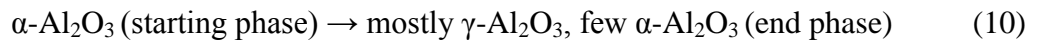


Figure 19. X-ray diffraction spectra of the ceramic coatings: (a) – GAC50, (b) – GAC250 and (c) – WAC500. The spectra are vertically shifted for clarity

The phase content of coating strongly depends on the spray parameters. The phase transformation from α - to γ - Al_2O_3 during thermal spraying under certain conditions may occur. Thus, using the plasma-spray technique, α - Al_2O_3 could be turned into the mixture of α - and γ - Al_2O_3 . The evidence of this transformation in case of GAC250 was confirmed by X-ray diffraction analysis. Figure 19 demonstrates XRD spectra of GAC50, GAC250 and WAC500. The XRD spectra from GAC50 and GAC250 clearly show that both coatings consist of α - and γ - Al_2O_3 mixture. According to (Shaw *et al*, 2000), at $I.V/\text{Ar}$ (electrical power to the primary Ar gas flow rate) ≥ 310 the following phase transformation may occur:



Thus, the second tested coating, which was supposed to be made of pure α - Al_2O_3

(Dzur B., PD Dr.), was turned into the mixture of α - and γ - Al_2O_3 during the plasma spray process.

The XRD spectrum of WAC500 (figure 19(c)) corresponds to almost pure α - Al_2O_3 . Sintering of pure α - Al_2O_3 did not change the coating composition, unlike in plasma-spray technique, as almost no admixtures in the XRD spectrum of WAC500 were observed.

2.3.2.2. Electric field strength

Many studies report on the effect of voltage pulse amplitude on the initiation and properties of electrical discharge. However, the applied voltage is not the important parameter, but the applied electric field. It is apparent that the higher applied voltage and the shorter the inter-electrode distance (electrode gap) will result in a higher probability of electrical discharge inception. Both parameters determine the value of averaged electric field strength given according to the equation 2.

The influence of the inter-electrode distance on the threshold voltage of electrical discharge inception is presented in figure (20) (the error bars are overlapped by the symbols).

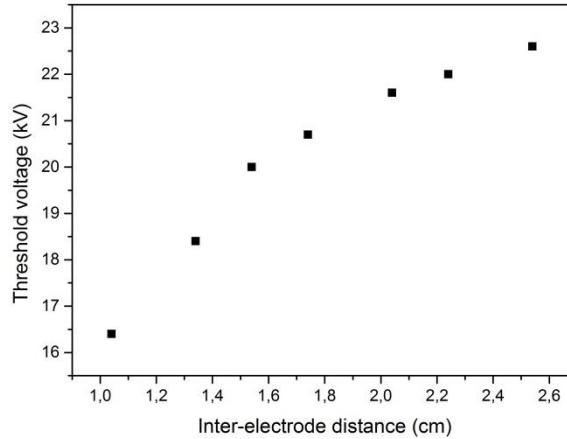


Figure 20. Influence of the inter-electrode distance on the threshold voltage of the electrical discharge inception

The range of the tested d values was limited by the dimensions of the plasma reactor ($d_{\min} = 1.04$ cm, $d_{\max} = 3.24$ cm). The threshold voltage was determined as the voltage at which a sustainable electrical discharge appears. The obtained results

demonstrated that the threshold voltage is lower for the shorter inter-electrode distances and higher for the longer discharge gaps. From practical point of view, it is easier to adjust voltage than inter-electrode distance, because the latter requires modification of the hardware. As it follows from the figure, the dependence of the threshold voltage on the inter-electrode distance is not a straight line and, therefore, the threshold value of the AEFS is not constant. For the short inter-electrode distances, higher values of the AEFS are required. Lower values of AEFS for long inter-electrode distances suggest that less power is required for electrical discharge inception under these conditions.

2.3.2.3. Solution conductivity

Along with the electrode coatings and AEFS, solution conductivity is a key parameter in the electrical discharge initiation. Its effect was investigated varying C_s and R_s values (figure 9), whereas C_d was constant and R_d was omitted from considerations.

Since the water is a resistive medium, the threshold value of the applied voltage depends on the conductive properties of the water layer. Threshold voltage of the electrical discharge inception was measured for different solution conductivities (figure 21) (the error bars are overlapped by the symbols). The results demonstrate that the increase in the solution conductivity leads to the decrease in the threshold voltage. Thus, in solution with higher conductivity, one needs to apply lower voltage to generate electrical discharge. The resistance of the aqueous layer decreases by the addition of ionic substances. Thus, the charge transfer is more efficient in solutions with high conductivities. Since the probability of the electrical discharge inception directly depends on the current flow, the electrical discharge is generated likelier at high values of solution conductivity. The slope of the curve decreases as the solution conductivity increases (figure 21). The discharge inception voltage is almost independent on the solution conductivity higher than 3 mS/cm. It suggests that at further increase of the solution conductivity (> 4 mS/cm) the electrical discharge inception will take place at the applied voltage of ~ 12 kV. For the electrical discharge inception in solutions with very high resistivity (low conductivity), one needs to apply very high voltages to breakdown the liquid. It is very difficult to manage such discharges, because the range of voltage at which the discharge occurs is very narrow.

Thus, in the solution with conductivity of 0.1 mS/cm the threshold voltage was found to be 24.5 kV and the electrical discharge turned into the arc discharge as the voltage was increased up to 28 kV. It must be noted that in the present study, using the distilled water with $\sigma = 0.3 \mu\text{S/cm}$, no electrical discharge was observed under any values of AEFS ($\text{AEFS}_{\text{max}} = 38.46 \text{ kV/cm}$, i.e. $d = 1.04 \text{ cm}$, $U = 40 \text{ kV}$).

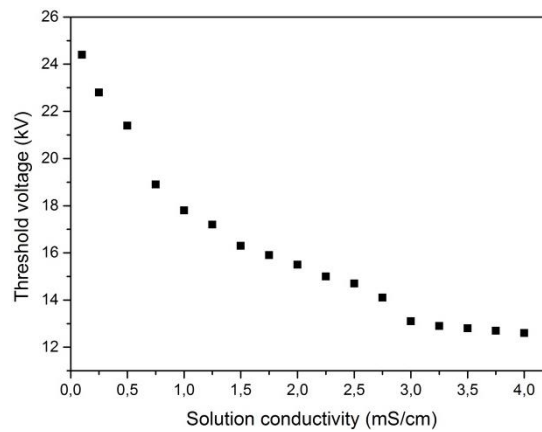


Figure 21. The effect of solution conductivity on the threshold voltage of the electrical discharge inception

The detailed explanation of the observed phenomenon could be found from the analysis of current and voltage waveforms. Figure 22 presents the difference in voltage waveforms for different solution conductivities. All measurements were carried out with the constant voltage across electrodes (30 kV). The voltage rise time is independent on the solution conductivity and estimated to be of 100 ns (90% of amplitude, figure 22), while the voltage fall after the maximum is different. The faster current dissipation in the discharge gap, inherent to the high solution conductivity (low resistance of the water layer), results in the shortening of the voltage pulse width as the solution conductivity increases. The discharge process is faster when the resistance is smaller, thus for the solution conductivity of 2 mS/cm, for example, the discharge occurs much faster (the pulse width at 50 % of amplitude is 160 ns) than that in case of 0.25 mS/cm solution (the pulse width at 50 % of amplitude is 700 ns). Thus, the supplied power dissipates faster in case of high solution conductivity and slower in case of the lower solution conductivity.

The effect of the solution conductivity on the current waveforms was also observed (figure 23). Three main features can be distinguished: (i) the current pulse duration increases as the solution conductivity decreases resembling the voltage pulse

behavior; (ii) unlike in the case of voltage effect, the rise time of current pulse is dependent on the solution conductivity; (iii) the current amplitude increases with increase of solution conductivity.

In a highly conductive solution, the concentration of ions is high, therefore more charged species are present. When the electric field across electrodes is applied, the charges start moving and heating the liquid. Due to the enhanced Joule heating, more intense bubble formation occurs when the electrical discharge is initiated in the solution with high conductivity. This fact simplifies the bubble formation – a process that precedes the electrical discharge initiation. Therefore, electrical discharge inception will occur faster, when solution conductivity is high. Thus, the current rise time becomes shorter when solution conductivity increases.

The longer rise time of the current pulse in case of low conductivity is explained by the slower propagation of the discharge channels. In highly conductive solutions, the discharge channels propagate simultaneously in many different directions (branching of the discharge channels is described in Chapter 3); whereas in low conductive solutions, the discharge channel preferentially propagates in a straight direction towards the opposite electrode. Thus, in the first case, the dissipation of the discharge power and the breakdown occur faster than in the second case, which is reflected in the shorter rise time of the current pulse for high solution conductivities.

The higher current pulse amplitude in case of high solution conductivity is explained by the fact that the water layer, acting as a better conductor than the one in case of low solution conductivity, transfers more charges and therefore more current flows in solution between the electrodes.

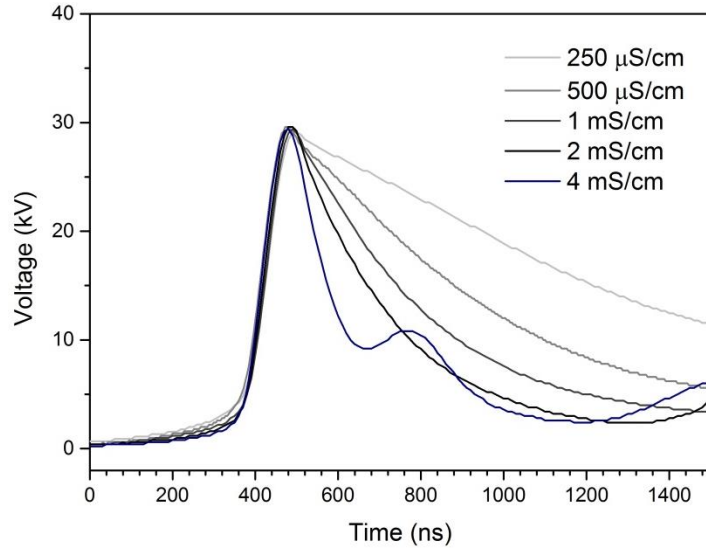


Figure 22. Voltage waveforms of electrical discharge generated at different values of solution conductivity

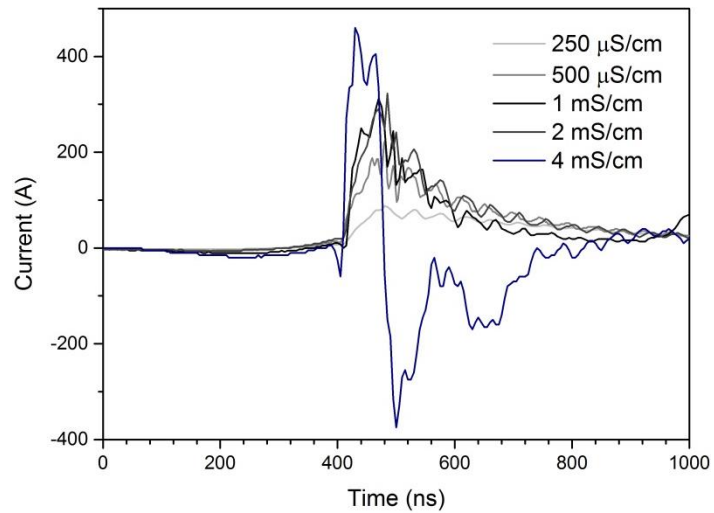


Figure 23. Current waveforms of electrical discharge generated at different values of solution conductivity

2.3.2.4. Pulse repetition rate

The effect of the pulse repetition rate on the electrical discharge inception was tested in a broad range of F values (1 - 50 Hz). The high pulse repetition rate of the electric pulse leads to the higher consumption and dissipation of the electric power. Thus, higher pulse repetition rate will result in faster heating of the surrounding media, uprising its conductivity and thus, facilitating electrical discharge inception. However, in the present study, the pulse repetition rate was found to make no

influence on the electrical discharge inception. Moreover, using high pulse repetition rate, more efficient solution circulation and cooling are required. Additionally, every event of electrical discharge influences, in some extent, the lifetime of electrode coating. Even very stable materials (e.g. white alumina) are affected by such effects as shock waves, unavoidable arc discharges and high temperature which accompany electrical discharge. Thus, the use of high values of pulse repetition rate will speed up the deterioration of electrode coating.

2.3.3. Electrical discharge formation

As described above, the high-voltage electrode used in the present study was covered with a ceramic layer in which five pinholes ($\varnothing = 0.1$ mm) were drilled. The insulating role of the electrode coating consists in the prevention of electrolysis and protection of the electrode from corrosion. In this subchapter, the role of the pinholes in the electrical discharge generation is discussed. The way the electrical discharge is generated in the present study using WAC500 has much in common with the “diaphragm discharge” (Baerdemaeker *et al*, 2007, Sato *et al*, 1999). On the one hand, the pinholes have the function of the pores i.e. the pinholes serve as the points of the local electric field enhancement. The bigger diameter of the pinholes compared to the dimension of pores, however, enables to avoid the disadvantages of the porosity (electrical discharge disappearance). Additionally, the pinholes can be considered as the capillaries, but with very small value of the length-to-diameter ratio ($l/\varnothing = 5$, in the present study). However, this value is assumed to be enough to generate the electrical discharge not in contact with metal electrode.

When the voltage pulse is applied across the electrodes, a weak conductive current inside the pinhole occurs heating the aqueous solution. As the input energy increases, the solution in the pinhole starts vaporizing forming a bubble of the water steam. The formed water bubble inside the pinhole undergoes to the electrical breakdown. The observable optical emission becomes possible after a further increase of the input power, when the energy released from the micro-bubble breakdown becomes enough to sustain continuous bubble formation by vaporization of the surrounding liquid. Thus, the discharge initiation in an aqueous solution passes the stages of the solution heating, micro-bubble formation and breakdown in the micro-bubble before the breakdown of the bulk solution takes place.

2.3.4. Energy per electric pulse

The determination of energy per electric pulse is necessary for the calculation of the energy consumption during the electrical discharge generation. The pulse energy could be determined from the analysis of voltage and current waveforms. Multiplication of the corresponding transient values of voltage ($U(t)$) and current ($I(t)$) allows the determination of the transient discharge power ($P(t)$) according to:

$$P(t) = U(t) \cdot I(t) \quad (11)$$

The obtained values of the transient power are plotted against time in figure 24 for the solution conductivity of 2 mS/cm ($U = 30$ kV). The integration of the power curve by time gives the total energy (E_{pulse}) dissipated during one electrical discharge:

$$E_{pulse} = \int_{t_1}^{t_2} P(t) dt \quad (12)$$

The limits of integration in this equation correspond to the duration of the active phase of the discharge. Time limits of the discharge process can be determined by tracing the development of the discharge light in time. The detailed description is performed in Chapter 3.3.2.4., where the method of time-resolved emission spectroscopy is employed. Thus, for solution conductivity of 2 mS/cm, the active phase of the discharge was found to be 200 ns, which was taken as the ($t_2 - t_1$) in the equation 12. The pulse energy, thus, was calculated to be 0.94 J for 2 mS/cm.

Since solution conductivity has a great influence on the electric pulse characteristics, it would also influence the electric pulse energy. The effect of the solution conductivity on the energy per electric pulse is shown in figure 25. The integration limits for all other solution conductivities were determined analogically to the 2mS/cm.

The discharge energy increases with increase of solution conductivity. At the low values of solution conductivity this effect is more pronounced than at the high values as the steeper slope of the curve is observed in figure 25 for lower values of solution

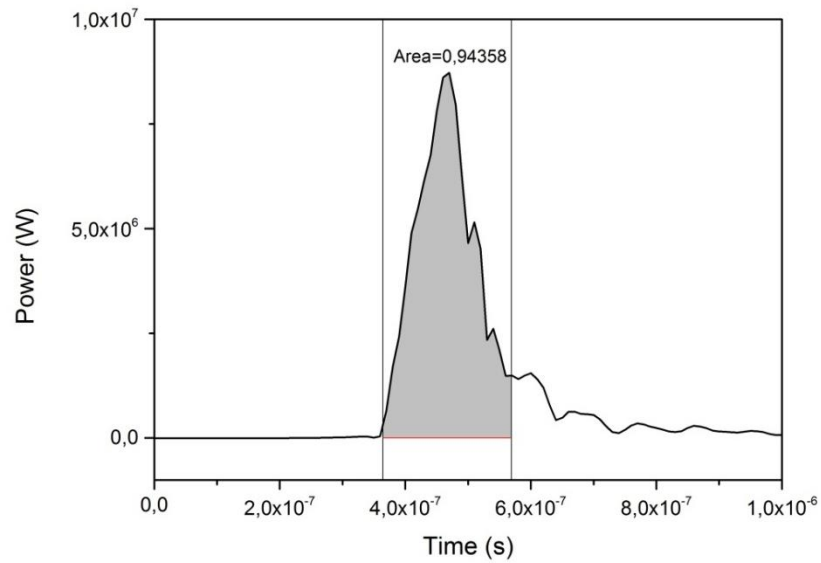


Figure 24. Calculation of the energy per electric pulse on the example of solution conductivity of 2 mS/cm

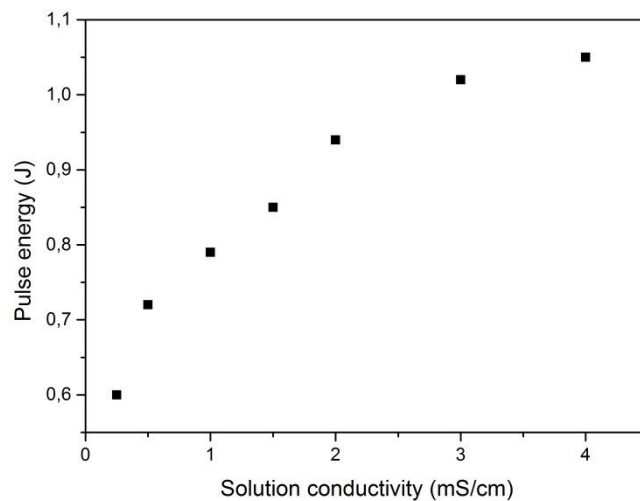


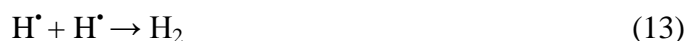
Figure 25. Effect of the solution conductivity on the energy per electric pulse

conductivity. As mentioned above, the capacitive properties of the discharge gap increase with decrease of solution conductivity. The water layer, acting as a capacitor, is not fully discharged in low conductive solutions, which results in the lower discharge energy for the less conductive solutions. The fact that in highly conductive solution the energy per electric pulse is higher suggests the electrical discharge generation in solutions with high conductivity leads to the more efficient use of the input power.

2.3.5. Chemical activity of underwater electrical discharge

The chemical activity of the electrical discharge was estimated by quantification of the chemical species generated by the discharge. In the chapter “Electrode coatings”, it was found that the contribution of electrolysis in the H_2O_2 and OH^\bullet formation is negligible for WAC500. Thus, the measured quantities of H_2O_2 and OH^\bullet are to be attributed to the formation through the plasma chemical reactions. In this chapter, the liquid phase reactions induced by electrical discharges are studied. The effect of different discharge parameters on the H_2O_2 and OH^\bullet formation is discussed.

The hydroxyl radicals can diffuse into the bulk or recombine to form H_2O_2 . The recombination of the OH^\bullet , H^\bullet and O^\bullet leads to the relatively stable molecular products according to the reactions (13) – (16):



Thus, O_2 , H_2 , OH^\bullet , H_2O_2 are present in the bulk solution for the long time (in the range of microseconds for OH^\bullet , in the range of several days for H_2O_2) after the electrical discharge and could be detected and quantified by chemical methods.

For the OH^\bullet quantification the method using 2-hydroxyterephthalic acid (HTA) was used which employs the NaTA as a scavenger for the OH^\bullet (equation 7). It allowed the OH^\bullet quantification before the recombination to form H_2O_2 . However, Mark *et al*, 1998 reported on the reduced yield of 2-hydroxyterephthalate (HTA, up to 35%) in the presence of O_2 . Thus, the method employed allows the relative quantification of OH^\bullet in the present study as all solutions were saturated with the air. In the present study, the obtained data on the HTA formation do not allow the direct quantification of OH^\bullet (not with 100% yield, nor with 35% yield). Therefore, it was assumed that the amount of the OH^\bullet present in the solution is proportional to the HTA.

2.3.5.1. Effect of the solution conductivity

The effect of the solution conductivity on the HTA formation (i.e. relative formation of OH^\bullet) is presented in figure 26(a). The reaction of the OH^\bullet formation is of a zero order for the chosen range of conductivity (250 $\mu\text{S}/\text{cm}$ – 4 mS/cm). After 90 min of applying high voltage pulses ($U = 30 \text{ kV}$, $d = 2.04 \text{ cm}$) the solution did not become saturated with the OH^\bullet as a stationary concentration was not achieved.

The amount of the generated OH^\bullet increases with the increase of the solution conductivity (figure 26(b)). When the conductivity is low, the electrical discharge is weak. As the solution conductivity rises, the electrical discharges of a higher energy are generated. Thus, the generation of electrical discharges in solutions with high conductivity leads to the more efficient OH^\bullet formation. The same tendency was observed by Sun *et al*, 1997 for solution conductivities up to 80 $\mu\text{S}/\text{cm}$ and Shih *et al*, 2010 for solution conductivities up to 250 $\mu\text{S}/\text{cm}$. Both authors reported on the decrease of the OH^\bullet formation with a further increase in the solution conductivity. Shih *et al*, 2010 proposed that the OH^\bullet decrease must relate to the different discharge properties in solution with high conductivity. The higher solution conductivity, the shorter are the discharge channels, the less is the water-plasma contact, the lower is the OH^\bullet yield. Thus, two opposite effects might influence the dependence of OH^\bullet formation from the solution conductivity: (i) more energetic electrical discharge formation in solutions with high conductivity; (ii) smaller area of the plasma/liquid interface with increase in the solution conductivity. The first effect leads to a direct proportionality of the OH^\bullet formation on solution conductivity, whereas the second effect leads to a reverse proportionality. What effect will predominate depends on the experimental conditions and might include a number of factors, e.g. the tested range of solution conductivity, reactor design, characteristics of the electric pulse etc. In the present study, the increase of OH^\bullet formation with increase of solution conductivity was observed suggesting that the effect of the discharge energy predominates over the effect of the discharge dimensions in the generation of OH^\bullet .

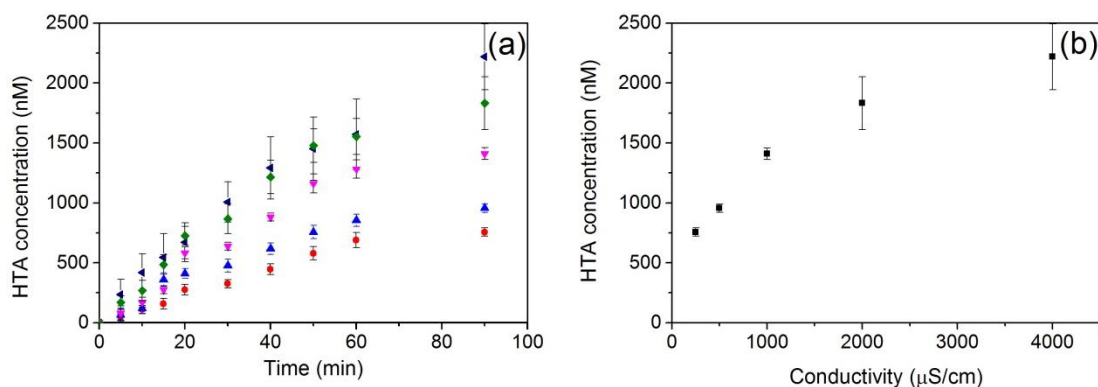


Figure 26. (a) – HTA formation in solutions of different conductivity; (b) - Effect of the solution conductivity on the HTA formation

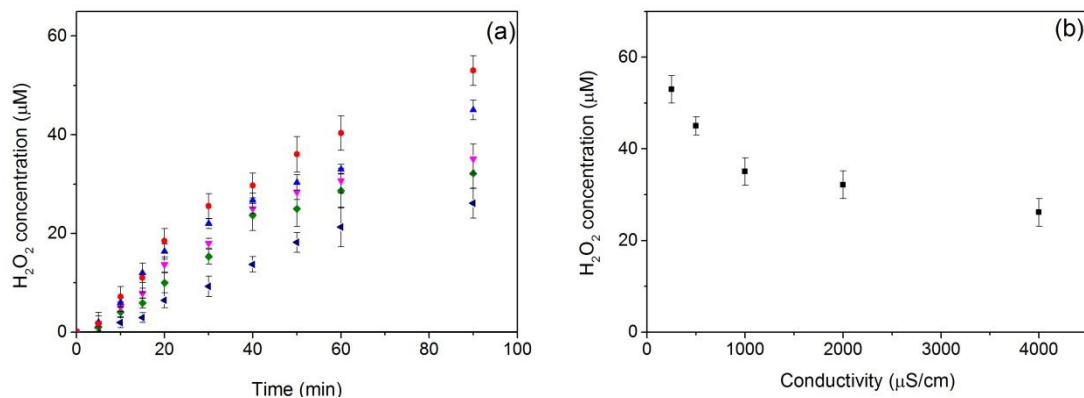


Figure 27. (a) – H₂O₂ formation in solutions of different conductivity; (b) - Effect of the solution conductivity on the H₂O₂ formation

The effect of the solution conductivity on the H₂O₂ formation is presented in figure 27. For these measurements the electrical parameters were the same as for the OH[•] measurements. The concentration of H₂O₂ increases with time (figure 27(a)) tracing the OH[•] behavior and does not become constant indicating that the formation of H₂O₂ has not reached the stationary concentration. The measured amount of H₂O₂ is roughly two orders higher than the detected amount of HTA suggesting that the yield of the HTA through the reaction with OH[•] (equation 7) is very low.

The H₂O₂ formation shows an opposite effect compared to the dependence of OH[•] formation on the solution conductivity. The increase of the solution conductivity has led to the decrease in the H₂O₂ yield (figure 27(b)). The highest H₂O₂ yield of 59 μM after 90 min of applying high voltage pulses was observed for the solution conductivity of 100 μS/cm, whereas only 26.4 μM of H₂O₂ were formed in the solution with conductivity of 4 mS/cm. The observed effect can be explained by the

fact that H_2O_2 undergoes the decomposition by the plasma effects. H_2O_2 formed after the electrical discharge could be decomposed by high temperature and the UV light of subsequent electrical discharges. Thus, the longer the duration of operating, the more efficient will be the H_2O_2 decomposition. Two effects influence the dependence of the H_2O_2 formation on the solution conductivity: (i) the higher OH^\bullet yield for the higher solution conductivities, which should lead to the higher amount of H_2O_2 ; (ii) H_2O_2 decomposition by UV light and high temperature of the discharge, which should lead to the lower concentration of H_2O_2 . Depending on what effect predominates, the concentration of H_2O_2 will grow up or fall down. In the present study, the second effect predominates, therefore, the observed results demonstrated the decrease of H_2O_2 concentration with increase of the solution conductivity.

Apparently, it is not possible to measure the true amount of H_2O_2 produced by the electrical discharge using the Allen's method. However, the quantification of the H_2O_2 , which is present in the solution after the action of all the effects, is possible. This result is less valuable in terms of the investigation of chemical yield of the electrical discharge, but more valuable in terms of the application for the organics removal, since it shows how much H_2O_2 is really available and can react with the organic compounds.

2.3.5.2. Effect of the pulse repetition rate

The formation of the reactive species depends on time of the electric pulses were applied. Therefore, it will also depend on the input power which can be altered by varying the pulse repetition rate. The effect of the pulse repetition rate on the H_2O_2 and OH^\bullet formation was studied and presented in figure 28. The measurements were carried out in the solution with conductivity of 1 mS/cm, the inter-electrode distance was of 2 cm, the voltage amplitude across the electrodes of 30 kV.

The HTA concentration increases with the increase of the pulse repetition rate (figure 28(a)). The lowest HTA yield (234 nM after 90 min of operation) was observed for the pulse repetition rate of 1 Hz, whereas the application of the HV pulses with the frequency of 40 Hz resulted in ~20 times higher HTA yield (4.85 μM after 90 min of operation). Theoretically, there is a direct proportionality between

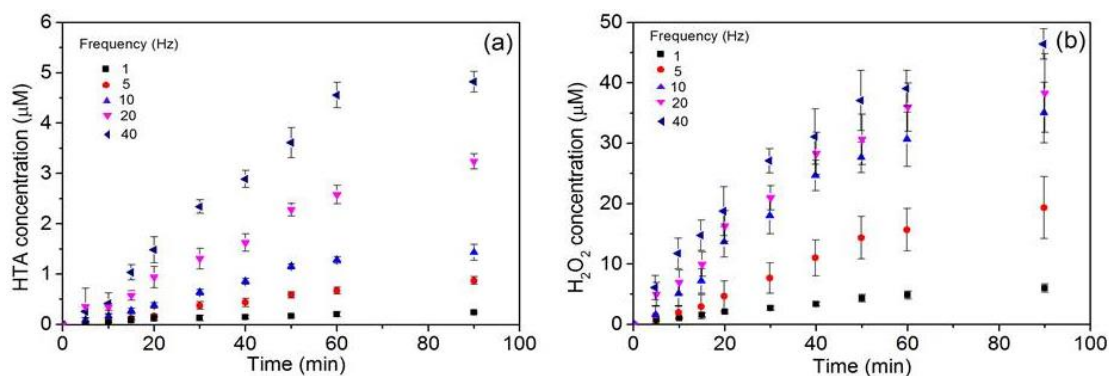


Figure 28. Effect of the pulse repetition rate on: (a) - HTA formation; (b) – H_2O_2 formation

frequency of applied electric pulse and the OH^\bullet (HTA) yield, since it was assumed that the equal amounts of the reactive species are produced after every discharge event. However, the increase of frequency in 40 times has led to the increase of the OH^\bullet production in 20 times, which is half as less than the expected value. This might be related to the saturation of the solution with the OH^\bullet and therefore the decrease of the formation rate of OH^\bullet . It is also evidenced by the more gradual slope of the curve for 40 Hz during the last 30 min of operation.

The formation of H_2O_2 increases with the increase of the pulse repetition rate (figure 28(b)). This dependence, however, is more considerable for the frequencies up to 10 Hz. For the higher frequencies (>10 Hz), the H_2O_2 formation does not increase significantly. It could be explained by two effects: (i) the higher the pulse repetition rate, the higher is the amount of the formed H_2O_2 , the slower is the further formation of H_2O_2 ; (ii) the effect of the decomposition of H_2O_2 by UV light and the increased temperature might contribute to the final amount of H_2O_2 present in the solution.

2.4. Summary

In this chapter, the electrical discharge generation in aqueous solution was discussed. The effect of different parameters on the electrical discharge inception was investigated.

Among the tested electrode coatings, the one containing pure $\alpha\text{-Al}_2\text{O}_3$ was shown to be the most suitable for the electrical discharge generation. Reproducible in time underwater electrical discharges were generated without the deterioration of the metal electrode. No evidence of electrolysis was observed or its part was negligible.

For the plasma reactor used in present work, the electrical discharge can occur in the wide range of the applied voltage. It is most reasonable to generate electrical discharge with the shortest possible inter-electrode distance for which the breakdown voltage is low ($U_{\text{breakdown}} = 16,4 \text{ kV}$ at $d_{\text{min}} = 1.04 \text{ cm}$, $\sigma = 1.5 \text{ mS/cm}$).

The effect of the solution conductivity was found to crucially influence the electrical discharge inception. Since the discharge inception was not possible in distilled water, the discharge gap must be filled with a conductive solution for successful discharge generation. The increase of solution conductivity was found to facilitate electrical discharge inception ($U_{\text{breakdown}} = 12.3 \text{ kV}$ at $\sigma = 4 \text{ mS/cm}$, $d = 1.04 \text{ cm}$). The higher output energy was calculated for the electrical discharge generated in a solution with high conductivity. Thus, it was found that the electrical discharge generation in the solution with high conductivity results in a more efficient use of the input energy.

The formation of H_2O_2 and OH^\bullet by the electrical discharge in aqueous solution was detected. The increase in solution conductivity was found to facilitate the formation of the reactive species.

The generation of the reproducible electrical discharge in aqueous solution allows performing the detailed investigation of this phenomenon.

2.5. List of literature

- Accuratus**, the company website: accuratus.com/alumox.html
- Ahn J.** and Rabalais J.W. 1997. Composition and structure of the Al_2O_3 0001-(1x1) surface. *Surface Sci.* 388, 121-131
- Akishev Y.**, Grushin M., Monich A.E., Napartovich A.P., Trushkin N. One-Atmosphere Argon Dielectric-Barrier Corona Discharge as an Effective Source of Cold Plasma for the Treatment of Polymer Films and Fabrics. *Proceedings of the 3rd International Symposium on Theoretical and Applied Plasma Chemistry.* September 16-21, 2002, Ples, Russia
- Allen A.O.**, Hochanadel C.J., Ghormley J.A. and Davis T.W. 1952. Decomposition of water and aqueous solutions under mixed fast neutron and gamma radiation. *J Phys Chem. B.* 56, 575-586
- Babaeva N.Y.**, Kushner M.J. 2008. Streamer Branching: The Role of Inhomogeneities and Bubbles. *IEEE Trans Plasma Sci.* 36(4), 892-893
- Baerdemaecker F.De.**, Simek M., Schmidt J and Leys C. 2007. Characteristics of ac capillary discharge produced in electrically conductive water solution. *Plasma Sources Sci Technol.* 16, 341-354
- Braun D.**, Kuchler U. and Pietsch G. 1991. Microdischarges in air-fed ozonizers. *J Phys D: Appl Phys.* 24, 564-572
- Bunkin N.F.** and Bunkin F.V. 1992. Bubbstons: stable microscopic gas bubbles in very dilute electrolytic solutions. *Zh Eksp Teor Fiz.* 101, 512-527
- Buxton G.V.** In "The study of fast processes and transient species by electron pulse radiolysis". Baxendale J.H.; and Busi F., Eds; Reidel: Dordrecht, 1982, 241-266
- Cheng L.**, Zhitao Z., Xiaofeng Z. and Yan Y. 2006. A study of the aging of α - Al_2O_3 dielectric material in DBD plasma. *Plasma Sci and Technol.* 8(6), 693-696
- Dhali S.K.** and Williams P.F. 1987. Two-dimensional studies of streamers in gases. *J Appl Phys.* 62(12), 4696—4707
- Dzur B.**, PD Dr. Personal communications. Institute for Materials Engineering, Technical University Ilmenau
- Gibalov V.I.** 1998. Dissertation abstract: Dynamics of barrier discharge and ozone synthesis (in Russian)

Hartmann W., Roemheld M., Rohde K-D. and Spiess F.-J. 2009. Large area pulsed corona discharge in water for disinfection and pollution control. *IEEE Trans Dielectr and Electr Insul.* 16(4), 1061-1065

Hensel K., Matsui Y., Katsura S. and Mizuno A. 2004. Generation of microdischarges in porous materials. *Czech J Phys.* 54C3, 683-689

Hensel K. and Tardiveau P. 2008. ICCD camera imaging of discharges in porous ceramics. *IEEE Trans Plasma Sci.* 36(43), 980-981

Heuser C. 1985. Doctoral Dissertation: Zur Ozonierung in elektrischen Gasentladungen. RWTH Aachen University, Aachen.

Hong Y.C., Park H.J., Lee B.J., Kang W.-S. and Uhm H.S. 2010. Plasma formation using a capillary discharge in water and its application to the sterilization of *E. coli*. *Phys Plasma.* 17, 1-5

Jang D.G., Kim M.S., Nam I.H., Uhm H.S. and Suk H. 2011. Density evolution measurement of hydrogen plasma in capillary discharge by spectroscopy and interferometry methods. *Appl Phys Lett.* 99, 1-3

Jones H.M. and Kurnhardt E.E. 1995. Pulsed dielectric breakdown of pressurized water and salt solutions. *J Appl Phys.* 77, 795-805

Joshi R.P., Qian J. and Schoenbach K.H. Proceedings of the 14th IEEE International Pulsed Power Conference. June 15th-18th, 2003, Dallas.

Joshi R.P., Qian J., Zhao G., Kolb J. and Schoenbach K.H. 2004. Are microbubbles necessary for the breakdown of liquid water subjected to a submicrosecond pulse? *J Appl Phys.* 96(6), 5129-5139

Joshi R.P., Kolb J.F., Xiao S. and Schoenbach K.H. 2009. Aspects of plasma in water: Streamer physics and applications. *Plasma Process Polym* 6(11), 763-777

Kogelschatz U. 2002. Dielectric-barrier discharges: their history, discharge physics, and industrial applications. *Plasma Chem Plasma Proc.* 23(1), 1-46

Kolb J.F., Joshi R.P., Xiao S. and Schoenbach K.H. 2008. Streamers in water and other dielectric liquids. *J Phys D: Appl Phys.* 41(23), 234007

Korobeinikov S.M., Melekhov A.V. and Besov A.S. 2002. Breakdown initiation in water with the aid of bubbles. *High Temperature.* 40(5), 706-713 (in Russian)

Kostov K.G., Honda R. Y., Alves L.M.S. and Kayama M.E. 2009. Characteristics of dielectric barrier discharge reactor for material treatment. *Braz J Phys.* 39(2), 322-325

Laenen R., Roth T., and Laubereau A. 2000. Novel precursors of solvated electrons in water: evidence for a charge transfer process. *Phys Rev Lett.* 85, 50-53

Laroussi M., Alexeff I., Richardson J. P. and Dyer F. F. 2002. The resistive barrier discharge? *IEEE Trans Plasma Sci.* 30(1) 158-159

Lewis T.J. 2003. Breakdown initiating mechanisms at electrode interfaces in liquids. *IEEE Trans Dielectr Electr Insul.* 10(6), 948-955

Li R., Tang Q., Yin S. and Sato T. 2007. Investigation of dielectric barrier discharge dependence on permittivity of barrier materials. *Appl Phys Lett.* 90, 1-8

Li R., Tang Q., Yin S., Yamaguchi Y. and Sato T. 2004. Dense and strong plasma initiated by $\text{Ca}_{0.7}\text{Sr}_{0.3}\text{TiO}_3$ ceramic. *Phys Plasmas* 11, 3715-3720

Lukes P., Clupek M., Babicky V. and Sunka P. 2008. Ultraviolet radiation from the pulsed corona discharge in water. *Plasma Sources Sci Technol.* 17, 1-11

Lukes P., Clupek M., Babicky V. and Sunka P. 2009. The role of surface chemistry at ceramic/electrolyte interfaces in the generation of pulsed corona discharges in water using porous ceramic-coated rod electrodes. *Plasma Proc Polym.* 6(11), 719-728

Mahoney J., Zhu W., Johnson V.S., Becker K.H and Lopez J.L. 2010. Electrical and optical emission measurements of a capillary dielectric barrier discharge. *Eur Phys J D.* 60, 441-447

Marinov I.L., Guaitella O., Rousseau A., Starikovskaia S.M. 2011. Successive nanosecond discharges in water. *IEEE Trans Plasma Sci.* 39(11), 2672-2673

Mark G., Tauber A., Laupert R., Schuchmann H. P., Schulz D., Mues A. and Sonntag C. von. 1998. OH-radical formation by ultrasound in aqueous solution – Part II: Terephthalate and fricke dosimetry and the influence of various conditions on the sonolytic yield. *Ultrasonics Sonochem.* 5, 41-52

Mason T., Lorimer J., Bates D. and Zhao Y. 1994. Dosimetry in sonochemistry: the use of aqueous terephthalate ion as a fluorescence monitor. *Ultrasonics Sonochem.* 1 91-95

Meiners A., Leck M. and Abel B. 2010. Efficiency enhancement of a dielectric barrier plasma discharge by dielectric barrier optimization. *Rev Sci Instr.* 81, 113507(1-8)

Miclea M., Kunze K., Musa G., Franzke J. and Niemax K. 2001. The dielectric barrier discharge – a powerful microchip plasma for diode laser spectrometry. *Spectrochimica Acta Part B.* 56, 37-43

Morrow R. 1997. The theory of positive glow corona. *J Phys D: Appl Phys.* 30(22) 2672-2673

Namihira T., Sakai S., Matsuda M., Wang D., Kiyon T., Katsuki S., Akiyama H., Okamoto K. and Toda K. 2007. Temperature of and NO generation in pulsed arc discharge plasma. *Plasma Sci Technol.* 9, 747-751

Naugol'nykh K. A. and Roi N. A. *Electrical Discharges in Water (Hydrodynamic Model).* Nauka, Moscow, Russia, 1971, 190 pages (in Russian)

Naz M. Y., Ghaffar A., Rehman N. U., Shukrullah S. and Ali M.A. 2012. Optical characterization of 50Hz atmospheric pressure single dielectric barrier discharge plasma. *Progress In Electromagnetics Research M.* 24, 193-207

Piroi D., Magureanu M., Mandache N.B., David V. and Parvulescu V. Pulsed dielectric barrier discharge generated at the gas-liquid interface for the degradation of the organic dye methyl red in aqueous solution. *Proceedings of the 12th International Conference on Optimization of Electrical and Electronic Equipment, OPTIM.* 20th-22th May, 2010, Brasso, Romania

Qian M.-Y., Ren C.-S., Wang D.-Z., Fan Q.-Q., Nie Q.-Y., Wen X.-Q., and Zhang J.-L. 2012. Investigations on an atmospheric dielectric barrier discharge plasma jet with a concentric wire-mesh cylinder electrode configuration. *IEEE Trans Plasma Sci.* 40(4), 1134-1141

Qian J., Joshi R.P., Schamiloglu E. Gaudet J., Woodworth J.R. and Lehr J. 2006. Analysis of polarity effects in the electrical breakdown of liquids. *J Phys D: Appl Phys.* 39, 359-369

Sahni M. and Locke B.R. 2006. Quantification of hydroxyl radicals produced in aqueous phase pulsed electrical discharge reactors. *Ind Eng Chem Res.* 45, 5819–25

Saran M. and Summer K.H. 1999. Assaying for hydroxyl radicals: hydroxylated terephthalate is a superior fluorescence marker than hydroxylated benzoate. *Free Rad Res.* 31(5), 429-436

Sato M., Yamada Y. and Sun B. 1999. Pulsed streamer discharge in water through pin hole of insulating plate. *Inst Phys Conf Ser.* 163, 37-40

Sein M.M., Bin Nasir Z., Telgheder U. and Schmidt T. 2012. Studies on a non-thermal pulsed corona plasma between two parallel-plate electrodes in water. *J Phys D: Appl Phys.* 45(22), 1-9

Shaw L.L., Goberman D., Ren R., Gell M., Jiang S., Wang Y., Xiao T.D. and Strutt P.R. 2000. The dependency of microstructure and properties of nanostructured coatings on plasma spray conditions. *Surface and Coatings Technology*. 130, 1-8

Shih K.-Y. and Locke B.R. 2010. Chemical and physical characteristics of pulsed electrical discharge within gas bubbles in aqueous solutions. *Plasma Chem Plasma Process*. 30, 1-20

Shih K.-Y. 2010. Doctoral Dissertation. Analysis of external pressure and solution temperature and conductivity on pulsed electrical discharge in aqueous solution and bubbles. The Florida State University, 164 pages

Starikovskiy A., Yang Y., Cho Y.I., Fridman A. 2011. Non-equilibrium plasma in liquid water: dynamics of generation and quenching. *Plasma Sources Sci Technol*. 20, 1-7

Stelmashuk V. and Hoffer P. 2012. Shock waves generated by an electrical discharge on composite electrode immersed in water with different conductivities. *IEEE Trans Plasma Sci*. 40(7), 1907-1912

Sun B., Sato M and Clements J.S. 1997. Optical study of active species produced by a pulsed streamer corona discharge in water. *J Electrostatics*. 39, 189-202

Sunka P. 2001. Pulse electrical discharges in water and their applications. *Phys Plasmas*. 8(5), 2587-2594

Tepper J., Li P. and Lindmayer M. Effects of interface between dielectric barrier and electrode on homogeneous barrier discharges at atmospheric pressure. *Proceedings of the 14th International Conference on Gas Discharges and their Application*. 1st - 6th September, 2002, Liverpool

Trunec D., Brablec A. and Stastny F. Comparative study of the APG and silent discharge. *Contributed papers of the International Symposium on High Pressure, Low Temperature Plasma Chemistry*. August 31st - September 2nd, 1998, Cork

Wang X., Luo H., Liang Z., Mao T. and Ma R. 2006. Influence of wire mesh electrodes on dielectric barrier discharge. *Plasma Sources Sci Technol*. 15, 845-848

Williamson J.M., Trump D.D., Bletzinger P. and Ganguly B.N. 2006. Comparison of high-voltage ac and pulsed operation of a surface dielectric barrier discharge. *J Phys D: Appl Phys*. 39, 4400-4406

Yurikov P.A. Protection of power stations 3-500 kV against lightning. Energia, Moscow, 1982, 88 pages (In Russian)

Zhu T., Zhang Q., Jia Zhijie and Yang L. 2009. The effect of conductivity on streamer initiation and propagation between dielectric-coated sphere-plate electrodes in water. IEEE Trans Dielectr Electr Insul. 16(6), 1552-1557

CHAPTER 3: PLASMA DIAGNOSTICS

Chapter scope

For the successful implementation of electrical discharges for water treatment, the optimization of the generated plasma is required. In the present chapter, plasma diagnostics is performed by means of optical methods – discharge imaging and emission spectrometry.

The discharge imaging is used in order to study the spatial characteristics of plasma – the diameter of the active plasma zone, the propagation velocity, the streamer length and branching. The emission spectrometry is used in order to: (i) investigate the light emission caused by the discharge; (ii) estimate the chemical activity of underwater plasma phenomenon by measuring the emission spectra of reactive species; (iii) calculate the plasma parameters – plasma gas temperature and electron density. The effect of such experimental parameters as solution conductivity, applied electric field strength and gas bubbling on the above mentioned plasma characteristics is also investigated.

The main aim at this step is the enhancement of the effects induced by the electrical discharges, which influence the degradation of organic compounds. Thus, the main objectives at this step are (i) the increase of the discharge light intensity; (ii) the increase of the formation rates of reactive species; (iii) increase of the electron density of plasma.

3.1. Literature survey

3.1.1. Electrical discharge propagation

3.1.1.1. Streamer branching

Visually, electrical discharge represents a luminous channel. Depending on the type of the discharge, this channel can be of various shapes. The partial discharge is always featured by a non-linear shape, which means that during its development, the discharge channel changes its direction and/or splits into many daughter channels. The latter phenomenon – streamer branching – is accompanied by the increase of the discharge light intensity and the formation of shock waves. The propagation front of the daughter filaments has a hemispherical shape.

It is clear that the higher the branching degree, the bigger volume is occupied by plasma. Therefore, it is very important to understand and control the streamer branching for such applications as water treatment, where big plasma volumes are required. The fact that the branching phenomenon is random, complicates its description. The most widely discussed concept of the streamer branching was developed by Loeb and Meek (Loeb *et al*, 1941). According to this theory, secondary electron avalanches are randomly formed ahead the streamer head and propagate in different directions. However, the numerical simulations of the branching process performed in the recent years suggested another mechanism of the branching (Meulenbroek *et al*, 2004, Arrayas *et al*, 2002). According to these studies, the branching is caused by the surface instability of the streamer. Babaeva *et al*, 2008 investigated the branching in liquids and explained the phenomenon by the presence of randomly distributed regions of low density in the liquid (inhomogeneities, e.g. bubbles).

A number of experimental parameters (applied electric field strength, solution conductivity, polarity of the applied electric pulse) influence the degree of branching (Clements *et al*, 1987, An *et al*, 2007, Korobeinikov *et al*, 2002, Gavrilov *et al*, 1994). In general, the following regularities were observed: (i) the degree of streamer branching is higher for higher solution conductivities; (ii) at positive polarity of the

electric pulses, the streamers are less branched (“filamentary discharge”) than at negative polarity where the streamers have more branched structure (“bush-like discharge”); (iii) at long electrode gaps, the formation of a leader has higher probability rather than the streamer branching.

3.1.1.2. Streamer length

Another spatial parameter that defines the discharge shape is the streamer length. The streamer propagation length directly depends on how far the ionization front can develop. The higher rate of ionization front will lead to the formation of the longer streamers. The length of a single streamer of a highly branched discharge is shorter than in a non-branched discharge. Polarity effect on the streamer length originates from the fact that a positive streamer propagates against the direction of the electron drift, whereas the propagation of a negative streamer occurs in the same direction with the electron drift. Thus, it was found that the negative streamers are shorter than positive ones (Clements *et al*, 1987). Solution conductivity was shown to make a crucial influence on the electrical pulse shape and, therefore, on the streamer length as well. The lower the solution conductivity, the longer is the duration of electric pulse, therefore, the streamer propagation takes the longer time. In general, the longer streamer formation in solutions with low conductivity takes place (Lee *et al*, 2010, Ceccato *et al*, 2010). The applied electric field (Bruggeman *et al*, 2007) also influences the streamer length: at higher applied voltages longer streamers are formed. It is due to the higher amount of input power and, therefore, the higher amount of the power supplied to sustain the streamers.

3.1.1.3. Propagation velocity

Electrical discharges propagate very rapidly, although the streamer propagation velocity in the case of liquid discharges is much slower than for the gaseous discharges due to the different discharge mechanisms. Since the propagation velocity directly depends on the discharge mechanism, the discharges formed through the direct ionization of liquid would be of much higher velocity than the discharges formed through the formation of gaseous cavity. Starikovsiy *et al*, 2011 and Marinov *et al*, 2011 investigated direct liquid discharges using voltage pulses with the rise time

of the order of a few ns. The obtained propagation velocities reached 5000 km/s which is comparable to the gas phase discharges (Winands *et al*, 2008). The discharge formed using the electric pulses with longer rise time were reported to result in much slower streamer propagation: 120-140 km/s. Thus, for the electric pulses with rise time of up to a few μ s the propagation velocities were found to be in the range of 0.5 km/s - 120 km/s (Lee *et al*, 2010, An *et al*, 2007, Nieto-Salazar *et al*, 2005). The higher the magnitude of the applied electric field, the higher is the streamer propagation velocity. Some authors found that the propagation velocity is constant in the electrode gap and increases as the streamer comes closer to the opposite electrode (Winands *et al*, 2008). However, in general way (Ceccato *et al*, 2010) the propagation velocity alters exponentially across the gap, slowing down in the proximity of the opposite electrode for the homogeneous electric fields. Positive polarity of the applied electric pulses was found to facilitate the streamer propagation. Thus, the positive streamers propagate faster than the negative ones (Lee *et al*, 2010) and this difference can reach one order of magnitude. The influence of solution conductivity on the streamer propagation velocity in liquid was investigated by many authors. Most of authors observed no influence of solution conductivity on the propagation velocity (Lee *et al*, 2010, Ceccato *et al*, 2010). On the one hand, the higher solution conductivity facilitates the process of water heating and vaporization when applying HV pulses, thus speeding up the process of bubble formation and simplifying the breakdown. On the other hand, at high solution conductivity, too many charges can be accumulated on the bubble/liquid interface, which will act as a screen. The input power may not be sufficient to sustain the discharge and the discharge propagation may be slowed down or stopped in the highly conductive solutions.

3.1.2. Radiative processes induced by underwater electrical discharges

3.1.2.1. Discharge continuum

The formation of electrical discharge in water is accompanied by a number of physical effects. One of the most important effects is a strong light emission whose qualitative and quantitative investigation brings the information about the discharge

phenomenon. The discharge light measurements are usually performed using emission spectroscopy. Emission intensity is used as an objective parameter to evaluate the influence of experimental parameters on the discharge occurrence.

Typically, the emission spectrum of underwater discharge represents a combination of a broadband spectrum - continuum radiation - and the strong atomic line emissions due to the presence of excited atoms in the plasma discharge zone. In underwater plasma discharges, a large part of the input energy is spent on the formation of a high-temperature plasma channel. The discharge channels function as a source of a blackbody radiation. The emission spectra of underwater discharges originate from Joule heating of the discharge channel. Thus, the detection of a continuum indicates that the thermal processes, which are dependent on temperature of the emitter, take place.

A blackbody emits photons whose energy distribution obeys the Planck's distribution function. The law that describes the distribution of the blackbody photons was developed by Planck in the year 1900 and is expressed as:

$$\varepsilon_{\nu,T} = \frac{2\pi h \nu^3}{c^2} \frac{1}{\exp(h\nu/kT)-1} \quad (17)$$

or

$$\varepsilon_{\lambda,T} = \frac{2\pi c^2 h}{\lambda^5 (\exp(h\nu/\lambda kT)-1)}, \quad (18)$$

where ε is the spectral radiance, c is the speed of light, h is the Planck's constant, k is the Boltzmann's constant, T is the temperature, λ is the wavelength, ν is the frequency. These equations correlate with the experimental results and were obtained by Planck. The equation consists of two parts: $I_{\nu,T} = \frac{2\pi \nu^2 kT}{c^2}$ is the Rayleigh-Jeans limit (for $h\nu \ll kT$; $I_{\nu,T}$ is the intensity) and $I_{\nu,T} = \frac{2h\nu^3}{c^2} e^{-h\nu/kT}$ is the Wien's limit (for $h\nu \gg kT$). Figure 29 shows several curves describing the Planck's law. The shift of the maximum to the region of the short wavelengths is clearly observed with increase of the temperature. This fact is essentially the Wien's displacement law that could be expressed as:

$$\lambda_{max} T = const, \quad (19)$$

where λ_{max} is the wavelength of the maximal intensity and T is the temperature of the blackbody. This law could be used for the determination of the blackbody temperature.

Some authors (Vanraes *et al*, 2012, Sun *et al*, 1998) reported on the continuum formation caused by underwater electrical discharge, whereas most of the studies report on the line spectrum dominated by H, O, OH emission lines. Since the discharge continuum has a thermal nature, its formation is attributed to the formation of a thermal plasma, whereas the line spectrum is attributed to the formation of a non-thermal plasma. The significance of the continuum formation consists in the fact that it is the evidence of the intense light emission caused by the discharge. All the reported discharge continua occurred in the region of 200 – 900 nm, thus, covering the entire optical region of the electromagnetic radiation. The maximal intensity of the light emission lies in the visible region which is important for the degradation of the compounds that undergo solar decomposition. Considerable part of the spectrum lies in the UV region (< 400 nm). The light emitted in the near and middle UV can be utilized for water disinfection or direct photolysis of organic compounds. The vacuum UV (70 – 190 nm) is responsible for the water photolysis and, therefore, plays the crucial role in the formation of hydroxyl radicals. Lukes *et al*, 2008 have performed quantitative analysis of the UV light emitted by the electrical discharge in aqueous solution using the method of actinometry. The authors reported on up to 28% of the input energy converted to the UV light by underwater electrical discharge.

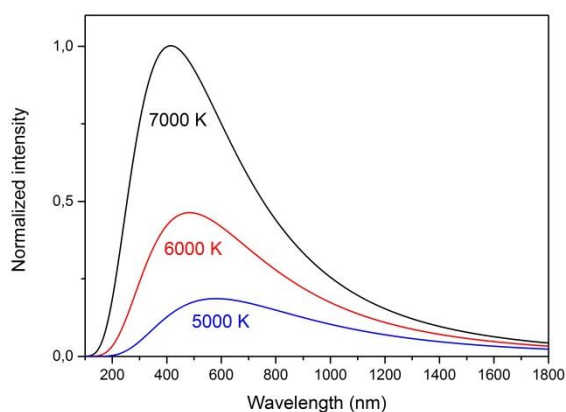


Figure 29. Dependence of spectral radiance on the wavelength at different temperatures. The simulated curves describe the Planck's radiation law

3.1.2.2. Line spectrum of primary species

The plasma-chemical reactions that take place on the border of plasma/liquid interface have been investigated by many research groups and significant achievements have been done. However, the complexity of the phenomenon does not allow to create an adequate theory that could describe all the involved processes.

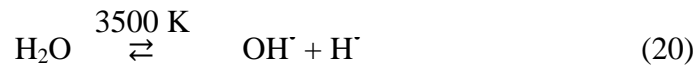
According to the bubble theory of the liquid discharges, electrical discharge initiation starts from the breakdown of the water bubble ($\text{H}_2\text{O}_{\text{vapor}}$) formed due to Joule heating when applying HV pulses. The breakdown of $\text{H}_2\text{O}_{\text{vapor}}$ leads to the formation of OH^\bullet and H^\bullet which is evidenced by the presence of strong atomic lines in the discharge continuum (Vanraes *et al*, 2012, Sun *et al*, 1988). The great variety of the possible pathways of the $\text{H}_2\text{O}_{\text{vapor}}$ breakdown suggests that the list of species formed directly by the electron collisions with water molecules is not limited only by these two radicals. Dolan *et al*, 1992 reported on a number of possible reactions of water molecules in vapor with electrons (table 4):

Table 4. Possible routes of interactions of water molecules being in vapor with electrons
(Dolan *et al*, 1992)

Nr	Reaction	Products
1	$\text{H}_2\text{O} + \text{e}^- \rightarrow$	$\text{H}_2\text{O}^+ + 2\text{e}^-$
2	$\text{H}_2\text{O} + \text{e}^- \rightarrow$	$\text{OH}^+ + \text{H}^\bullet + 2\text{e}^-$
3	$\text{H}_2\text{O} + \text{e}^- \rightarrow$	$\text{O}^+ + 2\text{H}^\bullet + 2\text{e}^-$
4	$\text{H}_2\text{O} + \text{e}^- \rightarrow$	$\text{O}^+ + \text{H}_2 + 2\text{e}^-$
5	$\text{H}_2\text{O} + \text{e}^- \rightarrow$	$\text{H}^+ + \text{OH}^\bullet + 2\text{e}^-$
6	$\text{H}_2\text{O} + \text{e}^- \rightarrow$	$\text{H}^+ + \text{O}^\bullet + \text{H}^\bullet + 2\text{e}^-$
7	$\text{H}_2\text{O} + \text{e}^- \rightarrow$	$\text{H}_2^+ + \text{O}^\bullet + 2\text{e}^-$
8	$\text{H}_2\text{O} + \text{e}^- \rightarrow$	$\text{OH}^- + \text{H}^+ + \text{e}^-$
9	$\text{H}_2\text{O} + \text{e}^- \rightarrow$	$\text{O}^- + \text{H}^\bullet + \text{H}^+ + \text{e}^-$
10	$\text{H}_2\text{O} + \text{e}^- \rightarrow$	$\text{O}^- + \text{H}_2^+ + \text{e}^-$
11	$\text{H}_2\text{O} + \text{e}^- \rightarrow$	$\text{OH}^+ + \text{H}^- + \text{e}^-$
12	$\text{H}_2\text{O} + \text{e}^- \rightarrow$	$\text{H}^- + \text{O}^+ + \text{H}^\bullet + \text{e}^-$
13	$\text{H}_2\text{O} + \text{e}^- \rightarrow$	$\text{H}^- + \text{O}^\bullet + \text{H}^+ + \text{e}^-$
14	$\text{H}_2\text{O} + \text{e}^- \rightarrow$	$\text{OH}^\bullet + \text{H}^\bullet + \text{e}^-$
15	$\text{H}_2\text{O} + \text{e}^- \rightarrow$	$\text{O}^\bullet + 2\text{H}^\bullet + \text{e}^-$
16	$\text{H}_2\text{O} + \text{e}^- \rightarrow$	$\text{O}^\bullet + \text{H}_2 + \text{e}^-$

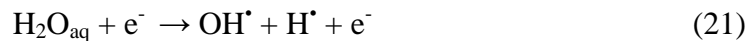
Although all the reactions may take place in the plasma discharge zone, the authors showed that the reactions 14 and 15 have the highest probabilities.

Apart from the immediate formation of the reactive radicals during the $\text{H}_2\text{O}_{\text{vapor}}$ breakdown, various physical effects are also induced. These effects may lead to the following water dissociation either by water thermolysis or by water photolysis. Additionally, the electron impact ionization of the water molecules in liquid state may take place. Studies on the plasma temperature determination usually report on the temperature values of up to 8000 K (Vanraes *et al*, 2012) for the liquid discharges. Thus, the discharge channels act as a source of a strong thermal radiation. Exposed to such high temperatures, water molecules may undergo thermal decomposition (equation 20). The most efficient formation of OH radicals occurs at $T = 3500 \text{ K}$:



At lower temperatures the efficiency of the water photolysis significantly decreases; at higher temperatures, the further splitting takes place to form various atomic species. Although, it should be noted that the volume that undergoes the thermal decomposition during electrical discharge is very small and is determined by the dimensions of the discharge channel. Thus, in the case of the thermal effects only the plasma discharge zone is affected, therefore the role of water thermolysis in the water splitting is relatively small. Moreover, the localized regions of high temperature are generated for a very short period of time, determined by the electrical pulse duration.

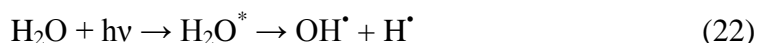
As well as in the case of the thermal effects, the electron impact ionization is characterized by a small reaction volume:



Because of the small mobility of electrons in water ($1.8 \times 10^{-3} \text{ cm}^2\text{V}^{-1}\text{s}^{-1}$, Farhataziz *et al*, 1987), the equation 21 takes place on the border of plasma/liquid interface. The formed radicals have a very small probability to diffuse into the bulk solution as they more probably react with the surrounding water molecules.

Unlike in water thermolysis and electron impact ionization, water photolysis is characterized by a higher probability. The UV light generated by the electrical

discharge is spread across the whole volume of the electrode gap which enables the photo-excitation of water molecules present in the bulk solution according to:



The highest quantum yield of this reaction occurs in the range of 120 – 170 nm (Atkinson *et al*, 2004), therefore, only the vacuum UV light plays significant role in this process.

The time scale of the events initiated by the absorption of energy by water is shown in figure 30 (Farnhataziz *et al*, 1987):

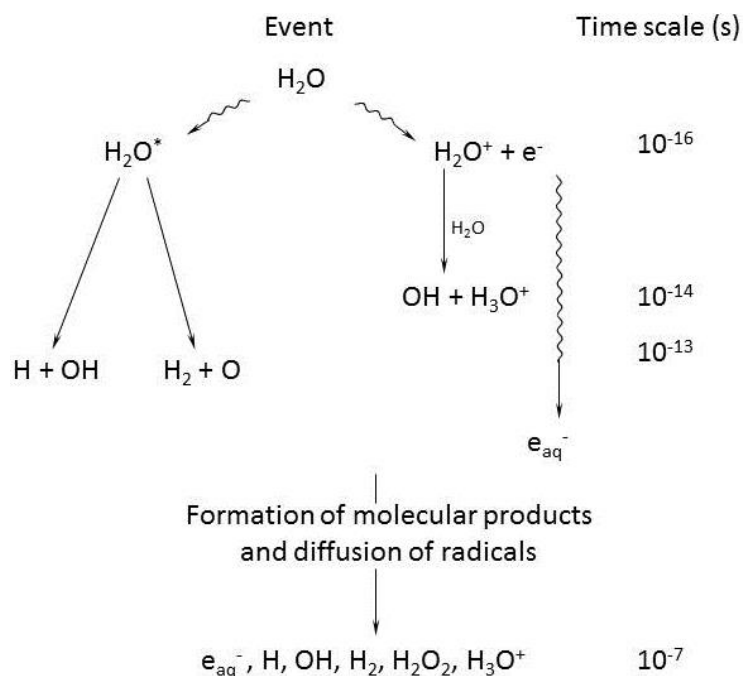
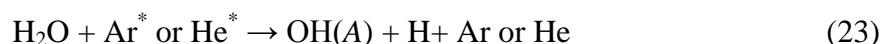


Figure 30. Radiolysis of water (Farnhataziz *et al*, 1987)

Initially, a water molecule is ionized or excited to upper electronic state by an energetic photon or an electron. The excited water molecules then dissociate to form primary species (OH^\bullet , H^\bullet , O^\bullet). The excitation event takes place on the time scale of an electronic transition. The physicochemical processes described above are complete by about 10^{-12} s after the ionization event. After this time, any radical and molecular species are in thermal equilibrium with the bulk medium. Next, the products start diffusing to form secondary products, which is complete by 10^{-7} s.

As shown above, plasma under water can be a very efficient ionization source. The variety of reactive species produced by plasma, however, is limited by the OH[•], H[•], O[•]. In the case of saturation of solution with gases (Nikiforov *et al*, 2011, Sarani *et al*, 2010), less input power is required for the discharge inception as there is no need to form the water bubbles. Thus, in terms of its commercial application, the advantage of underwater electrical discharges with saturation of the liquid with gases is the absence of dissipation of input power on ohmic heating and, thus, simplification of the discharge generation. Additionally, the introduction of the gases into the reactive plasma zone may lead to the formation of other reactive species by exciting the molecules of the introduced gases. These reactive species may directly react with organic compounds leading to their degradation or significantly influence the reaction rate of water splitting, thus, increasing the formation rates of OH[•]. Usually, argon, nitrogen and helium are used for these purposes. Nikiforov *et al*, 2011 proposed that Ar and He metastables formed during the discharge may cause dissociative excitation of water vapor:



Ar, He and N₂ are characterized by the very high chemical stability, thus, introducing these gases, the addition of chemically active substances is avoided, which is in agreement with the ultimate aim of the chemical-free method of water treatment developed in the present study. Finally, both Ar (in the less extent) and N₂ (~78%) are present in the environment and, therefore, can be easily supplied from the air.

3.1.3. Plasma parameters

The formation of plasma occurs through the intense and rapid ionization, which produces a large number of free electrons and positive ions. All plasma components – ions, neutrals, electrons - are characterized by the energy distribution functions. Plasma gas temperature refers to the average energy of all plasma components apart from the electrons. Since in the NTP electrons have much higher energy than other species, the gas temperature of NTP does not exceed a few thousand degrees, whereas the electron temperature may reach 10⁸ K.

Electron density - the number density of electrons in plasma - determines the intensity of electron and ion collisions providing a transfer of electrical energy to plasma. Provided that the plasma is quasi-neutral, the number density of electrons in a plasma is approximately equal to the number density of ions. Since the rate of the plasma-chemical reactions directly depends on the amount of the involved charged species, electron density determines the yield of the plasma-chemical reactions.

The plasma parameters, thus, determine the applicability of plasma for water treatment. The determination of plasma parameters is required for the effective optimization of the plasma source. The parameters of underwater plasma are the object of study of many research groups (Vanraes *et al*, 2008, Bruggeman *et al*, 2009, Nikiforov *et al*, 2011, Sarani *et al*, 2010). The generation of plasma with too high gas temperature must be avoided, since it leads to the destruction of reactor walls. Thus, at high gas temperatures, the input energy is wasted to the undesirable heating of the environment instead of being directed to the formation of chemically active species. At the same time, it is preferable to increase the electron density in order to increase the chemical activity of plasma. Thus, the optimization of a plasma source is very important and is necessary in order to produce a controllable, reproducible, high density and low-temperature plasma.

Characterization of plasma created by underwater electrical discharges is complicated due to: (i) small plasma volume; (ii) the electrical discharge is not reproducible, i.e. the spatial characteristics of the discharge vary from pulse to pulse; (iii) the liquid discharges are characterized by the much higher values of electron density compared to gas discharges.

Plasma parameters are unique characteristics of a plasma type. The plasma behavior depends on its temperature and electron density. Various examples of plasmas generated in laboratories, in industry and by the nature are placed on the density – gas temperature plane in figure 31. As it is shown in the figure, the plasmas are characterized by a great variety of the electron density values ($\Delta N_e > 25$ orders of magnitude) and gas bulk temperature ($\Delta T > 8$ orders of magnitude).

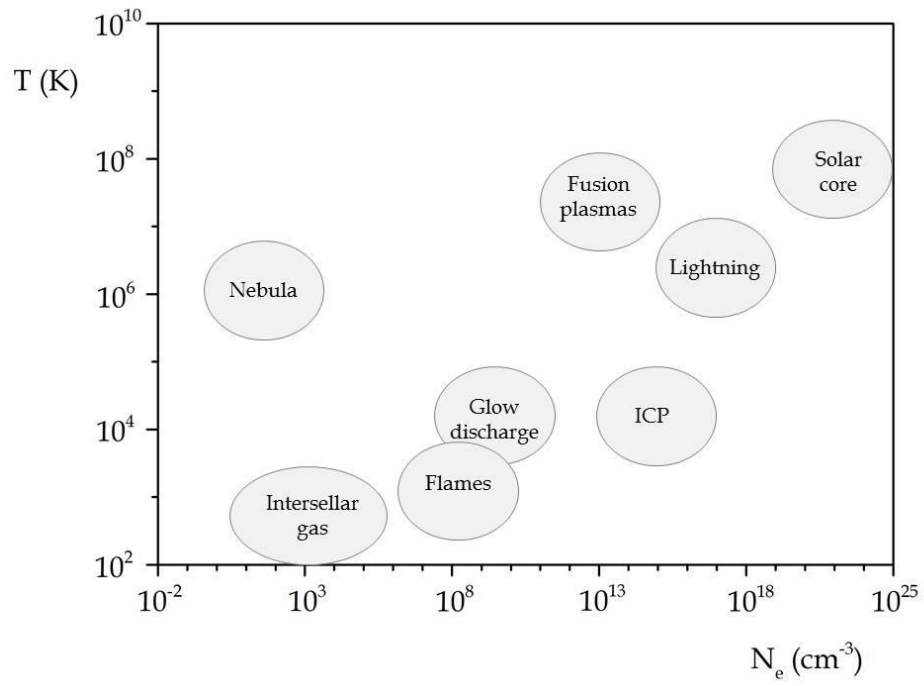


Figure 31. Density – gas temperature plane. The figure represents some examples of natural, industrial and laboratory plasmas

3.2. Experimental

3.2.1. Instrumentation

3.2.1.1. Reactor modification for spectroscopic measurements

For all experiments in the present chapter, the plasma reactor described in Chapter 2 was used (figure 32). WAC500 was used as a coating material for all measurements in the present chapter. The generation of multiple electrical discharges per one electric pulse complicates the description because of the possible overlapping of the discharge channels. Therefore, the electrode coating with only one pinhole positioned at the center of the round electrode was used for the plasma diagnostics. The Teflon[®] holder of the HV electrode was removed in order to provide the observation of the starting point of the discharge. The metal edges of the HV electrode were isolated with isolation tape. The distance between the plasma reactor wall and the fiber collimating optics was 5 cm. All optical measurements (imaging, ICCD (Intensified Charge Coupled Device) imaging and spectroscopic measurements) were performed in the dark. In order to provide the cooling, all experiments were carried out with the circulated solution (figure 7(b)).

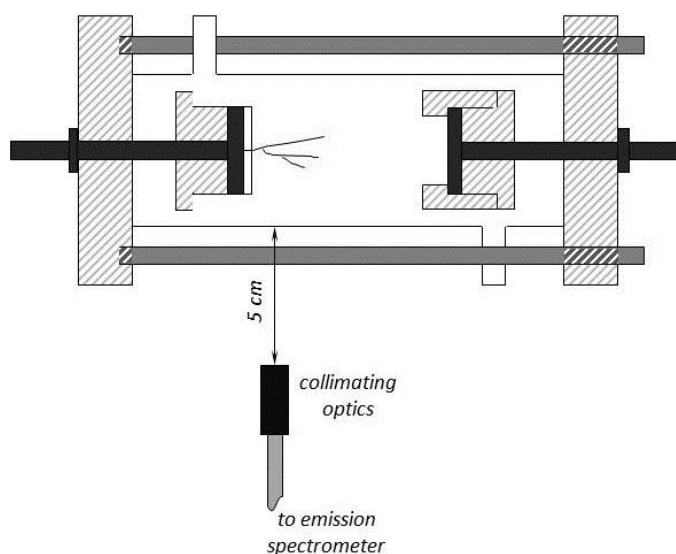


Figure 32. Placement of the optical equipment relating to the plasma reactor (the plasma reactor is described in Chapter 2.2.1)

3.2.1.2. Optical equipment

The block scheme of the experimental setup used for the plasma diagnostics is shown in figure 33.

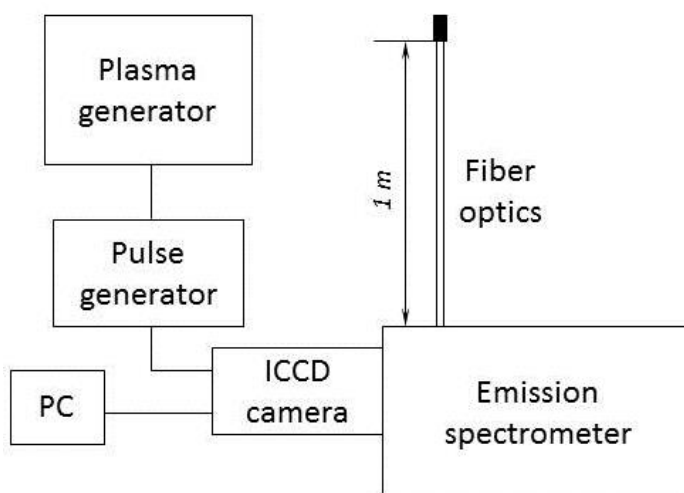


Figure 33. Block scheme of experimental setup

An iStar ICCD camera (DH734-18U-03, Andor, USA) was used to record ICCD images of the electric discharges. The active pixel size is 1024×1024 with the effective area of $13 \times 13 \mu\text{m}$. The camera has an ultimate temporal resolution of 1.2 ns (a minimal camera gate width) and a spectral response of 120 – 1090 nm. A quartz lens was used to focus the discharge gap to the photocathode. For the time-resolved ICCD imaging, a multichannel plate (MCP, the diameter of 18 mm) gain of 100, CCD exposure time of 0.2 s, gate pulse width of 10 ns were used. The camera was triggered by a pulse generator (TGP 110 10MHz, Thurbly Thander Instruments, UK) connected to the plasma generator. Additionally to the ICCD imaging, the side-view discharge photographs were recorded with a digital camera Canon EOS 400D.

For spectroscopic measurements, the ICCD camera was connected to a Shamrock spectrometer (SR-303i, Andor, USA). The spectrometer has a spatial and temporal resolution of 0.1 nm and 1.2 ns, respectively. The dimensions of the optic fiber of the spectrometer are $1 \text{ m} \times 85 \mu\text{m} \times 1.9 \text{ mm}$ (length x width x height). The discharge spectra were recorded in accumulating mode (1000 accumulations) with the MCP gain of 100 and the exposure time of 0.02 s. The grating of 300 lines/mm was used to record the full spectra (200 – 900 nm) and the grating of 1200 lines/mm was

used to record the line profiles, where the high spectral resolution was required (e.g. for the determination of FWHM). The camera gate width and delay time varied depending on a single experiment, therefore, their values are indicated in the description of each measurement in the Results and Discussions subchapter.

The instrumental response function of the spectroscopic diagnostic system was determined independently using the scattered light from a HeNe laser. The line profiles at 632.8 nm with different entrance slits are shown in figure 34. The FWHM of the profiles were found by fitting the experimental profiles with a Gaussian function. The optimal resolution of 0.32 nm was obtained at a slit width of 10 μm . This value exceeds by ~ 3 times the quoted 0.1 nm resolution of the spectrometer. Thus, the main source of the instrumental broadening is the settings of the optical devices. As long as the spectral resolution at a 50 μm slit is 0.33 nm and at a 10 μm slit it is 0.32, the use of the 50 μm slit did not much deteriorate the spectral resolution. Therefore, the entrance slit of 50 μm was used for all optical measurements.

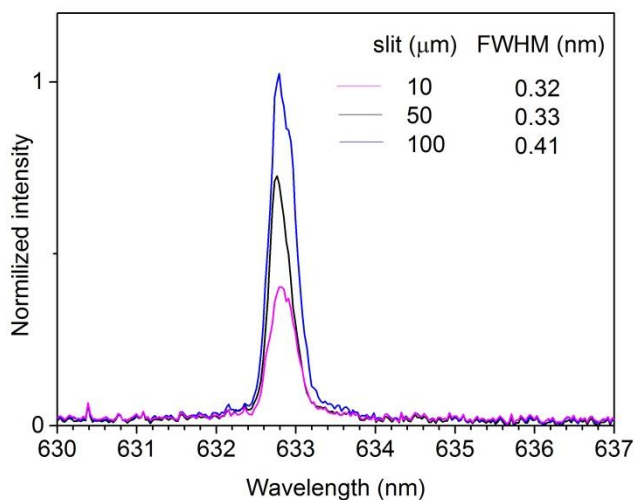


Figure 34. Calibration of the emission spectrometer with a HeNe laser

3.2.2. Determination of plasma parameters

3.2.2.1. Gas temperature measurements

The most usual way to determine plasma gas temperature is based on the investigation of line broadening. The thermal broadening of a spectral line is described by the Doppler effect (for H_α emission line):

$$\Delta\lambda_{1/2 D} = 7.16 \cdot 10^{-7} \cdot \lambda_0 \cdot \sqrt{T}, \quad (24)$$

where $\Delta\lambda_{1/2 D}$ is the full width at half maximum of the H_α line (nm); λ_0 is the H_α wavelength (nm); T is the plasma gas temperature (K). However, it appeared to be impossible to determine the plasma gas temperature in this way due to a large contribution of the Stark broadening in the experimental line profile caused by the high value of the electron density. Thus, the contribution of the Doppler effect in the H_α line broadening was neglected.

The use of the continuum radiation for the determination of the plasma gas temperature offers a number of advantages. For plasmas of high density, the continuum is optically thinner than the lines and its use, therefore, reduces systematic errors when self-absorption for lines becomes important.

Figure 29 shows the blackbody spectra for different plasma temperatures. As the temperature rises, the maximum is shifted to the region of short wavelengths according to the Wien's law, which consists in the linear dependency of the peak frequency from the temperature. Thus, the blackbody temperature of the plasma generated in the present study was found according to:

$$h\nu_{max} = 2.82kT_{bb} \quad (25)$$

or

$$\lambda_{max} = hc/2.82kT_{bb}, \quad (26)$$

where ν_{max} and λ_{max} are, respectively, the frequency (1/s) and wavelength (cm) at which the blackbody continuum reaches maximum; T_{bb} is the blackbody temperature

(K); k is the Boltzmann's constant; h is the Plank's constant. Although the real bodies emit less light than the blackbody at the same temperature, if the blackbody temperature is known, one can calculate a real temperature of a body. The corrected plasma gas temperature was found according to:

$$T = T_{bb} - \frac{\lambda T_{bb}^2 \ln \alpha_{\lambda,T}}{hc/k}, \quad (27)$$

where T is the real thermodynamic temperature (K); T_{bb} is the blackbody temperature (K), $\alpha_{\lambda,T}$ is the emissivity coefficient (for a blackbody is equal to 1, for the real bodies is < 1).

3.2.2.2. Electron density measurements

For the electron density determination, the Stark component of the line broadening was used. The Stark effect is caused by the influence of the electric field of the neighboring particles.

The plasma diagnostics is usually performed using H-Balmer lines. H_α has the highest intensity, but self-absorption of H_α line may lead to the overestimation of electron density. Therefore, H_β and H_γ emission lines are better candidates for more accurate plasma density and temperature measurements. However, in the present study the H_α emission line was used due to the low intensity of H_β and H_γ lines, which did allow their use for the electron density determination.

The electron density was calculated according to:

$$N_e = 8.02 \cdot 10^{12} \cdot \left(\frac{\Delta\lambda_{1/2}}{\alpha_{1/2}} \right)^{3/2}, \quad (28)$$

where N_e is the electron density (cm^{-3}), $\Delta\lambda_{1/2}$ is the full width at half maximum of the pure Stark component (\AA) and $\alpha_{1/2}$ is the fractional width from the line center ($\text{\AA}/\text{cgs}$ field strength units). The non-SI units of are taken from Griem *et al*, 1974, where $\alpha_{1/2}$ values are tabulated.

The values of $\Delta\lambda_{1/2}$ were found by subtraction of the background continuum and fitting the experimental H_α profile with a Voigt function. The deconvolution of

the fitted Voigt profile (equation 31) into the Lorentzian (Stark effect; equation 29) and Gaussian (instrumental function and Doppler effect; equation 30) components revealed the negligible effect of the latter one. Thus, in the present study, the Stark effect was shown to be the dominant mechanism of the H_α line broadening.

$$L(\lambda) = L_{max} \frac{W_L^2}{4(\lambda - \lambda_0)^2 + W_L^2} \quad (29)$$

$$G(\lambda) = G_{max} \exp\left(-\frac{4 \ln 2 \cdot (\lambda - \lambda_0)^2}{W_G^2}\right) \quad (30)$$

$$V(\lambda) = \int_{-\infty}^{\infty} G(\lambda - \lambda') L(\lambda') d\lambda', \quad (31)$$

where L_{max} and G_{max} are, respectively, Lorentzian and Gaussian peaks; W_L and W_G are, respectively, Lorentzian and Gaussian FWHM ($\Delta\lambda_{1/2}$).

3.2.3. Solution saturation with Ar and N₂

For the investigation of the effect of the dissolved gases on plasma characteristics, the aqueous solution was saturated with Ar and N₂. The gases were introduced into the flask filled with a solution at a pressure of 4 bar through a Teflon[®] tube (diameter of 8 mm) with a porous filter (the filter diameter is 10 mm, the pore diameter is 100 – 160 μm and the filter thickness is 2 mm). The gases were bubbled into the solution during 20 min prior to the electrical discharge generation. The solution circulation was used (as described in Chapter 2.2.) in order to transport the gas bubbles from the flask to the plasma reactor.

3.3. Results and discussions

3.3.1. Imaging diagnostic of electrical discharge

3.3.1.1. Discharge imaging

One of the most useful and obvious ways to trace the discharge behavior is to photograph it. The measurements of the discharge plasma with space resolution allow the determination of such parameters as the number of streamers, their length and branching, the volume of the active plasma zone. The investigation of the discharge properties by the imaging of the electrical discharges generated directly in liquids was performed by many authors (Ceccato *et al*, 2010, An *et al*, 2007). In order to trace the complete discharge path, long camera gates width should be used. In order to avoid the overlapping of multiple streamers, only one streamer per electric pulse was generated. For this, the ceramic coating (WAC500) with only one pinhole positioned at the center of the round electrode was used. The typical shape of the electrical discharge generated in a low-conductive solution (0.1 mS/cm) is shown in figure 35 with the counter electrode located on the right side. The image was recorded with a camera gate width of 1 s ($F = 1$ Hz, $U = 25$ kV, $d = 1.4$ cm), thus, the presented discharge image is time-integrated. The electrical discharge represents a filamentary streamer starting at the position of the pinhole on the HV-electrode. This discharge corresponds to the low-current discharge pulse. The discharge channel is split into three channels propagating towards the opposite electrode. As it could be seen from the figure, the partial discharge does not reach the opposite electrode. The average length of the longest visual streamer for $\sigma = 0.1$ mS/cm is (6 ± 2) mm (the average value is obtained by the analysis of 10 images). From this figure, one can clearly see the crisp plasma channels of white color surrounded by the diffuse magenta color, which originates from the emission of the excited hydrogen atoms.

Since the solution conductivity has a strong influence on the electric pulse characteristics, it would significantly influence the shape of the electrical discharge. The image of electrical discharge generated in solution of 1 mS/cm is shown in figure 36. The discharge structure significantly differs from the structure of the discharge generated in solution of 10 times lower conductivity (figure 35). The tips of the discharge channels depict a semicircle (for 2D imaging) or, which is more precise, a

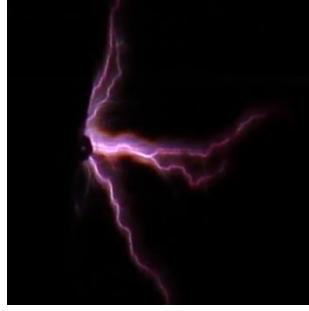


Figure 35. Image of the electrical discharge for $\sigma = 0.1$ mS/cm ($U = 30$ kV, $d = 1.4$ cm, camera gate width is 1 s). The image size is 11 x 11 mm

hemisphere (since the discharge is a 3D object) with a radius of (3 ± 1) mm (the average value is obtained by the analysis of 10 images). Since the streamer tips are the most active parts responsible for the propagation of the whole discharge, one can assume that the discharge propagation front in the conductive solutions has a hemispherical shape.

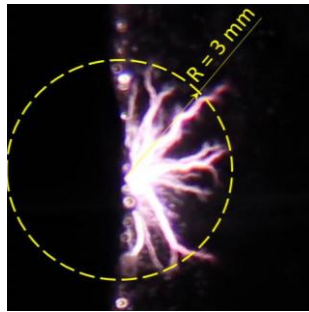


Figure 36. Image of the electrical discharge for $\sigma = 1$ mS/cm ($U = 30$ kV, $d = 1.4$ cm, camera gate width is 1 s). The image size is 8 x 8 mm

The effect of the solution conductivity on the discharge shape was investigated in a wide range of solution conductivities. The images of the electrical discharge generated in solutions of 0.1 – 10 mS/cm are shown in figure 37. It is clearly seen that the discharges generated in solution of high conductivity have more diffuse structure than the ones generated in low conductive solutions. As the solution conductivity increases, the discharge channels become more branched. It is explained by the fact that the higher current flows in solution of high conductivity, thus, supporting many daughter discharge filaments. The bush-like structure (i.e. high branching degree) of the discharge is observed for higher solution conductivity, whereas the tree-like structure (i.e. poor branching) occurs at low solution conductivity. Less daughter

filaments are formed and the discharge is composed mostly by from one to three main discharge channels propagating towards the opposite electrode.

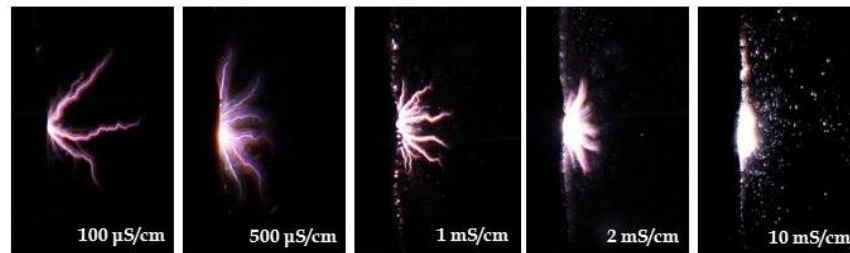


Figure 37. Effect of the solution conductivity on the discharge shape ($U = 30$ kV, $d = 1.4$ cm, camera gate width is 1 s). The size of each image is 10 x 16 mm

Solution conductivity also influences the streamer length. Streamers generated in low conductive solution are longer than the discharge radius of the bush-like discharge at high solution conductivity. It is explained by the faster current dissipation in the surrounding solution (Shih *et al*, 2011) when the ion concentration in solution is high. Additionally, the thickness and the brightness of the streamers increase with increase of solution conductivity. From the figure 37, it could be seen that the electrical discharge generation is accompanied by the formation of numerous micro-bubbles. This effect is more visible for high solution conductivities, where the more effective water vaporization takes place due to the higher current flow.

All electrical discharges discussed above are attributed to the partial discharges. When the electric field reaches a certain value, the full breakdown over the discharge gap may occur. The formation of the high current flow which connects both electrodes – spark discharge – is shown in figure 38. The image was recorded with the camera gate width of 1 s, applied voltage of 30 kV, electrode gap of 1.4 cm and solution conductivity of 0.1 μ S/cm (distilled water). The discharge channel of the spark is much thicker than the partial streamer discharge due to the much higher current flow in the electric circuit. The negative influence of spark discharges consists in the intense heating of the surrounding media, destruction of the electrode coating and the reactor walls. It originates from the fact that the plasma in sparks is tending to be thermal. Therefore, the formation of spark discharges must be avoided by applying lower voltage amplitude, increasing the electrode gaps and/or using higher solution conductivity (Yang *et al*, 2004).



Figure 38. Image of a spark discharge ($\sigma = 0.1 \mu\text{S/cm}$, $U = 30 \text{ kV}$, $d = 1.4 \text{ cm}$, camera gate width is 1 s). The image size is $13.5 \times 16 \text{ mm}$

3.3.1.2. ICCD imaging

As it was shown above by the discharge imaging, the shape of the electrical discharges varied from pulse to pulse. The discharge photography enables to obtain the spatial characteristics of electrical discharge, however, this method has limitations in terms of its application for determination of the time-resolved characteristics. A single shot per electric pulse is not enough to trace the temporal development of the discharge parameters. For the analysis of time-resolved discharge parameters, a very short camera gate width and, as a consequence, accumulation of the optical signal are required.

Figure 39 shows the time-resolved images of an electrical discharge with a counter electrode located on the right. The number of the accumulated shots was defined as a compromise between the necessity to obtain the reproducible optical signal of a considerably high intensity and to use the shortest possible camera gate width. Thus, the ICCD images presented in figure 39 were obtained by accumulating 1000 single-shots with a camera gate width of 10 ns for the discharge generated in solution of 2 mS/cm , 30 kV . The brightness scale for all images is the same. The sequence of images shows that the light emission is initially observed at the HV anode and becomes brighter during the first 50 ns . As it could be seen, the electrical discharge elongates towards the opposite electrode. The active plasma zone expands with time and reaches its maximum at $(50 \pm 10) \text{ ns}$ after the discharge inception, which is followed by the discharge attenuation during the following 500 ns . The plasma temperature is not constant inside the discharge channel as its maximal value occurs in the middle of the active plasma volume, which occupies a few mm. The discharge light intensity and, consequently, the plasma temperature decrease moving from the discharge center towards the opposite electrode. It should be noted that the region of the highest emission intensity does not change its position with time.

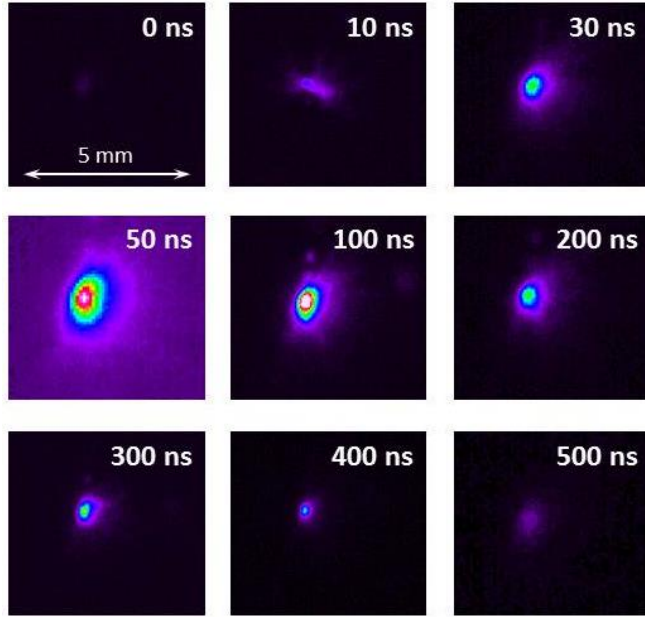


Figure 39. Time-resolved ICCD camera images of an underwater electrical discharge. Solution conductivity is 2 mS/cm, voltage pulse amplitude is 30 kV, electrode gap is 1.4 cm, camera gate width is 10 ns. HV electrode is located on the left side and grounded electrode is on the right side. The size of each image is 6 x 6 mm

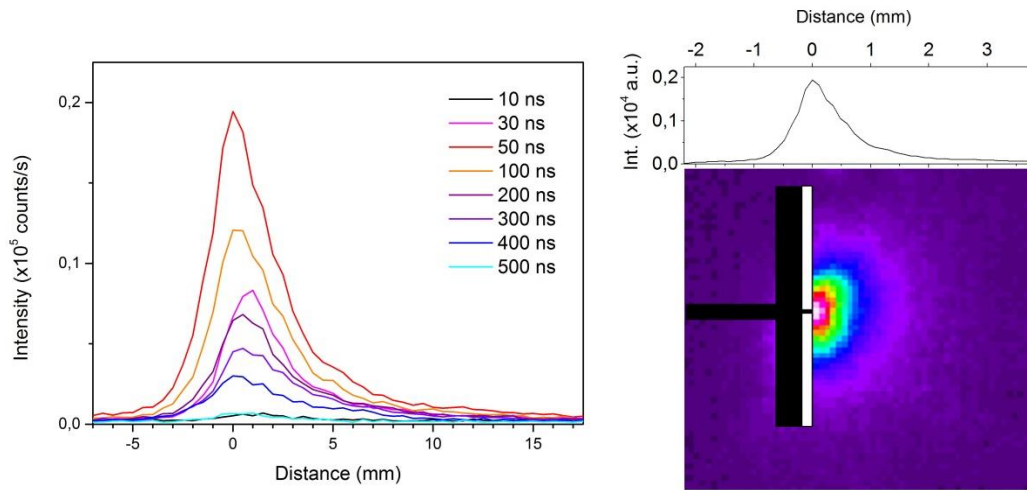


Figure 40. Time-resolved profiles of the discharge light collected in the range of 120 – 1090 nm ($\sigma = 2$ mS/cm, $U = 30$ kV, $d = 1.4$ cm, camera gate width is 10 ns), left image. An ICCD image (at 50 ns) and the corresponding discharge light profile, right image

In order to analyze the spatial discharge parameters, the full vertical binning operation was used. The integral emission profiles of the discharge light plotted

against the distance are shown in figure 40. The 0 mm on the X-axis was taken as the location of the maximal intensity of the discharge light. The length of the active plasma zone was determined as the distance at which the emission intensity of the light profile at 50 ns (maximal discharge intensity) decreases by 90% and estimated to be of (1.7 ± 0.5) mm. The discharge propagation velocity is approximately constant, as the emitting diameter expands linearly with time, and is estimated to be of (30 ± 10) km/s. These values are in agreement with previously reported values of the emitting diameter and propagation velocity for liquid phase discharges (Akiyama *et al*, 2000, An *et al*, 2007, Nieto-Salazar *et al*, 2005).

3.3.2. Discharge continuum

3.3.2.1. General view

A typical emission spectrum of underwater electrical discharge obtained in the present study is shown in figure 41. It represents a continuous spectrum with some atomic lines merged into it (OH line at 309 nm and H $_{\alpha}$ line at 656 nm). The spectrum occupies the entire optical range of the electromagnetic radiation. No line spectrum which could be attributed to the formation of plasma in non-thermal conditions was observed in the present study under any conditions. Thus, the continuous spectrum obtained in this study evidences the formation of plasma in thermal conditions.

Since the amount of light emitted by the discharge directly influences the discharge applicability for organics removal, it is very important to investigate the influence of different experimental parameters on the total light intensity. For this, the integral discharge light intensity was used as an evaluating parameter. In this chapter, the effect of the solution conductivity and the applied electric field on the integral discharge light intensity is discussed. Additionally, the temporal evolution of the discharge continuum is investigated.

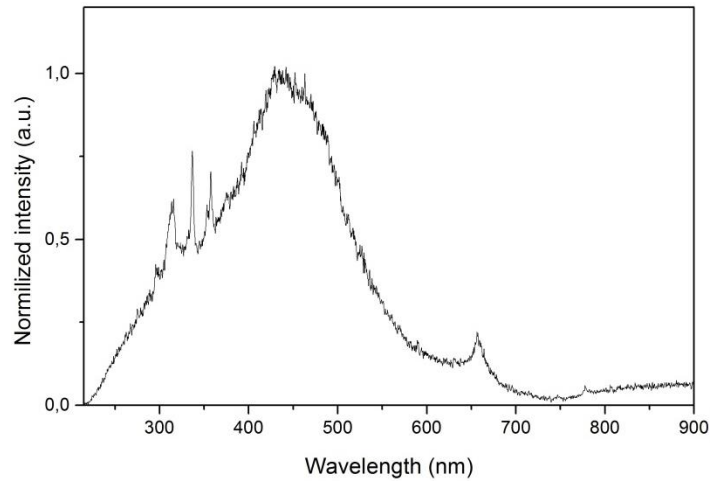


Figure 41. Continuous spectrum of underwater electrical discharge

3.3.2.2. Effect of the solution conductivity

The effect of the solution conductivity on the discharge intensity is shown in figure 42. The discharge continua were recorded with a camera gate width equal to the continuum duration, i.e. 500 ns and 1400 ns for solution conductivities of 2 mS/cm and 0.5 mS/cm, respectively (the determination of the duration of discharge continuum is discussed in Chapter 3.3.2.4.).

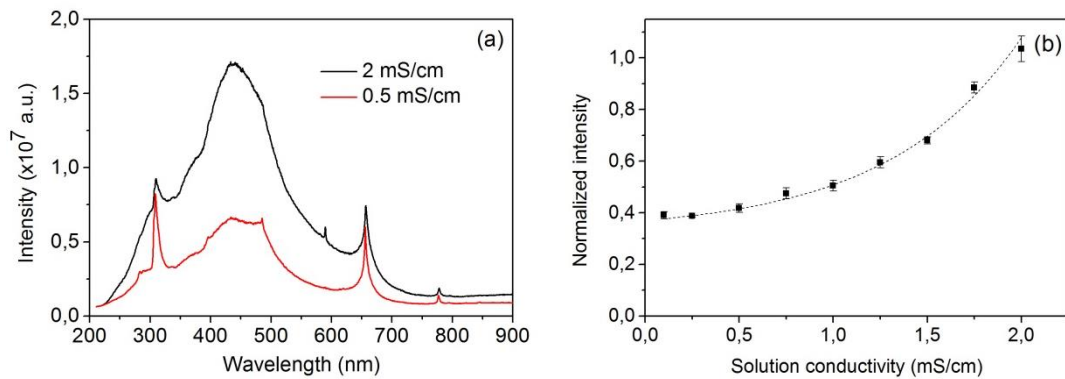


Figure 42. Effect of the solution conductivity on the discharge intensity ($U = 30$ kV, $d = 1.4$ cm, camera gate width is equal to the continuum duration): (a) – comparison of the discharge continua for 2 and 0.5 mS/cm; (b) – normalized integral intensity as a function of solution conductivity

The shape of the spectrum is affected by the solution conductivity (figure 42(a)) as the weaker continuum intensity is observed at low conductivity. The line

emissions become more distinct at lower solution conductivity, where the discharge continuum is less intense.

The total discharge light intensity was calculated by integrating the continuum (from 200 to 900 nm) and plotted in figure 42(b) for different values of solution conductivity. The highest integral intensity obtained in this experiment (for $\sigma = 2$ mS/cm) was taken as 1. The discharge light intensity increases with increase of solution conductivity. Thus, the discharges generated in solution of 2 mS/cm are characterized by ~2.5 higher light intensity than the discharge generated in solution of 0.1 mS/cm. It is explained by the higher discharge current flow in solution with higher conductivity, where more charged species are available. This tendency is non-linear as the faster increase of the discharge continuum intensity is observed for the high values of solution conductivity. In the measured range of σ values, the experimentally obtained data were fitted with function $I = 0.32 + 0.02 \cdot \exp((\sigma + 0.85)/0.78)$, where I is the normalized intensity and σ is solution conductivity (mS/cm). However, it is hardly possible to predict the shape of the dependency for the lower σ values (< 0.25 mS/cm) as no electrical discharge took place in the low conductive solutions and, therefore, no light emission could be detected (Chapter 2.3.2.3). The non-linear shape of the dependency could be explained by the fact that solution properties (C_s and R_s , figure 9) make different effect on the total capacity and resistivity of the system depending on solution conductivity.

3.3.2.3. Effect of the electric field strength

The effect of the average electric field strength (AEFS) on the discharge continuum is shown in figure 43 for solution conductivity of 2 mS/cm and a camera gate width of 500 ns.

The increase of the AEFS has no influence on the shape of the discharge continuum, but only affects the continuum intensity. The values of the integrated continuum intensity are plotted against the AEFS values in figure 43(b). The increase of the continuum intensity by ~3 times is observed when the AEFS is increased from its minimal value (9.26 kV/cm) to the maximal value (28.84 kV/cm). The observed effect is explained by the higher discharge energy in the case of the pulse energy. The experimentally obtained data were fitted with function $I = -0.048 + 0.036 \cdot x$, where I is the normalized intensity and x is the average electric field strength (kV/cm). Unlike in

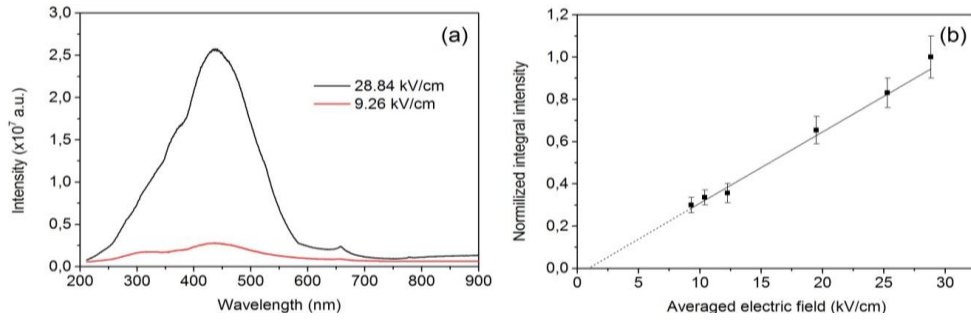


Figure 43. Effect of the averaged electric field strength on the discharge intensity ($\sigma = 2$ mS/cm, camera gate width is 500 ns): (a) - comparison of the discharge continua for 28.84 kV/cm and 9.26 kV/cm; (b) – normalized integral intensity as a function of averaged electric field strength

the effect of solution conductivity, the effect of the AEFS on the discharge continuum is constant in the tested range of AEFS values. Although the experimentally obtained values of intensity were fitted with a straight line, the behavior of this dependency near lower and higher AEFS values is different. As it was shown in Chapter 2.3.2.2, at $\text{AEFS} < 9$ kV/cm no electrical discharge takes place, therefore, the discharge light intensity is tending to be zero. At $\text{AEFS} > 29$ kV/cm, transition to spark discharge takes place, which significantly increases the light intensity. Thus, the extrapolation of the fitted straight line to the lower or higher AEFS values does not reflect the real shape of the dependency out of the tested range of AEFS.

3.3.2.4. Temporal evolution of discharge continuum

The shape and intensity of the discharge continuum change in time. In order to trace it, the time-resolved emission spectroscopy was employed. Figure 44 represents the time-resolved discharge continuum ($\sigma = 2$ mS/cm, $U = 30$ kV, $d = 1.54$ cm). The camera gate width was chosen as a compromise between the necessity to record the spectra of considerably high intensity and, at the same time, the necessity to have the highest possible temporal resolution. Thus, the measured continuous spectra were recorded with a camera gate width of 10 ns and a step of 50 ns (for the time range of 0 – 50 ns, the step was 10 ns).

The time moment of the first light emission was taken as 0 ns. Intensity of the discharge continuum reaches its maximum within the first 50 ns. The following continuum attenuation with time takes a few hundred ns. The discharge continuum duration was determined as the time during which the integral intensity decreases to 10% of its maximal value (at 50 ns) and was found to be of 500 ns (for $\sigma = 2$ mS/cm).

The discharge continuum duration (i.e. discharge duration) was found to be dependent on the solution conductivity. It increases with decrease of solution conductivity. Thus, the light emission from the electrical discharge generated in solution of 2 mS/cm lasts 500 ns and in solution of 0.5 m/cm the discharge duration is 1400 ns. It is explained by the longer electric pulse duration for lower solution conductivities discussed in Chapter 2.3.2.3.

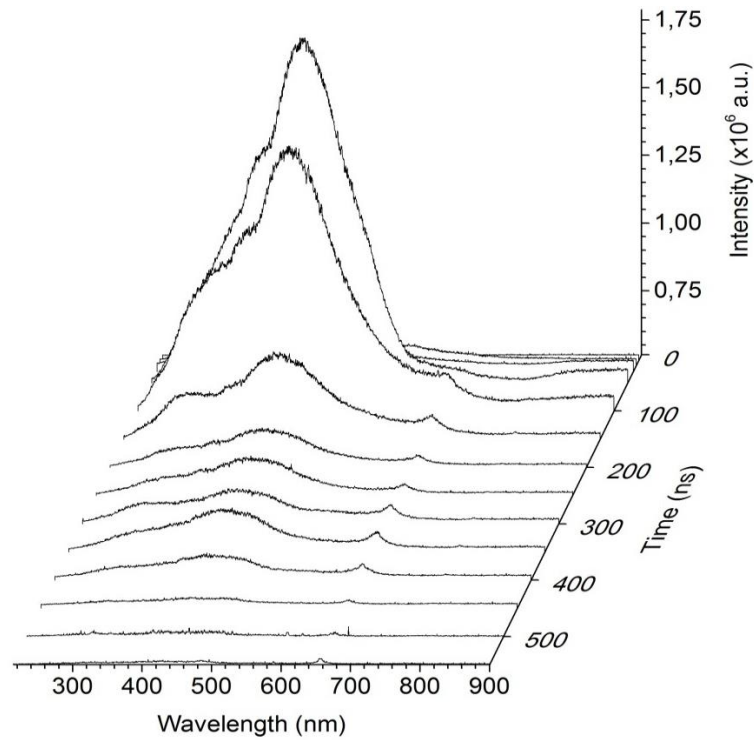


Figure 44. Time-resolved discharge continuum ($U = 30$ kV, $\sigma = 2$ mS/cm, $d = 1.54$ cm, camera gate width is 10 ns)

The temporal evolution of the integral discharge light intensity is compared with the corresponding voltage and current waveforms in figure 45 for $\sigma = 2$ mS/cm. The evolution of the discharge light (red) was obtained by collecting the total light in the range of 200 – 900 nm during 10 ns with the step of 50 ns. The light profile is narrower than the corresponding voltage pulse, but, in general way, it follows the shape of the voltage pulse. The moment of the first light emission lies on the rising slope of the voltage waveform and corresponds to the rapid increase of the discharge current. It is followed by the rapid increase of the discharge light intensity alongside with the further increase of voltage and current. The maximal discharge light emission

(50 ± 10 ns) coincides with the current maximum. At this point the discharge development reaches its maximum. The following attenuation of the discharge intensity can be divided into two parts: the rapid decrease of intensity, which occurs from (50 ± 10) ns till (200 ± 10) ns; and a more gradual decrease, which lasts from (200 ± 10) ns till (500 ± 10) ns. No light emission is observed after 500 ns. The most active phase of the discharge, during which the most intense light is emitted, thus, occurs for (200 ± 10) ns (i.e. from 0 ns to 200 ns, $\sigma = 2$ mS/cm).

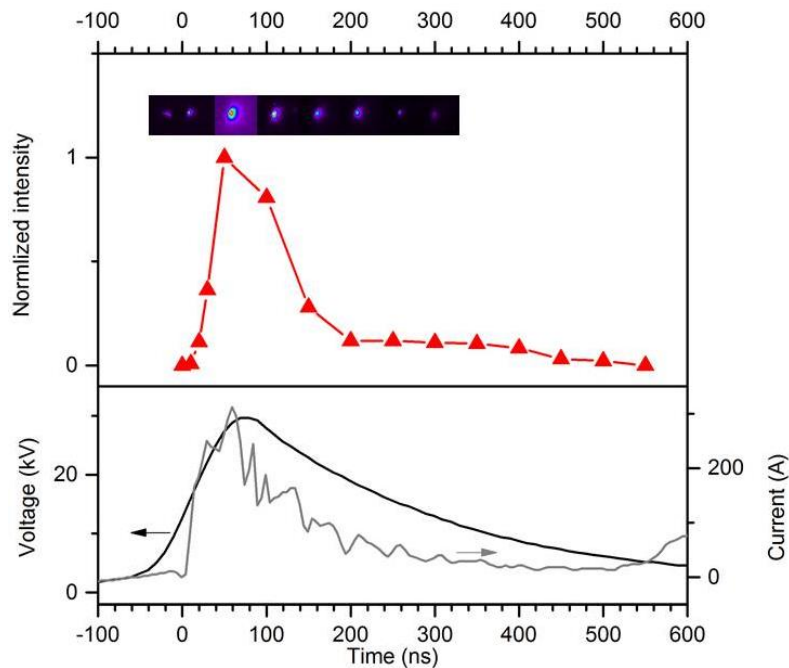


Figure 45. Temporal evolution of the discharge light. Top image is the integral light intensity (normalized) with the corresponding ICCD images; bottom image is the current and voltage waveforms for $\sigma = 2$ mS/cm, $U = 30$ kV

The beginning of the discharge light emission is independent on solution conductivity as the start of the optical emission occurs at the same time in the whole tested range of solution conductivity (0.1 – 2 mS/cm). However, the discharge light duration was found to be dependent on solution conductivity. Figure 46 represents the effect of the solution conductivity on the discharge light duration. The high solution conductivity leads to the shortening of the discharge light duration. It is explained by the shortening of the corresponding electric pulse for higher solution conductivity. Thus, the duration of the discharge light was found to be 500 ns, 1100 ns and 1400 ns

for solution conductivities of 2 mS/cm, 1 mS/cm and 0.5 mS/cm, respectively. Thus, the relation between the discharge light duration (t_{light} , ns) and solution conductivity (σ , mS/cm) is expressed by $t_{light}=1700-600\cdot\sigma$ in the measured range of σ values. However, the lack of data in this experiment does not allow the unambiguous conclusion on the shape of the dependency in the wider range of σ values.

It should be noted that the decrease of the discharge intensity which follows the maximum (figure 46), is not as rapid for low solution conductivity, as it is for high solution conductivity. It indicates that in the case of the less conductive solutions, the discharge power is spread in time, whereas in the case of highly conductive solutions, it is released during the considerably shorter period of time. Additionally, the discharge light (as well as the discharge power) was shown above to increase with increase of solution conductivity (figure 42). These two facts allow to suggest that the discharges generated in highly conductive solutions are characterized by a higher power and consequently a higher plasma density.

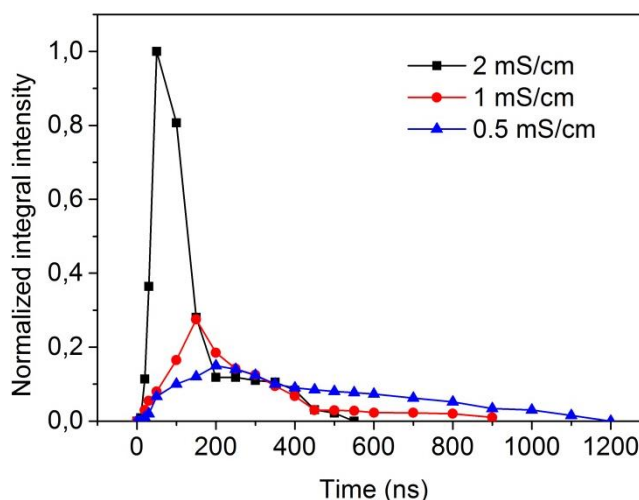


Figure 46. Effect of the solution conductivity on the discharge light duration

3.3.3. Post-discharge emission spectrum

3.3.3.1. Reactive species and the respective emission lines

After the continuum radiation of electrical discharge ceases, a number of reactive radicals are formed in the bulk solution. It results in the post-discharge line spectrum presented in figure 47. The spectrum dominated by the strong emission lines:

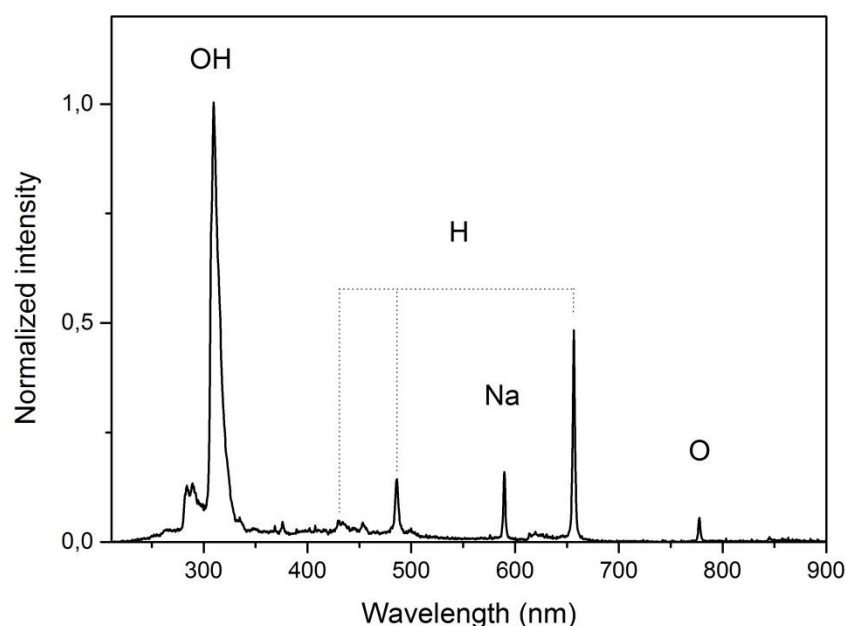


Figure 47. Post-discharge emission spectrum of reactive species ($\sigma = 2$ mS/cm, $U = 30$ kV, camera gate delay is $5.2 \mu\text{s}$, camera gate width is $2.5 \mu\text{s}$)

1. The peaks in the middle ultraviolet region are due to the emission of hydroxyl radicals:
 - $A^2\Sigma^+ (\nu = 1) \rightarrow X^2\Pi (\nu = 0)$ transition at 282 nm
 - $A^2\Sigma^+ (\nu = 0) \rightarrow X^2\Pi (\nu = 0)$ transition at 309 nm
2. The peaks in the visible regions – atomic hydrogen lines – are responsible for the magenta color around the discharge channel: H_γ at 434 nm, H_β at 486 nm, H_α at 656 nm.
3. Sodium atomic emission line at 588 nm is observed in highly conductive solutions (for $\sigma > 1$ mS/cm).
4. The peaks of the atomic oxygen in the infrared region:
 - $3p^5P^0 \rightarrow 3s^5S^0$ transition at 777 nm
 - $3p^3P \rightarrow 3s^3S^0$ transition at 844 nm

These results are in agreement with the previously reported set of radicals formed by the electrical discharges in water (Sun *et al*, 1997, Ono *et al*, 2002, Su *et al*, 2002, Bruggeman *et al*, 2009a, Sunka *et al*, 1999).

The post-discharge emission spectrum demonstrates the formation of reactive species by underwater electrical discharge, thus, evidencing a great chemical activity of underwater plasma. The hydrogen atom is an important species in the radiation chemistry of acidic solutions, where it is the major reducing radical ($E_{\text{red/ox}} = -2.3$ V).

With organic compounds it reacts by abstracting H atoms from saturated organic molecules.

The hydroxyl radical is a powerful oxidant having the oxidation potential of 2.82 V. It behaves as an electrophile in the reactions with organic molecules. OH[•] readily adds to unsaturated bonds. Although OH[•] and H[•] undergo similar types of reaction with organic molecules, OH[•] is less selective and more reactive than H[•].

Although it is assumed that the solvated electron is present in the list of the primary species, its formation was not detected in the present study due to its short lifetime (a few ps).

The line of the atomic oxygen is more often observed when electrical discharge is generated in gases or in the O₂ bubbles. For the liquid phase discharges, the line of the excited oxygen can originate either from direct breakdown of the oxygen dissolved in water or from the water splitting by energetic electrons in plasma (table 4).

The experimental conditions (AEFS and solution conductivity) determine such features of the post-discharge emission spectrum as the number of emission lines, their intensity and decay time of the respective species. The radical line intensity is proportional to the number of the species (Sun *et al.*, 1997):

$$I_{ij} = \nu_{ij}hcA_{ij}N_i, \quad (32)$$

where $\nu_{ij}hc$ is the energy of each light quantum of a wave number ν_{ij} emitted in the transition, A_{ij} is the transition probability from energy state i to energy state j , N_i is the number of radicals in the energy state i . Thus, analysis of the radical line intensity enables to estimate the number of the species in the excited state.

For the spectroscopic measurements of the reactive species, the collimating optics was positioned as shown in figure 32. Additionally, the measurements were performed with the collimating optics positioned near the opposite electrode, so that it enabled to measure the radical emission far from the discharge spot. The emission spectra obtained in the two ways did not differ from each other, neither did the line intensity change its value. It suggests that the radical formation takes place not only in the plasma discharge zone, but also in the entire volume of the discharge gap. Since the plasma discharge zone has a very small volume (see Chapter 3.3.1.), the formation

of reactive species by electron impact and/or water thermolysis can only take place near the HV electrode. Thus, it is assumed that the water photolysis is a dominant mechanism of water splitting as the UV light may penetrate into the bulk solution, leading to the formation of the reactive species (Lukes *et al*, 2008).

3.3.3.2. Effect of the solution conductivity

Figure 48 shows the effect of solution conductivity on the reactive species formation. The figure represents the comparison of post-discharge emission spectra for 2 and 0.5 mS/cm. In order to provide the adequate comparison of the emission signal of the reactive radicals, one needs to collect the light emitted during the entire emission time which is dependent on the solution conductivity. The lifetime of the radicals in the excited state was determined by the time-resolved analysis and will be discussed below. The compared spectra of solution conductivities of 2 and 0.5 mS/cm were taken with the camera gate width of 3 and 18 μ s, respectively. In order to record the radical light emission without the continuum light, the camera gate delays equal to the continuum duration and the camera gate widths equal to the duration of radical emission were used.

The spectrum at lower solution conductivity is characterized by the higher intensity of the emission lines (apart from the Na emission line). Taking into account the relation between the emission intensity and the number of the emitting species (equation 32), one can assume that significantly higher amount of the species in the excited state are present in the solution of lower conductivity. Figure 48(b) shows the change of integral emission intensity (obtained by integration of the respective emission peak by wavelength) of the OH (309 nm), H $_{\alpha}$ (656 nm) and O (777 nm) emission lines depending on solution conductivity. The highest intensity of each radical line was taken as 1 and compared with all others for clarity.

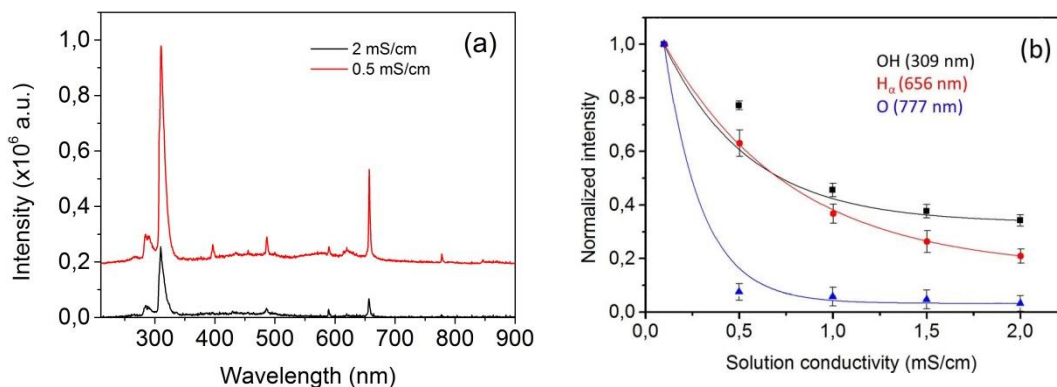


Figure 48. Effect of the solution conductivity on the radical formation by electrical discharges ($U = 30$ kV, $d = 1.4$ cm, camera gate width is equal to the duration of the radical emission): (a) – comparison of the post-discharge emission spectra for $\sigma = 2$ and 0.5 mS/cm; (b) – normalized radical intensity as a function of solution conductivity

The intensity of all emission lines decreases with increase of solution conductivity and the tendency is non-linear. The faster increase of the radical emission intensity is observed for the lower values of solution conductivity, suggesting that the less conductive solution, the bigger is the influence of solution conductivity on the radical line intensity. From the figure it can be seen that the relations between line intensity and solution conductivity are close to exponential functions. The obtained values were fitted with functions $I=0.33+0.67 \cdot \exp((\sigma-0.1)/0.45)$, $I=0.16+0.84 \cdot \exp((\sigma-0.1)/0.68)$ and $I=0.03+0.97 \cdot \exp((\sigma-0.1)/0.2)$ for, respectively, OH (309 nm), H_{α} (656 nm) and O (777 nm) emission lines (where I is normalized intensity and σ is solution conductivity (mS/cm)).

In general, the intensity of all emission lines decreases with increase of solution conductivity. There are two reasons to the decrease of the line intensity in solutions with high conductivity: (i) the lower probability of the light emission by the excited species during the transition from the excited to ground state (i.e. lower quantum yield); (ii) the lower number of the species in the excited state. The first assumption is explained by the formation of complex between the excited species and quenchers (quenching), which changes the properties of the initial species. The second assumption is explained by the fact that at high solution conductivity less species transit to the excited state.

The shape of dependency of the radical line intensity from solution conductivity is affected by the discharge light intensity and/or by the quenching of the species. It is assumed that conditions that lead to the higher discharge light intensity

should lead to the higher radical formation rates as more energy is available for the transition of the radicals to the excited state. The increase of solution conductivity was shown to lead to the more intense light radiation. Therefore, one could assume that at high solution conductivities, more intense radical emission should be observed. However, an opposite effect of solution conductivity on the radical formation was obtained.

The obtained trend of the decrease of the radical line intensity with increase of solution conductivity could be explained by the more intense quenching effect in more conductive solutions which was also observed by Shih *et al*, 2011 and Sun *et al*, 1997. The authors suggested that the decreased number of radicals in the excited state in solutions with high σ values could be explained by with higher ion concentration. Additionally, the faster quenching could take place due to the increased plasma temperature in highly conductive solutions. Thus, on the basis of the obtained in the present study results one may conclude that it is quenching rather than the discharge light intensity that has a stronger influence on the amount of the radicals in the excited state.

3.3.3.3. Effect of the electric field strength

Figure 49 shows the effect of the AEFS on the emission spectrum of reactive species formed by underwater electrical discharge for solution conductivity of 0.5 mS/cm. The camera gate width was 18 μ s, which is equal to the lifetime of the OH \cdot for the given solution conductivity. As it could be seen from the figure 49(a), the change of the AEFS does not significantly influence the shape of the spectra. The intensity of all emission lines increases with increase of the applied electric field. It could be explained by the more intense discharge light due higher energy input at higher AEFS values. Figure 49(b) demonstrates the dependence of the integral intensity of the OH (309 nm), H α (656 nm) and O (777 nm) emission lines from AEFS. The experimentally obtained data were fitted with functions $I = -0.28 + 0.09 \cdot x$, $I = -0.25 + 0.09 \cdot x$ and $I = -0.51 + 0.11 \cdot x$ for, respectively, OH (309 nm), H α (656 nm) and O (777 nm) emission lines (where I is the normalized integral intensity of emission line and x is the average electric field strength (kV/cm)). The higher magnitude of AEFS was shown to lead to the higher discharge intensity. Thus, at high AEFS values, more energy is available for the excitation of the species. It results in the

higher amount of the radicals in the excited state and, consequently, in the higher radical line intensity.

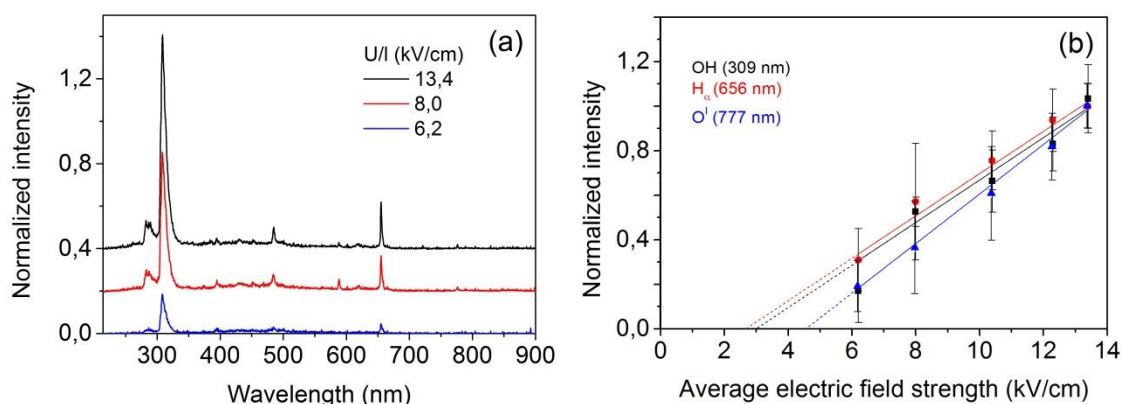


Figure 49. Effect of the average electric field strength on the radical formation by electrical discharges ($\sigma = 0.5$ mS/cm, $U = 30$ kV, a camera gate width is 18 μ s): (a) – comparison of the post-discharge emission spectra for 13.4, 8.0 and 6.2 kV/cm, the spectra are normalized and vertically shifted for clarity; (b) – normalized radical intensity as a function of average electric field strength

As it is shown in figure, the experimentally obtained data were fitted with straight lines. However, in the range of low values of AEFS no electrical discharge takes place and, therefore, no reactive radicals could be formed. It suggests that the shape of the dependency differs from straight line and the following extrapolation with the fitted lines to the lower AEFS is not reasonable.

3.3.3.4. Temporal evolution of reactive species

Depending on solution conductivity, electrical discharges were shown to emit light during the time of up to ~ 1.5 μ s. Formed by the electrical discharge reactive species (OH^\bullet , O^\bullet , H^\bullet) were found to have different lifetime. Additionally, their lifetime is dependent on solution conductivity.

Figure 50 shows an example of the temporal evolution of the OH emission line for solution conductivity of 1 mS/cm and the AEFS of 20 kV/cm. The spectra were recorded with a short camera gate width of 50 ns. The spectral line profiles at different times were integrated and the highest value was taken as 1. The lifetime of the radicals in the excited state was determined by the decrease of the normalized integral intensity by 50%. The H_α and O emission lines were treated in the same way

as the OH emission line. The results are summarized in figure 51 for solution conductivities of 0.5 mS/cm, 1 mS/cm and 2 mS/cm (figure 51 (a), (b) and (c), respectively). Independently on solution conductivity, all three cases show the same trend: the fastest decay was determined for O emission line and the most long-lived specie appeared to be the excited OH radical. The experimentally obtained data were fitted with the following functions:

for $\sigma=0.5$ mS/cm (figure 51(a)):

- OH (309 nm): $I = -0.54 + 1.07 \cdot \exp(-(t-4.54)/8.7)$
- H_α (656 nm): $I = -0.23 + 1.26 \cdot \exp(-(t-0.93)/5.5)$
- O (777 nm): $I = -0.02 + 0.95 \cdot \exp(-(t-0.04)/1.7)$

for $\sigma=1$ mS/cm (figure 51(b)):

- OH (309 nm): $I = -1.07 + 1.45 \cdot \exp(-(t-2.45)/6.4)$
- H_α (656 nm): $I = -0.38 + 1.2 \cdot \exp(-(t-0.4)/2.9)$
- O (777 nm): $I = 0.03 + 0.98 \cdot \exp(-(t+0.02)/0.45)$

for $\sigma=2$ mS/cm (figure 51(c)):

- OH (309 nm): $I = -0.28 + 1.2 \cdot \exp(-(t-0.13)/1.42)$
- H_α (656 nm): $I = -0.06 + 0.99 \cdot \exp(-(t-0.02)/0.7)$
- O (777 nm): $I = -0.01 + \exp(-(t-0.001)/0.27)$

where I is the normalized integral intensity and t is the time (μ s).

From the figure it can be seen that the obtained data could be fitted with more than one exponential function. This would suggest the transition of the excited species to the ground state in more than one direction. However, the presented fitting of each set of data with one exponential function indicates the domination of one process over all others that could possibly take place. In general, the exponential decay of radical line intensity in time indicates the first order decay kinetics of the excited species formed in water by electrical discharges.

Table 5 summarizes the time constants which characterize the decrease of the radical line intensity in time by 1/e times. The values reflect the lifetime of the respective species in the excited state. The lifetimes of the radicals in the excited state were determined to occur on a μ s timescale and vary depending on solution conductivity. The values increase with decrease of solution conductivity. As it was discussed above, the increase of solution conductivity could make two opposite effects on the chemical activity of electrical discharge. On the one hand, higher solution conductivity leads to the more intense discharge light resulting in higher

amount of the species in excited state, which should have led to the higher radical line intensity. However, the observed decrease of radical line intensity suggests that in the present experiment the effect of the quenching in solutions with high conductivity predominates. The latter leads either to the smaller amount of the species in excited state or to the lower probability of light emission during the transition to the ground state.

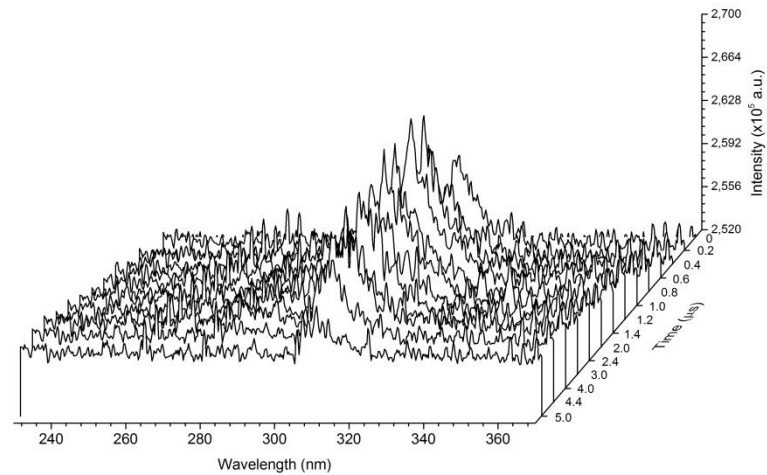


Figure 50. Temporal evolution of the OH emission line (309 nm) ($\sigma = 1$ mS/cm, $U = 30$ kV, $d = 1.4$ cm, camera delay time is 1100 ns, camera gate width is 5 μ s)

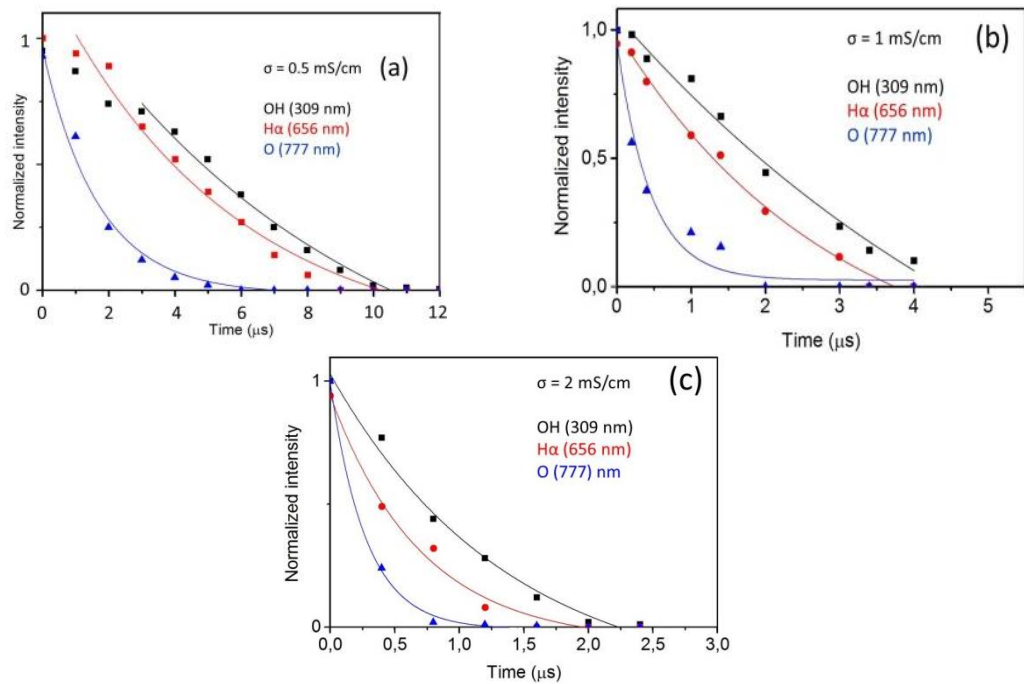


Figure 51. Evolution of radical line intensity in time depending on solution conductivity ($U = 30$ kV, $d = 1.4$ cm): (a) – 0.5 mS/cm, (b) – 1 mS/cm, (c) – 2 mS/cm

Table 5. Mean lifetime of reactive species in excited state (μs)

	0.5 mS/cm	1 mS/cm	2 mS/cm
OH (309 nm)	8.70	6.40	1.42
H $_{\alpha}$ (656 nm)	5.50	2.90	0.70
O ^I (777 nm)	1.70	0.45	0.27

3.3.3.5. Effect of the solution saturation with gases

A line spectrum of reactive species produced during the electrical discharge when feeding with nitrogen is shown in figure 52 for $\sigma = 2$ mS/cm, $U = 30$ kV, $d = 1.4$ cm. The upper image represents the full spectrum recorded from 200 to 900 nm (with a grating of 300 lines/mm) and the lower image is the detailed spectrum of the region of the most intense N emission lines recorded with a higher spectral resolution (with a grating of 1200 lines/mm). The emission spectrum is composed of the OH, H $_{\alpha}$ and O emission lines. Additionally, some N lines that were previously reported in literature (Keller *et al*, 2012, Rajasekaran *et al*, 2011) are observed in the near UV and visible spectral regions:

1. N $_2^*$ at 337.1 nm
2. N $_2^*$ at 380.0 nm
3. N $_2^+$ at 391.4 nm
4. N $_2^+$ at 427.0 nm

The addition of N $_2$ into the water exposed to plasma discharges made no influence on the lifetime of the OH, H and O radicals. The lifetime of N $_2^+$ was determined in the same way as for OH radical and estimated to be of ~ 10 μs ($\sigma = 2$ mS/cm). The emission intensity of the OH line was significantly increased when the solution was saturated with N $_2$.

A line spectrum of reactive species produced by the electric discharge when saturating with Ar is shown in figure 53. The experimental conditions and the camera settings were the same as in case of N $_2$ bubbling. As well as the spectrum without gas addition, it is dominated by OH, H and O emission lines. The Ar emission lines are

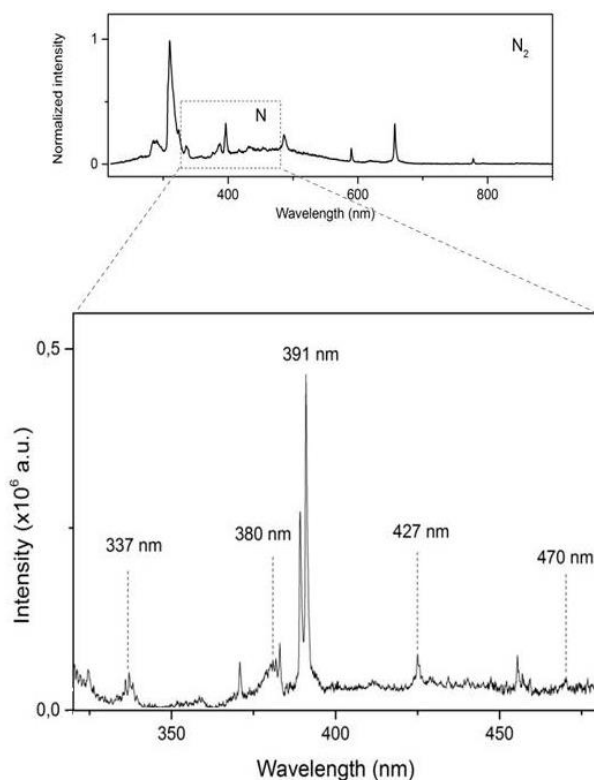


Figure 52. Effect of the solution saturation with N_2 on the post-discharge emission spectrum. Top image is the full spectrum of reactive species recorded with low resolution (grating of 300 lines/mm); bottom image is the (320 – 480) nm spectral region recorded with high resolution (grating of 1200 lines/mm); $\sigma = 2$ mS/cm, $U = 30$ kV, $d = 1.4$ cm, camera gate delay and camera gate width are 500 ns and 10 μ s, respectively

not visible in the spectrum as the region of the most intense Ar lines (650 – 900 nm, Shih *et al*, 2011) is composed only by H_α at 656 nm and O at 777 nm emission lines. The possible reasons could be: (i) inefficient amount of the dissolved Ar in water due to the poor solubility; (ii) low intensity of the emission lines due to the poor excitation of Ar molecules by plasma. In most studies dealing with underwater electrical discharge generation using the gas bubbling, the tested gases are introduced directly into the discharge gap (Shih *et al*, 2011, Sahni *et al*, 2006, Nikiforov *et al*, 2011). It provides the immediate contact of the dissolved gas bubbles with plasma, which is known as “discharge in gas bubbles”. In the present study, Ar and N_2 were introduced far from the reactor chamber and, therefore, needed to be transported to the plasma reactor. Such operation could not be attributed to the discharge in gas bubbles. Thus, the generation of electrical discharge in aqueous solution saturated with gases has led to different results compared to the literature. Since the solubility of Ar is three times

higher than of N₂ (62 mg/L and 20 mg/L, respectively) and the N₂ emission lines were observable in the spectrum, an assumption was made that the reason of absence of the Ar lines should be rather its poor excitation by plasma than the poor solubility in water. Since the mean excitation energy (I) of argon is approximately two times higher than that of nitrogen, (I(Ar) = 188 eV and I(N) = 82 eV, (Caso *et al*, 1998) and (Dalgarno *et al*, 1969), respectively) the excitation of argon by plasma should be less probable.

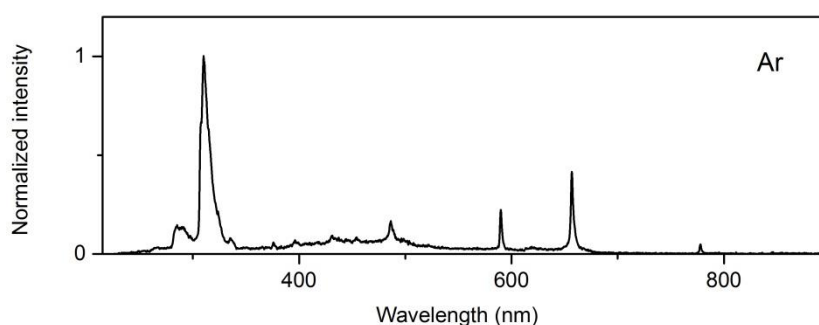


Figure 53. Emission spectrum of reactive species formed by underwater electrical discharge when saturating with Ar. The experimental parameters are the same as in figure 52

Saturation of the solution with gases was found to influence the formation rates of OH[•], H[•] and O[•]. Figure 54 shows the comparison of the emission intensities of OH (309 nm), H_α (at 656 nm) and O (at 777 nm) emission lines without gas saturation and with the addition of Ar and N₂. The highest intensity of all three emission lines was obtained when saturating with N₂ and the lowest intensity - when the discharge occurred directly in water without the gas addition. Thus, the addition of both gases has led to higher formation rates of the reactive species. It could be explained by the higher amount of the micro-discharges taking place in the solution because of the higher amount of the gas bubbles present in the solution when gas bubbling. On the contrary, at no gas bubbling, the micro-discharges only occur in the formed water bubbles. Consequently, lower amount of micro-discharges occur in this case leading to the decrease of the chemical activity of plasma compared to the discharges with gas bubbling.

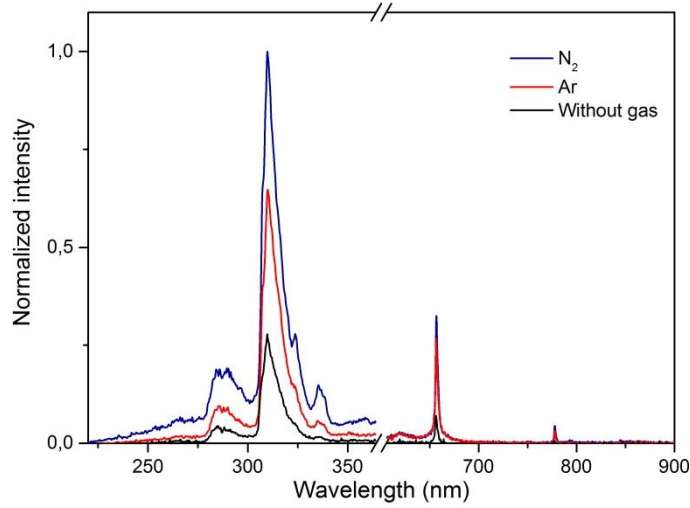


Figure 54. Comparison of OH, H $_{\alpha}$ and O emission lines in the case of no gas bubbling (black), saturation with N $_2$ (blue) and Ar (red) ($\sigma = 2$ mS/cm, $U = 30$ kV, camera gate delay and camera gate width are 500 ns and 10 μ s, respectively)

3.3.4. Plasma temperature analysis

Electrical discharge generated in the present study was shown to emit a continuous spectrum. It represents a blackbody radiation of the heated discharge channels. Since the position of the continuum maximum is determined by the temperature of the blackbody, the analysis of the discharge continua allows the estimation of the plasma temperature according to Wien's law (equation 26).

Effect of the solution conductivity and the applied electric field on the position of the continuum maximum (λ_{max}) as well as its temporal dependence are presented in figure 55. As it can be seen, λ_{max} remains constant for the tested values of solution conductivity (figure 55(a)) and AEFS (figure 55(b)). It suggests that the tested experimental conditions did not make any considerable influence on the plasma temperature or their effect was negligible. It could be explained by the fact that the analyzed spectra were averaged over the entire plasma volume. It is obvious that the plasma gas temperature is high at the discharge epicenter and decreases in the direction of the discharge channel propagation. The experimental parameters, thus, would significantly influence the local plasma temperature, whereas the temperature of the entire plasma volume would be constant. Thus, although some authors assume

that the plasma temperature is dependent on the solution conductivity and the AEFS (Vanraes *et al*, 2012), the utilized spectroscopic technique does not allow to trace it in the present study.

Figure 55(c) represents the discharge continua at different moments of a discharge. Again, no λ_{max} shift is observed. The plasma temperature is assumed to increase during the discharge propagation (0 – 50 ns), achieve its maximal value at the moment of the most intense light radiation (at 50 ns) and decrease during the discharge attenuation (50 – 500 ns). However, the obtained results indicate the constancy of the plasma temperature. It could be explained by the fact that the discharge continua were recorded with a relatively long camera gate width (10 ns). Thus, the spectra were temporally averaged, which did not allow the more precise temperature determination. For the investigation of the influence of the experimental parameters on the plasma temperature with spatial and temporal resolution, other diagnostic methods should be used.

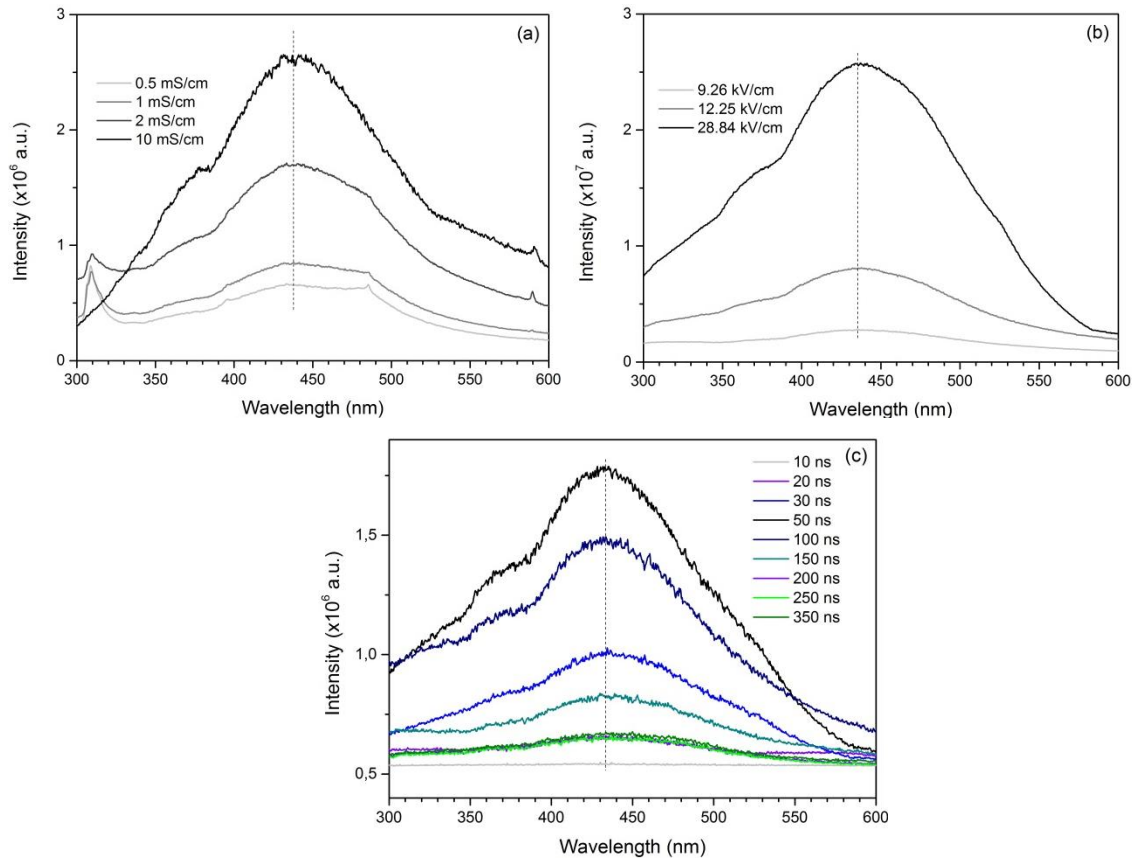


Figure 55. Effect of experimental parameters on the position of the continuum maximum: (a) – effect of the solution conductivity, (b) – effect of the applied electric field, (c) – temporal evolution

The value of the averaged plasma temperature was obtained from equation 26 and is estimated to be of 6600 K as the λ_{max} is 437 nm. The difference between the corrected temperature determined according to the equation 27 and the blackbody temperature (6600 K) was found to be of $\Delta T \approx 70$ K. Thus, the corrected values of the temperature did not significantly differ from the calculated values of the blackbody temperature.

Effect of the gas bubbling on the λ_{max} position is shown in figure 56. A slight, but reproducible in time, shift of the λ_{max} to the region of the short wavelength was observed as the aqueous solution was fed with N₂ and Ar. The continuum maximum occurs at 427 nm in the case of N₂ and at 429 nm in the case of Ar. These values are reproducible in time and did not change at different values of solution conductivity and the applied electric field. The averaged plasma temperature when the solution is saturated with Ar and N₂ is estimated to be of 6800 K. Thus, the plasma generated with the addition of the gases is of ~ 200 K hotter than the plasma generated in water without gases.

There are considerably less studies on the investigation of thermal underwater electrical discharges with plasma temperature in the range of 5000 – 9000 K compared to the numerous investigations of non-thermal discharges. The blackbody temperature of underwater electrical discharge determined from the blackbody continuum was reported for the first time by Vanraes *et al*, 2012. The obtained values varied from 6300 to 9400 K depending on the experimental conditions. The authors also did not observe the influence of solution conductivity on the blackbody temperature explaining it by a stronger leakage current towards the surrounding solution. However, the authors reported on the influence of gas bubbling on the blackbody temperature. Thus, when bubbling N₂, Ar and He, the temperature was up to 1500 K higher than that of the direct liquid discharges with no bubbles. The possible reason of no influence of the gas bubbling on the temperature obtained in the present study could be explained by a different discharge nature. Thus, Vanraes *et al*, 2012 generated electrical discharge in bubbles, introducing the gases directly into the discharge gap, which has led to the different electric characteristics of the discharge. Oppositely, in the present study, the discharges were generated in water saturated with gases, but not in the gas bubbles. Thus, electrical discharges generated in the present study with and without gas addition had the same nature and mechanism, which resulted in the generation of plasma of approximately same temperature.

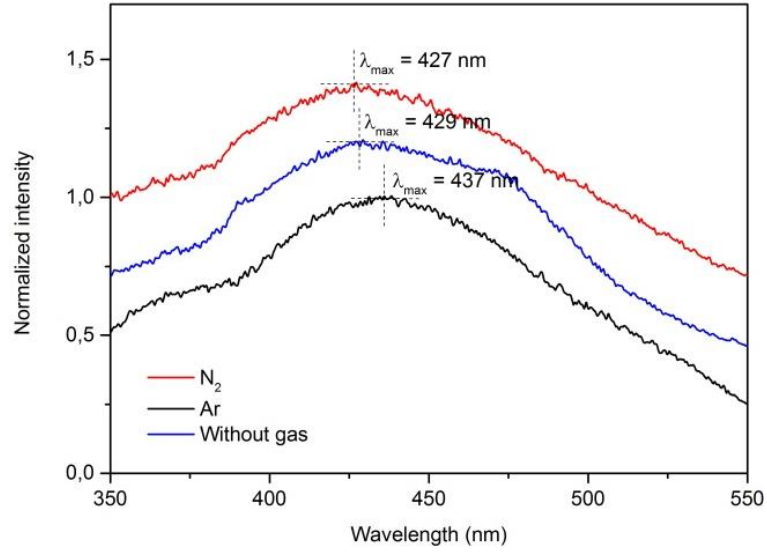


Figure 56. Effect of the saturation of solution with N₂ and Ar on the discharge continuum maximum

3.3.5. Electron density analysis

Plasma density (N_e) was determined from the Stark broadening of the H $_{\alpha}$ line present in the discharge continuum. The full width at half maximum of the H $_{\alpha}$ ($\Delta\lambda_{1/2}$) was determined by fitting the experimental profile with a Voigt function (equation 31) after the background subtraction (figure 57). The influence of other broadening mechanisms that are characterized by a Gaussian profile (Doppler effect, instrumental broadening etc; equation 30) was negligible as the fitting of the H $_{\alpha}$ profile with a Lorentzian function (equation 29) has showed a convergence of the same extent as with the Voigt function. Thus, the main mechanism of H $_{\alpha}$ line broadening in the present study was assumed to be the Stark effect (Sunka *et al*, 1999, Barmann *et al*, 1996, Bruggeman *et al*, 2010). The $\Delta\lambda_{1/2}$ of the H $_{\alpha}$ lines was used to estimate the effect of different experimental parameters on the electron density.

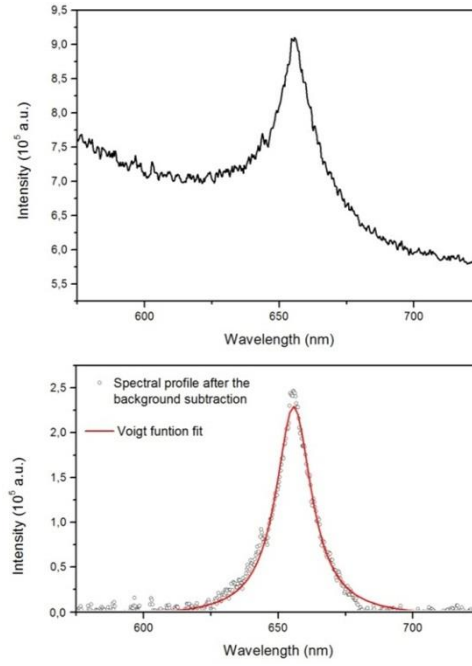


Figure 57. Example of the H_α line treatment. On the top - the experimental profile; on the bottom - the spectral profile after the background subtraction fitted with a Voigt function (equation 31)

As well as the plasma temperature, all the data presented in this chapter refer to the temporally and spatially averaged electron density. The precision of $\Delta\lambda_{1/2}$ and N_e measurements is directly defined by the integration time of the spectroscopic equipment. The obtained $\Delta\lambda_{1/2}$ values are averaged over time equal to the camera gate width.

3.3.5.1. Effect of the solution conductivity

Figure 58 shows the experimental profiles of H_α line for different solution conductivities ($U = 30$ kV, $d = 2.04$ cm, a camera gate width is equal to the continuum duration for each σ value). The figure shows the broadening of the H_α line with increase of solution conductivity. The background subtraction and fitting of the experimental profiles are presented at the bottom of the figure. The obtained $\Delta\lambda_{1/2}$ values are plotted against solution conductivity in figure 59. The dependency indicates the stronger effect of solution conductivity on $\Delta\lambda_{1/2}$ in low conductive solutions. As the solution conductivity grows, its effect on $\Delta\lambda_{1/2}$ becomes weaker.

The largest $\Delta\lambda_{1/2}$ value of 21.68 nm was determined for solution conductivity of 10 mS/cm. For the higher values of solution conductivities, the line broadening was so large that the determination of $\Delta\lambda_{1/2}$ was no longer possible. The increase of $\Delta\lambda_{1/2}$ from 9.5 nm at 0.5 mS/cm to 21.68 nm at 10 mS/cm corresponds to the increase of the

electron density by ~ 3.5 times (equation 28). Thus, the electrical discharge generated in solutions with higher conductivity forms plasma of higher electron density. It is explained by the higher amount of the charged species in solution with high conductivity and, therefore, the higher current flow. The higher the ion concentration, the more effective is the space charge electric field compensation (Sunka *et al*, 2001). It leads to the limited propagation length of the discharge channels. Because of the shorter streamer length and, at the same time, the higher current flow, the plasma density is higher for solutions with high conductivity. In solutions with low conductivity, on the contrary, the ion concentration is low, which allows the discharge propagation instead of its quenching. In this case, the generated plasma channels are longer, but the current is lower, which leads to the decrease of electron density. Thus, at the same input power, the plasma generated in solution with high conductivity has higher electron density than the plasma generated in solution with low conductivity.

An opposite effect of the solution conductivity on the N_e value was reported by Vanraes *et al*, 2012. The authors did not observe the increase of N_e with increase of solution conductivity explaining it by a different discharge nature. Thus, according to them, N_e does not depend on solution conductivity in spark discharges generated in their study, whereas the direct proportionality of N_e on solution conductivity evidences the formation of corona discharge.

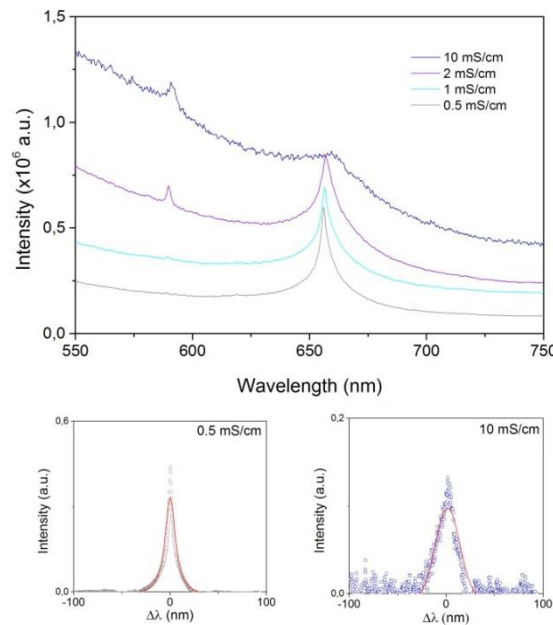


Figure 58. Effect of the solution conductivity on the H_α line broadening

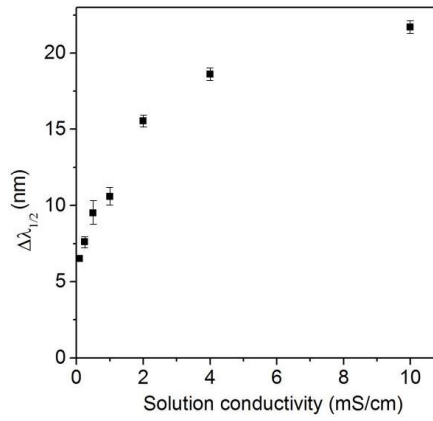


Figure 59. Effect of the solution conductivity on the $\Delta\lambda_{1/2}$ of the H_α line

3.3.5.2. Effect of the electric field strength

Figure 60 shows the experimental profiles of H_α line for different values of AEFS ($\sigma = 4$ mS/cm, a camera gate width is 300 ns). The obtained H_α profiles were treated in the same way as it was for the effect of the solution conductivity. The figure shows the broadening of the H_α line with increase of the magnitude of AEFS.

The obtained values of the $\Delta\lambda_{1/2}$ of H_α line are plotted against AEFS in figure 61. The electric field strength was found to make no considerable influence on the H_α line broadening as the difference between $\Delta\lambda_{1/2}$ for the highest (32.5 kV/cm) and the lowest (9.3 kV/cm) tested AEFS values was less than 3 nm. It corresponds to the difference in the electron density less than by $1 \cdot 10^{18} \text{ cm}^{-3}$. It is explained by the fact that the magnitude of the AEFS does not significantly influence the electrical discharge nature unlike in solution conductivity, for instance. The dependency between $\Delta\lambda_{1/2}$ and AEFS demonstrates a close to linear behavior and is fitted with function $y = 15.8 + 0.11 \cdot x$ in the measured range of AEFS values (where y is $\Delta\lambda_{1/2}$ (nm) and x is AEFS (kV/cm)). However, it is assumed that at the lower AEFS values, this relation will have a different shape as no electrical discharge occurs at $\text{AEFS} < 9$ kV/cm.

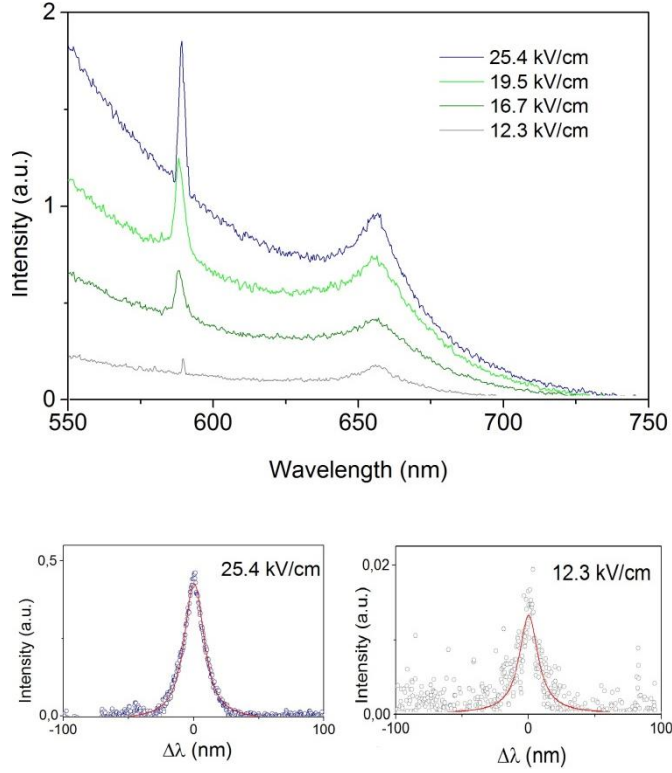


Figure 60. Effect of the average electric field strength on the H_α line broadening ($\sigma = 4$ mS/cm, a camera gate width is 300 ns)

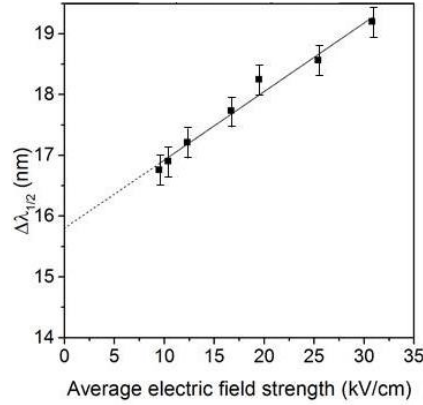


Figure 61. Effect of the average electric field strength on the $\Delta\lambda_{1/2}$ of the H_α line

3.3.5.3. Temporal evolution of electron density

The H_α line profiles were measured at different moments of discharge in order to investigate the temporal evolution of the electron density during the discharging. The spectra are presented in figure 62 ($\sigma = 2$ mS/cm, $U = 30$ kV, $d = 1.4$ cm). A camera gate width was set at 50 ns and the spectra were taken with a time step of 100

ns. The figure represents the narrowing of the H_α line in time. The obtained values of $\Delta\lambda_{1/2}$ of the H_α line are plotted against time in figure 63.

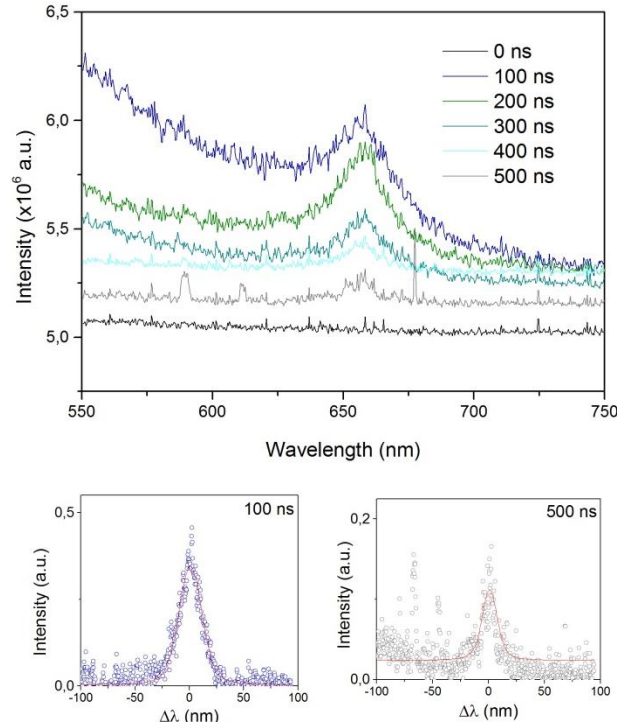


Figure 62. Time-resolved H_α line profiles ($\sigma = 2$ mS/cm, $U = 30$ kV, $d = 1.4$ cm). A camera gate width is 50 ns, a step is 100 ns

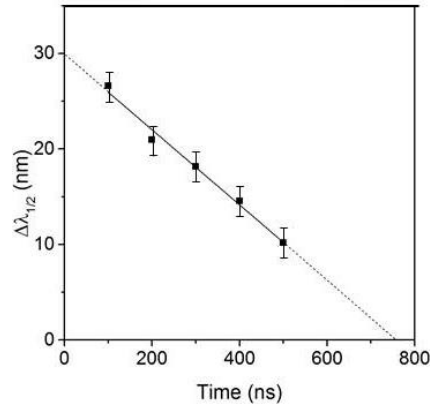


Figure 63. Temporal dependence of the $\Delta\lambda_{1/2}$ of H_α line

The decrease of experimentally obtained $\Delta\lambda_{1/2}$ values in time was fitted with function $y=29.9-0.04 \cdot t$, where y is $\Delta\lambda_{1/2}$ (nm) and t is the discharge time (ns). Assuming the linear shape of this dependency, one can expect the broadening of H_α line up to 29.9 nm at the beginning of the discharge ($t \simeq 0$ ns). Extrapolation of the

line to the longer time values ($t > 500$ ns) suggests the following narrowing of H_α . However, after 500 ns the detection of light emission from the discharge as well as the detection of H line signal was not possible due to the low intensities. The obtained by the fitting straight line does not reflect the real behavior of $\Delta\lambda_{1/2}$ the shorter and the longer times and can hardly be used for the extrapolation.

The largest H_α broadening was measured to be at the initial stage of the discharge (100 ns) and is equal to $\Delta\lambda_{1/2} = 26.61$ nm. It decreases with time as shown in figure 63 and reaches $\Delta\lambda_{1/2} = 10.16$ nm at 500 ns. It corresponds to the decrease of the electron density during the active phase of discharge by ~ 5 times. The high value of N_e of the plasma at the initial stage of the discharge is related to the more intense discharge light emission due to the high values of discharge current during the first 100 ns of the discharge. As the discharge channel propagates and expands, the plasma occupies the bigger volume and at the same time, the decrease of the current takes place. Both facts lead to the decrease of the electron density during the discharge.

3.3.5.4. Effect of the solution saturation with gases

The effect of the gas bubbling (Ar and N_2) on the H_α line broadening is shown in figure 64 ($\sigma = 2$ mS/cm, $U = 30$ kV, $d = 1.4$ cm, a camera gate width is 100 ns). The $\Delta\lambda_{1/2}$ of the H_α line in the case of saturation with Ar was found to be of 17.6 nm and for N_2 of 18.1 nm. The much smaller values of $\Delta\lambda_{1/2}$ of the H_α line in the case of saturation with gases compared to the $\Delta\lambda_{1/2}$ in the case of no gas bubbling (26.6 nm) obtained at the same conditions, indicate that the plasma generated without addition of gases has a larger electron density. Thus, the electron density in the case of saturation with gas is estimated to be ~ 2 times lower than in the case of electrical discharge without the addition of gases.

The lower values of electron density for the discharge with gas addition can be explained by the less power needed for the discharge propagation (Bruggeman *et al*, 2009, Nikiforov *et al*, 2011, Gershman *et al*, 2008). According to the bubble theory of the electrical discharge in liquid, the discharge generation passes the step of the bubble formation prior to the breakdown. At the direct liquid discharge, a significant amount of energy is spent on the solution heating in order to vaporize water and form

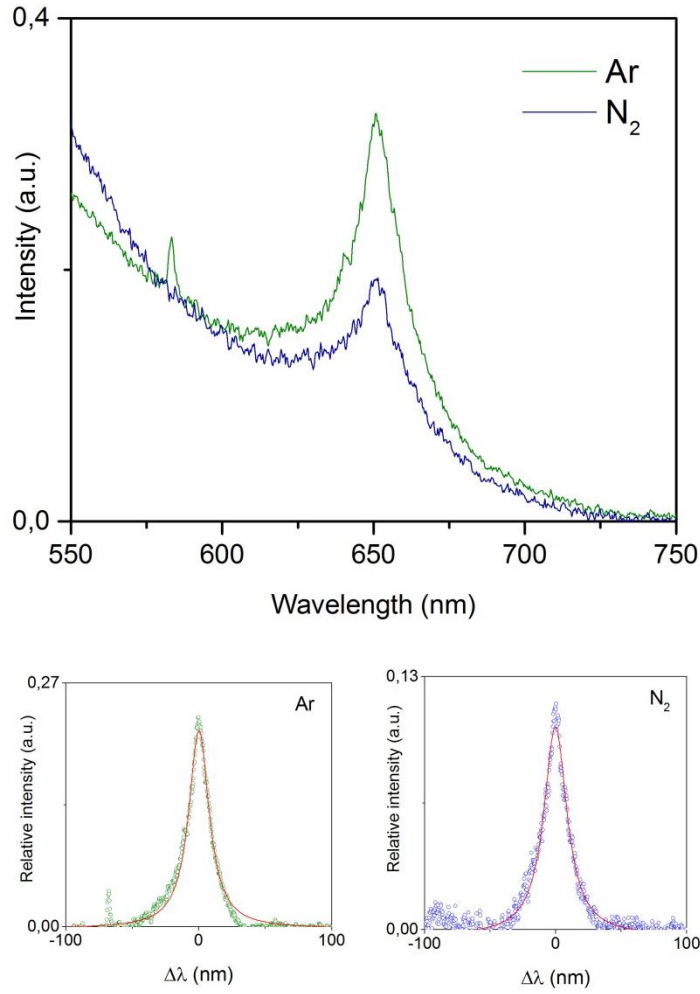


Figure 64. Effect of the solution saturation with Ar and N₂ on the broadening of the H_α line ($\sigma = 2$ mS/cm, $U = 30$ kV, $d = 1.4$ cm, a camera gate width is 100 ns)

Table 6. Values of $\Delta\lambda_{1/2}$ (nm) of the H_α line with and without solution saturation with Ar and N₂

Gas	$\Delta\lambda_{1/2}$ (nm)
Ar	17.6
N ₂	18.1
Without gas	26.6

water bubbles, thus, requiring the more input power. When solution is saturated with gases, the discharge propagation is simplified due to the presence of the existing bubbles. Thus, for the discharge development, less energy is spent on the bubble formation through the water vaporization resulting in the less consumption of the input power. More energetic direct liquid discharge leads to the formation of a denser plasma than the discharge in the case of saturation with gases. Higher values of N_e , on

one hand, lead to the higher rates of plasma-chemical reactions, resulting in the higher chemical activity. On the other hand, in terms of its application for water treatment, the direct underwater discharges with no bubble addition require higher energy consumption. The latter circumstance increases the costs of the water treatment process being one of the major disadvantages of the method.

3.3.5.5. Numerical values of N_e

The values of $\Delta\lambda_{1/2}$ obtained in the present study correspond to the N_e variations from $\sim 2 \cdot 10^{18} \text{ cm}^{-3}$ to $\sim 1.4 \cdot 10^{19} \text{ cm}^{-3}$ calculated according to equation 28 for $\alpha_{1/2}$ values of $1.89 \cdot 10^{-2} \text{ Å/cgs}$ units of electric field strength and $2.15 \cdot 10^{-2} \text{ Å/cgs}$ units of electric field strength (non-SI units are taken from Griem *et al*, 1974). Thus, depending on the experimental parameters, N_e could be increased by one order of magnitude. It corresponds to the typically obtained values of N_e for liquids phase discharges (Vanraes *et al*, 2012, Sunka *et al*, 1999, Locke *et al*, 2006, Nahimira *et al*, 2007). However, the authors investigating underwater electrical discharge in gas bubbles directly introduced into the reactor, usually report on the much lower N_e values of the order of $10^{14} - 10^{15} \text{ cm}^{-3}$ (Bruggeman *et al*, 2009, Nikiforov *et al*, 2011, Gershman *et al*, 2008).

3.4. Summary

In this chapter, the investigation of underwater electrical discharges was carried out. Underwater electrical discharges generated in the present study are partial discharges and were attributed to corona-like discharges by nature.

The discharge continuum measured in the present study was attributed to a blackbody radiation of the discharge channels. Increase of solution conductivity and average electric field strength makes a positive effect on the amount of light emitted during the discharge. The duration of the discharge light emission occurs in the range of up to $\sim 1.5 \mu\text{s}$ for the tested experimental conditions and decreases with decrease of solution conductivity.

Increase of solution conductivity makes a negative effect on the chemical activity of underwater plasma. Increase of average electric field strength makes a positive effect on the chemical activity of underwater plasma. The lifetime of the reactive species in the excited state occurs in the range of a few μs and is dependent on solution conductivity.

Underwater plasma discharges were found to be (i) able of excitation of N_2 molecules when the aqueous solution is saturated with N_2 ; (ii) unable of excitation of Ar molecules when the aqueous solution is saturated with Ar under the tested conditions. The increase of the chemical activity of underwater plasma by saturation of the solution with N_2 was proven.

The blackbody temperature of plasma generated in the present study is $\sim 6000 - 7000 \text{ K}$. The blackbody temperature of the plasma is independent on solution conductivity and average electric field strength and slightly dependent on the saturation of solution with Ar and N_2 gases.

Plasma generated in the present study is characterized by the spatially and temporally averaged electron density of $10^{18} - 10^{19} \text{ cm}^{-3}$ depending on the experimental conditions. Increase of solution conductivity makes a positive effect on the increase of electron density. Average electric field strength makes no considerable influence on the electron density. Solution saturation with gases leads to the decrease of the electron density. Plasma with the highest values of electron density occurs at the initial stage of the discharge.

3.5. List of literature

- Akiyama H.** 2000. Streamer discharges in liquids and their applications. IEEE Trans Dielectr Electr Insul. 7, 646-653
- An W.**, Baumung K. and Bluhm H. 2007. Underwater streamer propagation analyzed from detailed measurements of pressure release. J Appl Phys. 101, 1-10
- Arrayas M.**, Ebert U. and Hundsdorfer W. 2002. Spontaneous Branching of Anode-Directed Streamers between Planar Electrodes. Phys Rev Lett. 88(17), 1-4
- Atkinson R.**, Baulch D.L., Cox R.A., Crowley J.N., Hampson R.F., Hynes R.G., Jenkin M.E., Rossi M.J. and Troe, J. 2004. Evaluated kinetic and photochemical data for atmospheric chemistry: Volume I-gas phase reactions of O_x, HO_x, NO_x and SO_x species. Atmos Chem Phys. 4, 1461-1738
- Babaeva N.Y.**, Kushner M.J. 2008. Streamer branching: The role of inhomogeneities and bubbles. IEEE Trans Plasma Sci. 36(4), 892-893
- Barmann P.**, Kroell S. and Sunesson A. 1996. Spectroscopic measurements of streamer filaments in electric breakdown in a dielectric liquid. J Phys D: Appl Phys. 29(5), 1188 - 1196
- Bruggeman P.** and Leys C. 2009. Non-thermal plasmas in and in contact with liquids. Topical Review. J Phys D: Appl Phys. 42, 1-28
- Bruggeman P.**, Schram D.C., Kong M.G. and Leys C. 2009a. Is the rotational temperature of OH(A-X) for discharges in and in contact with liquids a good diagnostic for determining the gas temperature? Plasma Process Polym. 6(11), 751-762
- Bruggeman P.**, Verreycken T., Gonzalez M.A., Walsh J.L., Kong M.G., Leys C. and Schram D.C. 2010. Optical emission spectroscopy as a diagnostic for plasmas in liquids: opportunities and pitfalls. J Phys. D: Appl Phys. 43(12), 1-8
- Caso C.** 1998. Review of particle physics. Euro Phys J. C 3, 146
- Ceccato P.H.**, Guaitella O., Le Glohec M.R. and Rousseau A. 2010. Time-resolved nanosecond imaging of the propagation of a corona-like plasma discharge in water at positive applied voltage polarity. J Phys D: Appl Phys. 43(17), 175202
- Ceccato P.H.** 2010. Doctoral Dissertation: Filamentary plasma discharge inside water: initiation and propagation of a plasma in a dense medium. LPP laboratory in Ecole Polytechnique Palaiseau, Paris, 203 pages

Clements J.S., Sato M and Davis R.H. 1987. Preliminary investigation of prebreakdown phenomena and chemical reactions using a pulsed high voltage discharge in water. IEEE Trans Indust Appl. 23, 224-235

Dalgarno A., McElroy M.B. and Stewart A.I. 1969. Electron impact excitation of the Dayglow. J Atmos Sci. 26, 753-726

Dolan T.J. 1992. Electron and ion collisions with water vapour. J Phys D: Appl Phys. 26, 4-8

Farhataziz and Rogers M.A.J. 1987. Radiation Chemistry: Principles and Applications. VCH Publishers, New York. ISBN: 0895731274

Gavrilov I.M., Kukhta V.R., Lopatin V.V. and Petrov P.G. 1994. Dynamics of prebreakdown phenomena in a uniform field in water. IEEE Trans Dielectr Electr Insul. 1, 496-502

Gershman S. 2008. Doctoral Dissertation: Pulsed electrical discharge in gas bubbles in water. The State University of New Jersey, New Brunswick, 186 pages

Griem H.R. Spectral line broadening by plasmas. Vol. 39. Elsevier Science & Technology Books, 1974, 408 pages, ISBN-10: 0123028507, ISBN-13: 9780123028501

Keller S., Rajasekaran P., Bibinov N and Awakowicz P. 2012. Characterization of transient discharges under atmospheric-pressure conditions applying nitrogen photoemission and current measurements. J Phys D: Appl Phys. 45, 1-11

Korobeinikov S.M., Melekhov A.V. and Besov A.S. 2002. Breakdown initiation in water with the aid of bubbles. High Temperature. 40(5), 706-713 (in Russian)

Lee B.-H., Kim D.-S. and Choi J.-H. 2010. Underwater discharge phenomena in inhomogeneous electric fields caused by impulse voltages. J Electr Eng Technol. 5(2), 329-336

Locke B.R., Sato M., Sunka P., Hoffmann M.R. and Chang J.-S. 2006. Electrohydrolic discharge and nonthermal plasma for water treatment. Ind Eng Chem Res. 45, 882-905

Loeb L.B. and Meek J.M. The mechanism of the electric spark. Stanford University Press, 1941, ISBN: 080473139X, 9780804731393, 188 pages

Lukes P., Clupek M., Babicky V. and Sunka P. 2008. Ultraviolet radiation from the pulsed corona discharge in water. Plasma Sources Sci Technol. 17, 1-11

Marinov I.L., Guaitella O., Rousseau A., Starikovskaia S.M. 2011. Successive nanosecond discharges in water. *IEEE Trans Plasma Sci.* 39(11), 2672-2673

Meulenbroek B., Rocco A. and Ebert U. 2004. Streamer branching rationalized by conformal mapping techniques. *Phys Rev E.* 69(6), 1-4

Namihira T., Sakai S., Matsuda M., Wang D., Kiyan T., Katsuki S., Akiyama H., Okamoto K. and Toda K. 2007. Temperature of and NO generation in pulsed arc discharge plasma. *Plasma Sci Technol.* 9, 747-751

Nieto-Salazar J., Bonifaci N., Denat A. and Lesaint O. Characterization and spectroscopic study of positive streamers in water. *Proceedings of the 15th IEEE International Conference on Dielectric Liquids (ICDL)*, June 26th – July 1st, 2005, Coimbra, Portugal

Nikiforov A.Y., Leys C., Li L., Nemcova L. and Krcma F. 2011. Physical properties and chemical efficiency of an underwater dc discharge generated in He, Ar, N₂ and air bubbles. *Plasma Sources Sci Technol.* 20, 1-10

Ono R. and Oda T. 2002. Dynamics and density estimation of hydroxyl radicals in a pulsed corona discharge. *J Phys D: Appl Phys.* 35(17), 2133-2138

Rajasekaran P., Ruhrmann C., Bibinov N and Awakowicz P. 2011. Space-resolved characterization of high frequency atmospheric-pressure plasma in nitrogen, applying optical emission spectroscopy and numerical simulation. *J Phys D: Appl Phys.* 44, 1-9

Sahni M. and Locke B.R. 2006. Quantification of hydroxyl radicals produced in aqueous phase pulsed electrical discharge reactors. *Ind Eng Chem Res.* 45, 5819–25

Sarani A., Nikiforov A.Y. and Leys C. 2010. Atmospheric pressure plasma jet in Ar and Ar/H₂O mixtures: Optical emission spectroscopy and temperature measurements. *Phys Plasmas.* 17(6), 063504

Shih K.-Y. and Locke B.R. 2010. Chemical and physical characteristics of pulsed electrical discharge within gas bubbles in aqueous solutions. *Plasma Chem Plasma Process.* 30, 1-20

Sun B., Sato M and Clements J.S. 1997. Optical study of active species produced by a pulsed streamer corona discharge in water. *J Electrostat.* 39, 189-202

Sun B., Sato M., Harano A and Clements J.S. 1998. Non-uniform pulse discharge-induced radical production in distilled water. *J Electrostat.* 43, 115-126

Starikovskiy A., Yang Y., Cho Y.I., Fridman A. 2011. Non-equilibrium plasma in liquid water: dynamics of generation and quenching. *Plasma Sources Sci. Technol.* 20, 1-7

Su Z.Z., Ito K., Takashima K., Katsura S., Onda K and Mizuno A. 2002. OH radical generation by atmospheric pressure pulsed discharge plasma and its quantitative analysis by monitoring CO oxidation. *J Phys D: Appl Phys.* 35, 3192-3198

Sunka P. Babicky V., Clupek M., Lukes P., Simek M., Schmidt J. and Cernak M. 1999. Generation of chemically active species by electrical discharges in water. *Plasma Sources Sci Technol.* 8, 258-265

Sunka P. 2001. Pulse electrical discharges in water and their applications. *Phys Plasmas.* 8(5), 2587-2594

Vanraes P., Nikiforov A. and Leys C. 2012. Electrical and spectroscopic characterization of underwater plasma discharge inside rising gas bubbles. *J Phys D: Appl Phys.* 45, 1-10

Winands G.J.J., Liu Z., Pemen A.J.M., Heesch E.J.M. and Yan K. 2008. Analysis of streamer properties in air as function of pulse and reactor parameters by ICCD photography. *J Phys D: Appl Phys.* 41, 1-9

Yang B., Lei L.C. and Zhou M.H. 2004. Effects of the liquid conductivity on pulsed high-voltage discharge modes in water. *Chin Chem Lett.* 15, 1-8

4

CHAPTER 4: DEGRADATION OF ORGANIC COMPOUND

Chapter scope

This chapter finalizes the investigation of underwater electrical discharges as an alternative method of water treatment. In this chapter, the conclusions made in the previous two chapters on generation and diagnostics are used in order to optimally apply electrical discharges for water treatment.

The degradation of five pharmaceutical compounds (diclofenac, iopamidol, metoprolol, bisphenol A and carbamazepine) and trifluoroacetic acid by electrical discharges was investigated. The main parameter to evaluate the feasibility of the method was the removal rate. Liquid chromatography was the main technique used at this step of investigation to determine the values of the removal rates. The effect of the following experimental parameters on removal of the selected compounds was studied: initial concentration, solution conductivity, reactor configuration, treatment time.

The main aim of this part of the study is to prove the applicability of underwater electrical discharges for water treatment. To achieve this aim, the following objectives were set: (i) obtain the highest possible removal rates; (ii) estimate the energy yield and increase its value; (iii) check the influence of experimental parameters on the removal rates and the energy efficiency.

4.1. Literature survey

4.1.1. Current studies on removal of organics by electrical discharges

The capability of electrical discharges for water treatment was extensively investigated over the last few decades. Although every year the number of research groups dealing with water treatment by electrical discharges increases, there is still a lack of studies which does not allow to transfer the method from the laboratory to the commercial scale. In the evaluation of the decontaminating capability of electrical discharges, the most frequently used compounds are organic dyes (Magureanu *et al*, 2007, Sugiarto *et al*, 2001, Vujevic *et al*, 2004, Zhang *et al*, 2010, Stara *et al*, 2008, Stara *et al*, 2009, Pawlat *et al*, 2007, Wang *et al*, 2008a, Wang *et al*, 2008b, Bozic *et al*, 2004, Gao *et al*, 2008). The reasons for that are the simplicity of the analytical techniques (usually UV absorption spectroscopy) and the relatively high tendency of dyes to the destruction by the reactive radicals. Among the other model compounds, there are phenols (Hoeben *et al*, 1999, Hoeben *et al*, 2000, Hayashi *et al*, 2000, Sato *et al*, 2007, Yan *et al*, 2005, Piskarev *et al*, 1999, Kusic *et al*, 2005, Bubnov *et al*, 2006) because of their relatively simpler molecular structure. Finally, the potential of electrical discharges to disinfect water was evaluated on example of several bacteria (Edebo *et al*, 1968, Edebo *et al*, 1969, Sato *et al*, 1996, Ching *et al*, 2001, Abou-Ghazala *et al*, 2002, Li *et al*, 2006, Sale *et al*, 1967, Mizuno *et al*, 1988).

The energy efficiency of water purification by electrical discharges depends on the type of the discharge. Malik *et al*, 2010 and Grabowski *et al*, 2005 carried out a comparative study on different discharge types in terms of the degradation efficiency. The authors showed that the highest efficiencies were achieved for the hybrid reactors, where one electrode is submerged in the aqueous solution and another one is placed in the gas phase. The lowest efficiencies were obtained for the direct liquid discharges. Removal rates and efficiency could be greatly improved by gas bubbling directly into the discharge gap. Yet, even the most energy demanding discharge method requires significant costs. It suggests that it is only worth to use electrical discharges for really recalcitrant compounds which are impossible to degrade by the conventional water treatment methods. Following this aim, some authors have

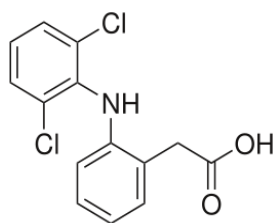
recently reported on the degradation of several pharmaceutical compounds using electrical discharges (Magureanu *et al*, 2010, Magureanu *et al*, 2011, Magureanu *et al*, 2012, Krause *et al*, 2009, Krause *et al*, 2011, Gerrity *et al*, 2010). Among the reasons of the lacking reports on the pharmaceutical removal by electrical discharges are: (i) the complex molecular structure compared to the more simple structure of the more frequently investigated phenols which complicates the study of degradation mechanism; (ii) the high recalcitrance which does not allow to achieve significant removal rates.

4.1.2. Pharmaceutical compounds

Pharmaceuticals are a group of chemical substances characterized by a great variety of properties. The high activity of pharmaceuticals towards bio-organisms determines their application in such fields as human health, medicine, agriculture, veterinary etc. The rapid development of the pharmaceutical industry in the last decades has led to the increased consumption of pharmaceutical compounds. Because of their extremely high persistence, many pharmaceuticals do not undergo the biodegradation and the common water treatment techniques fail to degrade the compounds. As a consequence, pharmaceutical residuals are constantly found in water treatment plant effluents. Thus, the continuous introduction of pharmaceuticals into the environment and the inability of the water treatment methods to degrade them lead to the continuous accumulation of pharmaceuticals in human body. It negatively influences the human health and may cause many chronic diseases. Although the concentration of pharmaceuticals in the environment (surface, drinking, ground waters) is low, water, containing them, is consumed many times a day, so the dose accumulated could be much higher than it may seem.

Diclofenac is one of the representatives of NSAIDs - non-steroidal anti-inflammatory drugs – which is used as an analgesic, antirheumatic agent and an effective pain killer. Diclofenac was originally synthesized by Ciba-Geigy in the year 1965 and was launched as Voltaren in 1988. It is mostly used as the sodium salt ($C_{14}H_{10}Cl_2NNaO_2$) due to the higher water solubility of the latter one compared to the acid form. Hundreds of tons of diclofenac are produced annually worldwide (Buser *et al*, 1998). Nikolau *et al*, 2007 reported on the annual consumption of diclofenac in Germany in amount of 86 tons. As a result, diclofenac is one of the most frequently

4.1.2.1. Diclofenac



Properties (Safety Data Sheet):

Brutto formula: C₁₄H₁₁Cl₂NO₂

Molecular weight: 296.15 g/mol

IUPAC classification: 2-(2,6-dichloranilino) phenylacetic acid

Solubility in water: 2.37 mg/L (25 °C)

Figure 65. Structural formula of diclofenac

detected pharmaceutical compounds in the water cycle (Ternes *et al*, 1998, Buser *et al*, 1998, Buser *et al*, 1999, Stumpf *et al*, 1999).

The ecotoxicity of diclofenac is relatively low, however, its ecotoxicity could be increased drastically in combination with other pharmaceutical agents which are present in the environment resulting in toxic effects (Perez-Estrada *et al*, 2005).

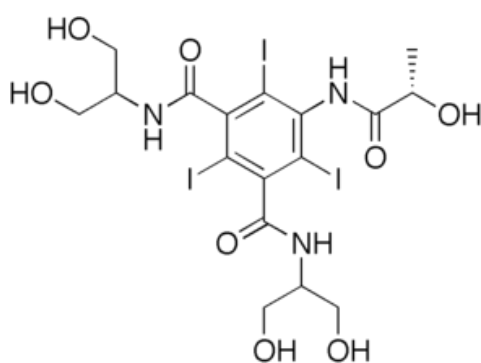
The complete elimination of diclofenac by biological treatment in water treatment plants (WTP) is not possible (Joss *et al*, 2006, Bound *et al*, 2005). The concentration of diclofenac in the WTP effluents is estimated to be of the order of a few µg/L (Soulet *et al*, 2002, Heberer *et al*, 2002a,b,c, Tixier *et al* 2003). Diclofenac was found in ground and surface waters (Sacher *et al*, 2001, Schmitt-Jansen *et al*, 2007, Buser *et al*, 1998). Diclofenac is not considered to be a persistent compound since it could be eliminated relatively easily in the environment. Despite this, owing to the continuous release of the pharmaceutical into the environment and, therefore, a high value of its constant concentration, diclofenac is supposed to be “pseudo-recalcitrant”.

Many studies reported on the ability of diclofenac degradation by direct photolysis (Buser *et al*, 1998, Buser *et al*, 1999, Agüera *et al*, 2005, Görner *et al*, 2010, Salgado *et al*, 2012) including the degradation by the natural light (Koutsouba *et al*, 2001). However, the long duration of the photolytical degradation of diclofenac (hours or days, depending on the light source) is a significant disadvantage. The successful and more rapid degradation of diclofenac by Advanced Oxidation Processes (AOPs) was reported (Zwiener *et al*, 2000, Vogna *et al*, 2004, Huber *et al*, 2003). Diclofenac was shown to be easily and completely degraded by ozonation

(Sein *et al*, 2008, Sein *et al*, 2009, Huber *et al*, 2003, Huber *et al*, 2004) and the attack of the hydroxyl radicals (Yu *et al*, 2012).

Despite the high degradation rates in most of cases or even complete degradation, diclofenac removal by the listed above methods was reported to lead to a great variety of transformation products of various toxicity levels. Studies on determination of DFC products most frequently report on the formation 5-Hydroxydiclofenac, 4'-Hydroxydiclofenac and Diclofenac-2,5-iminoquinone by oxidation (Miyamoto *et al*, 1997, Kaphalia *et al*, 2006, Sein *et al*, 2008, Perez-Estrada *et al*, 2005, Kinne *et al*, 2009) and 2-(8-chloro-9H-carbazol-1-yl)acetic acid by photocyclization of diclofenac (Görner *et al*, 2010, Salgado *et al*, 2012).

4.1.2.2. Iopamidol



Properties (Seitz *et al*, 2004):

Brutto formula: C₁₇H₂₂I₃N₃O₈

Molecular weight: 777.09 g/mol

IUPAC classification: 1-N,3-N-bis(1,3-dihydroxypropan-2-yl)-5-[(2S)-2-hydroxypropanamido]-2,4,6-triiodobenzene-1,3-dicarboxamide

Solubility in water: freely soluble

Figure 66. Structural formula of iopamidol

The presence of iodine in its structure allows of the absorption of X-rays by iopamidol molecules. It is one of the representatives of non-ionic iodinated X-ray contrast media (ICM), which are widely used in the radiology diagnostics for imaging of soft tissues. ICM are known to be a source of iodine in the formation of highly toxic iodo-trihalomethane and iodo-acid disinfection by-products (Duirk *et al*, 2011).

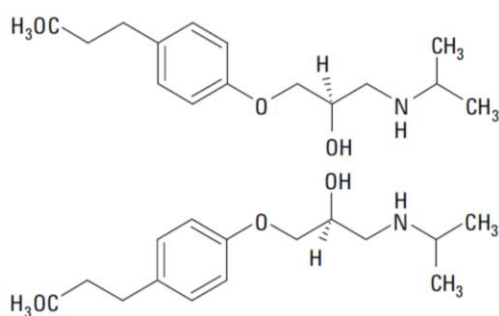
The annual usage of ICM is estimated to be of 3500 tons (Perez *et al*, 2007). ICM are not completely destroyed by the conventional water treatment. The WTP effluents were reported to contain ICM in amount of up to 100 µg/L (Ternes *et al*, 2000, Putschew *et al*, 2001). On the ng/L level, ICM were detected in drinking and

tap water samples (Putschew *et al*, 2000, Hirsch *et al*, 2000). Due to their wide use in the medicine, ICMs are chronic pollutants in the hospital waters (Gartiser *et al*, 1996).

The biodegradation of ICM in WTP is non-effective. However, approximately 85% of iopromide was transformed into its metabolites by activated sludge in the laboratory experiments (Kalsch *et al*, 1999). The removal of ICM by ozonation has shown to decrease the concentration by only 35-55 % (Seitz *et al*, 2008). However, the amount of organic bound iodine remains nearly constant (Putschew *et al*, 2003, Putschew *et al*, 2006). Significant degradation rates or complete elimination of some ICMs depending on the conditions were achieved with the direct photolysis (Perez *et al*, 2009), photocatalysis (Doll *et al*, 2003) and AOPs (Ternes *et al*, 2003, Jeong *et al*, 2010), however, the efficiencies of these processes are low.

The most frequently reported ICM used to study the degradation process are diatrizoate (ionic), iopermol and iopromide (non-ionic). Pitre *et al*, 1980 originally reported on the synthesis of iopamidol in the year 1980 as an alternative ICM with high water solubility. Despite the relatively long history of iopamidol and its apparent threat as an ICM, there are very few studies on its degradation in water (Jeong *et al*, 2010).

4.1.2.3. Metoprolol



Properties (ChemSpider, The free chemical database):

Brutto formula: C₁₅H₂₅NO₃

Molecular weight: 267.36 g/mol

IUPAC classification: 1-[4-(2-methoxyethyl)phenoxy]-3-(propan-2-ylamino)propan-2-ol

Solubility in water: practically insoluble

Figure 67. Structural formula of metoprolol (both isomers)

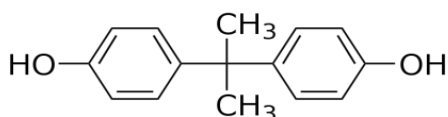
Metoprolol is a white crystalline odorless powder. In pharmacology, metoprolol acts as a cardioselective β_1 -receptor blocking agent. The β_1 -selectivity of metoprolol is thought to be due to the substituents in the *para* position. It is usually used for acute myocardial infarction, heart failure, angina pectoris, mild to moderate hypertension and arrhythmias (Swedberg *et al*, 1979, Ikehata *et al*, 2006). It may also

be used for migraine headaches. Due to the poor solubility, metoprolol is usually used in the form of its tartrate salt, which was originally synthesized by Novartis in the year 1978.

Sewage treatment plant effluents were reported to contain various β -blockers in amount of up to 2 $\mu\text{g/L}$ (Huggett *et al*, 2003). The occurrence of these drugs in rivers and surface waters was also detected (Zuccato *et al*, 2005, Gros *et al*, 2007, Gros *et al*, 2010, Coetsier *et al*, 2009). The incomplete degradation of β -blockers by conventional water treatment and the subsequent accumulation in human body may cause the failure of cardiac system.

Studies on metoprolol degradation report on its high resistance towards biodegradation (Baran *et al*, 2006, Mohring *et al*, 2009) and photolytical stability (Liu *et al*, 2009, Bokar *et al*, 2011, Piram *et al*, 2008). At the same time, metoprolol is degradable under the attack by OH^\bullet . The latter fact is thought to be due to a weakly/moderately activated aromatic ring, caused by a secondary amine, which is a target of OH^\bullet (Ikehata *et al*, 2006). Borkar *et al*, 2011 reported on the extensive hydrolysis of metoprolol at the increased temperature in acidic conditions. At the same time, the authors reported on the stability of the solid drug towards the direct photolysis and oxidation by H_2O_2 . Photocatalytical degradation of metoprolol was shown to lead to complete mineralization to form CO_2 and H_2O (Abramovic *et al*, 2011, Yang *et al*, 2010). The authors showed the key role of OH^\bullet in metoprolol degradation by using OH^\bullet scavengers. Metoprolol degradation by AOPs showed up to 70% mineralization by photo-Fenton process (Rivas *et al*, 2010, Romero *et al*, 2011).

4.1.2.4. Bisphenol A



Properties (ChemSpider, The free chemical database):

Brutto formula: $\text{C}_{15}\text{H}_{16}\text{O}_2$

Molecular weight: 228.29 g/mol

IUPAC classification: 4,4'-(propane-2,2-diyl)diphenol

Solubility in water: 300 mg/L (25 °C)

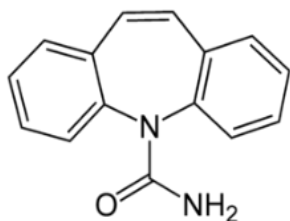
Figure 68. Structural formula of bisphenol A

Bisphenol A was originally synthesized by A. Dianin in the year 1891. Over the decades it was widely used as the key monomer in the production of epoxy resins, polycarbonate plastics, unsaturated polyesters (Rufus *et al*, 1994, Olea *et al*, 1996). The hormone-like properties of bisphenol A were discovered by C. Dodds in the early 1930s. Owing to its estrogenic activity, bisphenol A is used as an endocrine disrupting compound (EDC).

The production volumes of bisphenol A are one of the world's highest. The annual global production of bisphenol A in the early 2000s was estimated to be in the range of million tons (Staples *et al*, 2002). The adverse effects of bisphenol A consist in its potential to interfere the normal functioning of the endocrine system by duplicating, blocking or exaggerating hormonal responses (Ohko *et al*, 2001, Suzuki *et al*, 2004). Bisphenol A makes a particularly harmful effect on fetus, infants, young children because of the absence of the feedback regulating the activity. In the year 1996, the European Commission declared the harmful effect of bisphenol A on human body. In the year 2010, the government of Canada placed bisphenol A in the list of toxic substances (The Globe and Mail 2010, Canada Gazette 2010).

Bisphenol A was found in surface water samples (Suzuki *et al*, 2004). The average level of BPA in the leachates of hazardous waste landfill was reported by Yamamoto *et al*, 2001 to be of 270 ng/L. Many studies report on the capability of bisphenol A to biodegradation by different organisms such as bacteria, fungi, planktons, animals (Kang *et al*, 2006, Dorn *et al*, 1987, Atkinson *et al*, 1995, Kang *et al*, 2002, Ying *et al*, 2003, Spivack *et al*, 1994, Chai *et al*, 2005, Hirano *et al*, 2000, Hirooka *et al*, 2005). The electrochemical degradation appeared to be an effective method of bisphenol A elimination. Cui *et al*, 2009 and Tanaka *et al*, 2002 demonstrated the total destruction of BPA using different electrode materials (i.e. different amounts of charge consumption). The authors also showed that both – direct electrolysis of bisphenol A and oxidation by OH^\bullet – play important roles in the electrochemical degradation of BPA. Bisphenol A could also be degraded photocatalytically (Ohko *et al*, 2001) resulting in mineralization and by ozonation (Bin *et al*, 2007) especially at high ozone consumption.

4.1.2.5. Carbamazepine



Properties (Thome *et al*, 1994, Astier *et al*, 1979):

Brutto formula: C₁₅H₁₂N₂O

Molecular weight: 236.26 g/mol

IUPAC classification: 5H-Dibenz(b,f)azepine-5-carboxamide; 5-carbamoyl-5H-dibenz(b,f)azepine

Solubility in water: 20 mg/L (25 °C); soluble in acetone, alcohol, chloroform

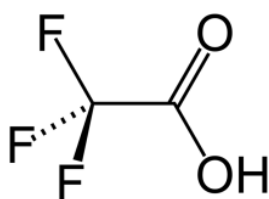
Figure 69. Structural formula of carbamazepine

The presence of an amine group in its structure causes the polar nature of carbamazepine. As a pharmaceutical, it is commonly used as an anticonvulsant, mood stabilizing antiepileptic drug (Grushka *et al*, 1971, Thome *et al*, 1994, Umweltbundesamt fact sheet Carbamazepine). As an organic compound it was originally synthesized by W. Schindler in 1953 and has been used as a drug since 1962 in many countries. In the year 1997, the consumed quantity of carbamazepine in Austria was 6334 kg per year, whereas the amount of the consumed carbamazepine in South Korea in the year 2003 was already 9155 kg (Schramm *et al*, 2006, Kim *et al*, 2007). The principle toxic effects of carbamazepine are depression in level of consciousness and convulsions.

Carbamazepine was found in municipal, surface and drinking waters (Ternes *et al*, 1998, Heberer *et al*, 2004), where its occurrence varies from the ng/L level (drinking water samples) to the µg/L level (surface water samples) (Stamatelatou *et al*, 2003). Among the investigated methods of carbamazepine degradation, there are biodegradation (Stamatelatou *et al*, 2003, Bernhard *et al*, 2006, Lesjean *et al*, 2005, Carballa *et al*, 2007, Clara *et al*, 2005, Ksjek *et al*, 2009), ozonation (Andreozzi *et al*, 2002, Ternes *et al*, 2002, Hua *et al*, 2006), UV photolysis (Petrovic *et al*, 2007, Vogna *et al*, 2004, Donner *et al*, 2012) and photocatalysis (Doll *et al*, 2005, Doll *et al*, 2004, Andreozzi *et al*, 2002, Andreozzi *et al*, 2003, Baker *et al*, 1973). The studies showed the inability of the biodegradation of carbamazepine, whereas significant removal rates were achieved with ozonation (> 90% (Ternes *et al*, 2002)). Photolysis of carbamazepine was shown to lead to the transformation products – acridine and

acridone – which toxicity much exceeds the toxicity of carbamazepine itself (Donner *et al*, 2012). Complete removal of carbamazepine by photocatalysis using TiO₂ was reported (Im *et al*, 2012), however, the formation of acridine (main intermediate) was also observed.

4.1.3. Trifluoroacetic acid



Properties (ChemSpider, The free chemical database):

Brutto formula: CF₃COOH

Molecular weight: 114 g/mol

IUPAC classification: 2,2,2-trifluoroethanoic acid

Solubility in water: miscible

Density: 1.489 g/cm³ (20 °C)

Boiling point: 72.4 °C

pKa: -0.25

Figure 70. Structural formula of trifluoroacetic acid

Owing to the presence of three fluorine atoms in its structure, trifluoroacetic acid is known as a very strong acid with pK_a = -0.25. The molecular structure of trifluoroacetic acid is presented in figure 70.

In the nature, trifluoroacetic acid could be formed from hydrofluorocarbons (HFC) and hydrochlorofluorocarbons (HCFC) which could react with OH[•] in the troposphere with the following oxidation by O₂ (Wallington *et al*, 1991, Scott *et al*, 2000). In the sea water, trifluoroacetic acid has been accumulating over many million years around sub-sea volcanic vents (Environmental fate of trifluoroacetyl halides) as a well-known HCFC source is volcanoes. Additionally, a source of trifluoroacetic acid was reported to be the degradation of the commercial fluoropolymers continuously charged into the environment during the manufacturing processes (Ellis *et al*, 2001, Ellis *et al*, 1997, Key *et al*, 1997). The typically reported level of trifluoroacetic acid in the rain water is estimated to be 100 ng/L (Boutonnet *et al*, 1999).

Although mammals are not affected by trifluoroacetic acid at the concentration thousand times higher than the one presented in the environment, trifluoroacetic acid is characterized by phytotoxicity (Berends *et al*, 1999) and may be harmful to aquatic organisms. There is no data on bioaccumulation of TFA.

The lack or absence of data on successful degradation of trifluoroacetic acid distinguishes it from other recalcitrant compounds. TFA was reported to be non-degradable under the environmental conditions (Martin *et al*, 2000, Ellis *et al*, 2001, Boutonnet *et al*, 1999, Pehkonen *et al*, 1995) and is currently considered to be highly persistent. Visscher *et al*, 1994 have shown the possibility of trifluoroacetic acid degradation microbially in oxic and anoxic conditions by up to 87%, however, the incubation periods were in the range of a few weeks. This result was not reproduced, therefore, generally, trifluoroacetic acid is supposed to be resistant to the biodegradation. Lifongo *et al*, 2010 predicted the extremely slow thermal degradation of trifluoroacetic acid which is estimated to be of thousand years, although the tested temperature was up to 100 °C. The low reactivity of OH[•] towards trifluoroacetic acid does not allow of its degradation by AOPs. Consequently, photocatalytical degradation of trifluoroacetic acid by TiO₂ is also not possible. Hori *et al*, 2003 reported on the 20% degradation of trifluoroacetic acid using H₃PW₁₂O₄₀·6H₂O as a photocatalyst in water saturated with oxygen after irradiation by the UV lamp during 48h. Francisco *et al*, 1992 studied the degradation pathways of trifluoroacetic acid using the computational methods. The authors predicted that the first step of trifluoroacetic acid degradation is likely to be C-C bond cleavage to form CF₃ and COOH radicals.

4.2. Experimental

4.2.1. Reactor configuration

The degradation of selected pharmaceutical compounds was performed either in a batch or in a flow reactor (BR and FR, respectively). Schematically both reactor configurations are shown in figure 71. In the batch configuration (figure 71(a)), the plasma reactor was not incorporated into the flow system. Therefore, the cooling and mixing of the solution were not provided in this reactor configuration. The stationary solution in the BR ($V = 25 \text{ mL}$) underwent the plasma treatment during 1, 2, 3, 4, 5, 10, 15 and 30 min. For each time period, the BR was filled with a new fresh solution. After the plasma treatment, the solution was removed from the reactor. In the flow configuration (figure 71(b)), the plasma reactor was incorporated into the flow system described in Chapter 2.2.1.2. The total volume of the flow system used for degradation experiments was 250 mL. The circulating solution underwent the plasma treatment during 4h with the sampling after 15, 30, 45, 60, 90, 120, 150, 180 and 240 min. For the operation in the FR, the solution was not removed during the entire treatment time. At each sampling point, the solution in amount of 1 mL was taken from the open vessel. Thus, by the end of plasma treatment the amount of the solution decreased by 8 mL, which was assumed to make negligible influence on the degradation rate. The solution flow rate was set at 80 L/h. With such settings, the residence time of the treated solution in the FR was equal to the residence time in the BR (30 min). Solution with a known concentration of a pharmaceutical was placed into the plasma reactor. The circulated (in the FR) or stationary (in the BR) solution was treated by the electrical discharges with $U = 30 \text{ kV}$, $F = 10 \text{ Hz}$, $d = 1.54 \text{ cm}$ and $\sigma = 2 \text{ mS/cm}$ for all experiments in the present study (apart from the experiments on the effect of the solution conductivity on removal rates, where σ was variable. The values of concentration in all described experiments are mean of three replicated degradation experiments.

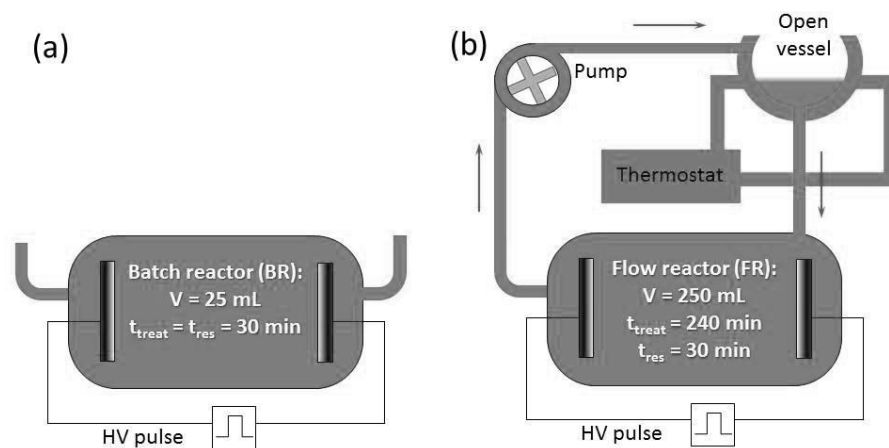


Figure 71. Reactor configurations used in the present study: (a) – a batch reactor; (b) – a flow reactor

4.2.2. Chemicals

Diclofenac (DFC, disodium salt, 99%), iopamidol (IOP, 99%), metoprolol (MP, tartrate salt, 99%), bisphenol A (BPA, 99%), carbamazepine (CBZ, 99%) and trifluoroacetic acid (TFA, 99%) were purchased from Sigma Aldrich (DFC, MP, CBZ and TFA) and Nycomed GmbH (IOP). Stock solutions were prepared on Milli-Q Plus water ($\sigma = 0.3 \mu\text{S}/\text{cm}$). The concentrations of the solutions of tested pharmaceutical compounds and TFA were 1, 10 and 100 mg/L. Due to the limited water solubility, CBZ degradation was investigated at $C_0 = 1$ and 10 mg/L. The conductivity of the solutions was adjusted by Na_2SO_4 . The prepared solutions and the samples with the treated solutions were stored in the dark at the temperature of 4°C .

4.2.3. HPLC measurements

The concentration of the compounds after the plasma treatment was determined using High Performance Liquid Chromatography (HPLC). Two HPLC systems were used. First one is Shimadzu (Japan) consisting of the following parts: a diode-array detector (model SPD-M10 AVP), an auto injector (model SIL-10AD), a degasser (model DGU-14A), a system controller (SCL-10A) and a pump (LC-10AT). The HPLC system was equipped with a Prontosil 120-5-C18 column (250 x 4.0 mm). The Shimadzu HPLC system was used for the analysis of transformation products of DFC, for which the detection at different wavelengths is required. Second HPLC

system is Agilent 1100 (Germany), with UV detection. The system was equipped with a SunFire™ column C18 (4.6 x 150 mm, 3.5 µm). The Agilent HPLC system was mostly used for the analysis of degradation of the initial compounds, for which the simultaneous detection at different wavelengths is not required. The following HPLC methods were used:

1. Diclofenac: the mobile phase (flow rate 0.4 mL/min) was a mixture of methanol and water (80 % MeOH), the water being acidified with HCl to pH 3, UV detection was set at 254 nm, injection volume was 50 µL.
2. Iopamidol: the mobile phase (flow rate 0.4 mL/min) was a mixture of acetonitrile and water (with the following gradient: 0-2 min 5% ACN, 6.5-10 min 35% ACN, post time 3 min), UV detection was set at 242 nm, injection volume was 50 µL.
3. Metoprolol: the mobile phase (flow rate 0.3 mL/min) was a mixture of acetonitrile and water (with the following gradient: 0-5 min 15% ACN, 10-15 min 30% ACN, post time 3 min), the water being acidified with 0.1% formic acid, UV detection was set at 225 nm, injection volume was 50 µL.
4. Bisphenol A: the mobile phase (flow rate 0.4 mL/min) was the mixture of acetonitrile (30%) and water (70%), UV detection was set at 280 nm, injection volume was 50 µL.
5. Carbamazepine: the mobile phase (flow rate 0.4 mL/min) was a mixture of acetonitrile (10%), methanol (60%) and water (30%), UV detection was set at 230 nm, injection volume was 50 µL.

The peak of each compound was integrated and the obtained areas were used for the quantitative analysis. The calibration curves were made using the solutions with known concentration of the compounds. The peak area (a.u.) versus the compound concentrations (mg/L) demonstrated the linear relationship.

4.2.4. Degradation of TFA

The ability of underwater electrical discharges to destroy polyfluorinated compounds (PFC) was checked on the example of the simplest representative (after

CHF₃) – trifluoroacetic acid (TFA). The solutions with the initial concentrations of 1 and 10 µM were made up using Milli-Q Plus water. The TFA degradation with a higher concentration (100 µM) was carried out, but not analyzed because of the overloading of the LC column. The degradation experiments were carried out in the BR with the treatment time of 2h. The concentration of TFA after plasma treatment was determined using ion chromatography (IC). The IC system 883 Basic IC plus (Metrohm AG, Switzerland) was equipped with a column Metrosep A Supp 4 (4.0 x 250 mm, 9µm). The mobile phase was sodium carbonate-bicarbonate buffer solution (1.8 mM Na₂CO₃ / 1.7 NaHCO₃), the flow rate was 1 mL/min, injection volume was 20 µL.

The change of TFA concentration during the plasma treatment was carried out by the analysis of the peak area of CF₃COO⁻ anion. The blank experiment revealed the formation of F⁻ released from the destruction of the Teflon[®] holders in the plasma reactor in amount of ΔC (F⁻) = (122 ± 0.8) µM. Thus, the release of F⁻ resulted from the possible cleavage of C-F bond of TFA was not possible to measure at the given experimental conditions. The second blank experiment was performed in order to measure the amount of TFA which could possibly be absorbed by the Teflon[®] parts of the plasma reactor. The change of TFA concentration was ΔC (CF₃COO⁻) = (0.4 ± 0.02)%.

4.2.5. Calculation of energy efficiency

The removal efficiency (W (mg/kWh)) was evaluated using the equation (Magureanu *et al*, 2010):

$$W = \frac{\text{the number of substance converted}}{\text{the required energy input}} \cdot \frac{X \times C_0 \times V}{E_p \times F \times t}, \quad (33)$$

where X is the conversion, C_0 is the initial concentration (mg/L), V is the treated volume (L), E_p is the pulse energy (kW), F is the frequency of high-voltage pulses (Hz) and t is the treatment time (s). The pulse energy was determined by integration of the discharge power by pulse duration time and was found to be of 0.94 J (2.8·10⁻⁴ Wh) for 2mS/cm (Chapter 2.3.4.).

4.3. Results and discussions

4.3.1. Removal of pharmaceuticals

All pharmaceuticals were partially degraded in aqueous solution exposed to electrical discharges. The degradation rates were found to be dependent on the initial concentration of the pharmaceuticals, the reactor type (batch or flow configuration, BR and FR, respectively) and the solution conductivity.

The degradation rates of diclofenac (DFC), iopamidol (IOP), metoprolol (MP), bisphenol A (BPA) and carbamazepine (CBZ) achieved within 30 min of operation using the plasma reactor in the batch configuration are presented in figure 72(a) for the initial concentrations of 1, 10 and 100 mg/L. As it could be seen, DFC appeared to be the most stable towards the electrical discharges with the degradation rate of $(90 \pm 4)\%$, whereas CBZ was the most stable among the investigated substances with the degradation rate of $(15 \pm 6)\%$ for $C_0 = 1$ mg/L. The removal rates for all compounds increase as the initial concentration is decreased.

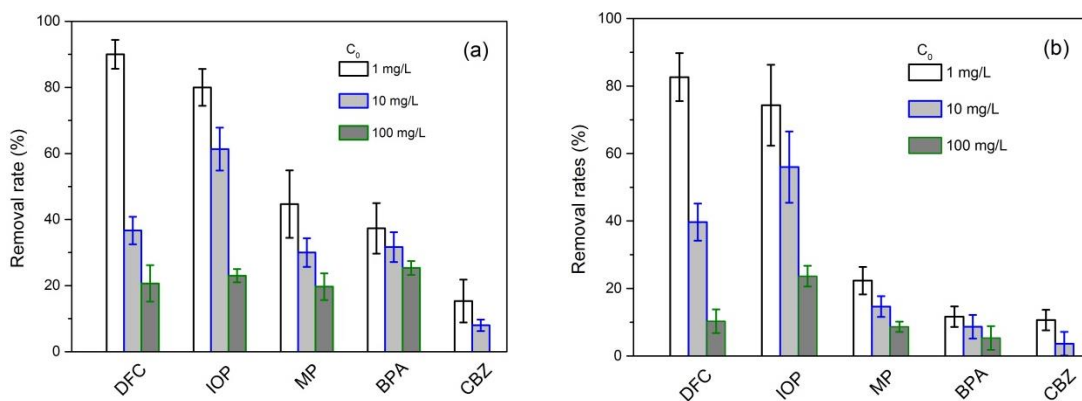


Figure 72. Effect of the initial concentration of pharmaceuticals on the removal rates: (a) – in the batch reactor and (b) – in the flow reactor

The degradation rates of DFC, IOP, MP, BPA and CBZ achieved within 240 min of operation using the plasma reactor in the flow configuration are presented in figure 72(b) for the initial concentrations of 1, 10 and 100 mg/L. Similarly to the BR, DFC and IOP showed the highest removal rates and CBZ and BPA appeared to be the

most recalcitrant. The removal rates for all compounds increase as the initial concentration is decreased as it was in the batch configuration. Very few studies report on the considerable degradation rates of pharmaceuticals using electrical discharges, which complicates the comparison of the obtained results with the literature. However, Krause *et al*, 2009 reported on almost complete elimination of CBZ (98%) by plasma treatment at C_0 comparable to the one used in the present study. The higher removal rates compares to the ones obtained in the present study could be explained by the fact that the authors used a different discharge type - corona in air. The same high removal rates of CBZ by electrical discharges were obtained by Gerrity *et al*, 2010 at $C_0 < 1\mu\text{g/L}$. The authors declared that CBZ was highly susceptible to non-thermal plasma treatment, however, the type of the electrical discharge was similar to the one in the work of Krause *et al*, 2009. Wang *et al*, 2007 reported on the elimination of BPA by ~60% by glow discharge in aqueous solution at $C_0 = 100\text{ mg/L}$. The authors also reported on complete elimination of BPA using NaCl solution instead of Na_2SO_4 because of the role of Cl_2^\bullet in the degradation of BPA. However, in that case, the authors assume the interaction of the target compounds with the added substances, which is against of the aim of the present study. Thus, neither CBZ nor BPA were reported in the literature to be recalcitrant towards the electrical discharges. One of the possible reasons of the limited degradation of these compounds obtained in the present study could be the lower efficiency of the liquid phase discharges compared to the discharge in air.

4.3.1.1. Effect of the initial concentration

In both reactors independently on the configuration, the higher removal rates were achieved for all compounds at lower initial concentrations. For example, in the BR, DFC was degraded by 90% at the initial concentration of 1 mg/L and by 21% at the initial concentration of 100 mg/L (figure 72). The smallest variations of the removal rates at different C_0 were observed for BPA and CBZ, which degradation was assumed to be slightly independent on the amount of the initial compound. The observed phenomenon could be explained by the difference in the degradation kinetics. At low initial concentration, the target compound is in a less excess relating to the main reactant (e.g. oxidative species, plasma photons etc). At the high initial concentration, the target compound is in a greater excess compared to the other

reactants, which are in a higher deficiency. The latter case will lead to the lower values of the rate constant and, consequently, to the lower degradation rates. Another possible explanation could be the formation of the transformation products which recalcitrance exceeds the recalcitrance of the initial substances. It leads to the prevention of the following degradation of the initial compounds. Thus, at higher initial concentrations of the target compound, the number of the recalcitrant products is higher than at the lower concentration. This fact leads to the lower degradation rates of the same compound at higher initial concentration compared to the lower concentration. The observed effect of the increase of the removal rates with the decrease of the initial concentration is in agreement with the results usually reported in literature for pharmaceuticals in the same range of C_0 (Magureanu *et al*, 2010, Krause *et al*, 2011).

4.3.1.2. Effect of the reactor configuration

The degradation rates were found to be dependent on the reactor configuration. The experiments on degradation were carried out either in the BR with a small volume and without stirring or in the FR with a bigger volume and with continuous circulation of the treated solution. An argument in favor of the use of the FR was that it simulated a commercial unit more closely than the BR; while the latter is more commonly used at the early stage of development due to the simplicity of its usage. Comparing the degradation at the same conditions in the batch and the flow reactors, it should be noted that for most of the cases the higher removal rates are achieved using the BR. For example, DFC at the initial concentration of 1 mg/L was degraded by $(90 \pm 4)\%$ in the BR, whereas in the FR the removal rate was $(83 \pm 7)\%$ provided that the residence time is equal for both reactors ($t_{\text{res}} = 30$ min). Smaller removal rates in the BR compared to the FR were achieved only for DFC at $C_0 = 10$ mg/L and IOP at $C_0 = 1$ mg/L. However, even in these cases the difference in the removal rates did not exceed 4% (figure 72).

The lower removal rates in the FR could be explained by the fact that using this reactor type, the entire solution volume is treated by portions. From the experimental conditions:

$$t_{\text{treatment}} = 4\text{h}, \text{ flow rate} = 80 \text{ L/min}, V_{\text{total}} = 200 \text{ mL}, V_{\text{reactor}} = 25 \text{ mL}$$

one may find the time during which the solution passes the reactor at one single run Δt :

$$\Delta t = V_{\text{reactor}} / \text{flow rate} = 1.8 \text{ s} \quad (34)$$

Each solution portion is treated n times:

$$n = (\text{flow rate} \cdot t_{\text{treatment}}) / V_{\text{total}} = 1600 \text{ times} \quad (35)$$

The residence time t_{res} is then:

$$t_{\text{res}} = \Delta t \cdot n = 30 \text{ min} \quad (36)$$

After 25 mL of the treated for 1.8 s solution leave the reactor, it is mixed with the untreated solution. By the time, this portion of solution reaches the reactor next time, the concentration of the initial compound ($C_{0\ n+1}$) is higher than it was when this portion left the reactor ($C_{0\ n}$). As it was discussed above, the increase of the initial concentration makes a negative effect on the removal rates. Thus, the removal rates at each run will be decreased compared to the case when $C_{0\ n+1} = C_{0\ n}$. It will finally result in the decreased removal rates at the end of the treatment. In contrast to the FR, in the BR, one solution portion is being continuously treated as $n = 1$ and $t_{\text{treatment}} = t_{\text{res}} = 30 \text{ min}$. Thus, the concentration of the initial compound decreases gradually during the treatment. It finally results in the higher removal rates at the end of the treatment compared to the FR.

4.3.1.3. Effect of the solution conductivity

As it was shown in Chapters I and II, solution conductivity is a key parameter that determines the generation and properties of the electrical discharge. The increase of solution conductivity was shown to facilitate the electrical discharge inception. Yet, the increase of solution conductivity makes an opposite effects of the chemical and physical activity of underwater electrical discharge. This fact does not allow to predict or make a conclusion on whether or not the increase of solution conductivity will lead to the higher or lower removal rates.

Figure 73 shows the effect of the solution conductivity on the removal rates of the tested pharmaceutical compounds in the BR at $C_0 = 10 \text{ mg/L}$.

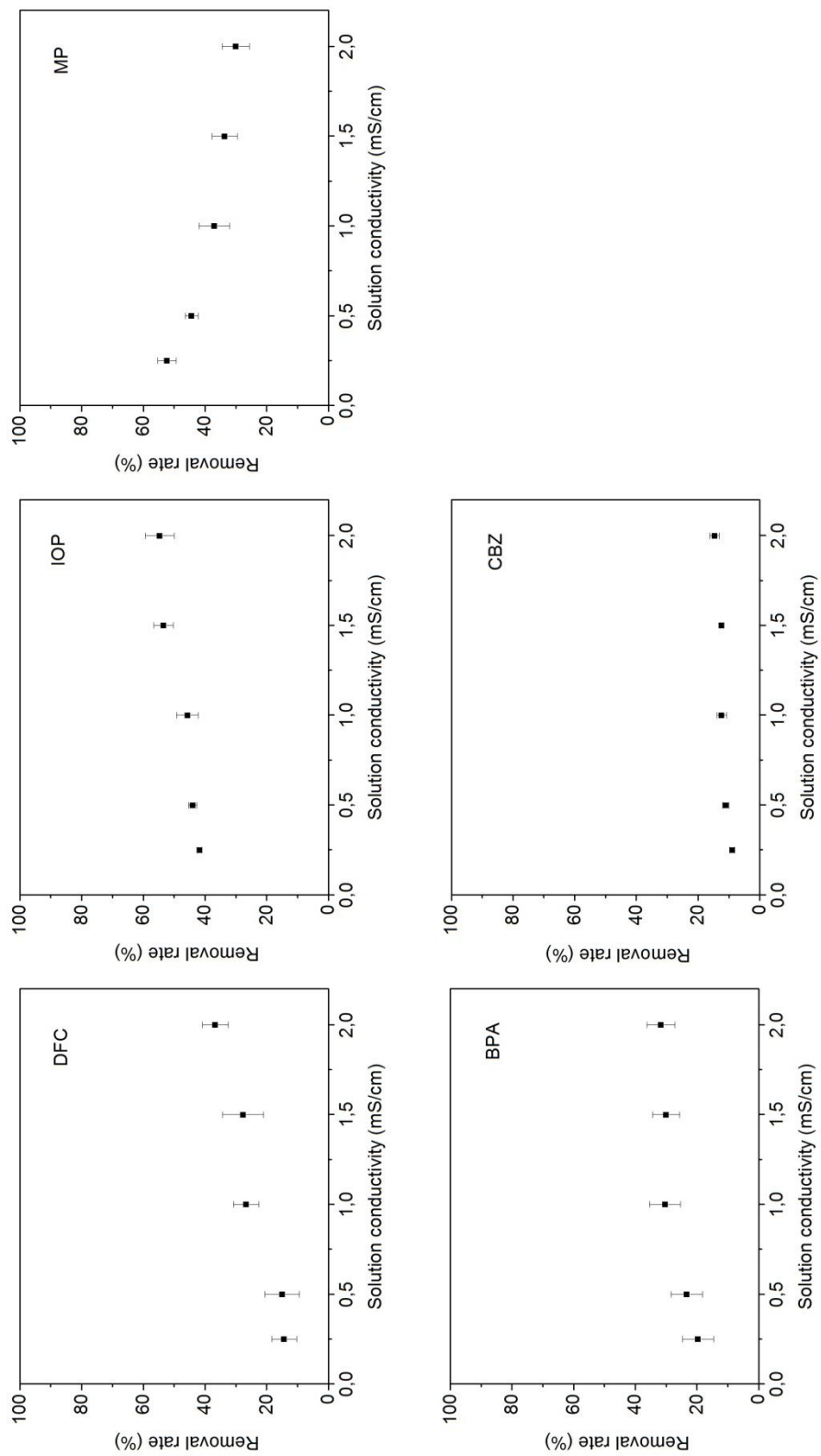


Figure 73. Effect of the solution conductivity on the removal rates of DFC, IOP, MP, BPA, CBZ (BR, $C_0 = 10 \text{ mg/L}$). The tendencies are expressed by the plots and the mean values of removal rates at 0.25 and 2 mS/cm are summarized in the table

From the figure it is seen that, by increasing the solution conductivity, the removal rates of all compounds, apart from MP, increase. The influence of solution conductivity on the degradation of some compounds is stronger and for other compounds is weaker. Among the tested compounds, solution conductivity makes the strongest effect on the removal of DFC as its removal rates were increased by three times using 2 mS/cm instead of 0.25 mS/cm. The least influenced by solution conductivity compound appeared to be CBZ. The opposite effect was found for MP, which removal rate was increased by more than two times when using ten times lower solution conductivity. Thus, the removal rate of $(30 \pm 4)\%$ was achieved at $\sigma = 2$ mS/cm, whereas the removal rate of $(52 \pm 3)\%$ was obtained at $\sigma = 0.25$ mS/cm.

The increase of solution conductivity leads to the more intense light emission (Chapter 3.3.2.2.) and higher electron density (Chapter 3.3.5.1.). However, the amount and the lifetime of the reactive species decrease with increase of solution conductivity: at high values of solution conductivity, the recombination of OH is faster (Chapter 3.3.3.2.). From this, one can assume that the compounds, which degradation is increased at higher solution conductivity, more likely undergo the decomposition by the physical effects induced by plasma (e.g. UV radiation); whereas the compounds, which degradation is not or slightly influenced by solution conductivity, more likely undergo decomposition by chemical effects (e.g. oxidation by OH[•]). This assumption is with a good agreement with the literature data that report on the higher tendency of MP to oxidation with OH[•] (Ikehata *et al*, 2006) rather than to photolytical decomposition (Liu *et al*, 2009, Bokar *et al*, 2011, Piram *et al*, 2008). Thus, at lower solution conductivity the amount OH[•] is higher, which leads to the higher removal rates of MP compared to high solution conductivity, when the amount of OH[•] is much less.

The effect of the solution conductivity on the removal rates of other tested chemicals – DFC, IOP, BPA, CBZ – could be explained by the possibility of their degradation by both – OH[•] and UV light. Yet, the slight increase of the removal rates at higher solution conductivity suggests the more decisive role of photolysis than oxidation by OH[•] in the removal of the tested compounds by underwater plasma discharges.

The similar effects made by solution conductivity on the organics removal by electrical discharges could be found in literature. In general way, the authors report on the positive effect of the increased solution conductivity in the case of the compounds

unstable towards the UV light; and the opposite effect in the case of the decomposition dominated by OH^\bullet . Dang *et al*, 2009 reported on the increased degradation yield of 4-chlorophenol and 4-nitrophenol by liquid phase electrical discharges at the elevated solution conductivity. The authors also pointed out at the significant role of UV radiation in degradation process at higher solution conductivity. Dors *et al*, 2007, on the contrary, demonstrated that at high solution conductivity (600 $\mu\text{S}/\text{cm}$, tap water), phenol cannot be decomposed by electrical discharges, whereas in the deionized water (1 $\mu\text{S}/\text{cm}$) the removal rates could be much increased. The authors explained this effect by the decreased yield of OH^\bullet at high solution conductivities, which were supposed to play the decisive role in the phenol degradation.

However, it should be noted that the effects induced by underwater plasma are not limited by the UV radiation and OH^\bullet formation, although those two are supposed to dominate in the degradation of organics. Other important effects (high temperature of the discharge channel, shock waves, formation of oxidative and reductive species) could be enhanced with the change of solution conductivity and should be taken into account when considering the degradation of organics.

4.3.2. Degradation kinetics

The decrease of concentration of the tested compounds exposed to the plasma discharges is shown in figure 74 as a function of treatment time (the error bars are omitted for clarity). The figure summarizes the degradation profiles of each compound at three initial concentrations (1, 10 and 100 mg/L) obtained in the batch and flow reactors.

From the figure 74 it is seen that the concentration of compounds decreases very fast in the first minutes of treatment and the rate slows down closer to the end of operation. Thus, for example, DFC was degraded by 50% within 4 min of treatment and by the end of the treatment (30 min), the removal was 90% (BR, $C_0 = 1 \text{ mg/L}$). In the case of BPA, the degradation is much slower indicating the higher recalcitrance of BPA towards the action of electrical discharges compared to DFC and IOP. The concentration of BPA decreases by 33% within the first 15 min of operation and achieves 39% within the next 15 min (BR, $C_0 = 1 \text{ mg/L}$). In case of CBZ, the

stationary concentration is achieved within the first 5 min of treatment (12%) after which no considerable decrease of concentration is observed (BR, $C_0 = 1$ mg/L). One

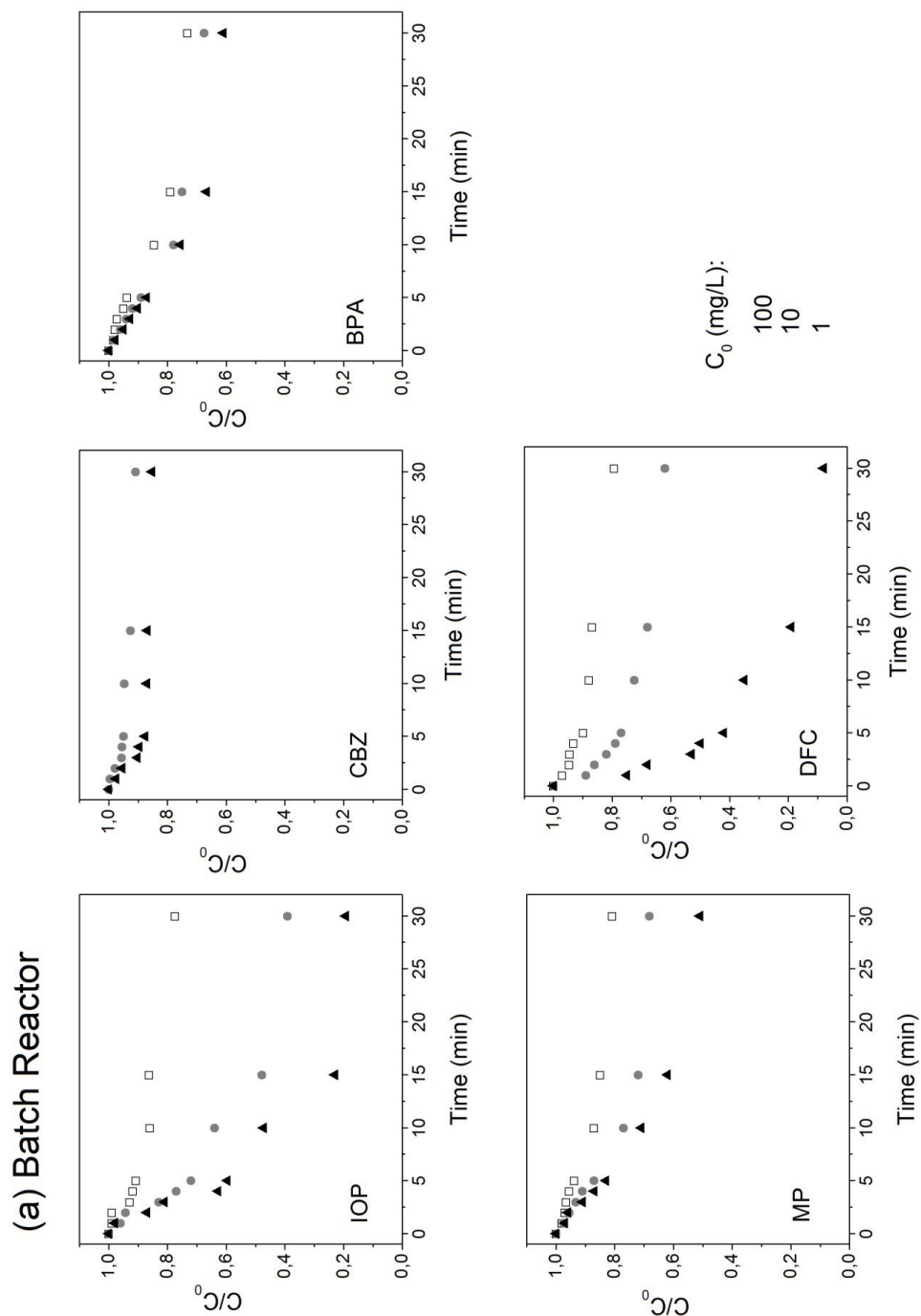


Figure 74. Degradation curves of DFC, IOP, MP, BPA and CBZ in (a) BR and (b) FR at initial concentrations of 1, 10 and 100 mg/L. Continued on the next page

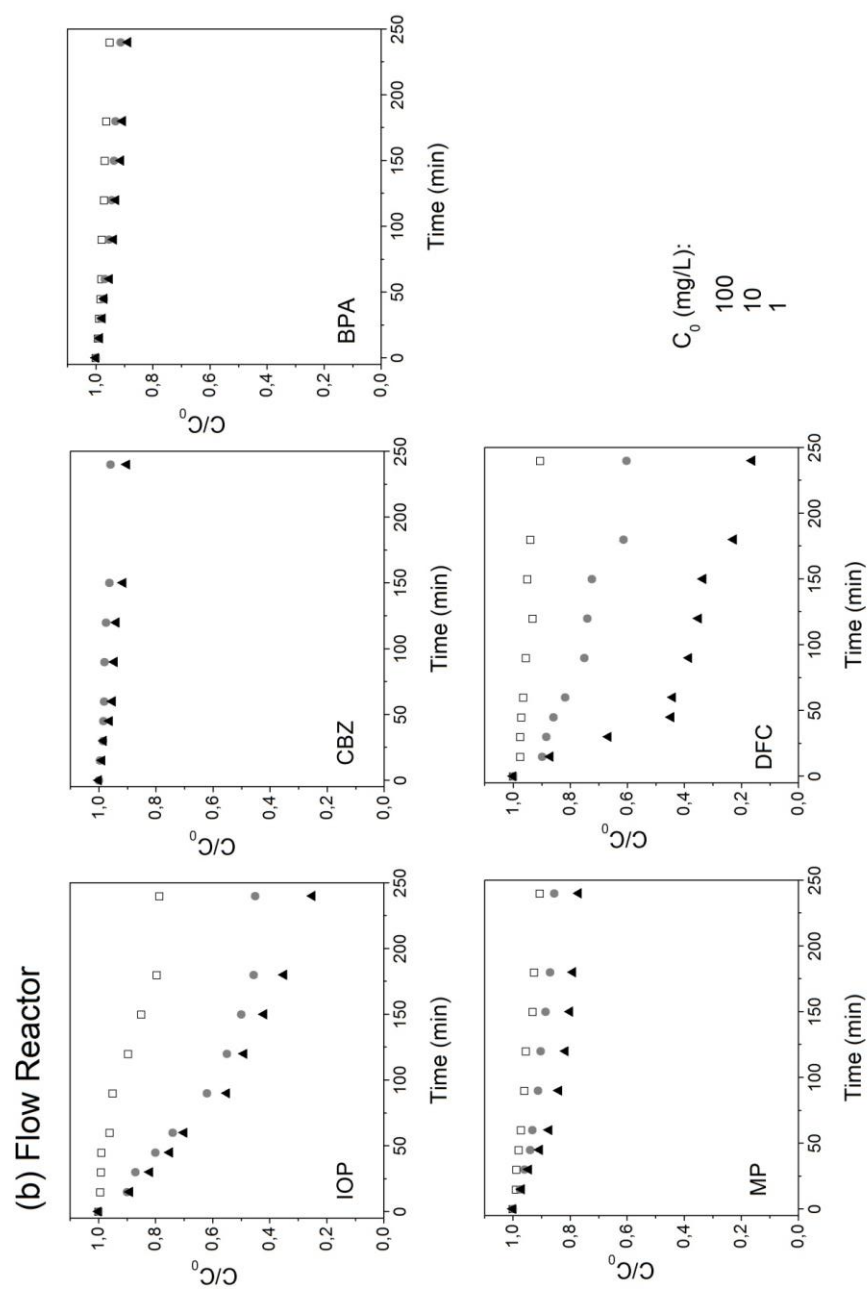


Figure 74. Degradation curves of DFC, IOP, MP, BPA and CBZ in (a) BR and (b) FR at initial concentrations of 1, 10 and 100 mg/L

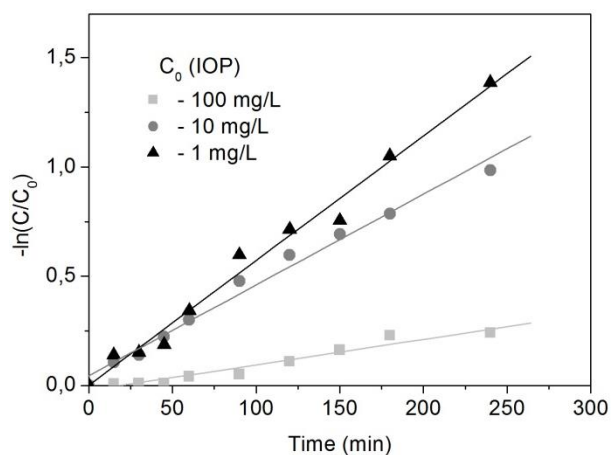


Figure 75. First order degradation plots on the example of iopamidol (FR)

Table 7. Observed pseudo-first order rate constants of degradation of pharmaceuticals in FR and BR for $C_0 = 1, 10$ and 100 mg/L

Compound	$C_0 \text{ (mg/L)}$	$k_{\text{obs}} \text{ (min}^{-1}\text{)}$	
		Flow reactor	Batch reactor
DFC	100	$(3.4 \pm 0.4) \cdot 10^{-4}$	$(6.9 \pm 0.8) \cdot 10^{-3}$
	10	$(2.0 \pm 0.2) \cdot 10^{-3}$	$(2.0 \pm 0.2) \cdot 10^{-2}$
	1	$(6.9 \pm 0.7) \cdot 10^{-3}$	$(7.9 \pm 0.6) \cdot 10^{-2}$
IOP	100	$(1.2 \pm 0.1) \cdot 10^{-3}$	$(8.2 \pm 1.1) \cdot 10^{-3}$
	10	$(4.2 \pm 0.3) \cdot 10^{-3}$	$(3.2 \pm 0.4) \cdot 10^{-2}$
	1	$(5.7 \pm 0.5) \cdot 10^{-3}$	$(5.9 \pm 0.8) \cdot 10^{-2}$
MP	100	$(4.2 \pm 0.2) \cdot 10^{-4}$	$(7.3 \pm 0.9) \cdot 10^{-3}$
	10	$(6.2 \pm 0.5) \cdot 10^{-4}$	$(2.3 \pm 0.1) \cdot 10^{-2}$
	1	$(1.1 \pm 0.1) \cdot 10^{-3}$	$(2.3 \pm 0.2) \cdot 10^{-2}$
BPA	100	$(1.8 \pm 0.1) \cdot 10^{-4}$	$(1.2 \pm 0.1) \cdot 10^{-2}$
	10	$(3.7 \pm 0.2) \cdot 10^{-4}$	$(1.5 \pm 0.2) \cdot 10^{-2}$
	1	$(5.2 \pm 0.5) \cdot 10^{-4}$	$(1.9 \pm 0.3) \cdot 10^{-2}$
CBZ	10	$(1.7 \pm 0.2) \cdot 10^{-4}$	$(1.6 \pm 0.3) \cdot 10^{-3}$
	1	$(4.6 \pm 0.6) \cdot 10^{-4}$	$(2.0 \pm 0.6) \cdot 10^{-3}$

of the possible reasons of the limited degradation rates of CBZ could be the formation of more recalcitrant transformation products which do not allow for the further degradation of the initial substance (Donner *et al*, 2012, Im *et al*, 2012).

The description of the obtained results on the degradation kinetics is complicated by the fact that the mechanism of the degradation is not known. The great variety of the physical and chemical processes induced by underwater plasma discharges leads to the complex processes occurring with the organic compounds. Another fact that does not enable to determine the real degradation kinetics is the formation of the transformation products simultaneously with the degradation of the initial substances. The parallel degradation of the transformation products should also be taken into account.

The degradation curves of the pharmaceuticals could be described by the equation:

$$\frac{dc}{dt} = -kc, \quad (37)$$

where C is the concentration of a compound (mg/L), t is the treatment time (min) and k is the observed rate constant (min^{-1}).

Thus, it was assumed that, in the present study, the degradation of the pharmaceuticals obeys the first order kinetics, showing the domination of one degradation pathway over the others. The linear dependence of $-\ln(C/C_0)$ on t shown in figure 75 on the example of IOP in the FR at $C_0 = 1, 10$ and 100 mg/L. As it could be seen, the experimental data are fitted with the straight lines. The observed pseudo-first order rate constants of the IOP degradation were calculated from the slope of the fitted lines and were found to be $(1.2 \pm 0.1) \cdot 10^{-3}$, $(4.2 \pm 0.2) \cdot 10^{-3}$ and $(5.7 \pm 0.2) \cdot 10^{-3} \text{ min}^{-1}$ for $C_0 = 100, 10$ and 1 mg/L, respectively. The data on degradation of all other compounds were treated analogically and the obtained results are summarized in table 7.

Several tendencies could be derived from the obtained values: (i) in general way, the observed rate constants are of one order of magnitude lower in the FR than in the BR, which suggests the faster degradation obtained in the BR; (ii) The values of the rate constants are higher for lower initial concentrations, confirming the results obtained in the previous subchapter; (iii) The highest values of the rate constants are obtained for DFC and IOP and the lowest ones are obtained for CBZ and BPA, confirming the higher recalcitrance of the latter ones.

From the analysis of the amount of OH^\bullet formed by the underwater electrical discharge (in the range of μM , figure 18, Chapter 2), it is obvious that the pharmaceuticals would be present in solution in a great excess compared to OH^\bullet at the high values of initial concentration; or the pharmaceutical concentration would be comparable to the one of OH^\bullet at the low initial concentrations (e.g. $C_0 = 1 \text{ mg/L}$ is equal to $3.2 \mu\text{M}$, $1.3 \mu\text{M}$, $1.5 \mu\text{M}$, $4.4 \mu\text{M}$ and $4.2 \mu\text{M}$ of DFC, IOP, MP, BP and CBZ, respectively). Thus, assuming the degradation caused only by OH^\bullet , one should expect the order of the reaction higher than the $n = 1$. However, the observed pseudo-first order degradation kinetics suggests that not only OH^\bullet participate in the degradation process, but also other effects such as the reactions with other oxidative species and/or the degradation by the discharge light.

The same pseudo-first order degradation kinetics was observed by the most of authors dealing with the degradation of organics by electrical discharges. However, the k_{obs} values reported in literature are $\sim 10^3$ times higher than the obtained in the present study. DFC was reported by Salgado *et al*, 2012 to undergo much faster photodegradation with $k = 2.5 (\text{min}^{-1})$ also following the pseudo-first order kinetics.

Magureanu *et al*, 2010 described the plasma induced degradation of a pharmaceutical compound – pentoxifylline – by the pseudo-first order. The authors reported on the higher values of rate constants at the same range of C_0 ($k_{obs} = 129.9 \pm 8.3 \text{ min}^{-1}$ for $C_0 = 25 \text{ mg/L}$ and $k_{obs} = 33.7 \pm 0.9 \text{ min}^{-1}$ for $C_0 = 150 \text{ mg/L}$). It is assumed that the main reason of the higher values of rate constants obtained by the authors is the different discharge type (corona in air). The authors also assumed an important, but not the decisive role of OH^\bullet in the degradation of the compound. The removal of phenols in water using corona in gas phase was reported by Lukes *et al*, 2005 to follow the first order kinetics and the degradation was dominated by the OH^\bullet attack. The degradation of more persistent pharmaceuticals – carbamazepine, clofibrac acid and iopromide – was shown by Krause *et al*, 2011 to follow the first order kinetics as well. Medevovic *et al*, 2007, on the contrary, assumed the degradation of atrazine only by OH^\bullet formed during electrical discharges. The authors described the degradation by the second order kinetics, excluding from the consideration UV induced photolysis due to the low efficiency of the latter one at $\sigma = 100 \mu\text{S/cm}$. DFC was reported by Salgado *et al*, 2012 to undergo much faster photodegradation with $k = 2.5 (\text{min}^{-1})$, pseudo-first order kinetics with).

4.3.3. Transformation products of DFC

The degradation of organic substances by different water treatment techniques often results in the formation of various degradation products. The degradation products and intermediates may have different, compared to the initial compound, ability towards the degradation by electrical discharges, i.e. they could be more degradable or more recalcitrant. In the case of higher stability, the products will be decomposed with a much slower rate. Moreover, the toxicity of the products is also a big issue

Normally, the identification of transformation products involves the use of mass-spectrometry (MS). However, the detection of transformation products using LC-MS in the present study was not possible as the obtained mass chromatograms contained no peaks which could be attributed to the products. The approaches included ESI-MS positive ion mode and ESI-QTOF. One of the possible reasons why no considerable signal was recorded with LC-MS could be the low concentration of the transformation products which was under the detection limit of the techniques ($\sim 10\mu\text{g/L}$). However, the probably formed products appeared to have high extinction coefficients which allowed of their detection using HPLC-DAD (will be discussed below) as several additional peaks to the initial one appeared on the chromatograms after the degradation experiment. Second possible reason could be the molecular structure of the products. The poor ionization degree of the products did not allow to obtain considerable signal using LC-MS. This assumption is particularly important taking into account that for the degradation experiments were performed in highly conductive solutions, where the ion concentration (Na^+ and SO_4^{2-}) much exceeded the concentration of the pharmaceuticals.

In the present study, the characterization of the transformation products was carried out using HPLC-DAD on the example of DFC. The choice of DFC for this study was due to (i) its higher removal rates compared to other tested compounds and (ii) lots of data available on its transformation products in the literature (Agüera *et al*, 2005, Goerner *et al*, 2010, Salgado *et al*, 2012, Sein *et al*, 2008, Miyamoto *et al*, 1997, Kaphalia *et al*, 2006, Perez-Estrada *et al*, 2005). First fact enables to obtain the considerable signal from the detected products and, thus, improve the chromatographic resolution. Second fact allows to carry out the comparison of the obtained results with the ones published before.

The chromatograms of DFC before and after plasma treatment are shown in figure 76 ($C_0 = 10 \text{ mg/L}$, $t = 1\text{h}$, BR). The multiple peaks on both chromatograms in the range of 5 – 10 min (dead time) correspond to the release of unretained components in the mixture. Significant decrease of the peak area of DFC at 16.7 min indicates the decrease of its concentration by 65% after the exposure to the electrical discharges. Five additional peaks appeared and were separated on the chromatogram after DFC degradation. The corresponding UV spectra of each peak are shown in figure 77. The peak I corresponds to a product with a retention time (t_{ret}) 11.3 min and the maximal absorption (λ_{max}) at 205 nm. The peak II appears at 13.2 min and the corresponding compound has two absorption maxima: $\lambda_{\text{max}1} = 205 \text{ nm}$ and $\lambda_{\text{max}2} = 361 \text{ nm}$. The peak III contains two bands (IIIa and IIIb) which separation is not visible on the chromatogram due to the low absorption at the selected wavelength (254 nm) and insufficient time resolution. The product IIIa with $t_{\text{ret}} = 14 \text{ min}$ and product IIIb with $t_{\text{ret}} = 14.5 \text{ min}$ both have $\lambda_{\text{max}} = 205 \text{ nm}$. The peak IV corresponds to a product with $t_{\text{ret}} = 18.9 \text{ min}$ and $\lambda_{\text{max}} = 236 \text{ nm}$. The peak V corresponds to a products with $t_{\text{ret}} = 23.9 \text{ min}$ and $\lambda_{\text{max}1} = 224 \text{ nm}$ and $\lambda_{\text{max}2} = 279 \text{ nm}$.

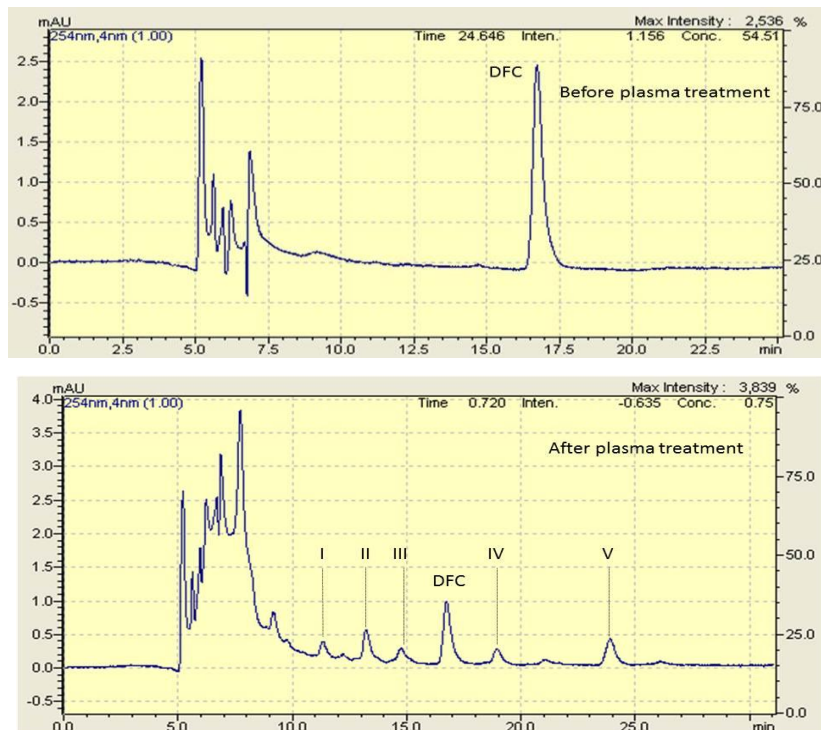


Figure 76. HPLC chromatograms of DFC before (upper image) and after (lower image) plasma treatment recorded at 254 nm

The oxidation of DFC by OH or O₃ is usually reported to proceed through the formation of 4'-hydroxydiclofenac (4'-OH DFC, $\lambda_{\text{max}} = 267 \text{ nm}$), 5-hydroxydiclofenac (5-OH DFC) and diclofenac-2,5-iminoquinone (DFC-2,5-iminoquinone, $\lambda_{\text{max}} = 455 \text{ nm}$) (Miyamoto *et al*, 1997, Kaphalia *et al*, 2006, Sein *et al*, 2008, Perez-Estrada *et al*, 2005, Kinne *et al*, 2009). It was assumed that the formation of 4'-OH DFC and 5-OH DFC did not take place as there were no compounds among the detected ones with the same λ_{max} . Additionally, the formation of DFC-2,5-iminoquinone was also excluded from consideration as no increase of the absorption

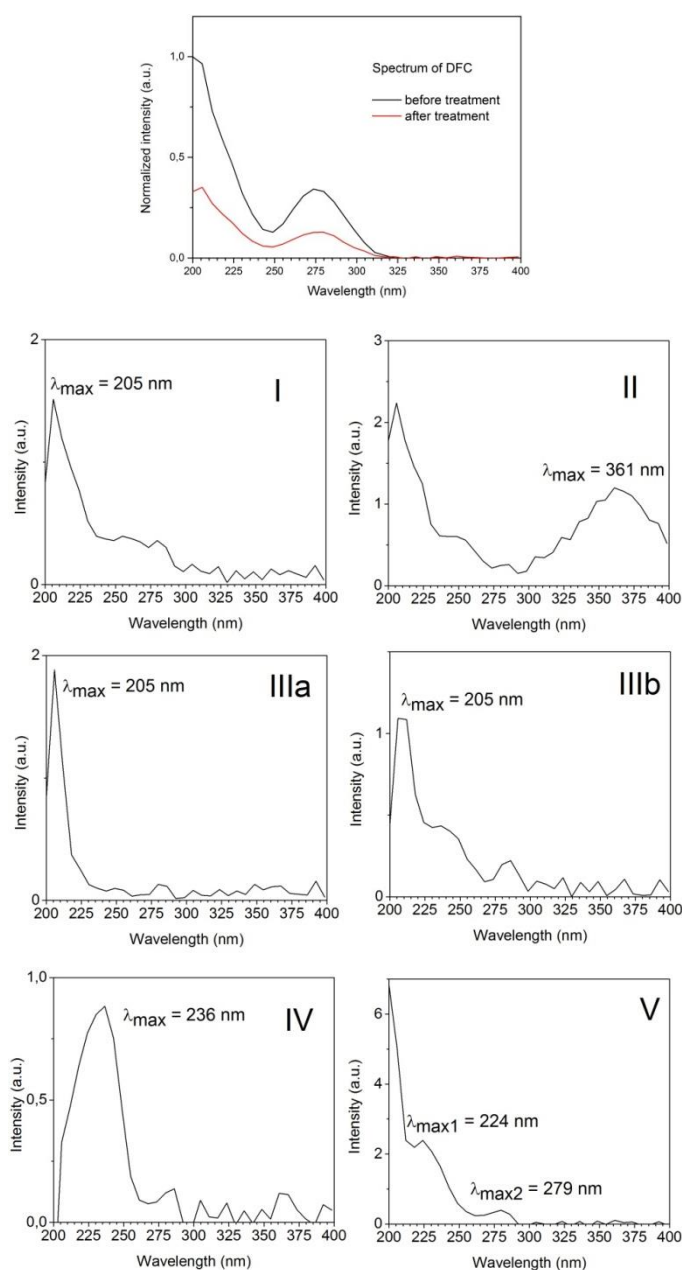


Figure 77. Absorption spectra of DFC and its transformation products

intensity took place in the region near 400 nm. It suggests that either the oxidation of DFC by OH did not take place or (5-OH DFC), (4'-OH DFC) and DFC-2,5-iminoquinone were fully decomposed during the plasma treatment.

The peaks I and III were attributed to the compounds that have a very short or have no conjugated system as the absorption maxima of the corresponding compounds are in the region of short wavelengths (205 nm). Thus, it was assumed that the degradation of DFC by underwater electrical discharges has led to the formation of three transformation products assigned at peaks II, IV and V. The product II has a retention time shorter than DFC, suggesting that it has a less polar structure. On the contrary, the products IV and V are retained stronger by the chromatographic column, therefore, they have a more polar structure than DFC. The absorption spectrum of the compound II suggests the formation of a long conjugated system as the λ_{max} lies in the region of the long wavelength (361 nm). The absorption maximum of product IV at 236 nm could suggest the formation of 1-(8-chlorocarbazolyl)acetic acid. The products of DFC containing carbazole fragments in their structure are resulted from the photocyclization of DFC reported by Görner *et al*, 2010, Agüera *et al*, 2005, Encinas *et al*, 1998 and Salgado *et al*, 2012. The cyclization of DFC proceeds through the loss of Cl and the ring closure, which could be followed by the further hydroxylation, dehalogenation and oxidation of the ring by O₂ (Salgado *et al*, 2012, Hofmann *et al*, 2007) or by decarboxylation to form chlorocarbazole (Agüera *et al*, 2005).

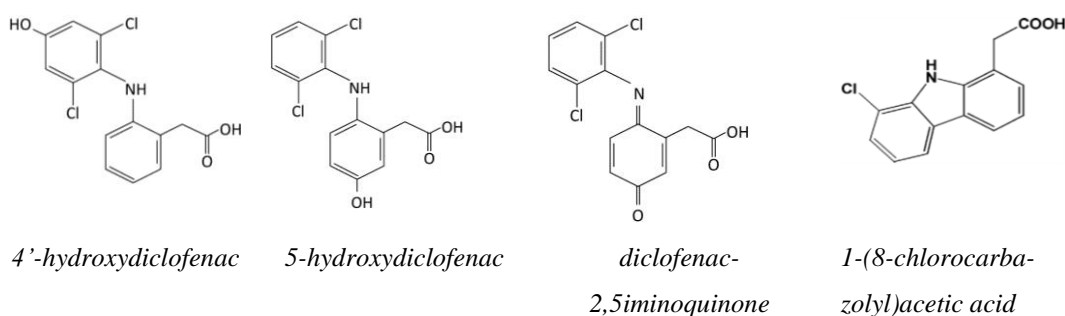


Figure 78. The main degradation products of diclofenac reported in literature

4.3.4. Energy efficiency

Energy efficiency is an important parameter that defines in a crucial way the applicability of the method for degradation of compounds. The energy efficiency of underwater plasma for degradation of organic compounds was evaluated using equation 33. In this subchapter, the effect of the reactor type, initial concentration and treatment time on the energy efficiency of the organics removal is discussed.

4.3.4.1. Effect of the treatment time

The highest values of energy efficiency are achieved in the beginning of degradation and these values decrease with time. The decrease of energy efficiency with treatment time is shown in figure 79 on the example of DFC degradation in the BR. As it could be seen, DFC degradation results in 230 mg/kWh efficiency after 5 min of operation at the removal rate of 10% ($C_0 = 100$ mg/L); while the removal of DFC by 21% after 30 min of treatment results in ~2 times lower energy efficiency (120 mg/kWh). Thus, the increase of treatment time leads to significant decrease of the energy efficiency. It is explained by higher energy consumption at longer treatment times. As it was shown above, the degradation rate is high in the beginning of the treatment and slows down at the end. As a result, the ratio *the number of substance converted/the number of energy required* would be more influenced by the value of the removal rate in the beginning and less at the end of the treatment. Thus, the reverse proportionality of the energy efficiency and the removal rates should be taken into account when compromising between the necessity to obtain high removal rates and high energy efficiency.

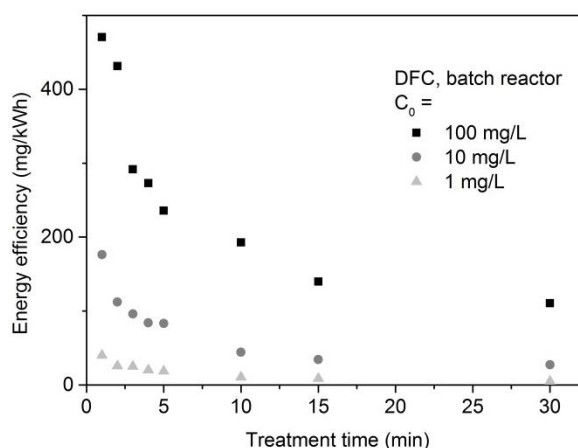


Figure 79. Effect of the treatment time on the energy yield on the example of DFC degradation in the BR at $C_0 = 100, 10$ and 1 mg/L

4.3.4.2. Effect of the initial concentration

The higher energy efficiency of degradation is achieved at the same value of removal rate when the initial concentration is higher (table 8, figure 79). For example, the removal of DFC by 21% (BR) results in energy efficiency of 100 mg/kWh at $C_0 = 100$ mg/L (after 30 min of treatment) and 20 mg/kWh at $C_0 = 1$ mg/L (after 4 min of treatment). It suggests that organics removal by the present method is more efficient when the concentration of pollutants is high. However, in the real samples with the pollutant concentrations in the range of $\mu\text{g/L}$, the energy efficiency is expected to be much lower.

4.3.4.3. Effect of the reactor configuration

The reactor configuration was proved to influence significantly the energy efficiency. The values of energy efficiency were calculated for both reactor types at fixed values of the removal rates. The lowest achieved values of removal rates (for all compounds obtained in the flow reactor, $C_0 = 100$ mg/L) were taken as the values at which the energy efficiencies were compared. The results are summarized in table 8.

Table 8. Energy efficiency of DFC, IOP, MP, BPA and CBZ degradation at the fixed removal rate of 10, 21, 9, 5 and 4%, respectively, in the batch and flow reactors

Compound (at % of removal)	Batch reactor			Flow reactor		
	100 mg/L	10 mg/L	1 mg/L	100 mg/L	10 mg/L	1 mg/L
DFC (10%)	236	176	NA	51	86	NA
IOP (21%)	112	60	5	116	84	10
MP (9%)	170	36	5	51	10	1
BPA (5%)	155	13	2	26	6	1
CBZ (4%)	NA	2	1	NA	24	4

As it is seen from the table, a higher energy efficiency is achieved in the BR compared to the FR (provided that other conditions are kept constant) for DFC, MP and BPA. Thus, for example, the energy efficiency for DFC degradation is improved by almost five times using BR instead of FR at $C_0 = 100$ mg/L. However, for most of the cases this difference is not significant. An opposite effect of the reactor type on the energy efficiency was obtained for IOP and CBZ as the values of energy efficiency are higher in the flow reactor for all tested concentrations.

Studies on degradation of organics by electrical discharges commonly report on three orders of magnitude higher energy efficiency. Magureanu *et al*, 2010, Gerrity *et al*, 2010 and Medevovic *et al*, 2007 also investigated the removal of organics by electrical discharges and reported on the degradation efficiency of the order of g/kWh. The reason of the lower energy efficiency obtained in the present study could be: (i) much higher recalcitrance of the compounds tested in the present study compared to the less recalcitrant phenols and organic dyes reported in the literature; and (ii) much higher values of energy per pulse for electrical discharges in liquids compared to the ones in gas phase. The first assumption is evidenced by the comparison of the works of Grabowski and Krause (Grabowski *et al*, 2006, Krause *et al*, 2009), who both used the same gas-phase discharge operation (corona above water), but different organic compounds. Thus, much higher recalcitrance of pharmaceuticals (carbamazepine, clofibric acid and iopromide) investigated by

Krause et al has led to the lower energy efficiency (a few mg/kWh) compared to Grabowski et al (a few g/kWh) who studied the degradation of phenol. To prove the second assumption, one may refer to the work of Malik *et al*, 2010, who carried out a comparative study of different discharge operations in terms of energy efficiency. The authors showed the much high efficiency of reactors in which electrical discharges are generated in gas-phase to treat a thin water layer. The lowest efficiencies were reported to be attributed to the reactors utilizing electrical discharges in liquid phase. In the present study, $E_p \simeq 1$ J, whereas E_p reported in the literature for corona above water is of the order of mJ. Since the formation of electrical discharge in liquid is ~ 1000 times more energy consuming, the energy efficiency of a treatment technique involving liquid-phase discharges will be much lower than the treatment by gas-phase discharges.

4.3.5. Degradation of TFA

Additionally to the pharmaceutical compounds, the ability of plasma discharges to degrade recalcitrant compounds was checked on the example of trifluoroacetic acid (TFA) known as a representative of the highly persistent polyfluorinated compounds (PFC). The decrease of TFA concentration after the plasma treatment was monitored by analyzing the peak area of CF_3COO^- anion. Figure 80 represents the ion chromatograms of TFA before and after the plasma treatment ($t = 2$ h, BR, $C_0 = 1$ μM). The peak at 4.1 min is attributed to SO_4^{2-} anion which is present in solution in order to adjust the conductivity (Na_2SO_4). The peak at 7.1 min is due to F^- anion released by the destruction of Teflon® holders. The decrease of the peak area of CF_3COO^- (retention time 8.6 min) after the plasma treatment corresponds to the decrease of TFA concentration by $(14.43 \pm 0.29)\%$. The peaks at 2.5 and 5.6 min were attributed to the presence of impurities in the solution after treatment. Analogical experiment with the same experimental conditions was carried out with $C_0 = 10$ μM . In this case, the TFA concentration was decreased by $(4.04 \pm 0.10)\%$.

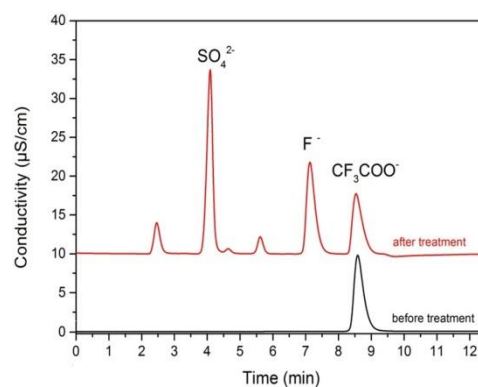


Figure 80. Ion chromatograms of TFA before and after plasma treatment. $C_0 = 1 \mu\text{M}$, BR, $t = 2\text{h}$, $U = 30 \text{ kV}$, $F = 10 \text{ Hz}$, $\sigma = 2 \text{ mS/cm}$. The chromatograms are shifted vertically for clarity

Under the utilized conditions it is not possible to measure the release of F^- during TFA degradation. The expected amount of F^- which is formed through the possible cleavage of the C-F bond in TFA is much smaller than the measured amount caused by the Teflon holder destruction. Thus, the question of the mechanism of TFA degradation by underwater electrical discharges is still open and needs further investigation. However, it is assumed that the complete defluorination of CF_3COO^- is unlikely to take place under the plasma conditions.

4.4. Summary

The capability of underwater electrical discharges to treat water was studied on the example of six recalcitrant compounds – five pharmaceuticals (diclofenac, iopamidol, metoprolol, bisphenol A and carbamazepine) and trifluoroacetic acid.

Underwater electrical discharges were proven to successfully degrade the tested pharmaceuticals. The higher removal rates are obtained for the lower initial concentration of the compounds. The use of the flow reactor for treatment of contaminated water does not significantly decrease the removal rates compared to the batch reactor. The removal was found to be higher in solutions with high conductivity for most of tested compounds (apart from metoprolol). Thus, the desalination of water in the case of real samples prior to the plasma treatment is not needed.

The degradation of highly persistent trifluoroacetic acid by underwater electrical discharges was shown to be possible during relatively short period of time.

The higher removal rates of the pharmaceuticals and trifluoroacetic acid could be achieved at lower initial concentration and longer treatment time.

The degradation of all pharmaceuticals was found to obey the pseudo-first order kinetics. The observed pseudo-first order degradation constants are higher for lower initial concentrations and for the reactor operation in the batch configuration.

In the present study, it was possible to detect three transformation products of diclofenac. None of them was previously reported in the literature.

The method of underwater electrical discharges for water treatment was found to be energy consuming, however, it is feasible for degradation of recalcitrant compounds.

4.5. List of literature

- Abou-Ghazala** A., Katsuki S., Schoenbach K.H., Dobbs F.C., Moreira K.R. 2002. Bacterial decontamination of water by means of pulsed-corona discharges. *IEEE Trans Plasma Sci.* 30, 1449-1453
- Abramovic** B., Kler S., Sojic D., Lausevic M., Radovic T., Vione D. 2011. Photocatalytic degradation of metoprolol tartrate in suspensions of two TiO₂-based photocatalysts with different surface area. Identification of intermediates and proposal of degradation pathways. *J Hazard Mater.* 198, 123-132
- Agüera** A., Perez-Estrada L.A., Ferrer I., Thurman E.M., Malato S., Fernandez-Alba A.R. 2005. Application of time-of-flight mass spectrometry to the analysis of phototransformation products of diclofenac in water under natural sunlight. *J Mass Spectrom.* 40, 908-915
- Andreozzi** R., Raffaele Marotta R., Gabriele Pinto G., Pollio A. 2002. Carbamazepine in water: persistence in the environment, ozonation treatment and preliminary assessment on algal toxicity. *Water Res.* 36(11), 2869–2877
- Andreozzi** R., Marotta R., Paxeus N. 2003. Pharmaceuticals in STP effluents and their solar photodegradation in aquatic environments. *Chemosphere.* 50, 1319-1330
- Astier** A., Maury M., Barbizet J. 1979. Simultaneous, rapid high-performance liquid chromatographic microanalysis of plasma carbamazepine and its 10,11-epoxide metabolite: applications to pharmacokinetic studies in humans. *J Chromatogr.* 164(2), 235-40
- Atkinson** A., Roy D. 1995. In vitro concersion of environmental estrogenic chemical bisphenol A to DNA binding metabolite(s). *Biochem Biophys Res Commun.* 210, 424-433
- Baker** K.M., Frigerio K.M., Morselli P.L., Pifferi G. 1973. Identification of a rearranged degradation product from carbamazepine-10,11-epoxide. *J Pharm Sci.* 62, 475-476
- Baran** W., Sochacka J., Wardas W. 2006. Toxicity and biodegradability of sulfonamides and products of their photocatalytic degradation in aqueous solutions. *Chemosphere.* 65(8), 1295-1299
- Berends** A.G., Boutonnet J.C., Rooij C.D. De, Thompson R.S. 1999 Toxicity of trifluoroacetate to aquatic organisms. *Environ Toxicol Chem.* 18(5), 1052-1059

Barnhard M., Mueller J., Knepper T.P. 2006. Biodegradation of persistent polar pollutants in wastewater: comparison of an optimized lab-scale membrane bioreactor and activated sludge treatment. *Water Res.* 40, 3419-3428

Borkar R.M., Raju B., Srinivas R., Patel P., Shetty C.K. 2011. Identification and characterization of stressed degradation products of metoprolol using LC/Q-TOF-ESI-MS/MS and MS(n) experiments. *Biomed Chromatogr.* 26, 720-736

Bin X.U., Naiyun G.A.O., Min R., Hong W., Haihui W.U. 2007. Degradation of endocrine disruptor bisphenol A in drinking water by ozone oxidation. *Front Environ Sci Engin China.* 1(3), 350-356

Bound J.P., Kitsou K., Voulvoulis N. 2005. Household disposal of pharmaceuticals and perception of risk to the environment. *Environ Toxicol Pharm.* 21(3), 301-307

Boutonnet J.C., Bingham P., Calamari D., Rooij C. De, Franklin J., Kawano T., Libre J.-M. McCulloch A., Malinverno G., Odom J.M., Rusch G.M. Smythe K., Sobolev I., Thompson R., Tiedje J.M. 1999. Environmental risk assessment of trifluoroacetic acid. *Hum Ecol Risk Assess.* 5, 59-124

Bozic A.L., Koprivanac N., Sunka P., Clupek M., Babicky V. 2004. Organic synthetic dye degradation by modified pinhole discharge. *Czech J Phys.* 54, C958-C963

Bubnov A.G., Burova E.Y., Grinevich V.I., Rybkin V.V., Kim J.K., Choi H.S. 2006. Plasma-catalytic decomposition of phenols in atmospheric pressure dielectric barrier discharge. *Plasma Chem Plasma Process.* 26(1), 19-30

Buser H.R., Poiger T., Mueller M.D. 1998. Occurrence and fate of the pharmaceutical drug diclofenac in surface waters: rapid photodegradation in a lake. *Environ Sci Technol.* 32(22), 3449-3456

Buser, H.-R., Poiger, T., Mueller, M.D. 1999. Occurrence and experimental behavior of the pharmaceutical drug ibuprofen in surface waters and in wastewater. *Environ Sci Technol.* 33, 2529-2535

Carballa M., Omil F., Ternes T., Lema J.M. 2007. Fate of pharmaceutical and personal care products (PPCPs) during anaerobic digestion of sewage sludge. *Water Res.* 41(10), 2139-2150

Chai W., Handa Y., Suzuki M., Saito M., Kato N., Horiuchi C.A. 2005. Biodegradation of bisphenol A by fungi. *Appl Biochem Biotechnol.* 120, 175-182

ChemSpider, the free chemical database <http://www.chemspider.com>

Ching W.K., Colussi A.J., Sun H.J., Nealson K.H., Hoffmann M.R. 2001. Escherichia coli disinfection by electrohydraulic discharges. *Environ Sci Technol.* 35(20), 4139-4144

Clara M., Strenna B., Gans O., Martinez E., Kreuzinger N., Kroissa H. 2005. Removal of selected pharmaceuticals, fragrances and endocrine disrupting compounds in a membrane bioreactor and conventional wastewater treatment plants. *Water Res.* 39, 4797-4807

Coestier C.M., Spinelli S., Lin L. 2009. Discharge of pharmaceutical products (PPs) through a conventional biological sewage treatment plant: MECs vs PECs? *Environ Intl.* 35, 787

Cui Y.-H., Li X.-Y., Chen G. 2009. Electrochemical degradation of bisphenol A on different anodes. *Water Res.* 43, 1968-1876

Dang T.H. Denat A., Lesaint O., Teissedre G. 2009. Pulsed electrical discharges in water for removal of organic pollutants: a comparative study. *Eur Phys J Appl Phys.* 47, 22818 p1-p7

Doll T.E., Frimmel F.H. 2004. Kinetic study of photocatalytic degradation of carbamazepine, clofibric acid, iopromol and iopromide assisted by different TiO₂ materials – determination of intermediates and reaction pathways. *Water Research.* 38, 955-964

Doll T.E., Frimmel F.H. 2005. Photocatalytic degradation of carbamazepine, clofibric acid and iopromol with P25 and Hombokal UV100 in the presence of natural organic matter (NOM) and other organic water constituents. *Water Res.* 39, 403-411

Doll T.E., Frimmel F.H. 2004. Kinetic study of photocatalytic degradation of carbamazepine, clofibric acid, iopromol and iopromide assisted by different TiO₂ materials – determination of intermediates and reaction pathways. *Water Res.* 38, 955-964

Donner E., Kosjek T., Qualmann S., Kusk K.O., Heath E., Revitt M., Ledin A., Andersen H.R. 2012. Ecotoxicity of carbamazepine and its UV photolysis transformation products. *Sci Total Environ.* 443C, 870-876

Dorn P.B., Chou C.-S., Gentempo J.J. 1987. Degradation of bisphenol A in natural waters. *Chemosphere.* 16(7), 1501-1507

Duirk S.E., Lindell C., Cornelison C.C., Kormos J., Ternes T.A., Attene-Ramos M., Osiol J., Wagner E.D., Plewa M.J., Richardson S.D. 2011. Formation of

toxic iodinated disinfection by-products from compounds used in medical imaging. *Environ Sci Technol.* 45(16), 6845-6854

Edebo L., Holme T., Selin I. 1968. Microbicidal action of compounds generated by transient electric arcs in aqueous systems. *J Gen Microbiol.* 53, 1-7

Edebo L., Holme T., Selin I. 1969. Influence of conductivity of discharge liquid on microbial effect of transient electric arcs in aqueous systems. *Appl Microbiol.* 17(1), 59-62

Ellis D.A., Mabury S.A., Martin J.W., Muir D.C.G. 2001. Thermolysis of fluoropolymers as a potential source of halogenated organic acids in the environment. *Nature.* 412, 321-324

Ellis D.A., Hanson M.L., Sibley P.K., Shahid T., Fineberg N.A., Solomon K.R., Muir D.C.G., Mabury S.A. 2001 The fate and persistence of trifluoroacetic and chloroacetic acids in pond waters. *Chemosphere.* 42, 309-318

Encinas S., Bosca F., Miranda M. 1998. Photochemistry of 2,6-dichlorodiphenylamine and 1-chlorocarbazole, the photoactive chromophores of diclofenac, meclofenamic acid and their major photoproducts. *Photochem Photobiol.* 68(5), 640-645

Environmental fate of trifluoroacetyl halides:
<http://www.afeas.org/environ.html>

Francisco J.S. 1992. Decomposition pathways for trifluoroacetic acid, $\text{CF}_3\text{C}(\text{O})\text{OH}$. *J Chem Soc Faraday Trans.* 88(24), 3521-3525

Gao J.Z., Yu J., Lu Q.F., He X.y., Yang W, Li Y., Pu L.M., Yang Z.M. 2008. Decoloration of alizarin red S in aqueous solution by glow discharge electrolysis. *Dyes Pigment.* 76(1), 47-52

Gartiser S., Brinker L., Erbe T., Kummerer K., Willmund R. 1996. Contamination of hospital wastewater with hazardous compounds as defined by 7a WHG. *Acta Hydrochimica Et Hydro-biologica.* 24(2), 90-97

Gerrity D., Stanford B.D., Trenholm R.A., Snyder S.A. 2010. An evaluation of a pilot-scale nonthermal plasma advanced oxidation process for trace organic compound degradation. *Water Res.* 44, 493-504

The Globe and Mail 2010 Canada Gazette <http://www.theglobeandmail.com>

Görner H. 2010. Photocyclization of 2,6-dichlorodiphenylamines in solution. *J Photochem Photobiol A: Chemistry.* 211, 1-6

Grabowski L.R. 2006. Doctoral Dissertation: Pulsed corona in air for water treatment. Technical University Eindhoven, Eindhoven, 127 pages

Gros M., Petrovic M., Barcelo D. 2007. Wastewater treatment plants as a pathway for aquatic contamination by pharmaceuticals in the Ebro river basin (Northeast Spain). *Environ Toxicol Chem.* 26, 1553

Gros M., Petrovic M., Ginebreda A., Barcelo D. 2010. Removal of pharmaceuticals during wastewater treatment and environmental risk assessment using hazard indexes. *Environ Int.* 36, 15

Gruska H., Beyer K.-H., Kubicki S.T., Schneider H. 1971. Klinik, Toxikologie und Therapie einer schweren Carbamazepin-Vergiftung. *Arch Toxikol.* 27, 193-203 (in German)

Hayashi D., Hoeben W., Doms G., Veldhuizen E.M. van, Rutgers W.R. Kroesen G.M.W. 2000. LIF diagnostics for pulsed-corona-induced degradation of phenol in aqueous solution. *J Phys D: Appl Phys.* 33, 1484-1486

Heberer T., Reddersen K., Mechlinski A., 2002a. From municipal sewage to drinking water: fate and removal of pharmaceutical residues in the aquatic environment in urban areas. *Water Sci Technol.* 46, 81-88

Heberer T., 2002b. Occurrence, fate, and removal of pharmaceutical residues in the aquatic environment: A review of recent research data. *Toxicol Lett.* 131, 5-17

Heberer T., 2002c. Tracking persistent pharmaceutical residues from municipal sewage to drinking water. *J Hydrol.* 266, 175-189

Hirano T., Honda Y., Watanabe T., Kuwahara M. 2000. Degradation of bisphenol A by the lignin-degrading enzyme, manganese peroxidase, produced by the white-rot basidiomycete. *Biosci Bio-technol Biochem.* 64, 1958-1962

Hirooka T., Nagase H., Uchida K., Hiroshige Y., Ehara Y., Nishikawa J., Nishihara T., Miyamoto K., Hirata Z. 2005. Biodegradation of bisphenol A and disappearance of its estrogenic activity by the green alga *Chlorella fusca* var. *vacuolata*. *Environ Toxicol Chem.* 24, 1896-1901

Hirsch R., Ternes T. A., Lindart A., Haberer K., Wilken R-D. 2000. A sensitive method for the determination of iodine containing diagnostic agents in aqueous matrices using LC-electrospraytandem-MS detection. *Fresenius J Anal Chem.* 366(8), 835-841

Hori H., Takano Y., Koike K., Takeuchi K., Einaga H. 2003. Decomposition of Environmentally persistent trifluoroacetic acid to fluoride ions by a homogeneous photocatalyst in water. *Environ Sci Technol.* 37, 418-422

Hoeben W., Velduizen E.M. van, Rutgers W.R. Kroesen G.M.W. 1999. Gas phase corona discharges for oxidation of phenol in aqueous solution. *J Phys D: Appl Phys.* 32(24), L133-L137

Hoeben W., Velduizen E.M. van, Rutgers W.R., Cramers C., Kroesen G.M.W. 2000. The degradation of aqueous phenol solutions by pulsed positive corona discharges. *Plasma Sources Sci Technol.* 9(3), 361-369

Hofmann J., Freier U., Wecks M., Hohmann S. 2007. Degradation of diclofenac in water by heterogeneous catalytic oxidation with H₂O₂. *Appl Cat B: Environ.* 70, 447-451

Hua W., Bennett E.R., Letcher R.J., 2006. Ozone treatment and the depletion of detectable pharma-ceuticals and atrazine herbicide in drinking water sourced from the upper Detroit River, Ontario, Canada. *Water Res.* 40, 2259-2266

Huber M., Canonica S., Park G. Y., Gunten, U. von. 2003. Oxidation of pharmaceuticals during ozonation and advanced oxidation processes. *Environ Sci Technol.* 37, 1016-1024

Huber M.M. 2004. Doctoral Dissertation: Elimination of pharmaceuticals during oxidative treatment of drinking water and wastewater: application of ozone and chlorine dioxide, Swiss Federal Institute of Technology, Zurich, 174 pages

Huggett D.B., Khan I.A., Foran C.M., Schlenk D. 2003. Determination of beta-adrenergic receptor blocking pharmaceuticals in United States wastewater effluent. *Environ Pollut.* 121, 199-205

Ikehata K., Naghashkar N.J., El-Din M.G. 2006. Degradation of aqueous pharmaceuticals by ozonation and advanced oxidation processes: a review. *Ozone-Sci Eng.* 28, 353-141

Im J.K., Son H.S., Kang Y.M., Zoh K.D. 2012. Carbamazepine degradation by photolysis and titanium dioxide photocatalysis. *Water Environ Res.* 84(7), 554-61

Jeong J., Jung J., Cooper W.J., Song W. 2010. Degradation mechanisms and kinetic studies for the treatment of X-ray contrast media compounds by advanced oxidation/reduction processes. *Water Res.* 44, 4391-4398

Joss A., Zabczynski S., Goebel A., Hoffmann B., Loeffler D., McArdell C. S., Ternes T. A., Thomsen A., Siegrist H. 2006. Biological degradation of

pharmaceuticals in municipal wastewater treatment: proposing a classification scheme. *Water Res.* 40, 1686-1696

Kalsch W. 1999. Biodegradation of the iodinated X-ray contrast media diatrizoate and iopromide. *Sci Total Environ.* 225(1-2), 143-153

Kang J.-H., Katayama Y., Kondo F. 2006. Biodegradation or metabolism of bisphenol A: from microorganisms to mammals. *Toxicol Review* 217, 81-90

Kang J.H., Kondo F. 2002. Bisphenol A degradation by bacteria isolated from river water. *Arch Envi-ron Contam Toxicol.* 43, 265-269

Kaphalia L., Kaphalia B.S., Kumar S., Kanz M.F., Treinen-Moslen M. 2006. Efficient high performance liquid chromatograph/ultraviolet method for determination of diclofenac and 4-hydroxydiclofenac in rat serum. *J Chromatography B.* 830, 231–237

Key B.D., Howell R.D., Criddle C.S. 1997 Fluorinated organics in the biosphere. *Environ Sci Technol.* 31(9), 2445-2454

Kim S.D., Cho J., Kim I.S., Vanderford B.J., Snyder S.A. 2007. Occurrence and removal of pharmaceuticals and endocrine disruptors in South Korean surface, drinking, and waste waters. *Water Res.* 41, 1013-1021

Kinne M., Poraj-kobielska M., Aranda E., Ullrich R., Hammel K.E., Scheibner K., Holfrichter M. 2009. Regioselective preparation of 5-hydroxypropranolol and 4'-hydroxydiclofenac with a fungal peroxxygenase. *Bioorg Med Chem Lett.* 19, 3085-3087

Kosjek T., Andersen H.R., Kompare B., Ledin A., Heath E. 2009. Fate of carbamazepine during water treatment. *Environ Sci Technol.* 43, 6256-6261

Koutsouba P., Dasenakis M., Hiskia A., Tsipi D. Photochemical studies of the anti-inflammatory drug diclofenac in aqueous solutions. *Proceedings of the 7th International Conference on Environmental Science and Technology.* 3rd – 6th September, 2001, Ermoupolis, Syros Island

Krause H., Schweiger B., Schuhmacher J., Scholl S., Steinfeld U. 2009. Degradation of the endocrine disrupting chemicals (EDCs) carbamazepine, clofibric acid, and iopromide by corona discharge over water. *Chemosphere.* 75, 163-168

Krause H., Schweiger B., Prinz E., Kim J., Steinfeld U. 2011. Degradation of persistent pharmaceuticals in aqueous solutions by a positive dielectric barrier discharge treatment. *J Electrostatics.* 69, 333-338

Kusic H., Koprivanac N., Locke B.R. 2005. Decomposition of phenol by hybrid gas/liquid electrical discharge reactors with zeolite catalysts. *J Hazard Mater.* 125(1-3), 190-200

Lesjean B., Gnirss R., Buisson H., Keller S., Tazi-Pain A., Luck F. 2005. Outcomes of a 2-year investigation on enhanced biological nutrients removal and trace organics elimination in membrane bioreactor (MBR). *Water Sci Technol.* 52(10-11), 453-60

Li Z., Sakai S., Yamada C., Wang D., Chung S., Lin X., Namihira T., Katsuki S., Akiyama H. 2006. The effects of pulsed streamerlike discharge on cyanobacteria cells. *IEEE Trans Plasma Sci.* 34, 1719-1725

Lifongo L.L., Bowden D.J., Brimblecombe P. 2010. Thermal degradation of haloacetic acids in water. *Int J Phys Sci.* 5(6), 738-747

Liu Q.-T., Cumming R.I., Sharpe A.D. 2009. Photo-induced environmental depletion processes of β -blockers in river waters. *Photochem Photobiol Sci.* 8, 768-777

Martin J.W., Franklin J., Hanson M.L. Solomon K.R., Mabury S.A., Ellis D.A., Scott B.F., Muir D.C. G. 2000. Detection of chlorodifluoroacetic acid in North American precipitation and surface waters *Environ Sci Technol.* 34, 274-281

Magureanu M., Piroi D., Mandache N.B., David V., Medvedovici A., Bradu C., Parvulescu V.I. 2011. Degradation of antibiotics in water by non-thermal plasma treatment. *Water Res.* 45, 3407-3416

Magureanu M., Piroi D., Mandache N.B., Bradu C., Medvedovici A., Parvulescu V.I. Degradation of pharmaceutical compounds in aqueous solution using non-thermal plasma. *Proceeding of 13th International Conference on Optimization of Electrical and Electronic Equipment (OPTIM).* 24th - 26th May 2012, Brasov, Romania.

Magureanu M., Piroi D., Mandache N.B., David V., Medvedovici A., Parvulescu V.I. 2010. Degradation of pharmaceutical compound pentoxifylline in water by non-thermal plasma treatment. *Water Res.* 44, 3445-3453

Magureanu M., Mandache N.B., Parvulescu V.I. 2007. Degradation of organic dyes in water by electrical discharges. *Plasma Chem Plasma Proces.* 27(5), 589-598

Malik M.A. 2010. Water purification by plasmas: which reactors are most energy efficient? *Plasma Chem Plasma Process.* 30, 21-31

Medevovic S., Locke B.R. 2007. Side-chain degradation of atrazine by pulsed electrical discharge in water. *Ind Eng Chem Res.* 46, 2702-2709

Medevovic S., Finney, Locke B.R. 2007. Aqueous-phase mineralization of s-triazine using pulsed electrical discharge. *Int J Plasma Environ Sci Technol.* 1(1), 82-90

Miyamoto G., Zahid N., Uetrecht J.P. 1997. Oxidation of diclofenac to reactive intermediates by neutrophils, myeloperoxidase, and hypochlorous acid. *Chem Res Toxicol.* 10, 414-419

Mizuno A., Hori Y. 1988. Destruction of living cells by pulsed high-voltage application. *IEEE Trans Ind Appl.* 24, 387-394

Mohring S.A.I., Strzysch I., Fernandes M.R., Kiffmeyer T.K., Tuerk J., Hamscher G. 2009. Degradation and elimination of various sulfonamides during anaerobic fermentation: a promising step on the way to sustainable pharmacy? *Environ Sci Technol.* 43(7), 2569-2574

Nikolaou A., Meric S., Fatta D. 2007. Occurrence patterns of pharmaceuticals in water and wastewater environments. *Anal Bioanal Chem* 387, 1225–1234

Ohko Y., Ando I., Niwa C., Tatsuma T., Yamamura T., Nakashima T., Kubota Y., Fujishima A. 2001. Degradation of bisphenol A in water by TiO₂ photocatalyst. *Environ Sci Technol.* 35, 2365-2368

Olea N., Pulgar R., Perez P., Olea-Serrano F., Rivas A., Novillo-Fertell A., Pedraza V., Soto A.M. Son-nenschein C. 1996. Estrogenicity of resin-based composites and sealants used in dentistry. *Environ Health Perspect.* 104, 298-305

Pawlat J., Ihara S. 2007. Removal of color caused by various chemical compounds using electrical discharges in a foaming column. *Plasma Process Polym.* 4(7-8), 753-759

Pehkonen S.O., Siefert R.L., Hoffmann M.R. 1995. Photoreduction of iron oxyhydroxides and the photooxidation of halogenated acetic acids. *Environ Sci Technol.* 29, 1215-1222

Perez S., Barcelo D. 2007. Fate and occurrence of X-ray contrast media in the environment. *Anal Bioanal Chem.* 387(4), 1235-1246.

Perez S., Eichhorn P., Ceballos V., Barcelo D. 2009. Elucidation of phototransformation reactions of the X-ray contrast medium iopromide under simulated solar radiation using UPLC-ESI-QqTOFMS. *J Mass Spectrom.* 44(9), 1308-1317

Perez-Estrada L.A., Malato S., Gernjak W., Agüera A., Thurman E.M., Ferrer I., Fernandez-Alba A.R. 2005. Photo-Fenton degradation of diclofenac: identification of main intermediated and degradation pathway. *Environ Sci Technol.* 39, 8300-8306

Petrovic M., Barcelo D. 2007. LC-MS for identifying photodegradation products of pharmaceuticals in the environment. *Trends in Analytical Chemistry.* 26(6), 486-493

Pitre D., Felder E. 1980. Development, chemistry and physical properties of iopamidol and its analogues. *Invest Radiol.* 15(6 suppl), 301-309

Piram A., Salvador A., Verne C., Harbreteau B., Faure R. 2008. Photolysis of β -blockers in environmental waters. *Chemosphere.* 73, 1265-1271

Piskarev I.M. 1999. Phenol oxidation by OH, H, O, and O₃ species formed in electric discharge. *Kinet Catal.* 40(4), 452-458

Putschew A., Wischnack S., Jekel M. 2000. Occurrence of triiodinated X-ray contrast agents in the aquatic environment. *Sci Total Environ.* 255(1), 129-134

Putschew A., Jekel M. 2001. Iodierte Röntgenkontrastmittel im anthropogen beeinflussten Wasser-kreislauf. *Vom Wasser.* 97, 103-114

Putschew A., Jekel M. 2006. Iodinated X-ray contrast media. *Organic Pollutants in the Water Cycle.* Eds. T. Reemtsma and M. Jekel. Wiley-VCH, Weinheim, ISBN 3-527-31297-8, 87-98

Putschew A., Jekel M. 2003. Induced in-source fragmentation for the selective detection of organic bound iodine by liquid chromatography electrospray mass-spectrometry. *Rapic Communications in Mass Spectrometry.* 17(20), 2279-2282

Rivas F.J., Gimeno O., Borralho T., Carbajo M. 2010. UV-C radiation based methods for aqueous metoprolol elimination. *J Hazard Mater.* 179, 357-362

Romero V., De la Cruz N., Dantas R.F., Marco P., Gimenez J., Esplugas S. 2011. Photocatalytic treatment of metoprolol and propranolol. *Catalysis Today.* 161, 115-120

Rufus I.B., Shah H., Hoyle C.E. 1994. Identification of fluorescent products produced by the thermal treatment of bisphenol A-based polycarbonate. *J Appl Polym Sci.* 51(9), 1549-1558

Sacher F., Lange F. T., Brauch H. J., Blankenhorn I. 2001. Pharmaceuticals in groundwaters. Analytical methods and results of a monitoring program in Baden-Wuerttemberg, Germany. *J Chromatography A.* 938, 199-210

Sale A.J.H., Hamilton W.A. 1967. Effect of high electric fields on microorganisms I. Killing of bacteria and yeasts. *Biochim Biophys Acta*. 148, 781-788

Salgado R., Pereira V.J., Carvalho G., Soeiro R., Gaffney V., Almeida C., Vale Cardoso V., Ferreira E., Benoliel M.J., Ternes T.A., Oehmen A., Reis M.A.M., Noronha J.P. 2012. Photodegradation kinetics and transformation products of ketoprofen, diclofenac and atenolol in pure water and treated wastewater. *J Hazard Mater*. 14662, 1-12

Sato M., Ohgiyama T., Clements J.S. 1996. Formation of chemical species and their effects on microorganisms using a pulsed high-voltage discharge in water. *IEEE Trans Ind Appl*. 32(1), 106-112

Sato M., Soutome T., Mii S., Ohshima T., Yamada Y. 2007. Decomposition of phenol in water using water surface plasma in wetted-wall reactor. *Int J Plasma Environ Sci Technol*. 1(1), 71-75

Schmitt-Jansen M., Bartels P., Adler N., Altenburger R. 2007. Phytotoxicity assessment of diclofenac and its phototransformation products. *Anal Bioanal Chem*. 387, 1389-1396

Schramm C., Gans O., Uhl M., Grath J., Scharf S., Zieritz I., Kralik M., Scheidleder A., Humer F. Carbamazepin und Koffein – potenzielle Screeningparameter für Verunreinigungen des Grundwassers durch kommunales Abwasser? Report Umweltbundesamt, Wien 2006 (in German)

Scott B.F., Mactavish D., Spencer C., Strachan W.M.J., Muir D.C.G. 2000. Haloacetic acids in Canadian lake waters and precipitation. *Environ Sci Technol*. 34, 4266-4272

Sein M.M., Zedda M., Tuerk J., Schmidt T., Golloch A., Sonntag C. von. 2008. Oxidation of diclofenac with ozone in aqueous solution. *Environ Sci Technol*. 42, 6656-6662

Sein M.M., Schmidt T.C., Golloch A., von Sonntag C. 2009. Oxidation of some typical wastewater contaminants (tributyltin, clarithromycin, metoprolol and diclofenac) by ozone. *Water Sci Tech*. 58, 1479-1485

Seitz W., Weber W.H., Flottmann D., Schulz W. 2004. Iodierte Röntgenkontrastmittel in Oberflächen-, Grund- und Trinkwasser. *CLB Chemie in Labor und Biotechnik*, Heft 12/2004 (in German)

- Seitz W.**, Jiang J.-Q., Schulz W., Weber W. H., Maier D., Maier M. 2008. Formation of oxidation by-products of the iodinated X-ray contrast medium iomeprol during ozonation. *Chemosphere*. 70(7), 1238-1246
- Soulet B.**, Tauxe A., Tarradellas J. 2002. Analysis of acidic drugs in Swiss wastewaters. *Int J Environ Anal Chem*. 82(10), 659–667
- Spivack J.**, Leib T.K., Lobos J.H. 1994. Novel pathway for bacterial metabolism of bisphenol A. *J Biol Chem*. 269, 7323-7329
- Sugiarto A.T.**, Sato M. 2001. Pulsed plasma processing of organic compounds in aqueous solution. *Thin Solid Films*. 386(2), 295-299
- Stamatelatou K.**, Frouda C., Fountoulakis M.S., Drillia P., Kornaros M., Lyberatos G. 2003. Pharmaceuticals and health care products in wastewater effluents: the example of carbamazepine. *Water Supply*. 3(4), 131–137
- Staples C.A.**, Dorn P.B., Klecka G.M., O’Block S.T. Hariis L.R. 1998. A review of the environmental fate, effects, and exposures of bisphenol A. *Chemosphere*. 36, 2149-2173
- Stara Z.**, Krcma F., Nejezchleb M., Skalny J.D. 2009. Organic dye decomposition by DC diaphragm discharge in water: effect of solution properties on dye removal. *Desalination*. 239(1-3), 283-294
- Stara Z.**, Krcma F., Nejezchleb M., Skalny J.D. 2008. Influence of solution composition and chemical structure of dye on removal of organic dye by DC diaphragm discharge in water solution. *J Adv Oxid Technol*. 11(1), 155-162
- Stumpf M.**, Ternes T.A., Wilken R.D., Rodrigues S.V., Baumann W. 1999. Polar drug residues in sewage and natural waters in the state of Rio de Janeiro. Brazil *Sci Total Environ*. 225 (1-2), 135–141
- Suzuki K.**, Hirai H., Murata H., Nishida T. 2003. Removal of estrogenic activities of 17 β -estradiol and ethinylestradiol by ligninolytic enzymes from white rot fungi. *Water Res*. 37, 1972-1975
- Swedberg K.**, Hjalmarson A., Holmberg S. 1979. Effects of work and acute beta-receptor blockade on myocardial noradrenaline release in congestive cardiomyopathy. *Clin Cardiol*. 2(6), 424-30
- Tanaka S.**, Nakata Y., Kimura T., Yustiawati, Kawasaki M., Kuramitz H. 2002. Electrochemical decomposition of bisphenol A using Pt/Ti and SnO₂/Ti anodes. *J Appl Electrochem*. 32, 197-201

Ternes T.A. 1998. Occurrence of drugs in German sewage treatment plants and rivers. *Water Res.* 32(11), 3245-3260

Ternes T. A., Hirsch R. 2000. Occurrence and behavior of X-ray contrast media in sewage facilities and the aquatic environment. *Environ Sci Technol.* 34(13), 2741-2748

Ternes T.A., Meisenheimer M., McDowell D., Sacher F., Brauch H.J., Haist-Gulde B., Preuss G., Wilme U., Zulei-Seibert N. 2002. Removal of pharmaceuticals during drinking water treatment. *Environ Sci Technol.* 36(17), 3855-3863

Ternes T. A., Stueber J., Herrmann N., McDowell D., Ried, A., Kampmann M., Teiser B. 2003. Ozonation: a tool for removal of pharmaceuticals, contrast media and musk fragrances from wastewater? *Water Res.* 37, 1976-1982

Thome J., Wiesbeck G.A., Vince G.H. 1994. Carbamazepin in der Behandlung des Alkohol-entzugssyndroms – Eine Übersicht zum aktuellen Forschungsstand. *Fortschr Neurol Psychiat.* 62, 125-133 (in German)

Tixier C., Singer H. P., Oellers S., Mueller S. R. 2003. Occurrence and fate of carbamazepine, clofibric acid, diclofenac, ibuprofen, ketoprofen, and naproxen in surface waters. *Environ Sci Tech.* 37, 1061-1068

Umweltbundesamt (2012) fact sheet Carbamazepine

Visscher P.T., Culbertson C.W., Oremland R.S. 1994. Degradation of trifluoroacetate in oxic and anoxic sediments. *Nature.* 370, 391

Vogna D., Marotta R., Napolitano A., Anderozzi R., d'Ischia M. 2004. Advanced oxidation of the pharmaceutical drug diclofenac with UV/H₂O₂ and ozone. *Water Res.* 38, 414-422

Vogna D., Marotta R., Andreozzi R., Napolitano A., d'Ischia M. 2004. Kinetic and chemical assessment of the UV/H₂O₂ treatment of antiepileptic drug carbamazepine. *Chemosphere.* 54(4), 497-505

Vujevic D., Koprivanac N., Bozic A.L., Locke B.R. 2004. The removal of direct orange 39 by pulsed corona discharge from model wastewater. *Environ Technol.* 25(7), 791-800

Wallington T. J., Nielsen O.J. 1991 Pulse radiolysis study of CF₃CFHO₂ radicals in the gas phase at 298 K. *Chem Phys Lett.* 187, 33-39

Wang H.J., Li J., Quan X., Wu Y. 2008. Enhanced generation of oxidative species and phenol degradation in a discharge plasma system coupled with TiO₂ photocatalysis. *Appl Catal B: Environ.* 83(1-2), 72-77

Wang Z.H., Xu D.X., Chen Y., Hao C.X., Zhang X.Y. 2008. Plasma decolorization of dye using dielectric barrier discharges with earthed spraying water electrodes. *J Electrostat.* 66(9-10), 476-481

Yamamoto T., Yasuhara A., Shiraishi H., Nakasugi O. 2001. Bisphenol A in hazardous waste landfill leaches. *Chemosphere.* 42, 415-418

Yan J.H., Du C.M., Li X.D., Sun X.D., Ni M.J., Cen K.F., Cheron B. 2005. Plasma chemical degradation of phenol in solution by gas-liquid gliding arc discharge. *Plasma Sources Sci Technol.* 14(4), 637-644

Yang H., Li G., Gao Y., Fu J. 2010. Photocatalytic degradation kinetics and mechanism of environmental pharmaceuticals in aqueous suspension of TiO₂: A case of sulfa drugs. *Catalysis Today.* 153, 200-207

Ying G.G., Kookana R.S. 2003. Degradation of five selected endocrine disrupting chemicals in seawater and marine sediment. *Environ Sci Technol.* 37, 1256-1260

Yu H., Nie E., Xu J., Yan S., Cooper W.J., Song W. 2012. Degradation of diclofenac by advanced oxidation and reduction processes: kinetic studies, degradation pathways and toxicity assessments. *Water Res.* 47, 1909-1918

Zhang Y.Z., Sun B.Y., Deng S.H., Wang Y.J., Peng H., Li Y.W., Zhang X.H. 2010. Methyl orange degradation by pulsed discharge in the presence of activated carbon fibers. *Chem Eng J.* 159(1-3), 47-52

Zuccato E., Castiglioni S., Fanelli R. 2005. Identification of the pharmaceuticals for human use contaminating the Italian aquatic environment. *J Hazard Mater.* 122, 205-209

Zwiener C., Frimmel H. 2000. Oxidative treatment of pharmaceuticals in water. *Water Res.* 34, 1881-1885

CONCLUSIONS

Electrical discharges generated in water is a subject of a great interest and is drawing attention of research groups which number increases every day. The research described in this work was aimed to fulfill the knowledge about the extremely complex phenomenon of underwater electrical discharges. Four goals that were set at the beginning have been successfully met at the end of the study. The following conclusions could be made:

1. In the present study, a novel approach was applied according to which all three aspects of electrical discharge - generation in water, characterization of the discharge phenomenon and application for organics removal – have been worked out.
2. The generation of electrical discharge in water with large-area electrodes using a pinhole geometry has the advantage over the classical corona with a tip electrode due to no deterioration of the metal surface of high-voltage electrode.
3. The described way of electrical discharge generation could be used for the formation of plasma of a non-thermal nature.
4. Among the investigated experimental parameters, solution conductivity tested in the range of 0.3 $\mu\text{S}/\text{cm}$ – 10 mS/cm was shown to make different effects on the discharge inception, physical and chemical activities of the electrical discharges. This fact should be taken into account for the future research and application.
5. The highest possible values of ratio of the *applied voltage/electrode distance* should be applied for the easier discharge generation, increased physical and chemical activity and the most effective application for organics removal. However, the upper limit determined by the formation of thermal plasma should be taken into account.

6. Electrical discharge in water have a great potential as a novel, chemical-free method of water treatment capable of degrading moderately and highly recalcitrant organic compounds. To our knowledge, the successful degradation of diclofenac, iopamidol, metoprolol, bisphenol A, carbamazepine and trifluoroacetic acid by electrical discharges in water using large-area electrodes has not been reported before in literature.
7. Nevertheless, the attempt to prove the applicability of electrical discharges for water treatment was only partially successful. The fact that this method is energy consuming limits its application on the commercial scale.

OUTLOOK

The present study could be used as a starting point for the future investigation of electrical discharges in terms of the application for water treatment. The recommendations for the future work are listed below:

1. The range of initial concentrations of pharmaceuticals tested in the present study (1-100 mg/L) is much higher than the concentration of the pharmaceuticals in the real wastewater samples. Therefore, the degradation of the compounds at lower initial concentrations (in the range of a few $\mu\text{g/L}$) should be investigated.
2. The low values of energy efficiency obtained in the present study suggest that the future improvement is required. The higher energy efficiency could be obtained for the degradation of pharmaceuticals at lower initial concentration, which is assumed to take shorter time.
3. The degradation of organic compounds by electrical discharges was shown to lead to the formation of transformation products. Their toxicity and recalcitrance could exceed the toxicity and recalcitrance of the target compounds. Therefore, the detailed study on determination of transformation products is required.
4. As it was shown in the thesis, solution properties make significant effect on the properties of the electrical discharges, thus, influencing organics removal. Therefore, the degradation of organic compounds in real solutions should be investigated in terms of the possible the matrix effect.
5. Generally, it is anticipated that the method of pulsed electrical discharges would be implemented in the municipal waste water treatment plants for the tertiary effluents treatment and for complete and effective remediation of drinking water wells

ACKNOWLEDGEMENTS

I would like to express my very great appreciation to my direct supervisor Dr. Ursula Telgheder for her invaluable inputs regarding my scientific work, assistance and support.

I am particularly grateful to the head of the Thin film group (Physical faculty) Prof. Volker Buck for his important remarks and recommendations that helped me to improve my thesis.

I would like to acknowledge the head of the department of Instrumental Analytical Chemistry (IAC) Prof. Torsten Schmidt for giving me the opportunity to start this project.

I would like to express the gratitude to Dr. Klaus Kerpen and Dr. Andriy Kuklya who were helping me during the course of my PhD. I would like to thank them for the continuous guidance and creative ideas they generated even in the most difficult periods of my work.

The first brick of this project - the manufacturing the plasma generator - was laid by Dr. Günter Böhm from Puls-Plasmatechnik (PPT) GmbH and Mr. Jürgen Kaiser from Kaiser Systemtechnik for which I am very grateful to them.

The staff and students of IAC are acknowledged for their help with any task no matter how complicated.

I also wish to thank the EU Framework 7 project “ATWARM” Marie Curie ITN, No. 238273 for the financial support.

My special thanks are extended to the managers of the ATWARM project Ciarán Prunty and Patricia McCrory from Queen’s University Belfast for the perfect organization of our project.

I would like to acknowledge Dr. Anne Morrissey from Dublin City University (DCU) for the supervision during my secondment at DCU.

I am also grateful to the ATWARM students for the scientific help, moral support and the great time spent on the ATWARM meetings and the Summer schools.

This research project would not have been possible without my parents and family to whom I express my sincerest gratitude for their dedication, their love and the faith in me throughout my whole life.

Curriculum Vitae

Svetlana Gasanova

Personal details

Born: 20.06.1988 Leningrad, Russia
Address: Zemskii pereulok 9
197375 Saint-Petersburg, Russia
Phone: +7 812 304 10 86
Email: svetlana.gasanova@stu.uni-due.de
Marital status: single, no children

Completions

06/2010 Saint-Petersburg State University (Diploma)
06/2005 Gymnasium №77, Saint-Petersburg

Studies

09/2005-06/2010 Department of Physical Chemistry, Faculty of Chemistry, Saint-Petersburg State University. Diploma title: Protonation and complexation of pyridine and pyrazine by Surface Enhanced Raman Spectroscopy (SERS)

PhD

10/2010-11/2013 Department of Analytical Chemistry, Faculty of Chemistry, University of Duisburg-Essen. PhD title: Aqueous-phase electrical discharges: generation, investigation and application for removal of organics

Work experience

10/2010-09/2013 EU-Scientist at the IWW Rhine-Westfalia Institute for Water Research.
Fellow of the EU project ATWARM – Advanced Technologies for Water Resource Management

Secondment

05/2012-08/2012 Dublin City University. Activity: Practical course in photocatalysis

Languages

Russian (mother tongue), English (fluent, reading, speaking, writing), German (good, reading, speaking), Spanish (basic knowledge, reading)

Principle skills

Instrumental methods of chemical analysis, scientific writing, oral presentations, work with high-voltage equipment, supervision of students, analysis the large amount of information

Personal qualities

capable to self-instruction, responsible, result-oriented

PC skills

MS Office, AutoCAD, OriginLab, Adobe Photoshop

Private Interests

Hiking, classic literature, flamenco

References

Available on request

List of publications

1. Gasanova S., Telgheder U., Kerpen K., Kuklya A. and Schmidt T. Al₂O₃ electrode coatings for electrical discharge generation in aqueous solution. Submitted to the Plasma Chemistry Plasma Processing, 2013
2. Proceedings of the Marie Curie Researchers Symposium "SCIENCE - Passion, Mission, Responsibilities". Warsaw, Poland, 25-27 September 2011. Abstract of poster presentation "Non-thermal plasmas created by corona-like discharges for eliminating recalcitrant organic contaminants"
3. Proceedings of the 4th IJAS International Conference. Gozo, Malta, 20-23 February 2012. Abstract of oral presentation "Non-thermal plasmas created by corona-like discharges for eliminating recalcitrant organic contaminants"
4. Proceedings of the IWA-WCE International Conference. World Congress on Water, Climate and Energy. Dublin, Ireland, 13-18 May 2012. Abstract of poster presentation "The application of corona-like discharges for eliminating recalcitrant organic contaminants"
5. Proceedings of the ATWARM International Conference. Water: the Greatest Global Challenge. Dublin, Ireland, 14-16 May 2013. Abstract of oral presentation "Underwater electrical discharges – removal of organic contaminants"
6. Proceedings of the 3rd International Conference on Environmental Pollution and Remediation. Toronto, Canada, 15-17 July 2013. Abstract of oral presentation "Removal of pharmaceuticals by underwater corona-like discharges"

Erklärung der eigenständigen Anfertigung der Arbeit

Hiermit versichere ich, dass ich die vorliegende Arbeit mit dem Titel

„Aqueous-phase electrical discharges: generation, investigation and application for organics removal from water”

selbst verfasst und keine außer den angegebenen Hilfsmitteln und Quellen benutzt habe, und dass die Arbeit in dieser oder ähnlicher Form noch bei keiner anderen Universität eingereicht wurde.

Essen, September 2013

